0-315-03651-6

National Library of Canada
Canadian Theses Division
Ottawa, Canada
K1A 0N4

Bibliothèque nationale du Canada
Division des thèses canadiennes

51546

# PERMISSION TO MICROFILM — AUTORISATION DE MICROFILMER

- Please print or type — Écrire en lettres moulées ou dactylographier

Full Name of Author — Nom complet de l'auteur
GARY F. MARGRAVE

Date of Birth — Date de naissance
6 FEB 1950

Country of Birth — Lieu de naissance
UNITED STATES OF AMERICA

Permanent Address — Résidence fixe
803 S.W. 32ND ST.
PENDLETON, OREGON 97801

Title of Thesis — Titre de la thèse
MICROGEODESY AND SOUTH AMERICAN TECTONICS

University — Université
UNIVERSITY OF ALBERTA

Degree for which thesis was presented — Grade pour lequel cette thèse fut présentée
PhD

Year this degree conferred — Année d'obtention de ce grade
1981

Name of Supervisor — Nom du directeur de thèse
EDO NYLAND

Permission is hereby granted to the NATIONAL LIBRARY OF CANADA to microfilm this thesis and to lend or sell copies of the film.

The author reserves other publication rights, and neither the thesis nor extensive extracts from it may be printed or otherwise reproduced without the author's written permission.

L'autorisation est, par la présente, accordée à la BIBLIOTHÈQUE NATIONALE DU CANADA de microfilmer cette thèse et de prêter ou de vendre des exemplaires du film.

L'auteur se réserve les autres droits de publication; ni la thèse ni de longs extraits de celle-ci ne doivent être imprimés ou autrement reproduits sans l'autorisation écrite de l'auteur.

3 April 1981

Date
3 April 1981

Signature
Gary F. Margrave

NL-91 (4/77)

National Library of Canada
Collections Development Branch

Canadian Theses on
Microfiche Service

NOTICE

The quality of this microfiche is heavily dependent upon the quality of the original thesis submitted for microfilming. Every effort has been made to ensure the highest quality of reproduction possible.

If pages are missing, contact the university which granted the degree.

Some pages may have indistinct print especially if the original pages were typed with a poor typewriter ribbon or if the university sent us a poor photocopy.

Previously copyrighted materials (journal articles, published tests, etc.) are not filmed.

Reproduction in full or in part of this film is governed by the Canadian Copyright Act, R.S.C. 1970, c. C-30. Please read the authorization forms which accompany this thesis.

THIS DISSERTATION
HAS BEEN MICROFILMED
EXACTLY AS RECEIVED

Bibliothèque nationale du Canada
Direction du développement des collections

Service des thèses canadiennes
sur microfiche

AVIS

La qualité de cette microfiche dépend grandement de la qualité de la thèse soumise au microfilmage. Nous avons tout fait pour assurer une qualité supérieure de reproduction.

S'il manque des pages, veuillez communiquer avec l'université qui a conféré le grade.

La qualité d'impression de certaines pages peut laisser à désirer, surtout si les pages originales ont été dactylographiées à l'aide d'un ruban usé ou si l'université nous a fait parvenir une photocopie de mauvaise qualité.

Les documents qui font déjà l'objet d'un droit d'auteur (articles de revue, examens publiés, etc.) ne sont pas microfilmés.

La reproduction, même partielle, de ce microfilm est soumise à la Loi canadienne sur le droit d'auteur, SRC 1970, c. C-30. Veuillez prendre connaissance des formules d'autorisation qui accompagnent cette thèse.

LA THÈSE A ÉTÉ
MICROFILMÉE TELLE QUE
NOUS L'AVONS REÇUE

Ottawa, Canada
K1A 0N4

NL-339 (Rev. 8/80)

THE UNIVERSITY OF ALBERTA

# Microgeodesy and South American Tectonics

by

© Gary Frank Margrave

A THESIS
SUBMITTED TO THE FACULTY OF GRADUATE STUDIES AND RESEARCH
IN PARTIAL FULFILMENT OF THE REQUIREMENTS FOR THE DEGREE
OF Doctor of Philosophy
IN
Geophysics

Physics

EDMONTON, ALBERTA
Spring 1981

University of Alberta

THE UNIVERSITY OF ALBERTA

RELEASE FORM

| | |
|---|---|
| NAME OF AUTHOR | Gary Frank Margrave |
| TITLE OF THESIS | Microgeodesy and South American Tectonics |

DEGREE FOR WHICH THESIS WAS PRESENTED Doctor of Philosophy

YEAR THIS DEGREE GRANTED Spring 1981

Permission is hereby granted to THE UNIVERSITY OF ALBERTA LIBRARY to reproduce single copies of this thesis and to lend or sell such copies for private, scholarly or scientific research purposes only.

The author reserves other publication rights, and neither the thesis nor extensive extracts from it may be printed or otherwise reproduced without the author's written permission.

(SIGNED) Gary F. Margrave

PERMANENT ADDRESS:

803 S.W. 32ND ST
PENDLETON, OREGON
97801

DATED 3 April 1981

University of Alberta

# THE UNIVERSITY OF ALBERTA

## FACULTY OF GRADUATE STUDIES AND RESEARCH

The undersigned certify that they have read, and recommend to the Faculty of Graduate Studies and Research, for acceptance, a thesis entitled Microgeodesy and South American Tectonics submitted by Gary Frank Margrave in partial fulfilment of the requirements for the degree of Doctor of Philosophy in Geophysics.

..........................................
Co-Supervisor

R St J Lambert
..........................................
Co-Supervisor

Donald D. Betts
..........................................

..........................................

..........................................
External Examiner

Date... August 15, 1980 ..........

University of Alberta

# Abstract

Repeated precision surveys of small heavily braced networks (about 2km aperture) can measure earth strains of $10^{-6}$ or larger using only inexpensive, highly reliable commercial surveying equipment. Practical difficulties of such a small survey experiment in remote areas can be eased with foresight, experience, and careful planning. Monumentation with concrete pillars speeds precision surveys. Less elaborate brass plugs in bedrock suffice when coupled with optical plummets.

Two dimensional survey data provide estimates of polynomial approximations to tensor strain components. The polynomial coefficients, not the benchmark positions, are the fundamental unknowns. The solution uses the generalized inverse of the rectangular design matrix to construct a direct linear relationship between the observations and the strain estimates. Analysis of synthetic data shows that standard commercial surveying instrumentation and techniques are adequate, distance measurements are much more important than angles, and resolution increases approximately linearly with increasing aperture to at least 10km. Non-constant approximations to strains are useful only if single measurement accuracy significantly exceeds the magnitude of the expected strains. Real data from a network astride the Huaytapallana reverse fault in Peru show a $3\times10^{-6}\text{yr}^{-1}$ shear strain event with better than 95% confidence. This fault, at 11.9°S and 75.1°W, is known to be seismically active and has

a history of lateral movement.

Such strain events must be interpreted in terms of South American tectonic history. Shallow subduction in Peru extends to beneath the Subandean ranges. The Pisco Deflection, where a continuous change from shallow to steep subduction occurs, is causally related to the Nazca Ridge. Maximum seismicity is 125-150 km beneath the Central Andean volcanic front. The Andean Seismicity Lineament (ASL), defined by the volcanic front, seismicity, and geology, lies along a great circle through the relative motion pole for South America and the Nazca Plate. It may be a megafracture penetrating the continental crust accommodating both tectonics and magma injection similar to the Tapacocha Axis in Peru. Linear plutonic structures may constrain paleo-positions of relative motion poles. Least squares fitting of the continental shelves of Africa and South America yields 90 km average misfit from the Amazon to the Falkland Escarpment, but the nothern and southern sections require different composite rotations. Motion of Patagonia relative to the South American craton from Triassic through Cretaceous times about a pole at 63°W and 36.5°S is the postulated cause. Modern Andean movements began perhaps 100my later in Peru (Cretaceous) than in Chile (Triassic). The onset of activity parallels the northward migration of the rifting of western Gondwana. Spherical geometry of such motion harmonizes with much of the continental structure. Suggested consequences include the Parana basalts, the

Argentine basins, the Arica Elbow, the Pampean massifs, and the ASL.

# Acknowledgements

I thank my co-supervisors Dr. Richard St. J. Lambert and Dr. Edo Nyland for their comprehensive and careful review of this work. Any remaining errors are, of course, my responsibility. I was fortunate to have many rewarding discussions with Dr. Lambert concerning plate tectonics and structural geology. Dr. Nyland introduced me to microgeodesy and suggested the singular value decomposition technique used in chapter 2.

Fellow student and good friend Richard Lamoreaux has helped me innumerable times in my work. Together with William Tighe, our frequent visits to the Canadian Rockies served both as inspiration and therapy during my work.

The initial version of the computer mapping progam used here was developed by Bruce Rout during the summer of 1979.

I am grateful to the staff of the Physics Department for many instances of kind service and especially Phyllis Tripp, who spent many hours at the photocopy machines in my behalf.

Thank you, Adam Balut, of the Department of Surveying Engineering at the University of New Brunswick, for teaching me the basic techniques of observing while I was there in 1977.

This work has been supported by research grants from the Natural Sciences and Engineering Research Council of Canada. I acknowledge the support of the University of Alberta in the form of a teaching assistantship.

The Department of Surveying Engineering of the UNB provided the instrumentation for the fieldwork in 1977. I thank all those involved in the gathering of the Huancayo survey data especially Robin Steeves, Peter Polak, Peter Chrzanowski, and Mark Dennler.

The surveying work reported here is part of a joint project between researchers at the University of Alberta, the University of New Brunswick and the Instituto Geofisico del Peru. Without the active cooperation of Alberto Giesecke, Ernesto Deza, Frederico del Castillo and Edgar Camargo in Peru this work would have been impossible.

The unselfish financial and emotional support I have received from my parents throughout my academic career is immeasurable.

Most of all, I wish to thank my wife Joan for coming into my life at just the right time. Her love and friendship are my most valued possessions.

# List of Tables

Table 2.1 (page 58) illustrates the ability of the Huancayo network to resolve constant strains with a constant strain model. The lower of the double entries represents one standard deviation. 38 distances and 81 angle measurements were used. All strains are given in microstrains.

Table 2.2 (page 62) shows the effects of increasing aperture on resolution. All strains are in microstrains. The aperture of a network is taken to be the longest measurable line length. In all cases, the "true" strains in this study were EXX=5.0, EXY=-2.5, EYY=-1.0. The second entry for each aperture was done with distance measurements only.

Table 2.3 (page 68) displays the fit of a constant strain model to the Huancayo survey data. Both distances and angles were used. All strains are in microstrains.

Table 2.4 (page 68) shows the fit of a constant strain model to the Huancayo data using distances only. All strains are in microstrains. Standard deviation estimates in brackets are corrected to agree with the variance ratio.

Table 2.5 (page 70) shows a repeat of the study of table 2.4 but here the pseudo-inverse was formed after the last (smallest) singular value was deleted. All strains are in microstrains.

# List of Figures

Figure 1.1a (page 8) illustrates the three basic types of plate boundaries. Figure 1.1b shows the possible modes of oblique subduction.

Figure 1.2a (page 14) is adapted from Windley (1977) and shows the structural elements of a typical island arc system. Figure 1.2b shows this author's conception of the structural elements of an Andean type subduction zone.

Figure 1.3 (page 16) illustrates the concept of paired "A" and "B" subduction zones as suggested by Bally and Snelson (1979).

Figure 1.4 (page 19) displays an idealized geosynclinal couple. The continental basement of the miogeosyncline is shown broken into a series of listric (curved) normal faults. Such a fault structure is thought to typify rifted continental margins and probably formed in response to stretching of the continental crust.

Figure 1.5 (page 26) shows a possible model of continental rifting incorporating crustal stretching. The continental crust is shown divided into brittle and ductile regimes. The ductile material flows in response to stretching stresses while the brittle regime forms a characteristic system of listric normal faults. The center of the stretched material is shown intruded by basic dikes forming a transitional crust preparatory to the emplacement of true oceanic crust. Compare with figures 1.4 and 1.6.

Figure 1.6 (page 28) shows one set of a dual system of orthogonal flow lines which would form in a perfectly plastic system as a response to a strong basal shear. The other set of flow lines are everywhere perpendicular to these. The upper surface of the material is assumed a free surface.

Figure 2.1 (page 32) shows a typical model for a strike-slip plate boundary. In the upper left, the fault motion is uniform at depth but "locked" near the surface. Strain accumulates in the locked portion as shown by the graph. The release of stored strain can be slow or abrupt, causing an earthquake.

Figure 2.2 (page 36) is a sketch map of Peru showing the locations of various places referred to in the text.

Figure 2.3 (page 37) is a schematic diagram of the Huancayo network.

Figure 2.4 (page 54) illustrates the method of strain analysis described in the text. Refer there for details.

Figure 2.5 (page 55) shows a test network used for the synthetic data studies discussed in the text.

Figure 2.6 (page 65) shows two studies of varying strain on network G10 using a varying strain model. In the lower figure, a linear strain is fitted with a linear model. The upper figure shows the shear strain expected from a locked strike slip fault 200 meters below the network fitted with constant and linear models. Error bars are 1 standard deviation.

Figure 3.1a (page 76) is a generalized structure map for the South American continent. Andean morphology is adapted from Aguirre et al. (1974). The remainder of the map is from numerous sources. Boundaries drawn for the Parnaiba and Parana basins conform to the mapped extent of the Mesozoic basalts.

Figure 3.1b (page 79) shows a spherical polar coordinate system drawn about the pole of relative motion for the Nazca and South American plates superimposed on the South American subduction zone. Small circles are labeled with their angular distance from the pole. Pole location is from earth model RM2 of Minster and Jordan (1978): 94.75°W and 59.08°N.

Figure 3.1c (page 80) is similar to 3.1b except that a coordinate system about the relative motion pole for the Nazca and Pacific plates was used. Pole position is 87.88°W and 56.64°N after Minster and Jordan (1978).

Figure 3.2 (page 83) is a structural map for the Andes between 5°S and 35°S.

Figure 3.3 (page 86) shows geologic and tectonic features near the Pisco Deflection in southern Peru. See figure 3.4a for the key to symbols and shading. The Pisco Deflection is adapted from Megard and Philip (1976).

Figure 3.4a (page 88) is a generalized geological map for the Andes between 5°S and 15°S.

Figure 3.4b (page 89) is a generalized geological map for the Andes from 15°S to 35°S.

Figure 3.5 (page 91) shows the geological structure of Peru as interpreted by E. J. Cobbing and W. S. Pitcher. The cross section is adapted from Cobbing and Pitcher (1972b) while the plan view is adapted from Pitcher (1978).

Figure 3.6 (page 98) shows two views of episodic orogenic activity in Peru. Figure A is adapted from Noble et al. (1974) and Figure B is modified from Pitcher (1978).

Figure 3.7a (page 105) is adapted from Clark et al. (1976) and shows the eastward migration of magmatism in northern Chile. (Compare with figure 3.6b.) Figure 3.7b is modified from Zentilli (1974) and shows the variation of Potash index across a transect of the Andes at about 26°S.

Figure 3.8 (page 111) displays contours of the approximate depth to the Moho beneath the Central Andes as estimated by James (1971a). Also shown is the approximate southern limit of the underlying Precambrian shield after Cobbing et al. (1977).

Figure 3.9 (page 112) indicates how the contours of figure 3.8 might be modified to agree with two seismic and gravity contours done by Ocola and Meyer (1973). The traverses are denoted by "AB" and "AC". Contours agree with Ocola and Meyer along the traverses and are hypothetical elsewhere.

Figure 3.10 (page 116) shows where significant Pliocene through Quaternary volcanism has been found in South America. Adapted from the Tectonic Map of South America (1978).

Figure 3.11 (page 120) is a geological sketch map of Patagonia. Primary source map was the Tectonic Map of South America (1978).

Figure 3.12 (page 125) displays the seismicity of South America. Data are taken from the NOAA catalogue from 1963 through 1977. Only events having body wave magnitude (Mb) greater than 5.0 are shown.

Figure 3.13 (page 129) is an expanded seismicity map for the Andean region between 5°S and 30°S. All events having Mb greater than 4.0 and which occurred between 1963 and 1977 are shown. Also shown are active volcanoes and contours of major geological features. The key to the labeling of the contours can be deduced from figures 3.4a and 3.4b.

Figure 3.14 (page 130) is a closeup of the northern half of figure 3.13. Additional detail is included in the geological structure.

Figure 3.15 (page 131) is a closeup of the southern half of figure 3.13.

Figure 3.16a (page 133) shows a vertical profile taken through the Peruvian Andes in the approximate direction of subduction. Only events having Mb greater than 4.0 are shown.

Figure 3.16b (page 134) is a seismicity profile along the same line as 3.16a but the threshold magnitude has been increased to 5.0. Two major areas of energy release are indicated: near the trench and beneath the Subandean Ranges.

Figure 3.17 (page 140) is a cartoon showing a probable geometry for the subducted Nazca Plate beneath central Peru.

Figure 3.18 (page 142) is a seismicity map of a portion of the Central Andes similar to 3.13. Only shallow and intermediate depth events are shown and depth coding has been chosen to be compatible with figure 3.19.

Figure 3.19 (page 143) shows approximate contours of the depth to "maximum" seismic activity beneath the Central Andes. Contours were constructed from a detailed analysis of numerous intersecting vertical profiles (not shown, but see Appendix 2). Most of the features of these contours can be confirmed in figure 3.18. Also shown is the location of the "tear" in the Nazca Plate postulated by Barazangi and Isacks (1976 and 1979).

Figure 3.20a (page 146) is a vertical seismicity profile, 1° wide, taken across northern Chile in the direction of subduction. Only events having Mb greater than 4.0 are shown. The dense cloud of activity between 125 and 150 km is directly beneath the volcanic front.

Figure 3.20b (page 147) shows the same profile as 3.20a but a higher threshold magnitude (5.0) has been used. Energy release is maximal beneath the volcanic front, but is distributed continuously along the slab to a depth of 250 km.

Figure 3.21 (page 148) is a cartoon depicting a possible mode of subduction beneath the Central Andes.

Figure 3.22 (page 151) shows the same seismicity map as figure 3.13 with a spherical coordinate grid drawn about the relative motion pole for the Nazca and South American plates. Pole position is 94.75°W and 59.08°N and is from earth model RM2 of Minster and Jordan (1978).

Figure 3.23 (page 152) is similar to figure 3.22 except the superimposed grid is drawn about the Nazca - Pacific pole of relative motion. Pole position is 87.88°N and 56.64°W after Minster and Jordan (1978).

Figure 3.24 (page 153) compares the Andean Seismicity Lineament as defined by the best fitting line of figure 3.22, with the locations of modern volcanism and the Pampean basement horsts.

Figure 3.25 (page 159) is adapted from Zambrano and Urien (1970) and Urien and Zambrano (1973) and shows major sedimentary basins and shear zones in Argentina which have formed since the Jurassic.

Figure 3.26 (page 163) is adapted from Hertz (1966) and shows the age distribution of K-Ar dating for the Parana Basalts. Determinations were made by various authors and summarized by Hertz.

Figure 4.1 (page 174) shows the fit of Africa and South America according to Bullard et al. (1965). The continents were matched at the 500 fathom isobath using a least squares technique. Africa is shown rotated clockwise 57.0° about a pole located at 30.6°W and 44.0°N. The average misfit according to Bullard et al. is 88 km. The points "P" indicate the limits of the continental shelves that were digitized.

Figure 4.2 (page 177) illustrates the technique of fitting conti together as discussed in the text. Opposing points are defined as pairs of points, one on each continent, lying on the same small circle about the rotation pole. The best rotation angle is chosen mathematically to minimize the squared misfit measured in km along the small circles.

Figure 4.3 (page 179) displays contours (at 5 km intervals) of the misfit in km between South America and Africa for the area in the immediate vicinity of the Bullard pole (figure 4.1). The Bullard pole is much better constrained in longitude than latitude. The shaded region indicates the possible range of optimal pole positions as discussed in the text.

Figure 4.4 (page 182) shows contours of the continental misfit when only the southern portions of Africa and South America are matched. Contour interval is 5 km. Minimum misfit is about 89 km at 31°W and 36°N.

Figure 4.5 (page 183) shows the best fit obtained when the southern portions of the continents are matched. Africa has been rotated clockwise 58.7° about a pole at 31°W and 36°N. This achieves a misfit of only 89 km between the limits marked "P".

Figure 4.6 (page 187) is a closeup of the southern gap between the continents as defined by the Bullard fit of figure 4.1. Note the matching offsets on the east flank of

Agulhas Bank and the Falkland Escarpment.

Figure 4.7 (page 189) shows the fit of the Agulhas Bank region of South Africa to the corresponding section of the Falkland Plateau. The continents were first rotated into the position of figure 4.1, then the Falkland Plateau was rotated counter clockwise 16.2° about a pole at 65°W and 42.5°S. The average misfit is about 17 km. The superimposed grid is drawn about the rotation pole.

Figure 4.8 (page 190) shows misfit contours for the best fit region of the fit shown in figure 4.4a. Contour interval is 2 km.

Figure 4.9 (page 193) shows the postulated boundary between the Patagonian Block and the Craton. The boundary is taken to be coincident with the southern extent of the shield as estimated by Cobbing et al. (1977).

Figure 4.10 (page 195) is a contour map of the misfit obtained by closing the southern gap between the continents in figure 4.1 with a rigid rotation of the Patagonian block. The best pole position is well defined in one dimension only. Contour interval is 2 km.

Figure 4.11 (page 198) shows the "best" rotation which closes the southern gap of figure 4.1. The pole position was chosen from figure 4.10 using the additional constraints described in the text. The average misfit is about 61 km. The Patagonian block has been rotated counter clockwise 12.5° about a pole at 63°W and 36.5°S.

Figure 4.12 (page 199) is an enlargement of the southern portion of figure 4.11 showing the closure of the southern gap. Compare with figure 4.6.

Figure 4.13 (page 201) is a cartoon sequence illustrating the continental distortion model proposed in the text.

Figure 4.14 (page 206) illustrates the geometric harmony found between the Patagonian pole and various geological features. See text for discussion.

Figure 4.15 (page 211) compares the structure of the modern Central Andes with the spherical geometry of the Patagonian pole. Sonnenberg's lines are major tectonic boundaries postulated by Sonnenberg (1963). Notice the remarkable alignment between the modern volcanic belt and a great circle. Compare with figures 3.24 and 4.14.

Figure 4.16 (page 219) shows the fit of the continents as postulated by Rabinowitz and Labreque (1979). The location of their early to middle Cretaceous pole for spreading on the South Atlantic is also shown (45°W and 2.5°S). Africa has been rotated clockwise 57.5° about a pole at 32.2°W and 45.5°N. The average misfit at the 500 fathom isobath is estimated in the text as 223 km. The worst misfit is along the northeastern coast of Brazil. Compare with figure 4.1.

Figure 4.17 (page 230) compares the Pisco deflection with spherical coordinate systems drawn about the Nazca - South America pole (figure A) and the Nazca - Pacific pole (figure B). The southern boundary of the deflection is well modeled as a slip line about the Nazca - South America pole. Compare with figure 3.3.

Figure 4.18 (page 233) is a cartoon depicting the possible evolution of a subduction system as a zone of buoyant oceanic crust encounters the trench. The figure reads from top to bottom. This construction was drawn assuming that both the buoyant slab (A) and the normal slab (B) move with the same horizontal velocity but that B feels a greater (constant) gravitational force. Thus the slabs follow parabolic trajectories with different curvatures.

## Table of Contents

Chapter Page

1. Preliminary Discussions ....................................1

1.1 Motivations ..............................................1

1.2 Spherical Geometry and Plate Motions .....................3

1.2.1 Euler's Theorem ........................................4

1.2.2 Angular Displacement and Angular Velocity ..............4

1.2.3 Plate Geometry and Poles of Rotation ...................6

1.2.4 Types of Plate Boundaries ..............................7

1.2.5 Types of Convergent Plate Margins .....................12

1.2.6 Two Types of Subduction ...............................15

1.3 Orogeny and Plate Margin Tectonics ......................17

1.3.1 Geosynclines ..........................................17

1.3.2 Plate Tectonic theories of Orogeny ....................20

1.4 Rifting and Stretching of the Lithosphere ...............23

1.4.1 Sedimentary Basins ....................................23

1.4.2 Rifting via Stretching ................................24

1.5 Concluding Remarks ......................................27

2. Microgeodetic Survey Networks and the Measurement of Earth Strains ....................................30

2.1 Introduction ............................................30

2.1.1 The Peruvian Survey Project ...........................34

2.2 Assessment of the 1977 Fieldwork ........................40

2.3 Strain Deduction Method .................................42

2.3.1 Tests with Synthetic Data .............................54

2.3.2 Analysis of Survey Data from Huancayo ....67

3. Highlights of the Tectonic History of South America ...73

- 3.1 Introduction ...73
- 3.2 General Plate Tectonic Setting ...77
  - 3.2.1 The Nazca Plate ...77
  - 3.2.2 Aseismic Ridges on the Nazca Plate ...80
  - 3.2.3 The South American Plate ...82
  - 3.2.4 The Huancabamba Deflection ...84
  - 3.2.5 The Pisco Deflection ...84
- 3.3 Plutonism and Volcanism in the Peruvian Andes ...87
  - 3.3.1 The Peruvian Coastal Batholith and Associated Volcanism ...90
  - 3.3.2 Emplacement of the Peruvian Coastal Batholith ...93
  - 3.3.3 Miocene to Recent Activity ...95
  - 3.3.4 Episodic Nature of Volcanism and Tectonism ...97
- 3.4 Tectonics of Central Peru ...99
  - 3.4.1 Vertical Block Tectonics ...99
  - 3.4.2 Present Day Tectonics of Central Peru ...101
- 3.5 Plutonism and Volcanism in the Central Andes ...102
  - 3.5.1 Intrusive Chronology ...103
  - 3.5.2 Eastward Migration of Magmatic Foci ...104
  - 3.5.3 The Miocene-Pliocene Magmatic Outbreak ...107
  - 3.5.4 Chemistry and Origin of Central Andean Andesites ...108
  - 3.5.5 Crustal and Lithospheric Thicknesses in the Central Andes ...110
- 3.6 Tectonic Style of the Central Andes ...114
  - 3.6.1 The Altiplano, Pampean Ranges, and Central Valley ...114

3.6.2 The Atacama Fault ........................117

3.6.3 The Ojos del Salado Lineament ...........117

3.7 On the Genesis of the Modern Andes ..............118

3.7.1 The Central Andes ........................118

3.7.2 Evidence from Patagonia .................119

3.7.3 Peruvian Andes ...........................121

3.8 Seismicity of South America .....................123

3.8.1 On the Accuracy of Hypocentral Determinations ...............................124

3.8.2 General Patterns .........................127

3.8.3 Central Peru .............................128

3.8.4 The 300-500 Kilometer Aseismic Zone .....136

3.8.5 The Shape of Subducting Plate beneath Central Peru .............................137

3.8.6 Low Angle Subduction and Peruvian Tectonics ................................140

3.8.7 The Central Andes ........................141

3.8.8 The Andean Seismicity Lineament .........149

3.8.9 Observations and Speculations on Geometric Symmetries ....................156

3.9 The South American Interior ....................158

3.9.1 The Argentine Basins .....................158

3.9.2 The Parana Flood Basalts .................161

3.9.3 The Chaco-Pampas Plains ..................164

3.10 Summary ........................................165

4. On the Tectonic Evolution of South America ...........170

4.1 Introduction ...................................170

4.2 The Fit of South America to Africa along their Continental Shelves ...........................171

4.2.1 The Bullard Fit ...........................171

4.2.2 A Revised Least Squares Method ..........175

4.2.3 The Bullard Fit Revisited ...............178

4.2.4 A Composite Pole for the Southernmost Regions ..................................180

4.2.5 On the Validity of Continental Shelf Reconstructions ..........................184

4.3 A Continental Distortion Model ..................186

4.3.1 Fit of the Falkland Escarpment to Agulhas Bank ..............................188

4.3.2 Boundaries of the Patagonian block ......191

4.3.3 Composite Pole of Opening for the Southern Gap ..............................193

4.3.4 Statement of the Model .................199

4.3.5 The Patagonian Pole .....................204

4.3.6 The Parana Basalts and Crustal Disruption ...............................205

4.3.7 The Southern Argentine Basins ...........208

4.3.8 The Cretaceous Marginal Basin in Patagonia ...............................208

4.3.9 The Structure of the Central Andes ......210

4.3.10 The Andean Seismicity Lineament Revisited ...............................212

4.3.11 The Atacama Fault as a Consequence of Oblique Subduction .....................213

4.3.12 Critical Evaluation of the Continental Distortion Model .......................215

4.4 The Model of Rabinowitz and Labreque ............217

4.4.1 The Rabinowitz and Labreque Fit .........218

4.4.2 The Ocean-Continent Boundary ............220

4.4.3 Comparison with the Fit at the Continental Shelves .....................222

4.4.4 Evaluation of the Rabinowitz and

Labreque Model ....................222

4.5 On Events Subsequent to the Western Gondwana Breakup ....................226

4.5.1 The Miocene Events ....................226

4.5.2 On Aseismic Ridges ....................227

4.5.3 Aseismic Ridges and the Miocene Event ...229

5. Future Directions in Tectonophysics ....................235

5.1 The Value of the Huancayo Microgeodetic Experiment ....................235

5.2 Directions in Design and Analysis ....................237

5.3 A Backus-Gilbert Formulation of the Strain Problem ....................238

5.4 Suggestions for Future Microgeodetic Experiments in South America ....................244

Bibliography ....................247

Appendix 1: Survey Data ....................267

Appendix 2: Vertical Seismicity Profiles ....................276

Appendix 3: Method for the Least Squares Matching of Plate Boundaries ....................290

# 1. Preliminary Discussions

## 1.1 Motivations

This thesis presents a survey of and contributions to knowledge of the structure and dynamics of a convergent plate margin. The particular margin of interest is the Andean mobile belt, but many of the topics discussed have general applicability. My involvement in this subject dates from early 1977 when I joined Dr. Edo Nyland's survey project in the Peruvian Andes. This project, the subject of chapter 2, is one of several geodetic experiments worldwide which are exploring the possibilities of direct measurement of the motions of the tectonic plates which form the surface of the earth.

In some instances, the relationship between large scale plate motions and geodetic strain is not difficult to imagine. For example, in southern California it is possible to lay a survey network across virtually the entire plate margin. The situation is further simplified since the motion along this particular margin is almost entirely horizontal. A similar situation occurs in New Zealand where geodetic measurements spanning the plate margin demonstrate a cumulative motion which agrees closely with the large scale plate motion predicted by less direct means (Walcott 1978).

Often, geodetic surveying involves measurement of angles and distances on lines approximately 20 km long. In New Zealand repetition of old British surveys done near the end of the last century has been a primary source of information. These generally involved lines of sight from mountain top to mountain top (e.g. Walcott 1978).

Waiting 100 years between surveys is one of two often practiced techniques for measuring earth strains. The other involves the application of the very latest technology to measure a few line lengths with great accuracy. This approach is taken in California where single measurement accuracies less than 1 part in $10^6$ are a reality (Prescott et al. 1979).

Our Peruvian project has investigated a technique different from either of these. We use small networks (2 kilometer line lengths) and moderate technology but make a large number of measurements in order to get a very high "redundancy" factor. In this way, we are able to measure tectonically interesting strains without waiting $10^2$ years or spending $10^5$ dollars. This technique has been referred to as "microgeodesy" (W. Welsch, 1977, personal communication) and that term will be used here.

The greatest problem facing us in Peru is not actually measuring the strains but rather interpreting them. A convergent plate margin (as we have along the western border of South America) is probably the most complex of the three major types (see section 1.2.4) showing great geometric variety and almost any imaginable style of deformation.

It was the attempt to understand our measurements that led to the vast subject broached in chapters 3 and 4: the evolution of the South American continent since the Mesozoic. I cannot truthfully say that my studies in this field have led to a full understanding of the fundamental forces driving the Huaytapallana thrust fault (where our survey network is). On the other hand, some unexpected discoveries were made and, at the very least, I have come to appreciate the vast diversity of the subject.

This thesis is thus multiple: this chapter concludes with some background information on plate interactions. Chapter 2 treats the subject of microgeodesy as applied in Peru. A summary of results from a study of the geology and seismicity of the South American continent is presented in chapter 3. Chapter 4 contains some models for certain aspects of the tectonic evolution of that continent. In chapter 5, some unexplored avenues for research in the application of survey methodology to problems in geodynamics are suggested.

## 1.2 Spherical Geometry and Plate Motions

Since the earth approximates a sphere, it is not surprising that spherical geometry is important in considering global tectonics. What is perhaps unexpected is the great wealth of information that comes from pursuing this subject and the strong constraints it places on the types of motion which may occur. "Plate tectonics" is the most successful theory of global geology and this success is in part due to investigation of these geometric constraints.

### 1.2.1 Euler's Theorem

A famous theorem of rigid body motion, first enunciated by Euler, forms the basis for the analysis of motions on a sphere:

> If two successive positions of a rigid body have a point in common, then the motion of the body, from the first to the second position, can be completely described by a rotation about an axis passing through the common point.

In the case of the relative motion of portions of the earth's surface, it may be said that any two successive positions of a crustal plate have the point at the earth's center in common. Thus, the motion of one rigid plate relative to another can be described by a rotation about an axis passing through the earth's center. The position of intersection of that imaginary axis with the earth's surface and the angular velocity about it suffice to characterize the instantaneous motion of one plate with respect to another. The validity of these conclusions rests directly upon the assumption that the tectonic plates behave rigidly.

### 1.2.2 Angular Displacement and Angular Velocity

Finite angular displacements can be specified by giving a "magnitude and a direction," but it is a well-known fact from classical mechanics that these are not vector quantities (Goldstein 1965, p124). This can be demonstrated by showing that they do not obey the laws of vector addition since the result depends on the order in which the addition is performed.

Angular velocity and infinitesimal angular displacements are vector quantities and can be added as vectors (Goldstein 1965, p125-126). Often average angular velocities are quoted in the literature and it is important to realize that these are not vectors. They are calculated by taking a total apparent displacement over a geological period and dividing by that period. Average angular velocities are only vector quantities if the motion has been steady state (constant), and then average and instantaneous angular velocities are identical. As Hobbs et al. (1976) point out, geometrical considerations (e.g. long transform faults) imply that steady motion is favored, but well documented instances of changes in both magnitude and direction of plate motion are found in the literature (Menard and Atwater 1968, Handschumacher 1976).

If $\underline{Wab}$ represents the instantaneous angular velocity vector of plate "b" with respect to plate "a", then for any three plates, a, b, and c, we must have (Hobbs et al. 1976, p 454):

$$\underline{Wab} + \underline{Wbc} + \underline{Wca} = 0$$

Thus, if any two of these instantaneous angular velocity vectors are known, the third may be found via vector addition laws. If three vectors sum to zero, they must be co-planar; thus, the relative rotation poles for any three plates must lie on the same great circle (Hobbs et al.

1976).

The velocity of any particle on plate b with respect to plate a is given by:

$\underline{Vab} = \underline{Wab} \times \underline{R}$

where $\underline{R}$ is the radius vector to the particle. At a triple junction where three adjacent particles on different plates have the same $\underline{R}$, the relation between angular velocity vectors becomes a relation between particle velocities:

$\underline{Vab} + \underline{Vbc} + \underline{Vca} = 0$

This equation, which was used by McKenzie and Morgan (1969) to investigate triple junction stability, is strictly valid only for points with no finite separation.

### 1.2.3 Plate Geometry and Poles of Rotation

The motions of the crustal plates are often reflected in the geometry of their boundaries and internal structures. This provides one of the primary methods of determining pole positions. A spherical coordinate system ("latitude" and "longitude") drawn about a pole of rotation determines a natural coordinate system in which to view a plate interaction. (The terms "latitude" and "longitude" will be considered synonymous with small and great circles about a motion pole. The same terms without the quotes will refer to conventional latitude and longitude.) The direction of relative motion between two plates is everywhere tangent to small circles about their pole.

At a speading ridge, two plates are being formed and are moving away from one another. This motion presumably takes place along a basal shear zone separating the plates from the mantle. The direction of motion is indicated by "transform faults" which should therefore be small circles about the corresponding pole of rotation. Fitting transform faults with "latitude" lines is a direct method for determining a pole position. The strikes of spreading ridge crests tend to be aligned with great circles about the pole of motion indicating that spreading takes place at right angles to ridge strike.

### 1.2.4 Types of Plate Boundaries

A useful classification of plate margins is based upon their relation to the direction of relative motion across them. Margins are said to be either transform (shear), divergent, or convergent depending on the direction of the normal component of relative motion (figure 1.1a). (These will be henceforth referred to as TPM, DPM, and CPM respectively.) As the name suggests, a TPM involves pure shear motion between the two plates and, hence, the component of V normal to the plate boundary (Vn) is zero. (The normal component of the relative velocity vector will be considered positive if it points outward from the reference plate a to plate b.) Examples include ocean floor transform faults and the San Andreas fault system. In this idealized definition, a transform boundary is always parallel to the direction of relative motion. This is

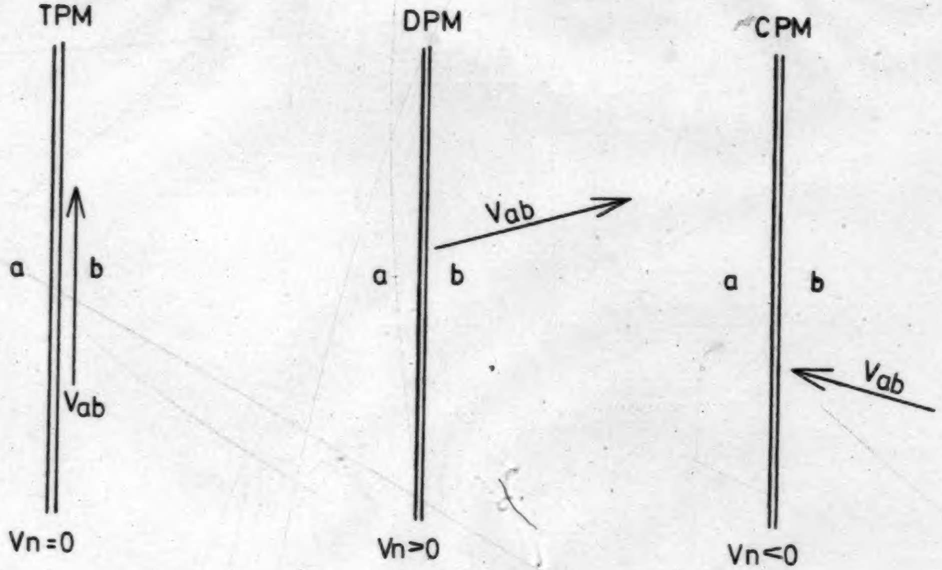
TPM
DPM
CPM
a
b
a
b
a
b
Vab
Vab
Vab
Vn=0
Vn>0
Vn<0

Figure A

Figure B

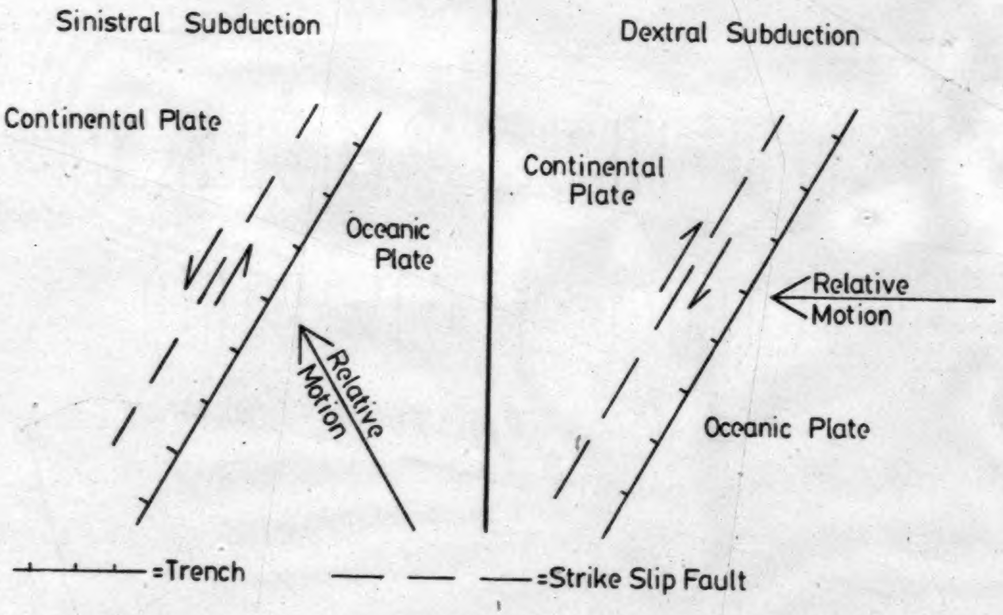
Sinistral Subduction
Dextral Subduction
Continental Plate
Oceanic Plate
Relative Motion
Continental Plate
Relative Motion
Oceanic Plate
=Trench
=Strike Slip Fault

Figure 1.1a illustrates the three basic types of plate boundaries. Figure 1.1b shows the possible modes of oblique subduction.

probably a good rule; however, in New Zealand, along the Alpine "Transform", there appears to be a definite component of relative motion normal to the boundary (Walcott 1978).

A divergent margin is characterized by positive Vn, the prime example being the world oceanic rift system. Spreading ridges, in the idealization of McKenzie and Morgan (1969), are always perpendicular to the direction of relative motion. However, there is no a priori necessity for the general DPM to have zero tangential motion.

The third type of plate margin (CPM) has negative Vn and is the subject of much of this thesis. Examples include the Tonga-Kermadec, Japan, and Peru-Chile trench systems and the India-Asia collision zone. The Tonga trench is the site of subduction beneath an immature island arc (one lacking a basement of continental crust) accompanied by active back arc spreading (Karig 1970), volcanism, and no compressional orogeny. The Japanese arc system is a mature arc (Uyeda and Miyashiro,1974), shows no active back-arc basin (Uyeda and Kanamori, 1979) (though the Japan Sea is thought to be an inactive basin (Uyeda and Miyashiro,1974)), and shows basically compressional tectonics. The Peru-Chile trench shows no island arc, active continental volcanism, no back-arc basin, and both compressional and extensional tectonics (Megard and Philip 1976). The India-Asia collision zone is caused by the collision of two relatively buoyant continental masses and shows no subduction or volcanism, large scale compressional tectonics, and effectively

2-dimensional plastic flow of crustal material (Molnar and Tapponier 1977b).

These definitions specify only Vn; nothing is said about the tangential component of the relative velocity vector (Vt) because both CPMs and DPMs may show large Vt. Subduction with a large component of Vt is called oblique subduction. Fitch (1972) and Hobbs et al. (1976) suggest that in such circumstances strike-slip faulting may be induced within the non-subducting plate. If the sense of shear across the trench is right-handed, it is a dextral trench system. Similarly, a sinistral trench system implies left-handed shear. Figure 1.1b illustrates dextral and sinistral subduction for an ocean - continent type CPM (see next section) and indicates the sense of strike slip faulting which might be found in the continent. (This is not the only possible response mechanism to oblique subduction. Refer to Hobbs et al. (1976 pp 458-459) for further details.)

Strike slip faults such as those hypothesized in figure 1.1b (called "Fitch faults" hereafter) are not transform faults. Superficial similarities such as extreme linearity over great distances can be expected, but the differences are more important. These would be true strike slip faults showing a sense of motion which agrees with the sense of offset along the fault. As Wilson (1965) first pointed out, transform faults show the opposite sense of motion. More importantly, there is no practical limit to the magnitude of offset which can occur on a transform fault, but geometry and surrounding structures severely limit the offset on a Fitch fault. Lateral motion exceeding a few tens of km would be extremely difficult to explain. Also, a Fitch fault might be expected to show considerable vertical motion because it exists in a region of vertical tectonics. With a complex system of eleven major plates jostling one another, it may be inevitable that some convergence zones should display large shear motions, but there may still be some energetic preference for normal over oblique subduction. A case for this can be made by noting that, with other parameters identical, normal subduction provides the contact surface of minimal area. Hence, the local work done against viscous forces to slide one plate over the other would almost certainly be less for normal subduction.

Such a local energy preference is not always sufficient to cause a reorganization of plate motions to achieve normal subduction, as is proved by the presence of oblique subduction. Such a reorganization would only occur if it were globally energy efficient. The local energy benefit can only be expected to be significant if the plates are strongly coupled. An old lithosphere, sinking passively under its own weight, will show minimal interaction with the overriding plate. On the other hand, a young hot plate being actively overridden will interact strongly with the upper plate.

It is a mistake to regard these definitions as statements about the tectonic stress field. For example, a CPM can display vast regions of tensional tectonics in addition to (or instead of) the expected compressive stresses. The basin and range province of the western United States shows considerable tensional character and has been called an ensialac back-arc basin (Scholz et al. 1971). Indeed, it is difficult to find non-tensile geological structures in some island arc systems with active back-arc basins. However there seems little evidence at present for compressive stresses of any significance in a DPM.

### 1.2.5 Types of Convergent Plate Margins

CPM's can be divided into three groups according to the nature of the interacting plates, whether oceanic or continental. Thus, we will say a CPM is either oceanic-oceanic (O-O), oceanic-continental (O-C), or continental-continental (C-C).

Dewey and Bird (1970) suggest four classifications in a scheme based on the geological structure of the interacting plates.

1. Continental - Continental. (Same as C-C above.) The prime example here is the collision zone between the Indian and Asian plates which has produced the Himalayas. This vast subject will not be broached here. For more information see the recent review paper by Roeder (1979)
2. Oceanic - island arc. This is basically the same as the

O-O classification used above.

3. Oceanic-Continental. (Same as O-C above)
4. Island arc - continental. This refers to the collision of a continent with an island arc trench system. The example suggested by Dewey and Bird is the northern New Guinea system where the Australian plate has collided with the Bismark arc.

An island arc - continental collision probably took place in southern Patagonia in the late Cretaceous (Dalziel et al, 1974) and has been suggested as part of the evolution of the Canadian Cordillera by Monger et al. (1972). Marginal seas may have periodically opened and closed behind an island arc off the western Canadian shore. The closure of such a back-arc basin causes ophiolite sequences and shallow water sediments to be scraped up onto the continent and eventual collision between the continent and island arc. The collision would result in intense local deformation and possibly plastic flow in the continental crust as is found in a C-C CPM. While certainly a complex collision process, we shall regard this type of CPM as a transition or intermediate structure marking the change of an O-O CPM to an O-C or even a C-C.

Figure 1.2a (adapted from Windley 1977, p245) is a cartoon showing the basic structural elements of an island arc system. This represents O-O subduction if the marginal basin is considered as a significant oceanic plate. Should the marginal sea close, the resulting collision would be an

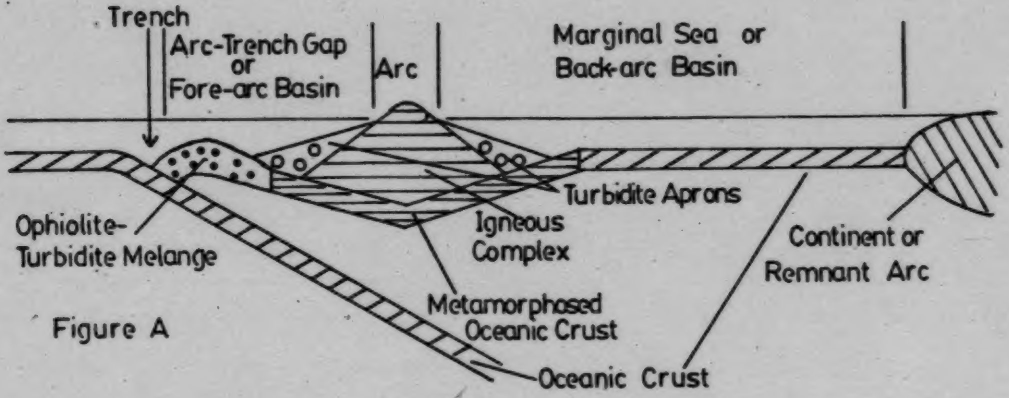
Trench
Arc-Trench Gap or Fore-arc Basin
Arc
Marginal Sea or Back-arc Basin
Turbidite Aprons
Ophiolite-Turbidite Melange
Igneous Complex
Continent or Remnant Arc
Metamorphosed Oceanic Crust
Oceanic Crust

Figure A

Figure B

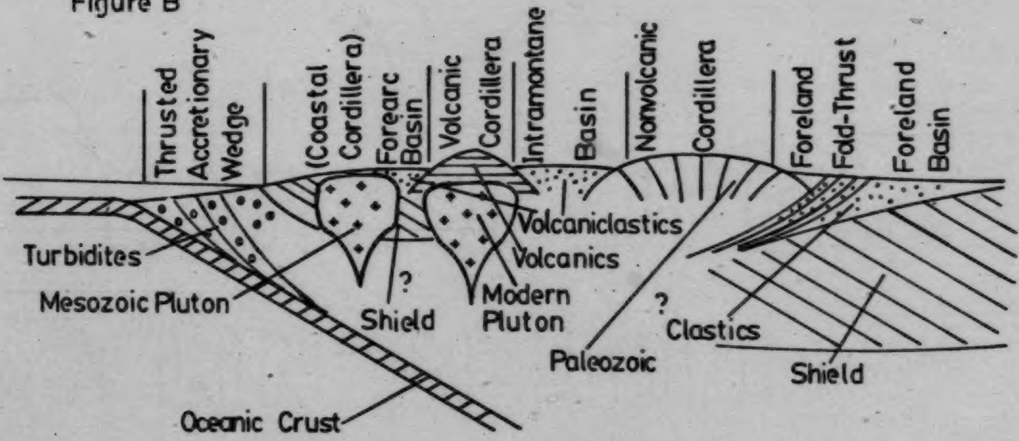
Thrusted Accretionary Wedge
(Coastal Cordillera)
Forearc Basin
Volcanic Cordillera
Intramontane Basin
Nonvolcanic Cordillera
Foreland Fold-Thrust
Foreland Basin
Volcaniclastics
Volcanics
Turbidites
Mesozoic Pluton
?
Shield
Modern Pluton
?
Clastics
Paleozoic
Shield
Oceanic Crust

Figure 1.2a is adapted from Windley (1977) and shows the structural elements of a typical island arc system. Figure 1.2b shows this author's conception of the structural elements of an Andean type subduction zone.

island arc - continental CPM, and after stabilization, we would have a O-C CPM. As shown, this is a so-called immature island arc because it lacks a significant basement of continental rocks (or sial). Such a system is characterized by extensional tectonics so long as the marginal basin is actively opening.

Figure 1.2b is a similar sketch showing the basic tectonic elements of an Andean type CPM (O-C). This diagram is a product of many months of study of the Andean system which will be discussed in detail in chapters 3 and 4. For now, it is sufficient to note some basic differences between this and the island arc system. Here we have shield rocks outcropping along the coast indicating a structurally rigid basement which resists horizontal deformation. Two cordillera, one volcanic and one not, are typical with the volcanic center having migrated away from the trench with time. Intramontane basins, and fore-arc and foreland basins receive erosives from the uplifted lands. Both the accretionary wedge and foreland basin show thrusting and decollement (detached) tectonics.

### 1.2.6 Two Types of Subduction

Bally and Snelson (1979) have proposed that there actually are two types of subduction zones called "A" and "B" subduction (figure 1.3). The idea is interesting because it suggests an easily envisioned mechanism for the formation of the opposing thrust belts of figure 1.2b.

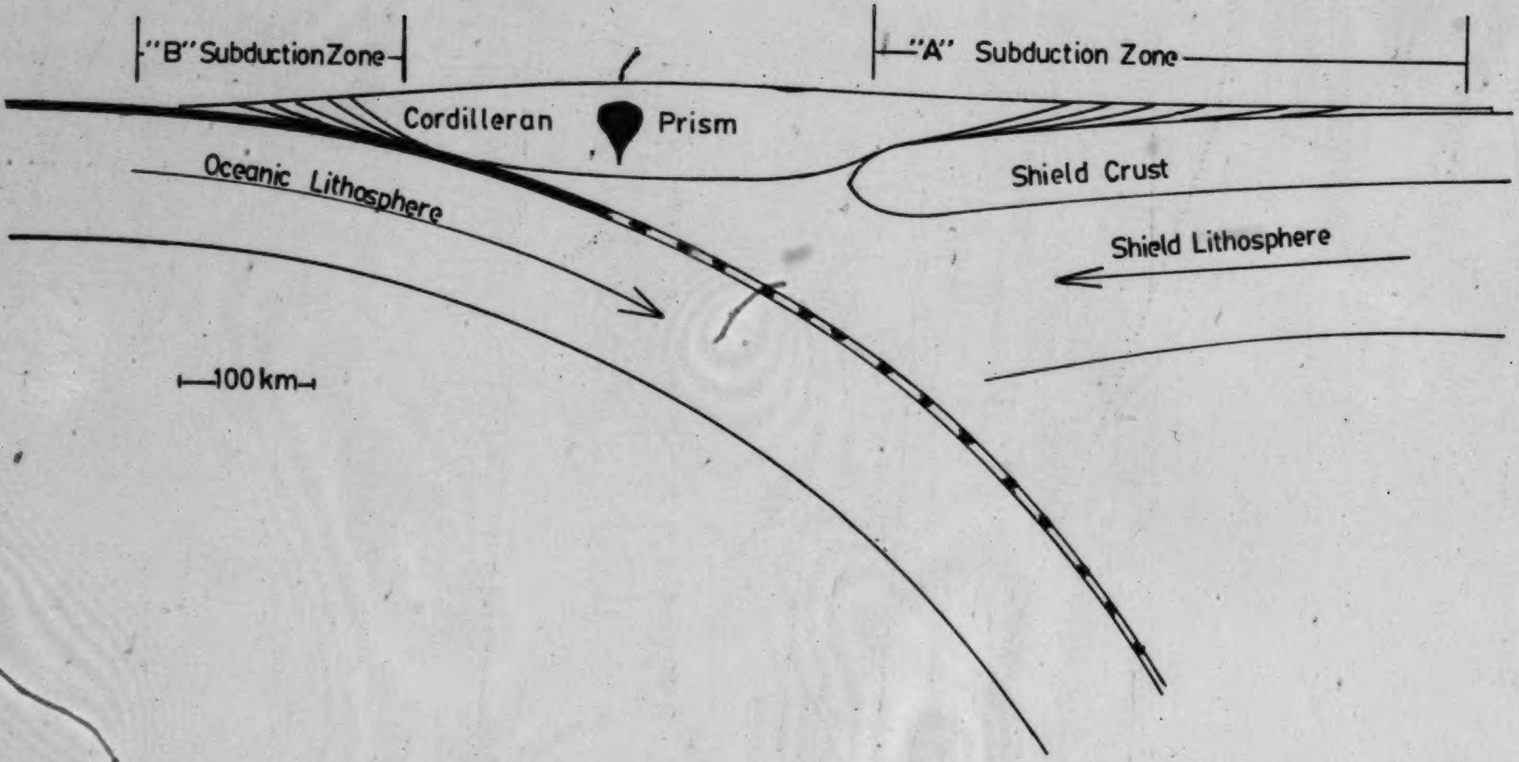
"B" Subduction Zone
"A" Subduction Zone
Cordilleran
Prism
Shield Crust
Oceanic Lithosphere
Shield Lithosphere
100 km

Figure 1.3 illustrates the concept of paired "A" and "B" subduction zones as suggested by Bally and Snelson (1979).

B subduction zones (B for Benioff) are those commonly recognized in plate tectonics, typified here by the thrusting of oceanic lithosphere beneath a mountain belt. Such a process is thought to actually involve the recycling of oceanic crust through the mantle.

A subduction (A for Ampferer, the famous Alpine geologist) involves the thrusting of a shield block beneath the same mountain belt, usually in opposition to B subduction. Recycling of shield material does not occur on a significant scale.

In this view, the orogenic belt is a prism of deformed material trapped between two opposing thrust systems. The thrust belts develop in response to a strong basal shear caused by the underthrusting tectonics. Bally calls this entire composite structure a "megasuture."

## 1.3 Orogeny and Plate Margin Tectonics

### 1.3.1 Geosynclines

Before the advent of plate tectonics, it was thought that orogenic movements were accomplished through the "geosynclinal cycle" (Kay 1951, Aubouin 1965). This idea developed from the field observations of many structural geologists who noted that mountains were characteristically formed from originally flat lying sedimentary beds. Though highly deformed and intruded, it was still possible to ascertain much about their original structure. The structural zones containing these pre-orogenic sediments, given the class name geosynclines, were observed to have a number of common denominators.

Kay(1951) recognized a basic form which he called a geosynclinal couple. Shown in figure 1.4 it is referred to as a miogeosyncline-eugeosyncline pair (often shortened to miogeocline and eugeocline). A miogeocline is typically a wedge of carbonate sediments deposited on a subsiding continental basement, whereas a eugeocline consists largely of turbidites and deep water marine sediments resting on oceanic crust. The eugeocline often contains ultra-basic intrusions. (Figure 1.4 is a more modern geosynclinal model than Kay proposed and shows several features, such as the listric normal faults which were not part of earlier models.)

Orogenic theories based on the geosynclinal cycle supposed the formation of mountains from geosynclines was a fundamental earth process and numerous complex schemes were proposed as driving mechanisms. For example, sediment weight was suggested as sufficient to produce heating and magma generation at depth leading to an eventual tectonic instability.

It was long thought that there were no modern examples of a geosyncline. However, beginning with Drake et al. (1959) it has gradually been realized that "living" geosynclines exist along most quiet continental margins. The eastern coast of North America is the type example. The carbonate wedge now being deposited on the continental shelf

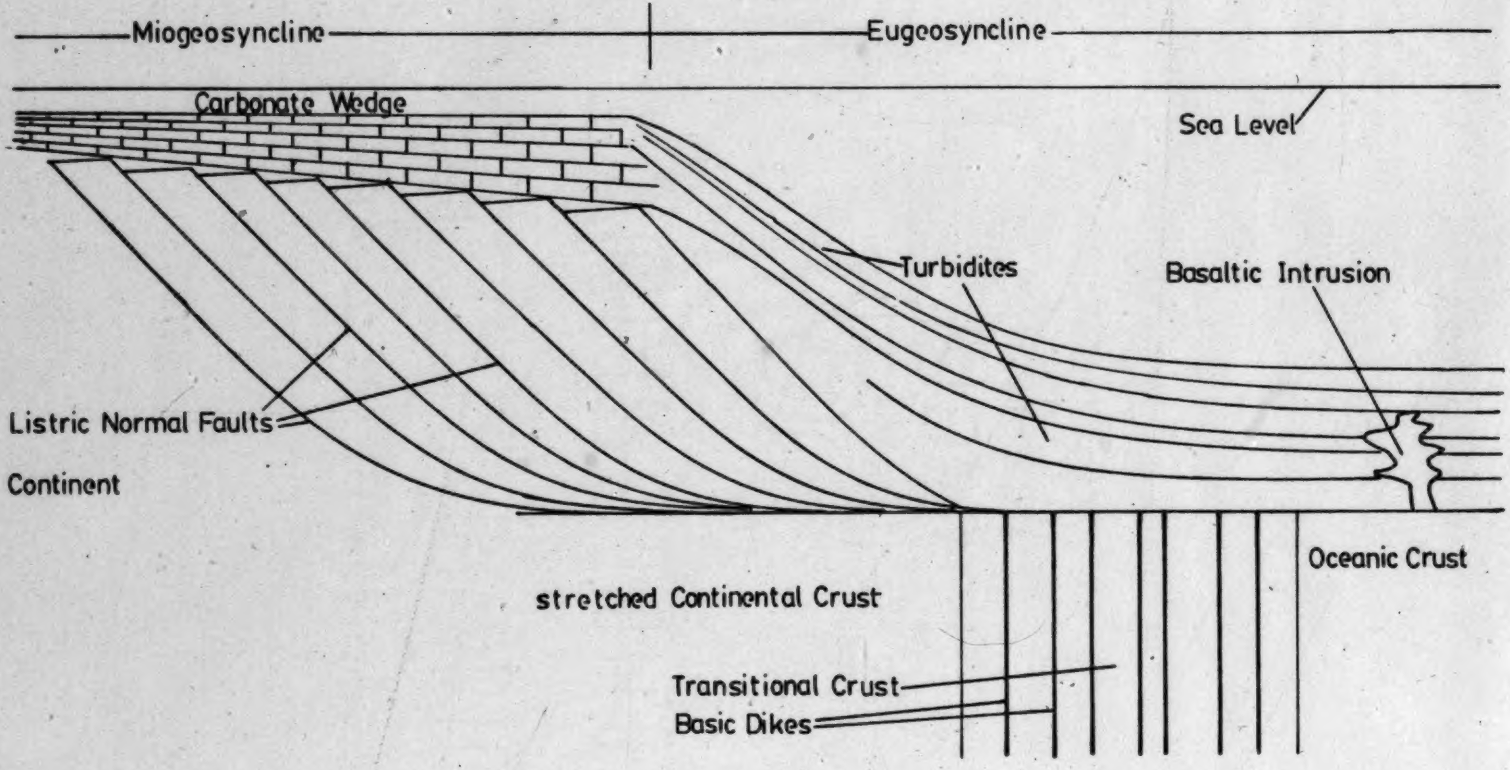
Miogeosyncline
Eugeosyncline
Carbonate Wedge
Sea Level
Turbidites
Basaltic Intrusion
Listric Normal Faults
Continent
Oceanic Crust
stretched Continental Crust
Transitional Crust
Basic Dikes

Figure 1.4 displays an idealized geosynclinal couple. The continental basement of the miogeosyncline is shown broken into a series of listric normal faults. Such a fault structure is thought to typify rifted continental margins and probably formed in response to stretching of the continental crust.

is a miogeocline while the sediments carried off the shelf and down the continental rise by turbidity currents form a eugeocline. As stated by Drake et al. (1959) and later by Dewey and Bird (1970), the recognition of the east coast of North America as a modern geosyncline serves to clarify the goals of a theory of orogeny. Any viable theory must account for the thickening, lateral compression, uplift, and heating necessary to convert eastern North America into a mountain belt.

### 1.3.2 Plate Tectonic theories of Orogeny

Plate tectonics is the framework for modern orogenic theories. Dewey and Bird (1970) offered perhaps the first comprehensive orogenic study based on plate tectonics concepts. They proposed two fundamental modes of mountain building, both being characteristics of particular CPM's.

1. Thermally driven uplift. This refers to island arc or cordilleran structures in which deformation is primarily in response to thermal perturbations from the immediately adjacent subduction zone. This is the dominant mechanism in O-O CPM's but can occur in an O-C as well. The prime determinant is probably the buoyancy of the subducting plate. An old oceanic plate passively subsiding beneath an island arc provides the type example of a thermal orogeny.
2. Mechanically driven movements. This type of deformation occurs when two buoyant non-subductable masses collide

such as continent - continent or continent - island arc interactions. The primary driving forces are horizontal compressive stresses. As such, a C-C margin would be the type example, but significant mechanical deformation could be expected in an O-C CPM if the oceanic plate was young or contained a large number of buoyant islands or ridges.

These generalizations have many exceptions, as a given system may show characteristics of both types. Cordilleran structures are characterized by movements along steeply dipping basement faults (block faulting) and associated forced folding (Stearns,1978), high heat flow, and some thrusting (high angle). In contrast, collisional (mechanical) orogenies show a marked predominance of low angle thrusting and free folding over block faulting, usually lower heat flow, and a tendency for extensive plastic deformation in the strike slip mode (Molnar and Tapponier,1975,1977a,1977b; and Tapponier and Molnar,1976).

Stearns(1978) suggests a similar classification and contrasts the deformation modes as either forced or free folding. What is meant by forced and free folding may be understood by the analogy of a rubber sheet laid across a set of wooden blocks. If the sheet is compressed by forces acting on its edges a pattern of free folds results. On the other hand, if the underlying blocks are moved vertically and/or rotated relative to one another, the sheet "drapes" over the uneven basement forming forced folds. A given mountain belt may undergo repeated cycles of both types of deformation in its history.

There is reason to believe that collisional orogenies must be transient in nature. Such a collision between two buoyant bodies usually results in the extinction of an active subduction system. If sea floor spreading continues elsewhere, geometric requirements force the spreading center to migrate away from the collision. The rate of migration plus the rate of crustal shortening in the collision zone must equal the spreading rate. This eventually results in very old oceanic crust off the trailing edge of the continent in addition to high compressive stresses. These conditions are generally thought to be sufficient to result in the formation of a new trench system (McKenzie 1977). Sykes (1970) suggests that the belt of shallow seismic activity from Australia to India represents a first stage in the development of a new trench.

While it is possible to imagine two extremes in mountain building, it is important to realize that there must exist a continuous spectrum between them. That is, a given orogeny may be classified as thermally driven and still exhibit appreciable deformation attributable to horizontal stresses.

## 1.4 Rifting and Stretching of the Lithosphere

The geosynclinal model of figure 1.4 is today called a rifted, passive continental margin. Such a system is thought to be the end result of rifting or disrupting continents. Evidence for the disruption of the megacontinent of Pangea in Mesozoic times is now so extensive that it is as near to being proven as anything can be in earth history (e.g. Dietz and Holden 1970). Thus, it is appropriate to include a few remarks on the nature of the rifting process. First, a discussion of recent theories of sedimentary basin formation because developments there have application to continental rifting.

### 1.4.1 Sedimentary Basins

The possibility of mechanically stretching continental crust has been receiving considerable attention recently. McKenzie (1978) proposed a model for the evolution of sedimentary basins beginning with an initial stretching of the continental crust. The stretching induces a thermally controlled lithospheric thinning and crustal subsidence which is accentuated by the weight of subsequently deposited sediments. (It is noteworthy that the theory indicates that uplift rather than subsidence would result from the stretching if the initial crustal thickness is less than about 20 km.) McKenzie concludes that the model is capable of accounting for observed patterns of subsidence. The amount of stretching required by such models is the prime objection raised by geologists. It usually requires at least 50% thinning of both crust and lithosphere to produce a satisfactory model.

An alternate model for sedimentary basins has been proposed by Beaumont (1978). He considers the response of a viscoelastic lithosphere to an applied load. The load induces an initial elastic subsidence which deepens with time as viscous relaxation of the lithosphere occurs. He applies this model to the formation of the foredeep basins of Alberta with remarkable success. The initial applied load is the weight of eastward moving thrust sheets.

Both of these models have sufficient free parameters to allow them to fit well in specific cases. Beaumont's model has the advantage of appealing to more traditional mechanisms.

### 1.4.2 Rifting via Stretching

Stretching as a mechanism for rifting the continental crust is one of the better models available today (see Memoir 29, The American Association of Petroleum Geologists, 1979). Bally, Oxburgh, and Beaumont concur that stretching was probably an important mechanism in initiating the subsidence observed on the circum-Atlantic rifted margins (unpublished notes: 18th Annual Conference on the Earth Sciences, Banff, Alberta, May 1980). The Beaumont subsidence mechanism is a better model in such cases as pericratonic basins like the Alberta foreland.

Perhaps the best evidence of crustal stretching is a recent investigation of the crustal structure in the Bay of Biscay region (unpublished notes, op. cit.). This work has apparently been carried out under the direction of X. LePichon and produced extremely high quality seismic profiles across the Bay. As is well known, Bullard et al. (1965) first proposed that Spain has been rotated away from France to produce the Bay of Biscay. The seismic sections across the Bay are very supportive of a stretching mechanism involving perhaps 75% thinning. The listric normal faults shown on figure 1.4 are a characteristic feature of the region (and of all rifted margins). The center of the Bay probably has true oceanic crust, which grades into stretched continental crust. A report of this work may be found in Montadert et al. (1979).

Listric normal faults probably represent the mechanism by which the upper brittle crust is thinned. Figure 1.5 is my representation of a possible rifting model. The continental plate is shown composed of brittle and ductile regimes with the transition occurring in the lower crust. The ductile material can respond to applied tensile stresses by a flow process while the brittle regime must fracture. Fractures take the shape indicated, showing a high dip at the surface but curving to become tangential to a decollement zone. The central region of stretched crust is shown cut by basic dikes. This forms a transition between thinned continental and oceanic crust. If the process shown

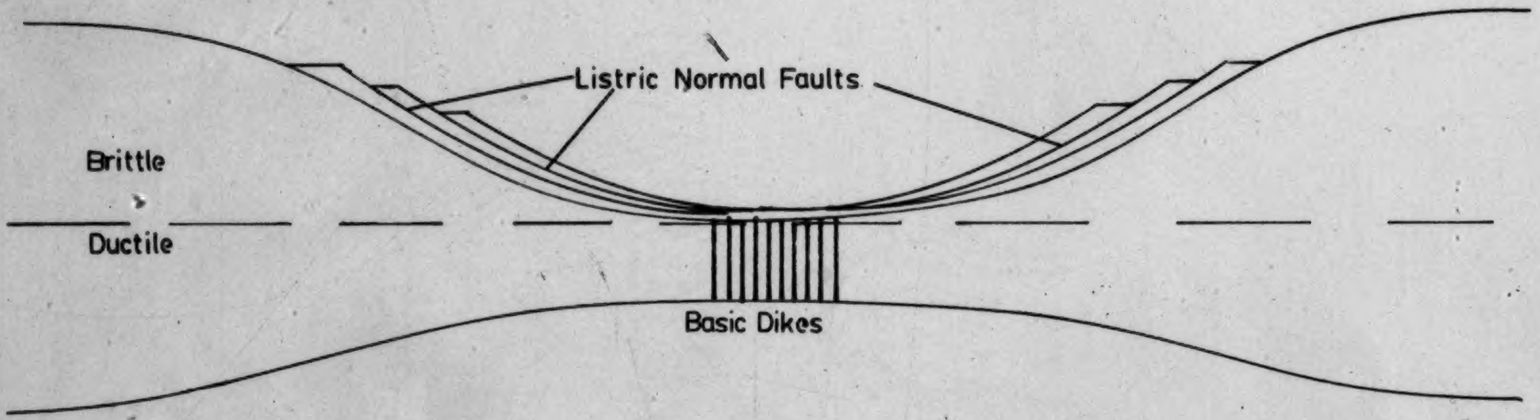

Figure 1.5 shows a possible model of continental rifting incorporating crustal stretching. The continental crust is shown divided into brittle and ductile regimes. The ductile material flows in response to stretching stresses while the brittle regime forms a characteristic system of listric normal faults. The center of the stretched material is shown intruded by basic dikes forming a transitional crust preparatory to the emplacement of true oceanic crust. Compare with figures 1.4 and 1.6.

in figure 1.5 were to continue, the next event would be the emplacement of true oceanic crust at the center of the rift. The mechanical behavior of continental crust cut by extensive basic dikes is difficult to distinguish from stretched crust (Beaumont, from unpublished notes, op. cit.).

## 1.5 Concluding Remarks

The visual similarity between the decollement tectonics of listric normal faults portrayed in figures 1.4 and 1.5 and the listric thrust faults of figures 1.2b and 1.3 is intentional. I feel that a similar mechanism is causing both structures. An analogy from 2 dimensional perfectly plastic flow will illustrate the point. The series of papers by Molnar and Tapponier (see bibliography) on Asian tectonics has demonstrated a striking analogy between systems of crustal faults and plastic slip lines. It is well known that plastic slip lines form an orthogonal grid whose trajectories are in the direction of maximum shear stress (Hill, 1950) which makes an angle of 45° to the direction of the maximum principle stress. This means that slip lines will intersect a free surface at 45° and become tangential to a strongly sheared surface. Figure 1.6 shows qualitatively the slip field expected in a medium whose lower surface is strongly sheared and whose upper surface is free. The effect of the weight of the material has been ignored here as well as possible pore pressure effects.

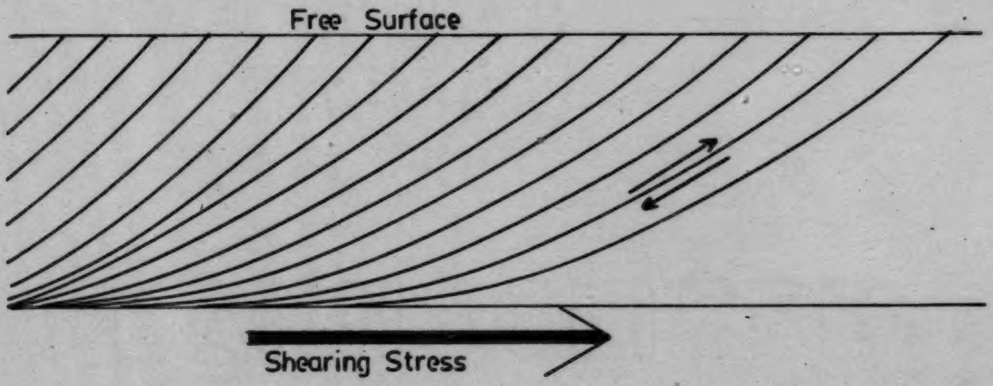

Figure 1.6 shows one set of a dual system of orthogonal flow lines which would form in a perfectly plastic system as a response to a strong basal shear. The other set of flow lines are everywhere perpendicular to these. The upper surface of the material is assumed a free surface.

Nevertheless, the structure of the flow lines is pleasingly similar to that seen in both tensional and compressional tectonics. The inference is that we are seeing structures whose lower surface is being strongly sheared.

# 2. Microgeodetic Survey Networks and the Measurement of Earth Strains

## 2.1 Introduction

It has been apparent for many centuries that the earth is an evolutionary world. Changes in the physical nature of the earth and its inhabitants occur on many time scales from the light travel time across the Bohr radius ($10^{-19}$ seconds) through daily changes ($10^{5}$ seconds) to short-term geological rhythms ($10^{13}$ seconds) and, finally, to processes comparable to the age of the earth itself, 4.5 billion years ($10^{17}$ seconds). Direct measurment of very short-lived phenomena is now a daily reality in atomic physics, however, the direct measurement of long-term processes is not so advanced.

The time scales involved in geological evolution have been known since the development of stratigraphic time scales and, later, radioisotope dating techniques. Structural studies of mountain ranges reveal that large horizontal motions (hundreds of km) can occur within time spans of a few million years. It has always been assumed that these movements must take place in a slow, but "continuous" fashion. The direct testing of this assumption is only just becoming feasible through the application of modern electromagnetic distance measuring techniques (e.g. Huggett and Slater 1975).

The term continuous will be used here in a somewhat imprecise way. Clearly motion directly attributable to earthquakes is not continuous, but averages of this motion over times much larger than the typical duration of earthquakes (minutes) can be considered continuous (though not constant).

It has been proposed that continuous motion takes place along boundary faults at depth but, typically, these faults lock near the surface (Turcotte and Spence (1974), Savage (1975), Savage (1977)). Though these references present models which conflict in detail, the important point is that near surface motion may be discontinuous in time. Such "locked" portions of plate boundaries will tend to deform in an elastic or plastic sense causing measurable earth strains (figure 2.1). Stored strain may be released either slowly through aseismic creep or abruptly in an earthquake.

Whether tectonic motion can be considered temporally uniform obviously depends upon the assumed time interval. The direct measurement of earth strains with geodetic techniques may soon permit the comparison of yearly strain rates with geological strain rates which usually are averages over several million years. In a geological context, yearly strain rates are effectively measurements of instantaneous response. If the instantaneous strain rate can be shown to correspond with the geological strain rate then the long term orogenic motions could be inferred to be temporally uniform. If they differ significantly, the geologic rates must be averages over some time period considerably longer than one year.

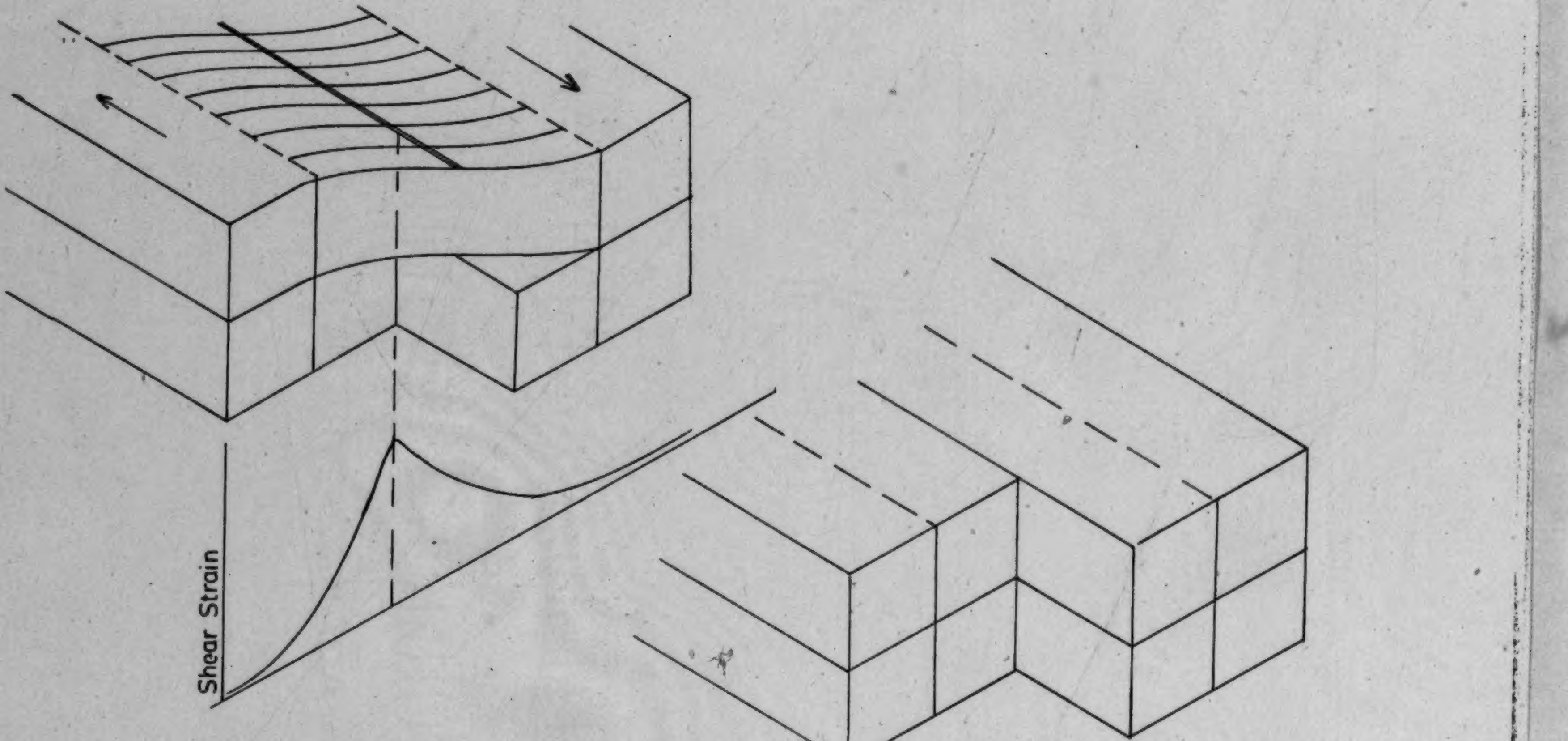

Figure 2.1 shows a typical model for a strike-slip plate boundary. In the upper left, the fault motion is uniform at depth but "locked" near the surface. Strain accumulates in the locked portion as shown by the graph. The release of stored strain can be slow or abrupt, causing an earthquake.

A simple example will serve to illustrate the magnitude of the deformations involved. Plate tectonics studies have shown that the large crustal plates comprising the earth's surface have relative motions as large as 10 cm/yr with an average probably closer to 1 cm/yr. Plate boundaries are not sharply defined lines but are rather broad transition zones 100 km and greater in width. Imagine an "average" situation with a plate boundary 100km across and a relative motion of 5 cm/yr. Perhaps an island on an oceanic plate is within 100km of the coastline on the other side of a trench system. If it is desired investigate the possible temporal uniformity of these plate motions on a yearly interval, then the $10^7$ centimeters separating the island from the coast must be measured to a precision of about 1 cm. This corresponds to strain rate of $10^{-7}$ $yr^{-1}$ or one part in ten million per year.

$10^{-7}$ $yr^{-1}$ is a fairly common estimate of what would probably be a geologically interesting strain rate. Given rather extreme assumptions about the size of plate boundaries and velocities, this can be pushed to $10^{-6}$ $yr^{-1}$ but not much further. Savage (1979) summarizes observations of straining on plate margins in various circum-Pacific locations and gives $3x10^{-7}$ $yr^{-1}$ as a typical maximum strain rate. (Local strains could be much larger.) If the range of interest is broadened to include such things as slow landslides, fault creep, tidal loading, and dilatant effects premonitory to earthquakes then the range of possible strain rates also increases.

### 2.1.1 The Peruvian Survey Project

Small aperture (about 2 km) strongly braced geodetic networks are useful tools for the study of recent crustal movement in areas where accumulated strains can be expected to exceed 2 microstrains (Nyland et al. 1979). I shall use the term "microgeodesy" to refer to the use of precision surveys over such networks to study local earth geometry and deformation. Specifically, I shall consider the potential of microgeodetic techniques for measuring tectonic straining in the earth.

Precision estimates of strains of the order of few microstrains and smaller are now routinely made throughout the western United States using geodimeters for trilateration combined with airborne meteorological observations (Prescott et al. 1979, or Thatcher 1979, for example). Though extremely accurate, these methods are quite expensive and require a high commitment of manpower and technology.

The Tectonophysics research group of the Physics Department of the University of Alberta, together with the Department of Surveying Engineering of the University of New Brunswick, has developed a surveying methodology for earth strain measurement. Only standard commercial instruments (such as the HP3800A E.D.M. for distance measurements and the Wild T2 theodolite for angles) and conventional surveying techniques are required. A complete discussion of the surveying techniques involved is presented in Chrzanowski et al. (1978) and Dennler and Chrzanowski (1979).

Here I present a method for the estimation of 2 dimensional strain components from repeated survey data. (Other approaches to this problem have been discussed by Brunner(1979), Snay and Gergen (1979), and Welsh (1979).) In general, both precise distance and angle measurements will be considered though the importance (but not necessarily accuracy) of the latter (at least for strain determinations) decreases rapidly with increasing network aperture.

Two small survey networks have been established in Peru (Nyland et al. 1979, figure 2.2) for investigation of active earthquake faults. The Huancayo network (figure 2.3), measuring 1.6km by .9km, is located at 11.9°S and 75.1° W some 30 km northeast of the city of Huancayo in the eastern cordillera of the Peruvian Andes. The network is bisected by the Huaytapallana fault which is a reverse fault striking N120°E and dipping 60° toward the northeastern (uplifted) block (Philip and Megard 1977). This fault was first ruptured by the very shallow focus Pariahuanca earthquakes of 1969 (Deza 1971) and probably represents a reactivation of much older faults paralleling the Huaytapallana cordillera just to the northeast of the network (Philip and Megard 1977).

The local deformation caused by these earthquakes was

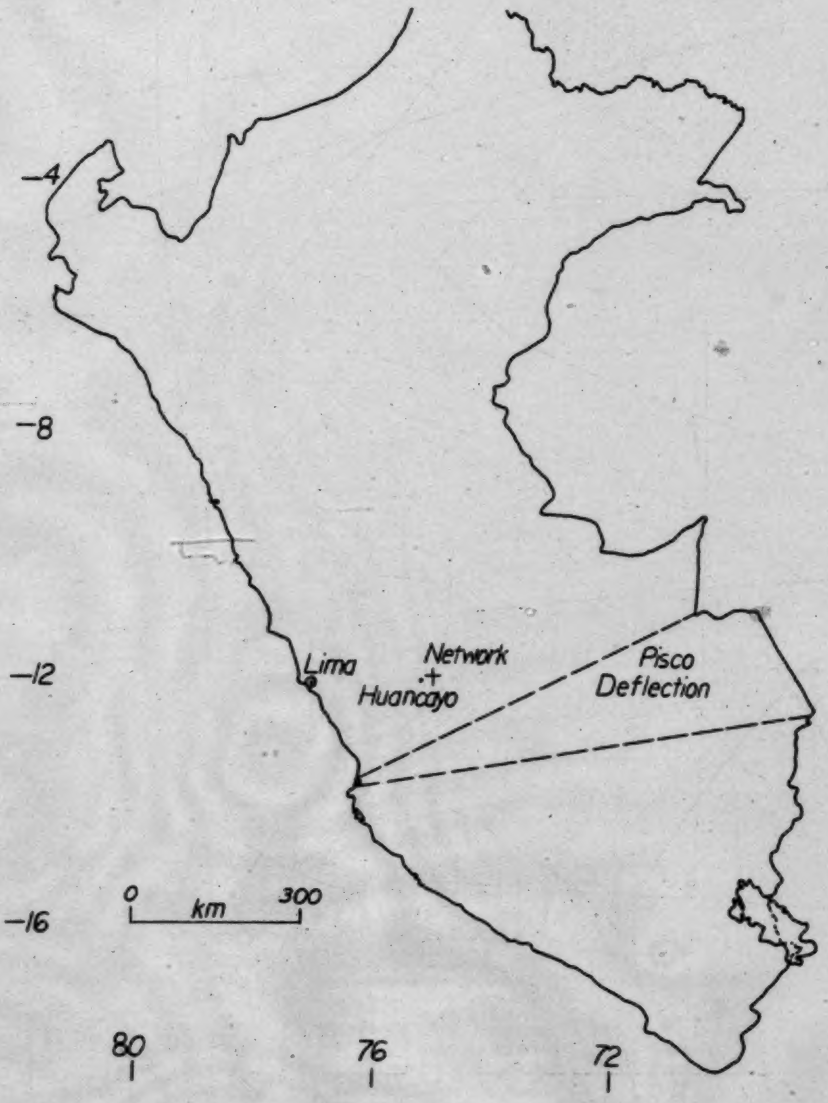
-4
-8
-12
-16
80
76
72
0
km
300
Lima
Network
Huancayo
Pisco
Deflection

Figure 2.2 is a sketch map of Peru showing the locations of various places referred to in the text.

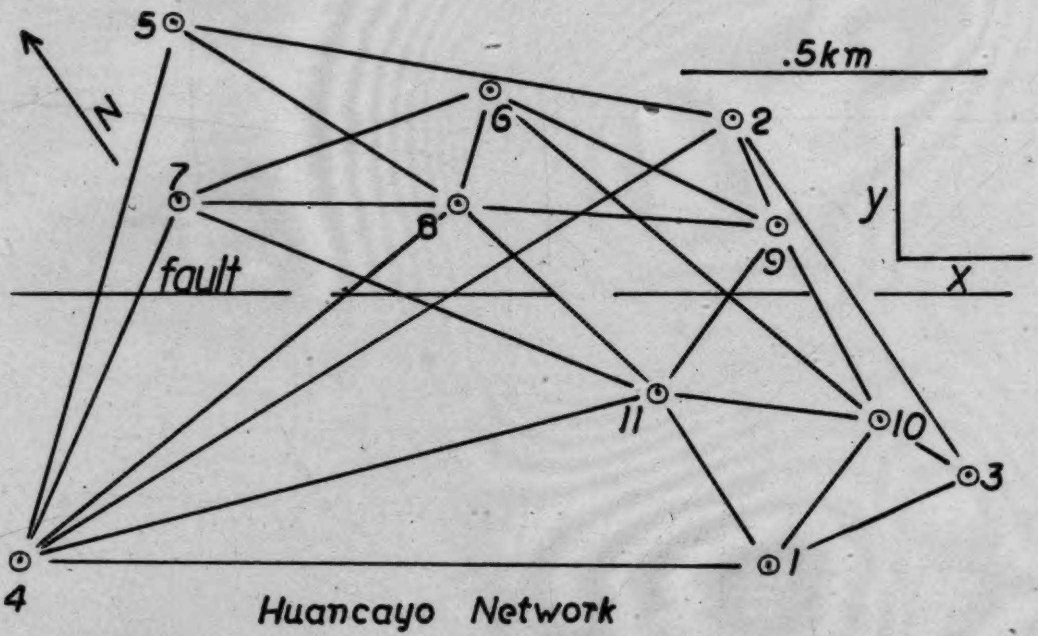

5
N
.5km
6
2
7
8
9
y
fault
x
11
10
3
4
1
Huancayo Network

Figure 2.3. A schematic diagram of the Huancayo network.

first summarized by Deza and later analyzed in detail by Philip and Megard. Both report the total fault displacement from the shocks as 1.6m vertical and .7m left lateral. Focal mechanism solutions, first given by Stauder (1975), are consistant with high angle reverse faulting with a component of strike-slip motion on the Huaytapallana fault. Philip and Megard note that most faults in the region are reverse faults which also display horizontal slickenslides indicating dextral motion. Thus, while the sinistral motion of the Pariahuanca events is opposite in sense to these trends, it is important to note that strike-slip motions are common here.

Philip and Megard supply a sketch map of the regional geology as well as abundant photographs of the fault trace. The Huancayo network covers approximately sections D through G of the Huaytapallana fault as noted in their figure 2. Benchmark monumentation was done by cementing brass plugs into bedrock outcrops. Surveys of the network have been conducted in 1975, 76, 77, and 78 measuring, on average, 36 distances and 81 angles each year (Chrzanowski et al., 1978).

A complete survey of these networks (measuring distances and angles) can be accomplished in about two weeks. Thus, for most purposes the set of measurements comprising a given survey can be regarded as having been made simultaneously. The relatively small size of the networks helps to minimize the effect of uncertainty in the refractivity of air along the line of sight. It has proven sufficient to measure atmospheric temperature and pressure at the instrument and target stations only. On the other hand the small size increases errors due to centering and pointing.

The Pitec network (not shown) was established in 1977 near the city of Huaraz across a normal fault. This network has been surveyed only once (1978) and hence will not be discussed further.

Due to the rugged terrain in the Peruvain Andes, it has not proven possible to achieve vertical control of the network motion through precise leveling. For this reason, vertical angle measurements at all observing points have been used to project all distance data onto a horizontal reference plane. The distance data analyzed here are "raw" or unadjusted data which were corrected (at the University of New Brunswick) only for elevation differences and atmospheric effects (Dennler and Chrzanowski 1979).

My involvement with the Peruvian survey project has been twofold. First, I was a member of the 1977 survey team as an observer and "strong back" and second, I have developed a mathematical technique for the direct estimation of tensor strain components from repeated survey data. The emphasis in this chapter will thus be a brief evaluation of the 1977 fieldwork and a presentation of the strain deduction method. For a detailed discussion of many of the other practical problems of microgeodesy as they apply to the Peruvian project, refer to Dennler and Chrzanowski (1979).

## 2.2 Assessment of the 1977 Fieldwork

A great variety of difficulties arose which, though unique, were certainly no greater than any of the other surveys had encountered. The main objective, which was to repeat trilateration and triangulation on the Huancayo network, was achieved. The secondary objective of establishing vertical control through precise leveling was a total failure.

Most of the problems were related to transportation. A reliable vehicle is absolutely essential. Camping at the network might solve some of these problems but would create others such as lack of charging facilities for the EDM and no medical facilities.

The second major difficulty, illness, probably has no easy solution, but certain basic rules do help. Physical conditioning and experience at high altitudes certainly are helpful. Surveying involves physical work which, at 4500 meters, can be devastating to those not properly prepared. Altitude effects rather than poor conditioning probably caused most of the illness. However, the local food can also be a problem for North Americans. A strict "don't eat the food" policy is impractical but it is possible to avoid commonly recognized problem items.

Other factors such as weather, instrument failure, and civil unrest can be anticipated and to some extent circumvented by careful planning. However, they will probably always be a factor. The 1977 survey was completed in 17 days, counting from the first day that we actually reached the network. Of those 17 days, surveying was actually done on 14 but only on less than half of those was a full day of work done. In ideal conditions, such a survey could probably be completed in less than a week. Given more normal circumstances, three weeks should be allowed.

It is my opinion that horizontal angle measurements are not worth the time and effort expended on them. The reasons for this will be clarified later after the analysis of the Huancayo data. For now, it is sufficient to remark that a typical survey of the Huancayo network measured 36 distances and 81 angles. Probably some 80% of actual surveying time is spent measuring angles for a gain in "resolution" of less than 10-15% over that obtained using distances alone (see section 2.6.3 and tables 2.1 and 2.2). This time could be spent repeating the distance measurements to obtain a better statistical determination. Alternately, if the accuracy obtained from repeating the distance measurements 5 or 10 times is satisfactory, then two or even three such networks could be trilaterated in the time necessary to complete trilateration and triangulation over one network.

One other success of the 1977 work should be mentioned. That summer, cooperation with Peruvian institutions was extended to include the Instituto de Geologia y Minas (Ingeomin) under the direction of B. Morales. This greatly aided the initial reconnaissance of the Pitec network. This network was established over a branch of the Cordillera Blanca normal fault near Huaraz. Initial layout and design was done by Walter Welch and me in the second week of August 1977. Actual monumentation was done later by Alcides Ames of Ingeomin using brass plugs which had been included in the instrument package for this purpose. This network has been surveyed in 1978 and 1979, however, the data is not available at this University at the time of this writing (June 1980).

## 2.3 Strain Deduction Method

The presentation of results from repeated surveys of such networks can be done in two ways. If at least 1 point and 1 direction is assumed fixed the relative motion of the other points in the network can be derived. This assumption is equivalent to saying there is no rigid translation or rotation of the entire network. Obviously the gradients of the displacements are not arbitrary to a rigid body rotation and translation. They contain deformation only which contains differential rotation as well as the more commonly considered strain. (The techniques developed here are used to estimate strains but can easily be extended to the estimation of differential rotations as well.) A presentation of displacement gradients is the second method of displaying results and is usually called strain analysis. Data processing methods for strain analysis are well-known (Frank, 1966 for example) but there is controversy and ambiguity about the location and the nature of the average strain derived by this method. It is very important to understand that the fundamental unknowns in my work are the components of the displacement gradient, not the positions of the network benchmarks.

Consider a two dimensional deformable medium which has undergone a "strain event". Before straining, the position of a point, p, relative to a point, q, is described by the vector $\vec{X}_{pq}$

After straining, the position of p with respect to q is now given by:

$$\vec{X}'_{pq} = \vec{X}_{pq} + \vec{U}_{pq} \qquad 1$$

where $\vec{U}_{pq}$ is called the relative displacement vector of p with respect to q. If displacements are small compared with interpoint distances, elementary geometry suffices to derive a relation for the change of euclidian distance, say S, between the points.

$$\frac{S'_{pq} - S_{pq}}{S_{pq}} = \frac{1}{S^2_{pq}} \vec{X}_{pq} \cdot \vec{U}_{pq} \qquad 2$$

In a similar fashion, though algebraically more complicated, an expression for the change in angle, $\phi$ , between the points k, 1, and m can be shown to be:

$$\frac{\phi'-\phi}{\phi} = \frac{-1}{\phi\sin\phi}\left[\vec{U}_{k\ell}\cdot\vec{\Delta}_{k\ell m} + \vec{U}_{m\ell}\cdot\vec{\Delta}_{m\ell k}\right] \tag{3}$$

where:

$$\vec{\Delta}_{k\ell m} = \frac{1}{S_{k\ell}^{2}S_{m\ell}}\left[S_{k\ell}\vec{X}_{m\ell} - \vec{S}_{m\ell}\vec{X}_{k\ell}\right] \tag{4}$$

Equations 2 and 3 are linear in the unknown displacement vectors. Their left hand sides are directly derived from observed changes in the network configuration. As such they form observation equations for data gathered in the course of repeated geodetic surveys. If observations of relative elevation changes are available, observation equations can be derived in a similar way. Note that the "observations" in these equations are the fractional changes in line lengths and angles formed through the direct comparison of two sets of survey data.

The above relations are not sufficient to determine the motion of the network unambiguously. It is sufficient to require that some point and some direction in the medium remain fixed. Usually the fixed point and direction are taken to be a survey point in the network and the azimuth between this point and one other. These, or some similar pair of constraints, remove the rigid translation and rotation components from the displacement vector field.

Equations 2 and 3 can be used as observation equations for the problem of determining displacements from survey data. Difficulties arise in trying to write an equivalent set of equations for the estimation of strain tensor components. Though displacements and strains can safely be regarded as truly infinitesimal, a similar assumption regarding the distance separating points in the network cannot be made. That is, if points p and q are infinitesimally close, then:

$$\vec{U}_{pq} = \underset{\sim}{E} \cdot \vec{X}_{pq} \qquad 5$$

where $\underset{\sim}{E}$ is the strain tensor. If the interpoint distance is finite, then this must be changed to:

$$\vec{U}_{pq} = \int_{p}^{q} \underset{\sim}{E} \cdot d\vec{S} \qquad 6$$

where the integral is taken along some curve connecting p and q.

The fact that the relative displacement vector is shown in equation 6 to be a path integral of the strains means that the observations depend on average values of the strains. If no information is available on the possible functional form of the strain field, then there is no justifiable alternative to assuming the strain to be constant along the line pq. It follows that assuming constant strain applies along a line is equivalent to saying this constant strain is the average of a varying strain. Such an average cannot be localized to any one part of the line.

Thus equations 2 and 3 directly determine only averages of the strain tensor components. Assuming that the strains are constant over the entire network leads to the simplest solution. If, as is often the case, the expected strains are of the same order of magnitude as uncertainties in the data then this is the only practical solution. If the time between surveys is large, or if accuracies of $10^{-7}$ can be achieved then it would be informative to examine higher order approximations to the strain field. I present a formalism for the least squares approximation of strain fields with a polynomial of arbitrary order.

If it is assumed that the state of strain over the network can be represented as a continuous tensor field, the observation equations can be regarded as stringent constraints upon the class of functions which could possibly describe these tensor components. Thus if the components of displacement and strain are approximated as linear combinations of suitably chosen expansion functions the observation equations can be used to estimate the expansion coefficients.

The nature of the functions used for interpolation is certainly a matter for discussion. I choose here to describe the kinematics of the deformation through the use of two dimensional polynomials of low order. (A more physical choice of expansion functions might be those describing the response of the surface of a half space to internal forces

(Nyland, 1977).) In effect, an (n-1)'th order Taylor series approximation to the two dimensional strain field (or order n for the displacements) is sought. Strictly speaking, the validity of such a scheme requires that the strains possess continuous derivatives to order n.

Let the displacement vector field have components u and v in the x and y coordinate directions, each possessing continuous derivatives to order n+1. Then the displacement components can be written as:

$$u = a_{oo} + \sum_{i=1}^{n} \sum_{j=0}^{i} a_{ij} x^{i-j} y^{j} \qquad 7$$

$$v = b_{oo} + \sum_{i=1}^{n} \sum_{j=0}^{i} b_{ij} x^{i-j} y^{j} \qquad 8$$

Formulae for the strain components, valid everywhere except possibly on the fault itself, are then:

$$e_{xx} = \sum_{i=1}^{n} \sum_{j=0}^{i} (i-j) a_{ij} x^{i-j-1} y^{j} \qquad 9$$

$$e_{yy} = \sum_{i=1}^{n} \sum_{j=0}^{i} j b_{ij} x^{i-j} y^{j-1} \qquad 10$$

$$e_{xy} = \frac{1}{2} \sum_{i=1}^{n} \sum_{j=0}^{i} \left[ j a_{ij} x^{i-j} y^{j-1} + (i-j) b_{ij} x^{i-j-1} y^{j} \right] \qquad 11$$

If the expansion coefficients, {a} and {b} are regarded as the fundamental unknowns, then the observation equations can be written in terms of them. This representation of the displacements to order n requires that the the expansion coefficients (including the zero'th order terms) number in total $N=n^2+3n+2$. At most, three of these can be eliminated through constraints against rigid body motion. This leads to the following linear system:

$$\underline{A}\underline{p}=\underline{y} \qquad 12$$

$$\underline{w}=\underline{B}\underline{p} \qquad 13$$

$$\underline{z}=\underline{C}\underline{p} \qquad 14$$

where $\underline{p}$ is an N length vector containing the parameters, $\underline{y}$ is an M length vector of observations, $\underline{w}$ is a vector containing the values of the displacements at the network points, $\underline{z}$ is a similar vector for the strains, and $\underline{A}$,$\underline{B}$,$\underline{C}$ are rectangular matrices depending upon the network geometry.

The pseudo or generalized inverse of a rectangular matrix is used here to solve this problem. Traditional least squares methods (IMSL 1979) lack numerical stability and precision required for this study. For a strictly overdetermined problem, the pseudo-inverse solution is formally identical to a minimum length least squares solution. However, the availability of extremely fast and accurate algorithms for pseudo-inverse calculations (e.g. Lawson and Hanson 1974) makes such an approach numerically more accurate than traditional least squares methods. Thus traditional least squares methods are contained in the generalized inverse approach, but some of the generalizations of interest to geophysicists dealing with incomplete, inadequate, and sometimes incorrect data are not amenable to traditional least squares treatment. Jackson (1972) presents a valuable summary of the advantages of this approach.

Following Penrose(1955), the pseudo-inverse of the M by N matrix A is the unique solution to:

$$\underline{AXA}=\underline{A} \tag{15}$$

$$\underline{XAX}=\underline{X} \tag{16}$$

$$(\underline{AX})^{+}=\underline{AX} \tag{17}$$

$$(\underline{XA})^{+}=\underline{XA} \tag{18}$$

where the superscript "+" denotes the transpose.

The pseudo-inverse of $\underline{A}$ will be denoted by $\underline{A}^{-1}$. It can then be shown (Penrose 1955) that the unique "best" solution to equation 12 is given by $\underline{p}'=\underline{A}^{-1}\underline{y}$. This is the best solution in the sense that:

$$\underline{e}^{+}\underline{e}= \text{a minimum} \tag{19}$$

where:

$$\underline{e}=\underline{Ap}'-\underline{y}= \text{the error vector} \tag{20}$$

and:

$$\underline{p}'^{+}\underline{p}'= \text{a minimum} \tag{21}$$

The solutions to equations 12,13,14 are then:

$$\underline{p}'=\underline{A}^{-1}\underline{y} \tag{22}$$

$$\underline{w}'=\underline{BA}^{-1}\underline{y} \tag{23}$$

$$\underline{z}'=\underline{CA}^{-1}\underline{y} \tag{24}$$

Thus, with relatively few assumptions, a linear relationship between the strain tensor components at the network points and the observations has been formulated.

In actual practice, the error vector of equation 20 is rarely minimized without first applying some sort of weighting scheme to the data. The procedure (Jackson 1972) of prescribing weights for each equation proportional to the inverses of the standard deviations of the data will be used here. (It is assumed that the line length and angle changes are uncorrelated. See Jackson 1972, Wiggins 1972). If $\underline{W}$ is a matrix of such weights, then multiplication of equations 12,13, and 14 from the left by $\underline{W}$ and appropriately renaming some terms, results in a system that is formally the same as before and which minimizes:

$$\underline{e}^{+}\underline{W}^{+}\underline{We} \qquad 25$$

If $\underline{dy}$ represents a vector containing the standard deviations of the observations then $\underline{W}$ is a matrix whose diagonal elements are proportional to the inverses of the corresponding elements of $\underline{dy}$. The constant of proportionality is usually chosen such that the largest weights are unity. The inverse of the square of this proportionality constant, say v, is called the "problem variance". (In all that follows the equations 12-14 and 19-24 are assumed to be weighted.)

The solutions 22-24 represent simple linear combinations of the observations. Therefore, their variances are relatively easy to calculate from the theory of the propagation of errors. This results (Jackson 1972) in:

$$\mathrm{var}(\underline{p}'_i)=v\sum_j(\underline{A}^{-1}_{ij})^2 \tag{26}$$

$$\mathrm{var}(\underline{w}'_i)=v\sum_j(\underline{B}'_{ij})^2 \tag{27}$$

$$\mathrm{var}(\underline{z}'_i)=v\sum_j(\underline{C}'_{ij})^2 \tag{28}$$

where $\underline{B}'=\underline{BA}^{-1}$ and $\underline{C}'=\underline{CA}^{-1}$

The standard deviations are then simply the square roots of the variances.

It is also possible to estimate the problem variance from the value of $\underline{e}^+\underline{e}$ (where $\underline{e}$ now denotes the weighted error vector) as:

$$v'=(N^{-1}\underline{e}^+\underline{e})^{.5} \tag{29}$$

where N (as before) is the number of unknown parameters. Wiggins (1972) suggests that v and v′ should agree to within an order of magnitude. If, for example, $v' \ll v$ then the data display an internal consistency greater than was estimated before the analysis. (This is a heuristic application of chi-squared significance tests which ought not to be important unless a gross error was made in estimating data uncertainties.)

The pseudo-inverse is usually calculated via a procedure known as singular value decomposition (e.g. Lawson and Hanson 1974). This is a generalized form of eigenvalue analysis (Lanczos 1961) by which an arbitrary M by N matrix, $\underline{A}$, may be written as the product of three submatrices. (For ease of presentation I assume M≥N.) This is usually written:

$\underline{A}=\underline{UQV}^{+}$ . 30

where:

$\underline{U}$ is an M by M orthogonal matrix whose columns are the eigenvectors of $\underline{AA}^{+}$.

$\underline{V}$ is an N by N orthogonal matrix whose rows are the eigenvectors of $\underline{A}^{+}\underline{A}$.

$\underline{Q}$ is an M by N matrix in which the only non-zero elements are the diagonal elements of the first N rows. These contain the non-negative square roots of the eigenvalues of $\underline{A}^{+}\underline{A}$ and are called the singular values of $\underline{A}$.

The pseudo-inverse of $\underline{A}$ can then be shown to be (Jackson 1972):

$\underline{A}^{-1}=\underline{VQ}^{-1}\underline{U}^{+}$ 31

where $\underline{Q}^{-1}$ is an N by M matrix whose only non-zero elements are in the diagonal positions of the first N columns and these are the inverses of the non-zero singular values of $\underline{A}$.

If this result is substituted into equations 26-28, the variances of the model are seen to depend on the inverse singular values. Thus unnecessarily large variance estimates can result if a few of the singular values are much smaller than the rest. This leads to the practice of examining the singular values and setting some of the smaller ones to zero. This has the effect of decreasing the variance estimates and the resolution of the model. The value of this procedure depends upon the problem under investigation and the judgement of the investigators. (See Jackson 1972 or Wiggins 1972 for a more complete discussion.)

My approach is to use this theoretical formulation, and a library (IMSL 1979) program for pseudo-inverse calculations to determine strain fields associated with repeated survey observations. Figure 2.4 is a schematic summary of this method.

### 2.3.1 Tests with Synthetic Data

Figures 2.3 and 2.5 show two networks which I have examined using synthetic data. In these studies with the Huancayo network I have assumed that 38 distances and 81 angles have been measured. Figure 2.5 shows the network G10 (for 10 point geometry). This is a theoretical network chosen to show average behavior and to be free of the design limitations usually imposed by terrain. Its behavior is examined in order to establish "ideal" response. It is assumed that all 45 possible distances and 90 of the 120 possible angles have been measured.

The method used to generate synthetic data for these studies was:

1. Assume a displacement field and a mathematically compatible strain field.
2. Using a set of "original" coordinates and a set of displaced coordinates calculated from the assumed displacement field, two sets of data simulating line

## OBSERVATION EQUATIONS

$$F(U_{pq}) = \frac{\Delta S_{pq}}{S_{pq}}$$

$$G(U_{kl}, U_{ml}) = \frac{\Delta \varphi_{klm}}{\varphi_{klm}}$$

## POLYNOMIAL REPRESENTATION

$$u(x,y) = a_{00} + \sum_{i=1}^{n}\sum_{j=0}^{i} a_{ij}\, x^{i-j} y^{j} \qquad v(x,y) = b_{00} + \sum_{i=1}^{n}\sum_{j=0}^{i} b_{ij}\, x^{i-j} y^{j}$$

$$exx(x,y) = \sum_{i=1}^{n}\sum_{j=0}^{i} (i-j)\, a_{ij}\, x^{i-j-1} y^{j} \qquad eyy(x,y) = \sum_{i=1}^{n}\sum_{j=0}^{i} j\, b_{ij}\, x^{i-j} y^{j-1}$$

$$exy(x,y) = \sum_{i=1}^{n}\sum_{j=0}^{i} \left[ j\, a_{ij}\, x^{i-j} y^{j-1} + (i-j)\, b_{ij}\, x^{i-j-1} y^{j} \right]$$

## LINEAR SYSTEM — SOLUTIONS

$$\left.\begin{array}{l} Ap = y \\ w = Bp \\ z = Cp \end{array}\right\} \xRightarrow{\text{weighting}} \begin{array}{l} p' = A^{-1}y \\ w' = BA^{-1}y \\ z' = CA^{-1}y \end{array}$$

p = parameter vector
y = observation vector
w = displacement vector
z = strain vector

A, B and C are rectangular matrices determined by network geometry

$A^{-1}$ pseudo inverse of A

Figure 2.4 illustrates the method of strain analysis described in the text. Refer there for details.

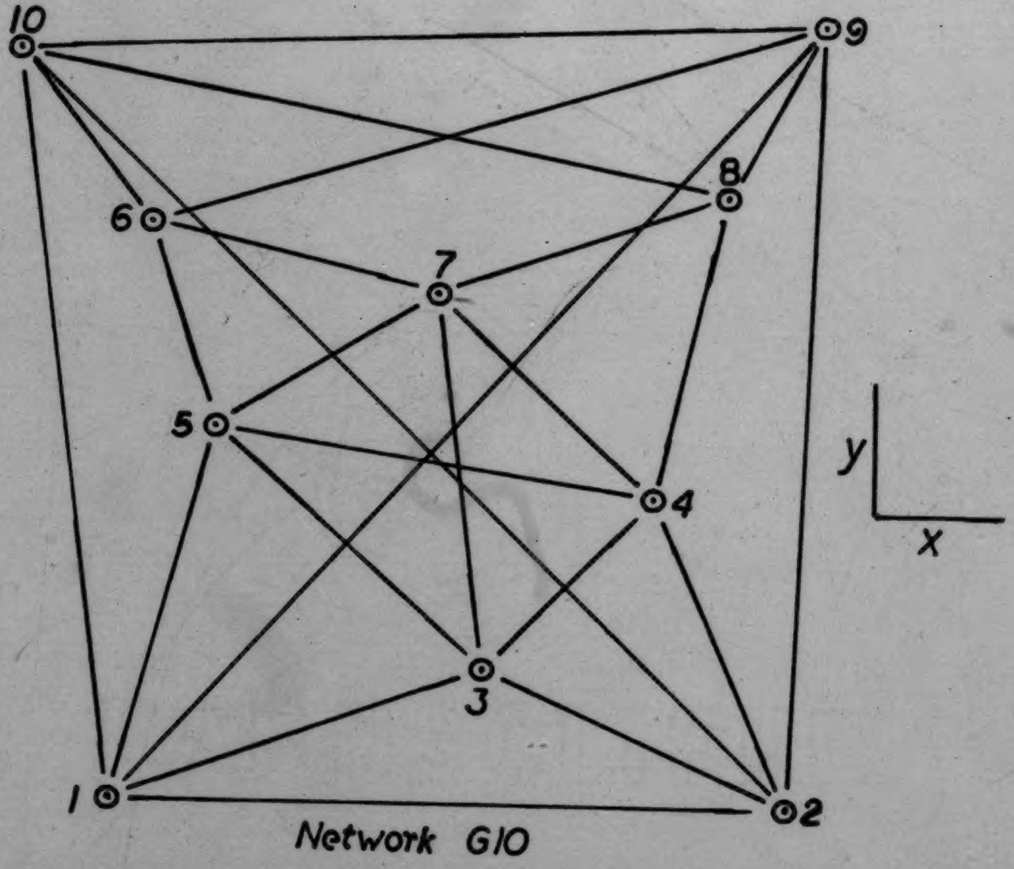
10
9
8
6
7
5
4
3
1
2
y
x
Network G10

Figure 2.5 shows a test network used for the synthetic data studies discussed in the text. This represents the author's vision of the "ideal" network.

length and angle measurements were generated.

3. These data sets were contaminated with zero mean, normally distributed, "random" noise. Standard deviations were chosen to be compatible with those attainable in the field

Unless explicitly stated otherwise, the random noise used for data contamination in these studies had standard deviations of 3mm for distance measurements and 3 sec for angles. Savage and Prescott (1973) have reported achieving standard deviations for distance measurements of $(a^2+b^2l^2)^{.5}$ where a=3mm, $b=2\times10^{-7}$, and l is the linelength in mm. This is only marginally greater than 3mm even for 10Km lines. In Peru, using much less sophistication than the California workers, we have achieved standard error estimates of :

| Survey | Distances (mm) | Angles (sec) |
|---|---|---|
| 1975 | 4.0 | 2.6 |
| 1976 | 1.8 | 2.2 |
| 1977 | 2.8 | 5.0 |
| 1978 | 2.8 | -- |

The 1975 and 1976 distance and angle estimates and the 1977 distance estimates are from Chrzanowski et al. (1978) and were determined from the residual vector obtained from least squares fits of coordinate systems to each individual survey. The 1977 angle estimates and the distance estimates for 1978 were assumed by me. (The accuracy of these estimates is supported by the results of the analysis of the Huancayo data in the latter part of this paper.)

That these precision estimates are on a par with those achieved in southern California is perhaps due to the shorter lengths involved in our surveys as well as the vastly different atmospheric effects between sea level in California and 5000m in the Andes. Regardless, the standard deviations used in this study represent those achievable in many parts of the world using modern techniques and equipment.

Table 2.1 summarizes the results of numerous studies designed to test the response on the Huancayo net to various constant strain fields. In the coordinate system of figure 2.3, compression is indicated by negative values for exx and eyy, and a negative exy means left lateral shear. It is apparent upon examination of this table that constant strains of a few microstrains can be resolved by the Huancayo net. Generally strains of absolute value less than about $10^{-6}$ were estimated for zero true strains. (Only in studies 6 and 9 was this not true.)

Of interest here are the standard deviation estimates for the various strain components. These suggest that the Huancayo network is better suited to measurement of exx and exy than eyy. This is regrettable but is consistent with the horizontal dimensions of the network being greater in x than y.

The standard deviation estimates in all of these

Table 2.1 illustrates the ability of the Huancayo network to resolve constant strains with a constant strain model. The lower of the double entries represents one standard deviation. 38 distances and 81 angle measurements were used.

### HUANCAYO NETWORK RESOLUTION OF CONSTANT STRAINS

| | TRUE STRAIN (MICROSTRAINS) | | | STRAIN ESTIMATES (MICROSTRAINS) | | | | |
|---|---|---|---|---|---|---|---|---|
| STUDY | EXX | EXY | EYY | EXX STD DEV | EXY STD DEV | EYY STD DEV | VARIANCE RATIO | COMMENTS |
| 1 | 0.0 | 0.0 | -5.0 | -.245<br>1.16 | .611<br>1.04 | -4.03<br>2.21 | .76659 | |
| 2 | 0.0 | 0.0 | -5.0 | -.136<br>1.16 | .715<br>1.04 | -6.46<br>2.21 | .96446 | |
| 3 | 0.0 | 0.0 | -5.0 | -.875<br>1.16 | -.616<br>1.04 | -5.12<br>2.21 | .87939 | |
| 4 | 0.0 | 0.0 | -5.0 | 0.0<br>0.0 | .639<br>1.02 | -3.92<br>2.05 | .76892 | SAME DATA AS IN 1 SYMMETRY ASSUMED |
| 5 | 0.0 | 0.0 | -5.0 | -.825<br>1.33 | -.875<br>1.24 | -5.61<br>2.72 | .94984 | SAME AS 3 EXCEPT DISTANCES ONLY |
| 6 | 0.0 | -5.0 | 0.0 | -.702<br>1.16 | -5.05<br>1.04 | 2.69<br>2.21 | .86302 | |
| 7 | 0.0 | -5.0 | 0.0 | -.807<br>1.33 | -4.54<br>1.24 | 1.24<br>2.72 | .88047 | SAME AS 6 EXCEPT DISTANCES ONLY |
| 8 | 0.0 | -3.0 | 0.0 | -.217<br>1.16 | -2.85<br>1.04 | 1.03<br>2.21 | .90776 | |
| 9 | 5.0 | 0.0 | 0.0 | 3.61<br>1.16 | .271<br>1.04 | .266<br>2.21 | .76736 | |
| 10 | 4.0 | -3.0 | -4.0 | 4.10<br>1.16 | -2.22<br>1.04 | -1.55<br>2.21 | .85901 | |
| 11 | -3.0 | 3.0 | -5.0 | -4.29<br>1.16 | 3.24<br>1.04 | -4.14<br>2.21 | .99196 | |

studies are dependent upon the assumed variance in the data, the number of measurements, and the network geometry (eqns 26-28). They provide a quantitative statement of the fundamental resolving power of a network. It can be stated that, given a data set of 38 distances and 81 angles measured to the aforementioned precision, the resolution limit of the Huancayo network is (in microstrains) $|exx|=1.16$ $|exy|=1.04$ and $|eyy|=2.21$. In this light, it may be instructive in studies of optimal network design to seek geometries which minimize these quantities.

In the great majority of cases in table 2.1, the strain estimates are well within one standard deviation of the true strain. (It has been brought to my attention that this table suggests the method is more successful than is statistically probable. Upon review of my research notes, I realize that subjective bias entered into the selection process for results shown in table 2.1. I estimated at least 111 constant strain tensor components from synthetic data of which 80 or 72% were within one standard deviation and 109 or 98% were within two standard deviations of the true values. Results in table 2.2 are a better statistical sample.) An overly optimistic interpretation of these results should be avoided. It is better to say that a measurement which differs from zero by 1.96 standard deviations is non-zero at the 95% confidence level (Chrzanowski et al. 1978).

The column labeled "variance ratio" in all of these data tables refers to the ratio of the problem variance as calculated from the squared length of the residual vector to the problem variance as determined from the specified uncertainties in the data. Thus if the variance ratio is significantly less (or greater) than unity, the internal consistency of the data is much greater (or less) than was estimated apriori. Multiplication by the square root of the variance ratio will convert the standard deviation estimates given into those which agree exactly with the sum of the squares.

A comparison of studies 5 and 7 with 3 and 6 respectively illustrates the much greater importance of distance measurements over angle measurements. On the Huancayo net, a small and non-negligible decrease in the standard deviation estimates is achieved by including the angles. However since angle measurements are much more time consuming than distance measurements, practical considerations may argue strongly against measuring angles. Table 2.2 gives the results of a more comprehensive study on this matter (using network G10). These 10 studies show how the resolution of the same assumed strain field increases with increasing network aperture. (I define the aperture of a network to be the longest measurable linelength. The Huancayo net has an aperture of 1.6km.) Two studies are shown for each aperture, the first having been done with angles and distances while the second used distances only. As can be seen, any advantage achieved by including angle

APERTURE SIZE AND RESOLUTION FOR NETWORK G10

| APERTURE (KM) | EXX STD DEV | EXY STD DEV | EYY STD DEV | VARIANCE RATIO |
|---|---|---|---|---|
| 1.6 | 5.90<br>1.25 | -2.35<br>.903 | -1.23<br>1.34 | 1.1265 |
| 1.6 | 6.37<br>1.31 | -2.49<br>.935 | -1.76<br>1.41 | .91012 |
| 3.2 | 5.40<br>.650 | -1.90<br>.464 | -1.99<br>.696 | .88199 |
| 3.2 | 5.40<br>.658 | -1.98<br>.468 | -1.99<br>.706 | 1.1094 |
| 6.4 | 4.70<br>.328 | -2.46<br>.234 | -.419<br>.351 | 1.1541 |
| 6.4 | 4.66<br>.329 | -2.44<br>.234 | -.364<br>.352 | 1.4167 |
| 12.8 | 5.05<br>.164 | -2.45<br>.117 | -1.03<br>.174 | 1.0235 |
| 12.8 | 5.05<br>.164 | -2.45<br>.117 | -1.03<br>.176 | 1.1243 |
| 25.6 | 5.21<br>.110 | -2.48<br>.078 | -.908<br>.118 | .87802 |
| 25.6 | 5.21<br>.110 | -2.48<br>.078 | -.910<br>.118 | .60106 |

Table 2.2 shows the effects of increasing aperture on resolution. All strains are in microstrains. The aperture of a network is taken to be the longest measurable linelength. In all cases, the "true" strains in this study were EXX=5.0, EXY=-2.5, EYY=-1.0. The second entry for each aperture was done with distance measurements only.

measurements is rapidly lost with increasing aperture.

These simulations deal only with short range EDMs and T2 theodolites. Although it can be argued that standard deviations of measured angles decrease with increasing length of lines (Vanicek, personal comminication, 1980) no allowance has been made for this effect. I feel that systematic errors due to other effects than pointing will, if anything, increase the uncertainty in the observed angles. Obviously more precise theodolites should be treated differently. If, in fact, the accuracy of measured angles does increase with distance, strain determinations should be made with theodolites and this has proven to be not as accurate in many cases (e.g. California).

I would classify only the first two or three apertures in table 2.2 as being "microgeodetic". It is clear that networks of this size are quite capable of measuring tectonically interesting strains and in many cases may be preferable to larger ones. While the predicted standard deviations decrease linearly with increasing aperture practical problems such as atmospheric disturbances and logistics must increase rapidly. A standard deviation of 4mm for distances was assumed for the 25.6 km aperture. (The average line length is considerably less than the aperture.) The assumption of a typical deviation of 4 mm may be optimistic, but it is not unreasonable. In any case it is an academic exercise. An HP3800 does not see beyond about 10 km even under ideal conditions. These preliminary estimates by no means exhaust the subject. There is room for further study by investigators who recognize the practicalities of geophysical field work.

Thus far only lowest order approximations to the strain field have been treated. The success of higher order approximations generally requires that the expected strains be an order of magnitude or so larger than the errors in observations. Fitting higher order polynomials to poorly determined data will result in "fitting to the noise". Some possible methods of achieving sufficiently accurate data for higher order analysis include:

1. allow a sufficiently long period between surveys for strains of $10^{-5}$ to accumulate.
2. use a distance measuring device capable of single measurement accuracies of $10^{-7}$.
3. make a number of repeated measurements with an instrument having single measurement accuracy of $10^{-6}$.

Assuming that one of these methods has been adopted, the resolution of linear trends in appropriate synthetic data can be examined. Figure 2.6 shows results from two such studies done with network G10 using a 6.2 km aperture. In one study (lower graph) a linear shear strain varying from $-2\times10^{-5}$ to $2\times10^{-5}$ across the network was fit with a linear model. The fit is quite good at all network points though the interior points have the smallest standard deviations. (The errors bars represent one standard deviation.) Fitting a constant strain to the same data approximates the average

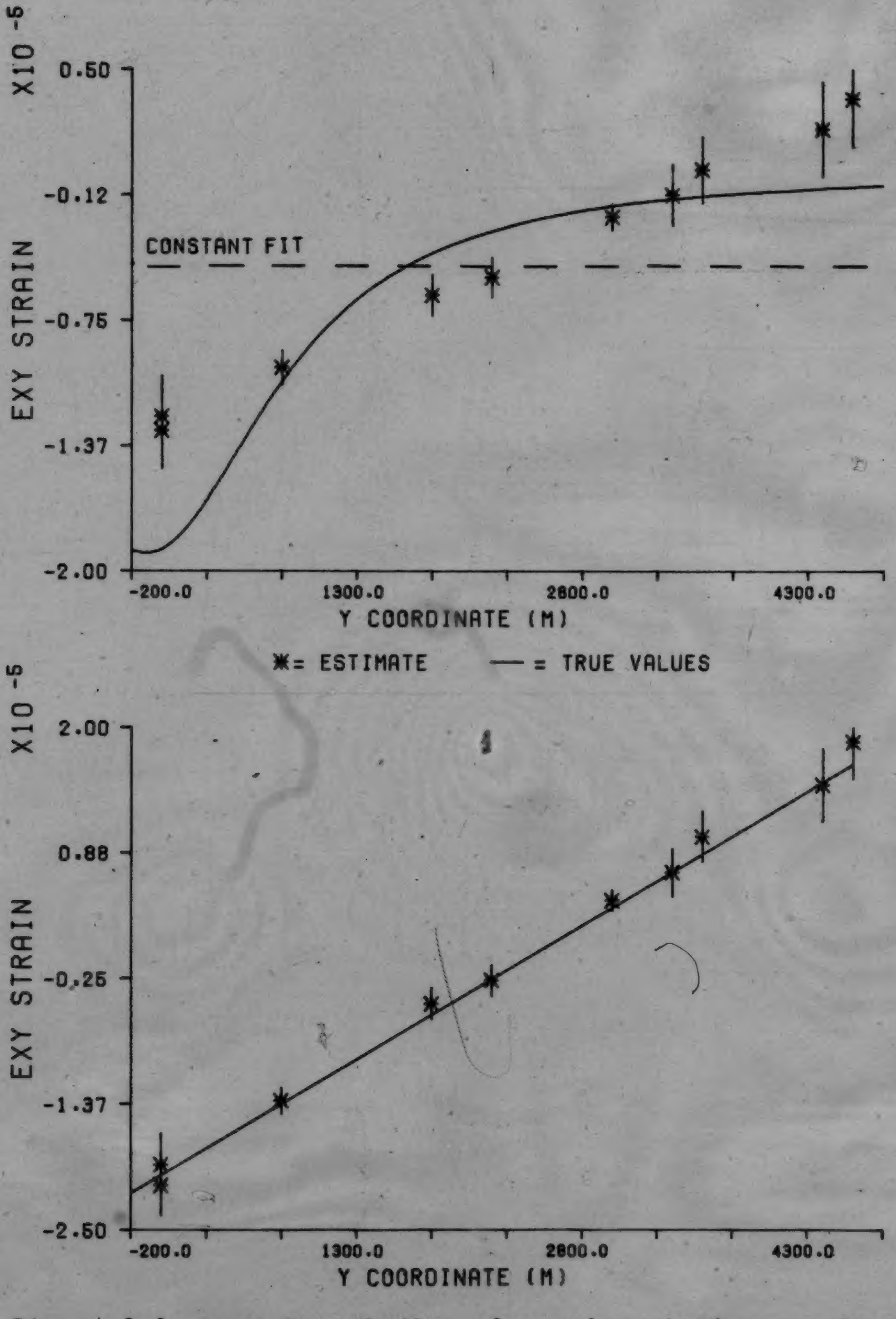

Figure 2.6 shows two studies of varying strain on network G10 using a varying strain model. In the lower figure, a linear strain is fitted with a linear model. The upper figure shows the shear strain expected from a locked strike slip fault 200 meters below the network fitted with constant and linear models. Error bars are 1 standard deviation.

value of the shear strain while a quadratic fit gives reasonable though slightly more scattered results. Both of these cases resulted in larger variance ratios than for the linear fit and can thus be discarded.

The study represented by the upper graph in figure 2.6 simulates an infinite, locked strike slip fault located 100m below points 1 and 2 (at y coordinate -100.). Chinnery (1961) used the results of Steketee (1958) to derive general expressions for the displacement field of a finite strike-slip dislocation. The limiting forms for an infinite strike-slip fault locked to a depth 'd' are easily obtained from Chinnery's expressions. Upon differentiaton, the shear strain for such a fault can be shown to be:

$$e_{xy} = -\frac{u}{2\pi d}\left(1 + y^2/d^2\right)^{-1} \qquad 32$$

where u is the magnitude of the displacement dislocation, y is the perpendicular distance from the fault, and the minus sign indicates left lateral shear. Choosing u=.012m and d=1km gives the synthetic strain shown on the graph. Fitting a constant strain model to this data gives exy=-4.75 ± .23 microstrains (shown by the horizontal line on the graph) and a variance ratio of 4.2. This high variance ratio is an indication that the constant model does not adequately represent the data. The actual mathematical average shear strain across the network was -2.98 microstrains. That the estimate achieved is slightly high is perhaps due to the loss of information on strains below the noise level.

The strain estimates plotted on the upper graph represent a linear fit to the data which achieved a variance ratio of .945. The linear trend of the actual shear strain is quite well defined by this model and the variance ratio lends support to this conclusion. These data proved to be inadequate for higher order resolution. A quadratic fit yields a smaller variance ratio however standard deviation estimates become so large the results are ambiguous. Deletion of small singular values before forming the pseudo-inverse reduces the standard deviations but I have found that the loss of resolution is generally large enough to yield results of questionable value.

### 2.3.2 Analysis of Survey Data from Huancayo

Most of the results described in this section have been obtained from distance measurements only. As discussed previously, there is little gain in resolution when using angle measurements. Additionally, the 1977 and 1978 surveys measured directions and not angles. Angles estimated from these directions were found to have considerably larger error estimates (Chrzanowski 1978) than angles measured directly in the field.

Table 2.3 shows a constant strain fit to the first three surveys using both distances and angles while table 2.4 gives the results of a more comprehensive study for all four surveys using only distances. A comparison quickly

CONSTANT STRAIN FIT TO HUANCAYO DATA

| SURVEYS COMPARED | EXX STD DEV | EXY STD DEV | EYY STD DEV | VARIANCE RATIO |
|---|---|---|---|---|
| 75-76 | -.23<br>1.18 | -2.86<br>1.04 | 1.28<br>2.22 | 1.1751 |
| 76-77 | .16<br>.98 | 1.62<br>.91 | -.78<br>1.96 | .85403 |
| 75-77 | -.11<br>1.40 | -.15<br>1.30 | .54<br>2.80 | 1.1101 |

Table 2.3 displays the fit of a constant strain model to the Huancayo survey data. Both distances and angles were used. All strains are in microstrains.

CONSTANT STRAIN FIT TO HUANCAYO DATA

| SURVEYS COMPARED | EXX STD DEV | EXY STD DEV | EYY STD DEV | VARIANCE RATIO |
|---|---|---|---|---|
| 75-76 | -.23<br>1.34 | -2.96<br>1.28 | 1.26<br>2.78 | .98228 |
| 76-77 | .35<br>1.01 | .93<br>.95(.85) | -1.56<br>2.09 | .79528 |
| 77-78 | .72<br>1.19(.85) | 1.92<br>1.12(.80) | .79<br>2.45 | .50882 |
| 75-77 | .10<br>1.49 | -1.88<br>1.43(1.23) | -.50<br>3.09 | .74541 |
| 75-78 | 1.07<br>1.49(1.36) | .56<br>1.43 | -.58<br>3.09 | .84078 |
| 76-78 | 1.35<br>1.01 | 3.16<br>.95 | -1.34<br>2.09 | 1.0406 |

Table 2.4 shows the fit of a constant strain model to the Huancayo data using distances only. All strains are in microstrains. Standard deviation estimates in brackets are corrected to agree with the variance ratio.

shows why I de-emphasize the angle measurements.

In both of these studies, all singular values were used. With synthetic data, I have found that deletion of singular values at the constant strain level before forming the pseudo-inverse can lead to incorrect conclusions. This is because the smallest singular value is, in this case, the primary determinant of the strain eyy. If it is deleted, a major decrease in resolution occurs. Thus, deletion of the last singular value in these studies gives some additional information but of doubtful reliability. For example, in table 2.4, if the 1975 1976 comparison is conducted in this fashion, we obtain exx=-.03 ± 1.13, exy=-2.99 ± 1.28, and eyy=.48 ± .33 (all in microstrains) with a variance ratio of .98451. Though the standard deviation estimate for eyy is considerably reduced, a definitive statement is impossible due to loss of resolution. Table 2.5 shows results obtained by deleting the smallest singular value from each of the studies in table 2.4.

Table 2.4 documents a remarkably consistent strain event over the entire three year period spanned by the surveys. The low variance ratios found indicate that the data fit a constant strain model remarkably well. In fact, the 1977 1978 standard deviations should be reduced by 25% and the 1976 1977 and 1975 1977 standard deviations are perhaps 10% too large. I regard three of the shear strain estimates as significant at the 95% confidence level (1975 1976, 1977 1978, and 1976 1978) and three additional

CONSTANT STRAIN FIT TO HUANCAYO DATA

| SURVEYS COMPARED | EXX STD DEV | EXY STD DEV | EYY STD DEV | VARIANCE RATIO |
|---|---|---|---|---|
| 75-76 | -.03<br>1.13 | -2.99<br>1.28 | .48<br>.33 | .98451 |
| 76-77 | .04<br>.86 | 1.04<br>.93 | -.37<br>.37 | .80423 |
| 77-78 | 1.09<br>1.03 | 1.71<br>1.07 | -.67<br>.58 | .51845 |
| 75-77 | -.10<br>1.26 | -1.85<br>1.42 | .27<br>.37 | .74715 |
| 75-78 | .88<br>1.26 | .59<br>1.42 | .13<br>.37 | .84227 |
| 76-78 | 1.23<br>.86 | 3.20<br>.93 | -.87<br>.37 | 1.0420 |

Table 2.5 shows a repeat of the study of table 2.4 but here the pseudo inverse was formed after the last (smallest) singular value was deleted. All strains are in microstrains.

estimates as significant at the 68% level (exy for 1976 1977, exy for 1975 1977, and exx for 1976 1978).

Between the 1975 and 1976 the network experienced a left lateral shear of exy= -2.96 ± 1.28 microstrains. Over the next two years another event, which could be a response to the first one, negated the initial straining such that a comparison of the 1975 and 1978 surveys shows no measureable strain. The 1976 1978 comparison shows a right lateral shear of exy= 3.16 ± .95 microstrains and a possible tensional exx= 1.35 ± 1.01 microstrains.

This compensatory event seems to have occurred very uniformly with time as is indicated by further examination of table 2.4. The 1977 1978 comparison yields strain estimates that are (within error bounds) half of the 1976 1978 estimates. The conclusion of temporal uniformity is further bolstered by the 1975 1977 comparison which shows a shear strain level of about half of the initial event. The 1976 1977 comparison, though inconclusive by itself, is entirely consistent with this interpretation.

The results of table 2.5 are consistent with table 2.4 and suggest a bit of additional information. If table 2.5 is taken at face value then the tensional exx measurement of 1976 1978 is enhanced and another tensional exx measurement (1977 1978) is significant at the 68% level. Also a possible pattern in the eyy estimates suggests tensional straining during the initial 1975 1976 event and compressional straining thereafter. The tensional exx estimates could be regarded as an elastic (or Poisson) spreading parallel to the fault caused by compression perpendicular to the fault. Though these conclusions are internally consistent, I hesitate to place too much reliance on them.

I advance the following kinematic model as an interpretation of these measurements:

1. Between 1975 and 1976 the Huancayo network and surroundings experienced a left lateral shear strain event of about -3 microstrains. This was not accompanied by any measurable exx straining but was possibly associated with tension (or a reduction of compression) perpendicular to the fault. Though this shear event is consistent with the 1969 Pariahuanca earthquakes (Deza 1971) we are unable to establish any specific relationship between them at this time.
2. From 1976 to 1978 the local strain state moved uniformly (in time) back to the state that existed just prior to the 1975 survey. A right lateral shear strain of about +3 microstrains occurred during this time span and was associated with a probable tensional straining parallel to the fault and some evidence of compression perpendicular to it.

# 3. Highlights of the Tectonic History of South America

## 3.1 Introduction

Geodesy can be a valuable tool for the direct measurement of earth deformation. It would be desirable to transform this purely kinematic description into meaningful constraints on physical models of the earth. Such models might include studies of the dynamics of faulting or small scale plastic deformation of the crust. On a larger scale, it might eventually prove possible to combine the results from a great many small networks with satellite-based laser ranging to model the instantaneous response of the tectonic plates to applied forces. Additionally, it is conceivable that geodetic networks may be valuable in monitoring the possible accumulation of tectonic strain before a major earthquake.

Interpretation of geodetic results must be guided by detailed understanding of the tectonic evolution of the land on which the network rests. Accordingly, a portion of this thesis is devoted to a study of the tectonic history of South America. It is virtually impossible to give a complete description of the state of modern knowledge on this subject. This is so, not only because many investigators have worked on elements of this problem, but also because of the vast extent in space and time of South America and the complexity of its structure. Therefore, this study covers only the past 200 million years since the beginning of the disruption of the Gondwana continent, and concentrates on certain areas I believe to be the locales of key tectonic events in South America. As a result, certain areas such as the Central Andes have received more attention than, say, the northernmost Andes of Colombia and Venezuela. Certainly such practices are dangerous but they are a practical necessity. One can only hope that the information gained from a detailed study of one region will be of more general applicability.

In this chapter I discuss the current state of knowledge of the tectonic history of the continent. Regions selected for special emphasis are the Andes of Peru and Northern Chile (down to about 30°S) and the vast subsiding basins of eastern Bolivia, Paraguay, southern Brazil, and northeastern Argentina. The history and areal distribution of volcanism and plutonism will be examined and modern ideas on the mode of emplacement of these magmas will be presented. Present knowledge of the history of tectonic movements will then be outlined together with a discussion of their possible structural control. Finally, the spatial distribution of seismicity beneath western South America and its plate tectonic interpretation will be summarized. In chapter 4, I present a plate tectonic model which appears to place much, but not all, of South American tectonics in a systematic framework.

In Chapters 3 and 4 "Peruvian Andes" will refer to that section of the Andes between the Huancabamba Deflection and the Pisco Deflection (figure 3.1a), from approximately the Peru-Equador border to about 15°S. "Central Andes" will refer to that portion of the Andean Cordillera between the Pisco Deflection and about latitude 30°S.

An accurate assessment of the capacity of plate tectonics to explain major continental geologic and tectonic features requires the comparison of morphology and setting of these structures with the spherical geometric principles of plate tectonics. The maps shown in this thesis were computer generated with a FORTRAN program which has the following capabilities:

1. Produces a transverse Mercator projection of an arbitrary quadrilateral on the earth's surface formed by four intersecting lines of latitude and longitude. All maps displayed in this thesis had a center of projection located at the physical center of the map, thus producing a relatively distortion-free map for the small surface areas considered.
2. Allows the display of any number of spherical coordinate systems in addition to normal latitude and longitude. For plate tectonics studies, this means that flow lines about relative motion poles can be shown on the plot.
3. Allows the display of sets of digitized earth features. A smooth curve is drawn through such input points using a cubic spline interpolation scheme.
4. Allows the display of epicenters of earthquakes in either magnitude or depth coded displays.

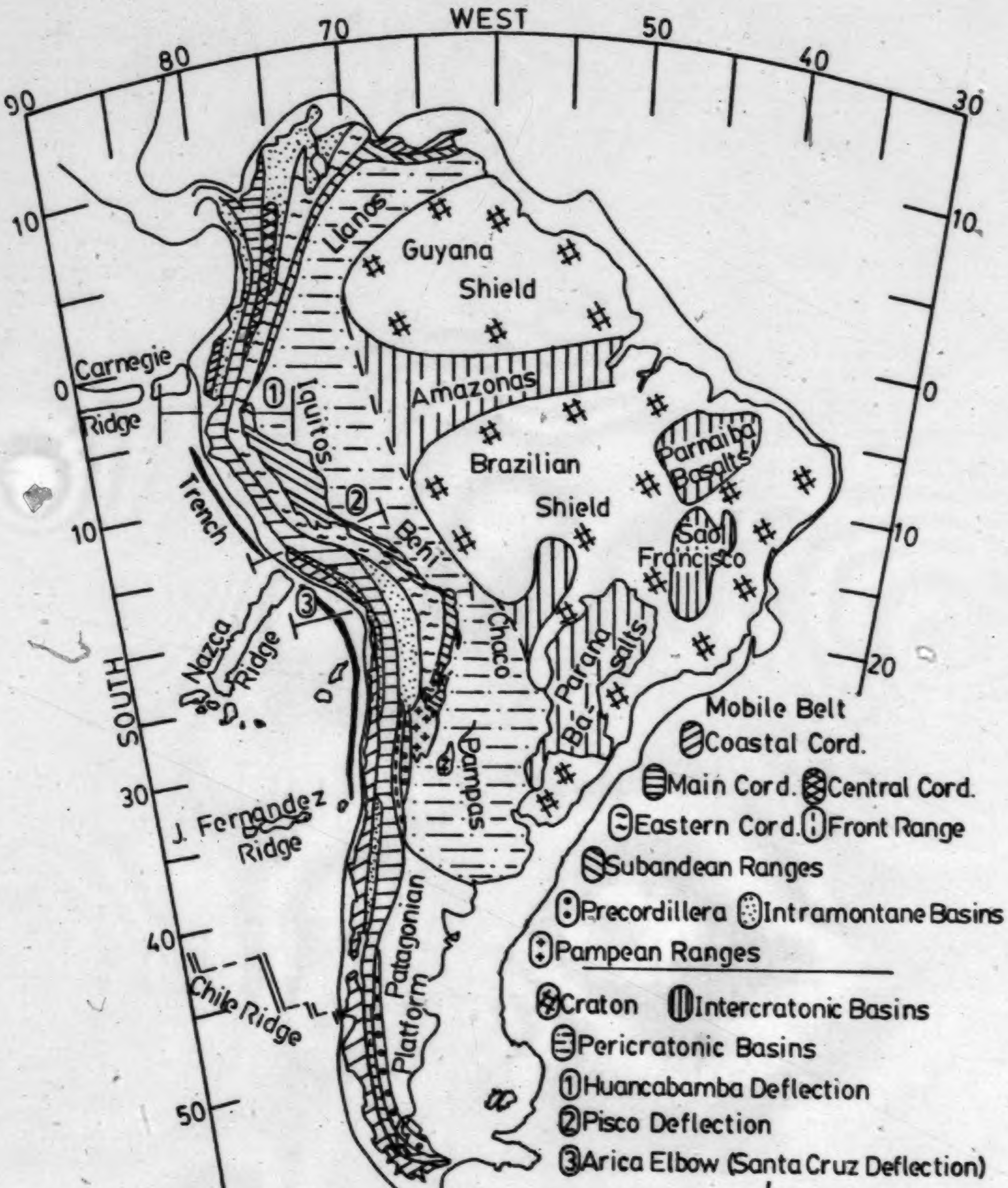
WEST
90
80
70
50
40
30
10
0
10
20
SOUTH
30
40
50
WEST
80
40
Carnegie Ridge
Trench
Nazca Ridge
J. Fernandez Ridge
Chile Ridge
Llanos
Guyana Shield
Amazonas
Iquitos
Beni
Brazilian Shield
Parnaiba Basalts
Sao Francisco
Chaco
Parana Basalts
Pampas
Patagonian Platform
①
②
③
Mobile Belt
Coastal Cord.
Main Cord.
Central Cord.
Eastern Cord.
Front Range
Subandean Ranges
Precordillera
Intramontane Basins
Pampean Ranges
Craton
Intercratonic Basins
Pericratonic Basins
① Huancabamba Deflection
② Pisco Deflection
③ Arica Elbow (Santa Cruz Deflection)

Figure 3.1a is a generalized structure map for the South American continent. Andean morphology is adapted from Aguirre et. al. (1974). The remainder of the map is from numerous sources. Boundaries drawn for the Parnaiba and Parana basins conform to the mapped extent of the mesozoic basalts.

Most of the tectonic and geologic features shown on maps in this thesis were digitized using about two points per degree. The actual point density used may vary by a factor of two depending on the desired accuracy and the complexity of the structure. Using the Tectonic Map of South America (UNESCO 1978), major plutons, major volcanic flows, major salars and lakes, the outline of the Subandean foredeep basin (or Subandean Cordillera), the outlines of the uplifted Pampean basement blocks, and locations of active volcanoes were digitized between 5°S and 30°S. The continental coastline was digitized from a standard National Geographic Society map.

## 3.2 General Plate Tectonic Setting

### 3.2.1 The Nazca Plate

Between the equator and 30°S the Nazca Plate subducts beneath the South America. (The collision zone between the two plates actually extends to 46°S but central and southern Chile will be only briefly discussed.)

The Nazca Plate is bordered by South America on the east, the Pacific Plate on the west, the Cocos Plate to the north, and in the south the Antarctic Plate. The actual boundaries are well determined by earthquake zones and major tectonic features. The $15 \times 10^6$ km$^2$ Nazca Plate has east and west boundaries formed by the Peru-Chile Trench and the East Pacific Rise respectively. Northern and southern boundaries are the Galapagos Rift Zone and the Chile Rise.

The relative motion pole for the South American and Nazca plates is approximately 59.08°W and 94.75°N (Minster and Jordan 1978). Figure 3.1b shows the same area of the earth as figure 3.1a with a spherical coordinate system drawn about this pole superimposed on the subduction zone. The small circles are labeled with the number of degrees from the pole and give the direction of relative motion which is maximum 90° from the pole. Subduction in Chile is oblique in the dextral sense while it is oblique in the sinistral sense in Peru.

The relative motion pole for the Nazca and Pacific plates (i.e. the pole of spreading for the East Pacific Rise) is located near 56.64°W and 87.88°N (Minster and Jordan 1978). Figure 3.1c shows a spherical coordinate system about this pole and is included for comparison with figure 3.1b. Since these poles are quite close together, the flow lines generated about each are quite similar and the relative motion between the Pacific and South American plates is very small.

### 3.2.2 Aseismic Ridges on the Nazca Plate

There are at least 3 significant aseismic ridge structures on the Nazca Plate or its boundaries (figure 3.1 b or c). Two of these, the Carnegie Ridge and the Juan Fernandez Ridge, are aligned approximately in the direction of subduction (or the direction of spreading on the East Pacific Rise). The third, the Nazca Ridge is oblique to the

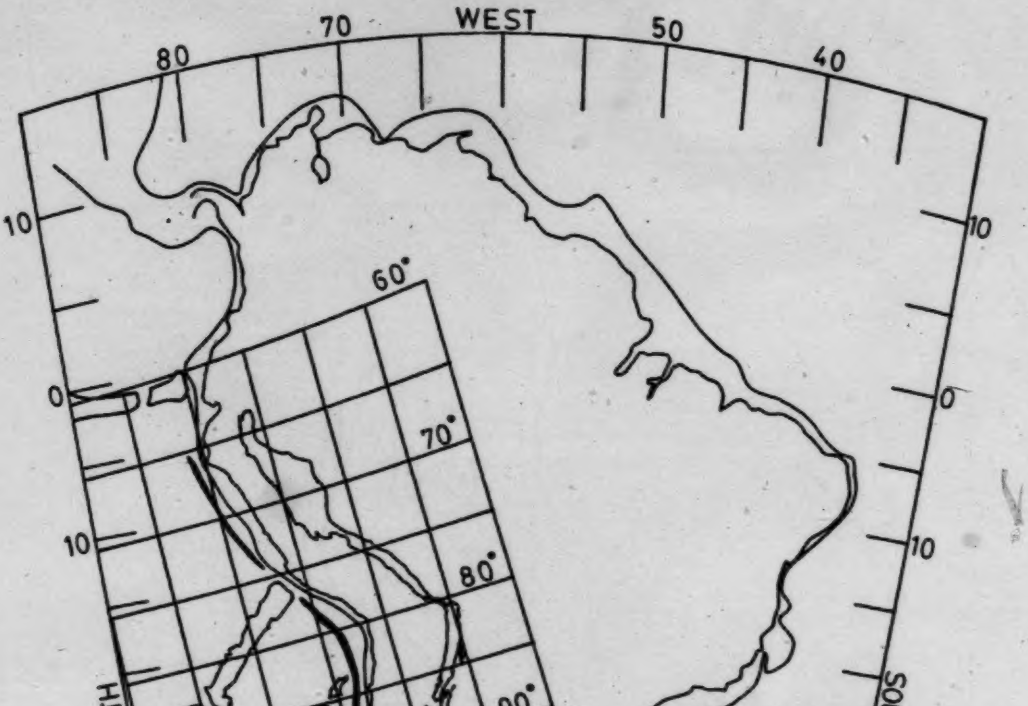
WEST
80
70
50
40
10
0
10
SOUTH
30
40
50
60°
70°
80°
90°
80°
WEST
80
40

Figure 3.1b shows a spherical polar coordinate system drawn about the pole of relative motion for the Nazca and South American plates superimposed on the South American subduction zone. Small circles are labeled with their angular distance from the pole. Pole location is from earth model RM2 of Minster and Jordan (1978): 94.75°W and 59.08°N.

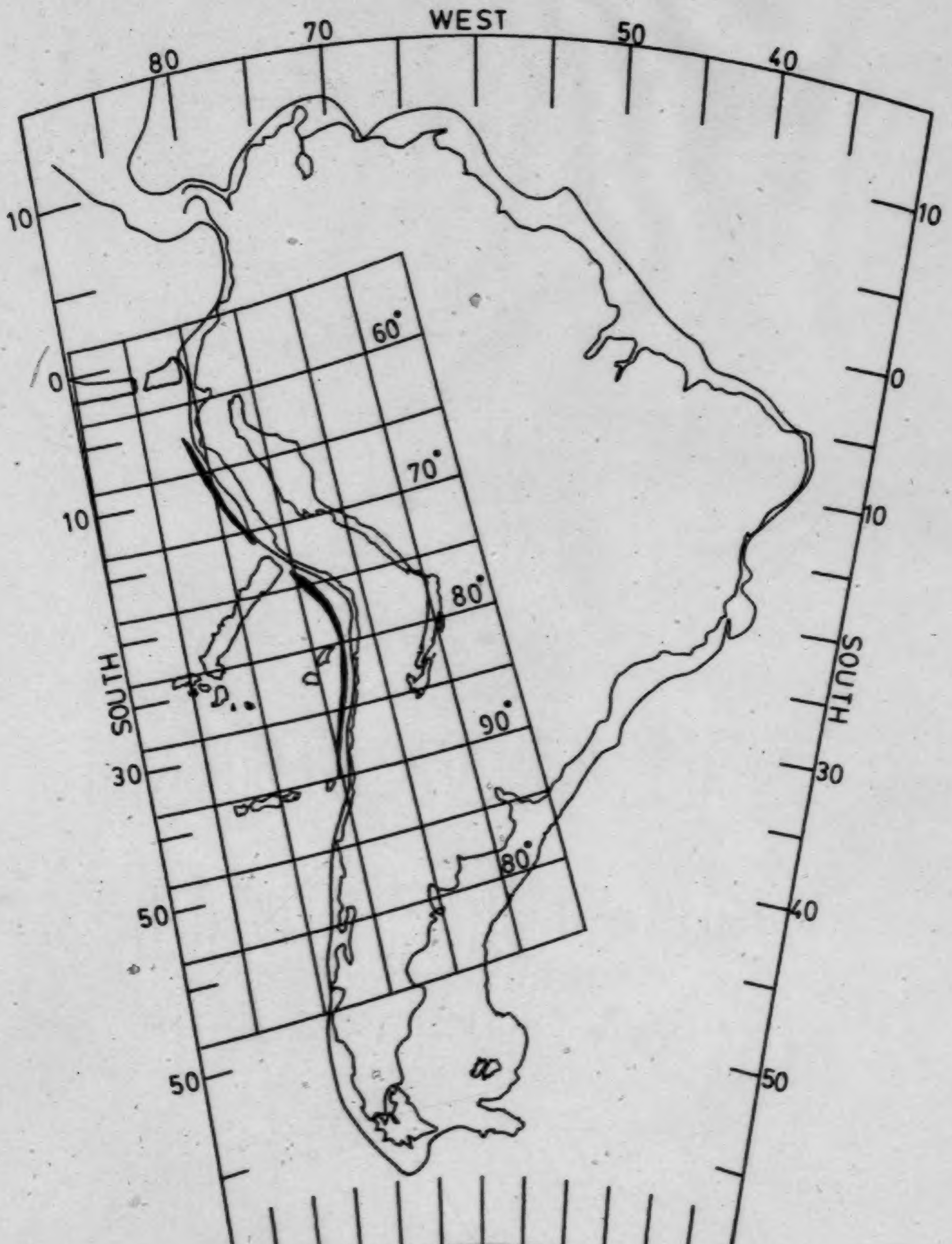
WEST
80
70
50
40
10
0
10
SOUTH
30
50
50
10
0
10
SOUTH
30
40
50
60°
70°
80°
90°
80°
WEST
80
40

Figure 3.1c is similar to 3.1b except that a coordinate system about the relative motion pole for the Nazca and Pacific plates was used. Pole position is 87.88°W and 56.64°N after Minster and Jordan (1978).

subduction direction. The group of seamounts just south of the Nazca Ridge, sometimes called the Sala y Gomez Ridge, is also aligned with the subduction direction.

These aseismic ridges, and other similar structures worldwide, are often spatially associated with anomalies in the subduction process (Vogt et al. 1976, Kelleher and McCann 1976). The Nazca Ridge in particular is associated with one of the major structural transition zones in the Andes, the Pisco Deflection.

Cutler (1977a&b) found that a crustal model similar to the Iceland-Faroes complex best fits the available data for the Nazca Ridge. This ridge model shows typical oceanic crustal layers but each has been anomalously thickened. A crustal root extends down to about 20 km making the effective thickness of the Nazca Ridge at least double that of ordinary oceanic crust. Thus it is not only more buoyant but will be considerably more rigid. Since the flexural rigidity of a thin elastic plate increases with the third power of the thickness, an aseismic ridge will make an oceanic plate more resistant to flexure about an axis perpendicular to the ridge. The ridge will have little effect if the axis of bending is parallel to the strike of the ridge.

The Emperor Seamount chain shows only one thickened layer and is well modeled as a basalt load poured out on a pre-existing oceanic plate (Walcott 1976). On the other hand the Nazca Ridge appears to have been created at a very productive spot (hot spot) on a spreading ridge. The Carnegie and Cocos ridges are also of this type. It has been suggested (e.g. Cutler 1977b) that the Tuamotu Ridge is an image ridge for the Nazca Ridge similar to the Walvis Ridge - Rio Grande Rise pair.

### 3.2.3 The South American Plate

Figure 3.1a is a generalized structure map of the South American continent. The Andean morphology is adapted from Aguirre et al. (1974) while the remainder of the map comes from numerous sources detailed in the references. The boundaries shown for the Parana and Parnaiba intercratonic basins correspond to the approximate limits of their Mesozoic basalt flows.

Figure 3.2 is a sketch map of Andean morphology for the region between 5°S and 35°S. A distinction is made between the Peruvian Andes and the Central Andes because they show very different structure and history and their boundaries are major tectonic features. Many authors have recognized that the Andes show significant longitudinal variation and numerous sets of tectonic boundaries have been proposed (Ham and Herrera 1961, Deza 1970, Gansser 1973, Sillitoe 1974, Kulm et al. 1977, Megard and Philip 1976 and others). The broad zonation proposed here is consistent with most authors.

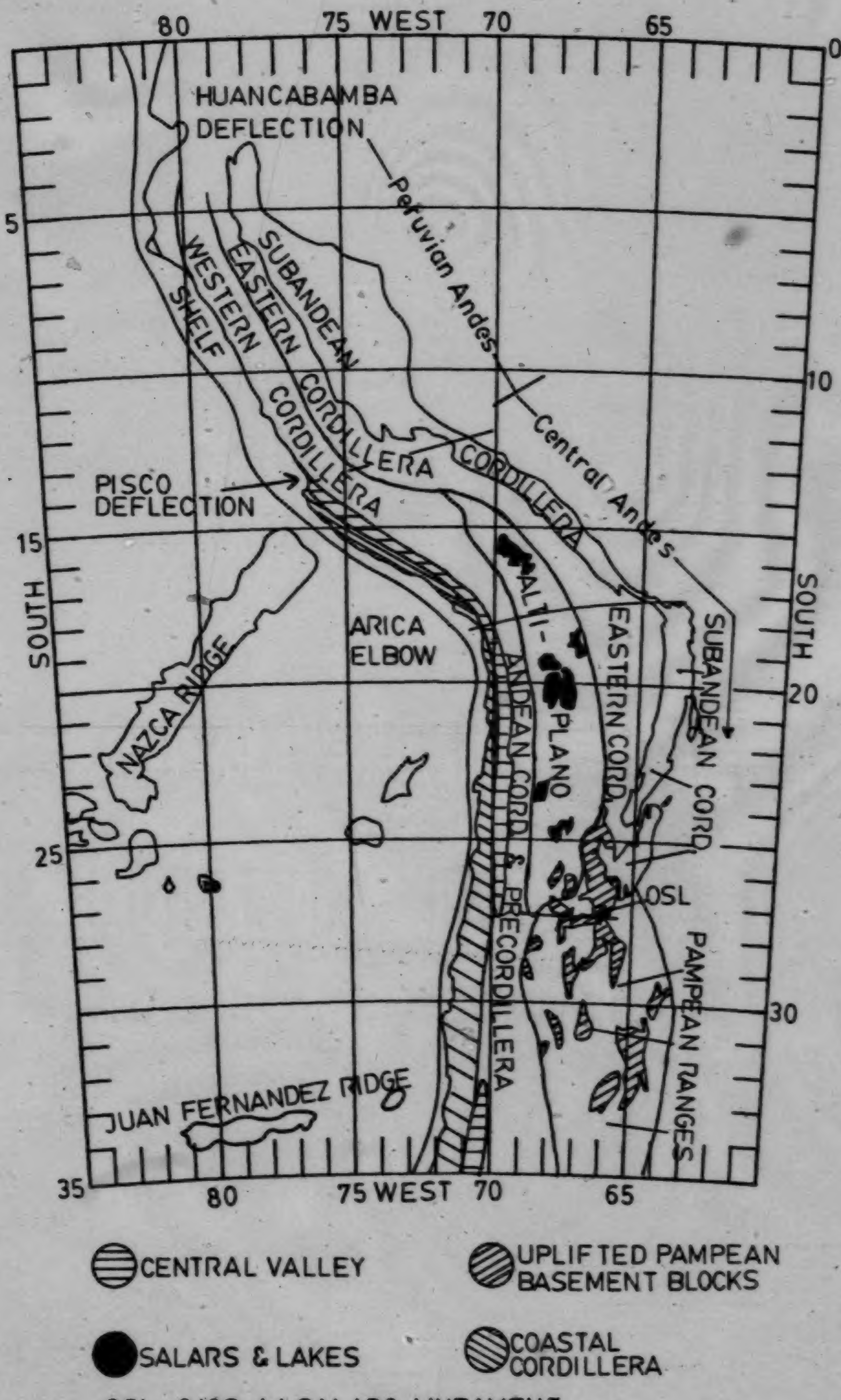
80
75 WEST
70
65
0
5
10
15
20
25
30
35
SOUTH
SOUTH
80
75 WEST
70
65
HUANCABAMBA
DEFLECTION
Peruvian Andes
Central Andes
SUBANDEAN
EASTERN
WESTERN
SHELF
CORDILLERA
CORDILLERA
CORDILLERA
PISCO
DEFLECTION
ARICA
ELBOW
NAZCA RIDGE
ALTI-
PLANO
EASTERN CORD
SUBANDEAN
CORD
ANDEAN CORD & PRECORDILLERA
OSL
PAMPEAN RANGES
JUAN FERNANDEZ RIDGE
CENTRAL VALLEY
UPLIFTED PAMPEAN
BASEMENT BLOCKS
SALARS & LAKES
COASTAL
CORDILLERA
OSL: OJOS del SALADO LINEAMENT

Figure 3.2 is a structural map for the Andes between 5°S and 35°S.

### 3.2.4 The Huancabamba Deflection

The Huancabamba Deflection at about 5°S (Ham and Herrera 1961, Gansser 1973, Sillitoe 1974) is the northern boundary of the Peruvian Andes. Gansser (1973) says that the region shown on figure 3.2 as the Huancabamba Deflection is also known as the Amotape Zone. Sillitoe (1974) refers to this region only as the Amotape zone and reserves the name Huancabamba Deflection for a smaller deflection near Santa Cruz (northern Peru) at about 6°S. Ham and Herrera (1963), while not using the term Amotape Zone, are in agreement with Gansser. Here the term Huancabamba Deflection will refer to the entire region from 3°S to 8°S which displays similar "anomalous" structure.

The east-west aligned Carnegie Ridge, the northeast trending Colombian Andes, and the southeast striking Peruvian Andes meet in roughly a 120° triad at the Huancabamba Deflection. East-west striking structures predominate (Gansser 1973) and the Quaternary volcanism of Colombia ends here (Barazangi and Dorman 1969, Megard and Philip 1976, Gansser 1973 and others) (figure 3.10). It has been suggested that the Carnegie Ridge, Huancabamba Deflection, Amazon Basin, and the Romanche Fracture Zone form a continuous trans-continental shear zone (Carey 1958).

### 3.2.5 The Pisco Deflection

The boundary between the Peruvian Andes and the Central Andes marks a major change in tectonic and structural style along the South American subduction zone (Ham and Herrera 1961, Deza 1970, Gansser 1973, Stauder 1975, Megard and Philip 1976, Barazangi and Isacks 1976), and is called the Pisco (or Abancay) Deflection. Figure 3.3 shows in detail some of the geological structure in the region of interest. The western end of the Pisco Deflection occurs at the Paracas Peninsula, just east of the juncture of the Nazca Ridge with the Peru-Chile Trench. This is also the northern limit of the Central Valley and the Coastal Cordillera of the Chilean Andes (figure 3.2) in which is found the Chilean Coastal Batholith of Jurassic to mid-Cretaceous age (Gansser 1973). The San Nicholas Batholith (possibly Jurassic) outcrops along the Paracas Peninsula with a structure that may imply a seaward extension onto the continental shelf (Pitcher 1974).

The Pisco Deflection is actually a broad transition zone within which structural changes occur (Megard and Philip 1976). This transition zone also appears in the seismicity beneath the continent. To the north, the Nazca Plate is probably underthrusting South America at about 10° which increases abruptly at the Pisco Deflection to about 30° through northern Chile (Barazangi and Isacks 1976). The Abancay fault system (trending east-west) has shown some recent vertical movement (Megard and Philip 1976) but the one earthquake focal mechanism which has been reported (Stauder 1975) shows strike slip motion with an east-west p axis.

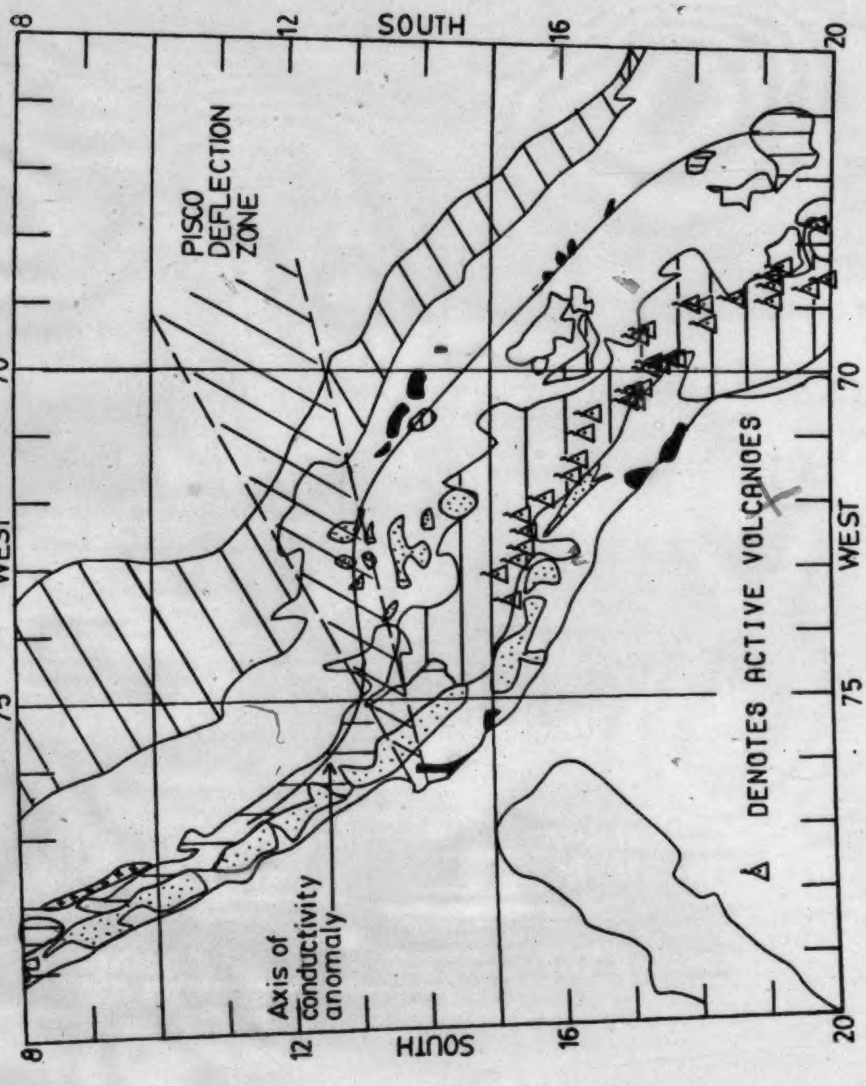
SOUTH
8
12
16
20
WEST
75
70
PISCO DEFLECTION ZONE
Axis of conductivity anomaly
Δ DENOTES ACTIVE VOLCANOES
SOUTH
WEST

Figure 3.3 shows geologic and tectonic features near the Pisco Deflection in southern Peru. See figure 3.4a for the key to symbols and shading. The Pisco Deflection is adapted from Megard and Philip (1976).

Other structural anomalies associated with the Pisco Deflection include the change in strike of the Andean ranges, the abrupt thickening of the continental crust from north to south (James 1971a and section 3.5.5), the east-to-west offset of the Andean fault system (Ham and Herrera 1961, Mapa Geologico del Peru, 1975), a similar offset of the axis of the anomaly of high conductivity beneath the Andes (Schmucker et al. 1964 and 1966), the sudden increase of Miocene to Recent volcanism from north to south (Noble et al. 1974, Baker and Francis 1978), and a shallowing of the Peru-Chile Trench between the Nazca Ridge and the Paracas Peninsula.

## 3.3 Plutonism and Volcanism in the Peruvian Andes

The geological structures shown on figures 3.4 a and b are highly generalized with emphasis on magmatic formations. The primary source maps for these figures were the Tectonic Map of South America (UNESCO 1978), Mapa Geologico del Peru (1975), and Mapa Geologico de America del Sur (1964). They are not complete geologic maps but show those features which seem to me to reflect key tectonic events.

The Peruvian plutons consist of 3 separate batholiths (Pitcher 1974): the San Nicholas Batholith, the Peruvian Coastal Batholith, and the Cordillera Blanca Batholith. Little is known about the San Nicholas Batholith which has only two major outcrops in southern Peru. It may be Jurassic for it intrudes an upper Paleozoic formation and there is

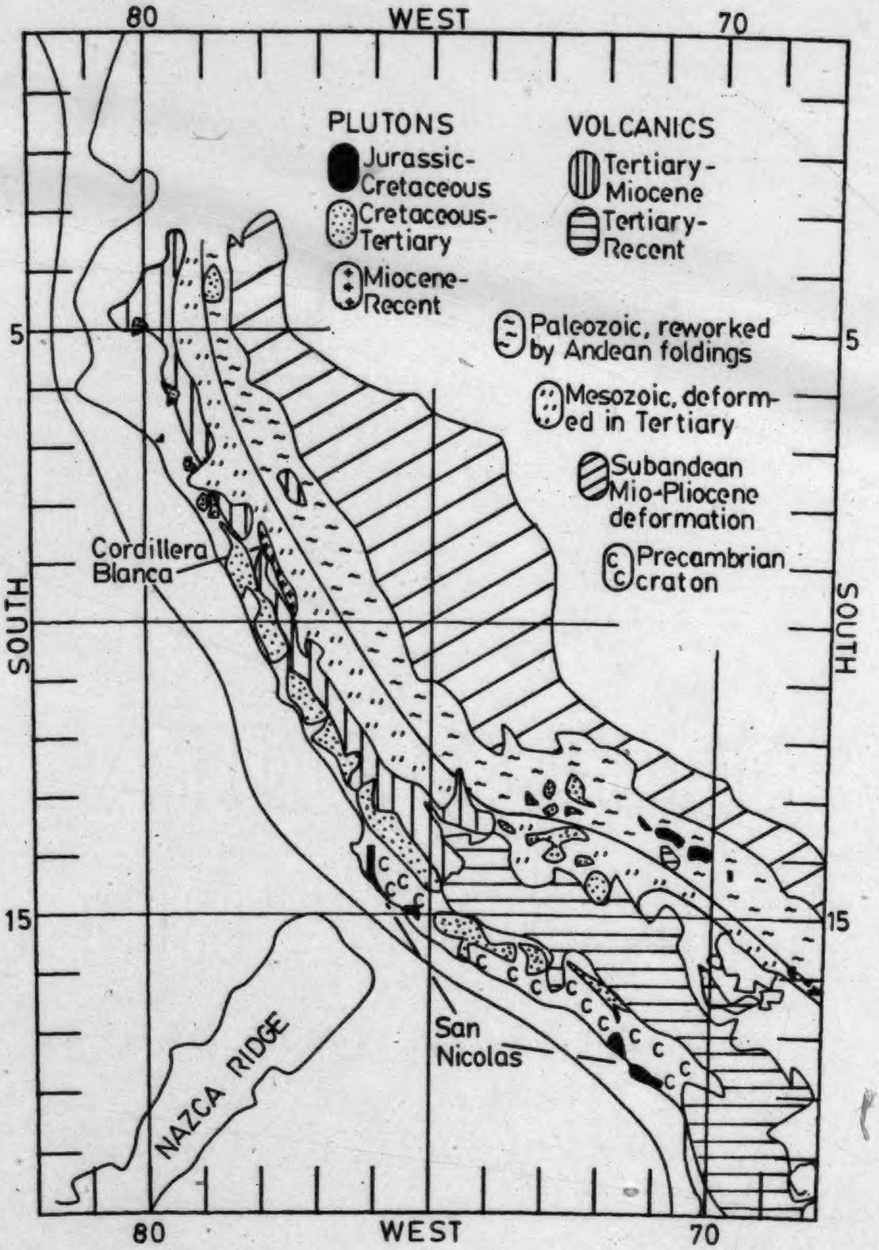
80
WEST
70
PLUTONS
Jurassic-Cretaceous
Cretaceous-Tertiary
Miocene-Recent
VOLCANICS
Tertiary-Miocene
Tertiary-Recent
Paleozoic, reworked by Andean foldings
Mesozoic, deformed in Tertiary
Subandean Mio-Pliocene deformation
Precambrian craton
5
5
SOUTH
SOUTH
Cordillera Blanca
15
15
San Nicolas
NAZCA RIDGE
80
WEST
70

Figure 3.4a is a generalized geological map for the Andes between 5°S and 15°S.

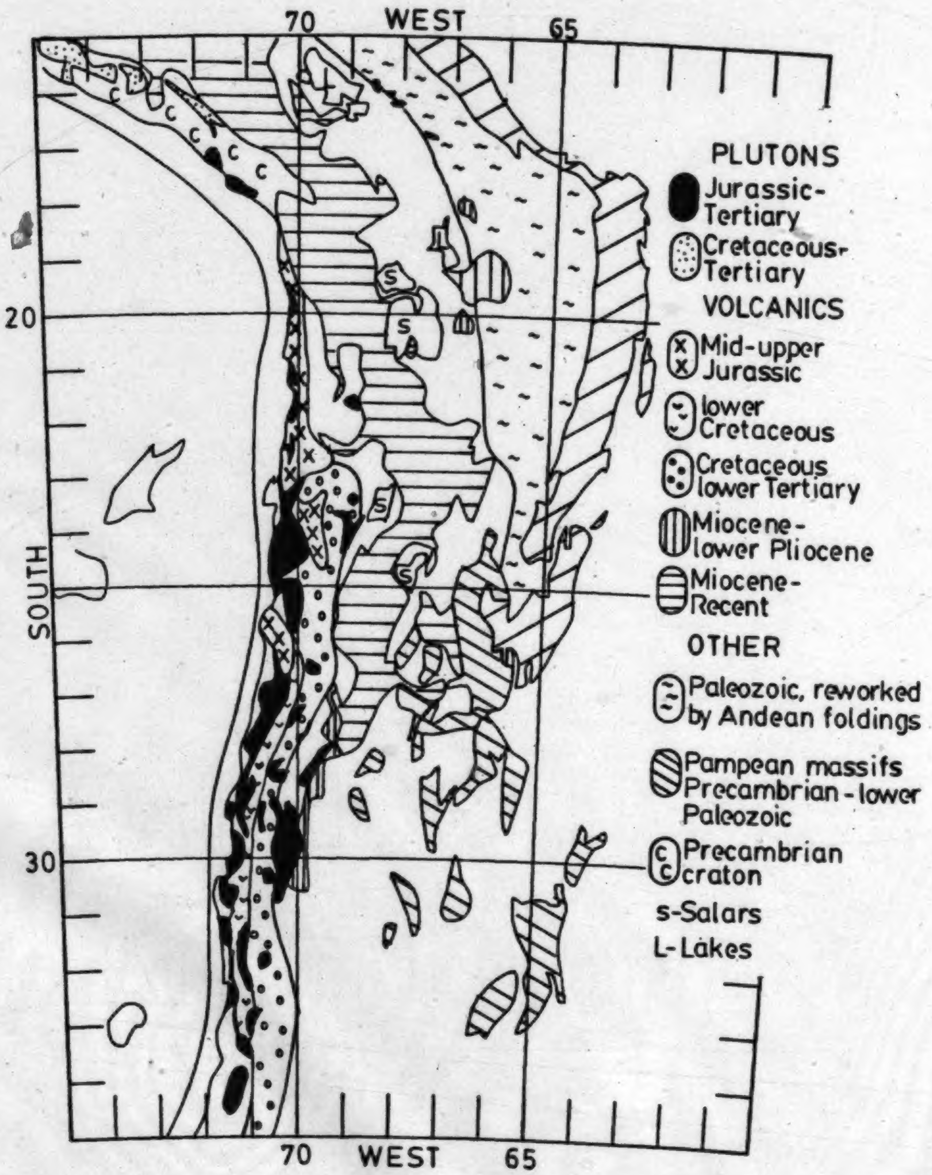
70
WEST
65
20
30
SOUTH
s
c
x
70
WEST
65
PLUTONS
Jurassic-Tertiary
Cretaceous-Tertiary
VOLCANICS
Mid-upper Jurassic
lower Cretaceous
Cretaceous lower Tertiary
Miocene-lower Pliocene
Miocene-Recent
OTHER
Paleozoic, reworked by Andean foldings
Pampean massifs Precambrian-lower Paleozoic
Precambrian craton
s-Salars
L-Lakes

Figure 3.4b is a generalized geological map for the Andes from 15°S to 35°S.

one Jurassic K-Ar age determination (Stewart et al. 1974).

### 3.3.1 The Peruvian Coastal Batholith and Associated Volcanism

The Peruvian Coastal Batholith was emplaced in a series of distinct pulses from the mid Cretaceous (about 105 ma) to the Paleocene (60 ma) (Cobbing and Pitcher 1972a, Noble et al. 1979) or even into the upper Oligocene (30 ma) (Pitcher 1978). It outcrops in a series of individual plutons averaging 50km by 100 - 200km. Emplacement was at a high level (Atherton and Brenchley 1972) in a thick sequence of Cretaceous basic to andesitic volcanics (Wilson 1963) whose lower members are marine showing black shales and pillow basalts (Cobbing and Pitcher 1972a). These volcanics are a major constituent of a deformed eugeosynclinal belt of volcaniclastics, some 3000m thick (Cobbing and Pitcher 1972a), occupying the coastal position in Peru from Trujillo in the north (8°S) to Pisco (14°S) where it strikes inland (Cobbing and Pitcher 1972b) (figure 3.5). These volcanics have been referred to as the Casma Formation (Cossio 1964, Myers 1975b) and the Quilmana Formation (Mapa Geologico del Peru, 1975), and were probably erupted between 100 and 95 ma (Myers 1975b). (See also figure 3.6b.)

To the east, the Peruvian Coastal Batholith is flanked by a thick pile of Cretaceous to lower Tertiary continental volcanics forming the crest of the Western Cordillera of Peru. This is referred to as the Calipuy Formation (Cobbing

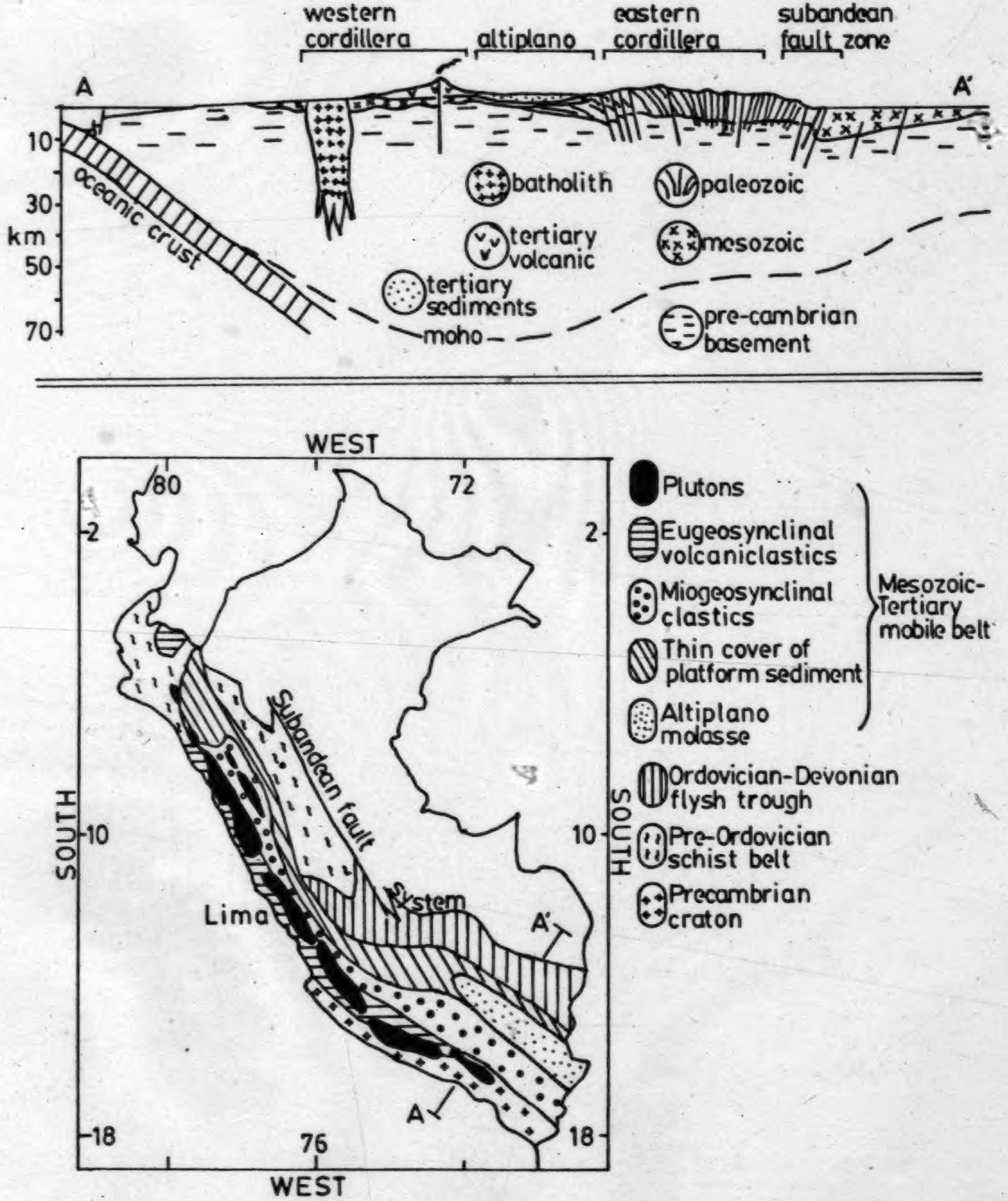
western cordillera
altiplano
eastern cordillera
subandean fault zone
A
A'
10
30
km
50
70
oceanic crust
moho
batholith
tertiary volcanic
tertiary sediments
paleozoic
mesozoic
pre-cambrian basement
WEST
80
72
2
10
18
76
SOUTH
Subandean fault System
Lima
A'
A
Plutons
Eugeosynclinal volcaniclastics
Miogeosynclinal clastics
Thin cover of platform sediment
Altiplano molasse
Mesozoic-Tertiary mobile belt
Ordovician-Devonian flysh trough
Pre-Ordovician schist belt
Precambrian craton

Figure 3.5 shows the geological structure of Peru as interpreted by E. J. Cobbing and W. S. Pitcher. The cross section is adapted from Cobbing and Pitcher (1972b) while the plan view is adapted from Pitcher (1978).

and Pitcher 1972a, Myers 1975b) and on the Mapa Geologico del Peru, 1975. These include the volcanics of the late Eocene - early Oligocene (41ma to 35ma) "Incaic" orogenic pulse (Steinmann 1929,Noble et al. 1979). The Calipuy Formation rests unconformably on intensely folded and faulted rocks of a Mesozoic miogeosyncline (Cobbing and Pitcher 1972b, Pitcher and Bussell 1977, Cobbing 1978, Noble et al. 1979) known as the Casapalca Formation composed of middle to upper Cretaceous marine sedimentary facies and continental sediments and volcaniclastics of upper Cretaceous to lower Tertiary age (Mapa Geologico del Peru, 1975). The volcaniclastics are the dominant sequence of the Casapalca Formation and are presumably erosives from the uplifted volcanic pile to the west (Noble et al. 1979). A major erosional unconformity (the "post Incaic unconformity" e.g. Noble et al. 1979) separates the Calipuy Formation from the miogeosynclinal rocks. The Calipuy formation is dominantly composed of andesites, rhyolites, and tuff (Cobbing and Pitcher 1972a, Noble et al. 1979). The contact between the Peruvian Coastal Batholith and the Calipuy Formation, the Tapacocha Axis (Myers 1975b), is quite sharp and is thought to represent part of a system of megafractures extending down through the continental basement which provided an injection route for the magmas (Cobbing and Pitcher 1972a, Myers 1975b, Pitcher and Bussell 1977).

The Peruvian Coastal Batholith is composed of some 55%

tonalite, 32% granodiorite, 7% gabbro-diorite, and 4% granite on the average (Cobbing and Pitcher 1972a). Other notable features include:

1. High emplacement to within 3km (Myers 1975a) to 5km (Atherton and Brenchley 1972) of the surface.
2. Narrow contact metamorphic aureoles (averaging 100m or so (Cobbing and Pitcher 1972a)).
3. Regular spatial arrangement of the various rock types. The intermediate forms (tonalites) tend to occur in long strips flanked by smaller, more basic plutons (gabbros) (Cobbing and Pitcher 1972a). The gabbros are the oldest type having K-Ar ages ranging from 105-95ma (Wilson 1975) while the tonalites range in age range from 84 to 93ma.
4. Systems of associated dike swarms (Cobbing and Pitcher 1972a, Myers 1975a, Pitcher and Bussel 1977).

### 3.3.2 Emplacement of the Peruvian Coastal Batholith

The consensus of many studies of the Peruvian Coastal Batholith is that its emplacement was highly structurally controlled. Apparently the intrusives rose along very large fractures in the Precambrian basement parallel to the trench. Metamorphic contacts and local faulting show the same two preferred directions: N45°E and N35°W (Cobbing and Pitcher 1972a). Deep seated basement fractures may have controlled the tectonics of Peru from Mesozoic to Recent times (Pitcher and Bussell 1977). Since the Tapacocha Axis has been the site of nearly continuous magmatic activity over many millions of years there must be a deep structural link between the eruptive sites and the Benioff Zone. Cobbing 1978 postulates similar systems of fractures with the Tapacocha Axis and the Cordillera Blanca fault being major examples.

Pitcher (1978) combined these ideas and suggests:

1. The primary source mechanism for the magmas is the subduction of an oceanic lithospheric plate.
2. Basic igneous materials (the gabbros) are generated along the subduction zone.
3. These rise along pre-existing lines of weakness in the continental crust.
4. The magmas rise on these "feeder" fractures (my term) until, in the upper crust, conditions become favorable for lateral branching. The lateral expansion forces huge blocks of crustal material to subside. This is known as the cauldron subsidence model.
5. While the basic gabbros probably had mantle origin, the more acid granitoids probably represent either gabbros contaminated by sialic crust or melted and reactivated sial mobilized by heat from the gabbros.
6. Simple crystal differentiation is responsible for the evolution of all elements of the batholith regardless of where generated.
7. Volcanism was simultaneous with emplacement and represents "ejecta" forced to the surface.
8. The major axis of plutonic injection remained stable for

some 70 million years (from 100ma to 30ma).

9. Basic dikes represent fissures venting to the surface.

Aguirre et al. (1974) see a fundamental rhythmic interplay between tectonic style and intrusive phases. An initial period of no compression (or possible extension) during which plutonic intrusion and acid volcanism occur is followed by a short, amagmatic interval of compressive tectonism. A third, final period of no compression follows in which there is some volcanism together with rapid uplift and erosion.

### 3.3.3 Miocene to Recent Activity

After the late Eocene Incaic orogeny, the entire western South America mobile belt experienced a period of relative quiescence (Noble et al. 1974, Zentilli 1974). This quiet period lasted virtually the entire Oligocene. The resumption of activity in the Miocene seems to correspond, at least temporally, with the major change of oceanic spreading patterns in the East Pacific (Handschumacher 1976). In the Peruvian Andes, this change was manifested in the shifting of the site of plutonic injection eastward from the Tapacocha Axis to the Cordillera Blanca fault and by considerable volcanic activity. The volcanics marked Tertiary - Miocene on figure 3.4a are, in fact, dominantly Miocene.

The Miocene orogenic activity in Central Peru was much less intense than in the Central Andes, and Pliocene -

Quaternary activity is almost non-existent. There are no active volcanoes in Central Peru and Quaternary volcanism is generally spoken of as "absent." Nevertheless, there were a few events of importance. The Cordillera Blanca Batholith (figure 3.3a) of central Peru has yielded K-Ar age determinations between 12 and 2.7 ma (Stewart et al. 1974). The Cordillera Blanca Batholith is associated with dramatic uplift and some volcanism. There are some silicic and ash-flow tuffs found in the Cordillera Blanca with K-Ar ages near the Miocene-Pliocene boundary (Megard and Philip 1976). The relatively minor intrusives of the Cordillera Huayhuash (just south of the Cordillera Blanca), though undated, are probably of the same age as the Cordillera Blanca Batholith (Coney 1971).

Noble et al. (1974) report K-Ar ages in the early-middle Miocene (21 to 14 ma) for a series of samples from the Huancavelica Department in Peru all taken from the same general area (13°S and 75°W). These flows, and the associated Ayacucho Formation, (Mapa Geologico del Peru, 1975) are not extensive and not easily related to simple plate tectonics models (Megard and Philip 1976). Another very limited distribution of probable Miocene volcanics is found near Santa Cruz in northern Peru at about 6° to 7°S and 79°W.

Despite these examples, Pliocene - Quaternary volcanism in Central Peru is dwarfed by the massive eruptives of the same era beginning just south of the Pisco Deflection and extending the entire length of the Central Andes (Megard and Philip 1976) (figure 3.10). The major Miocene magmatic event was the emplacement of the Cordillera Blanca Batholith. Even this, however, is small in comparison to the coastal batholiths of Peru and Chile. It may be that the processes responsible for the Cordillera Blanca Batholith were either of vastly diminished strength or were of a different nature altogether than those which created the Peruvian Coastal Batholith.

### 3.3.4 Episodic Nature of Volcanism and Tectonism

Both volcanism and tectonism have occurred in a series of distinct "episodes" since at least the late Cretaceous (Noble et al. 1974). Figure 3.6a (adapted from their figure 2) shows at least three and possibly four temporally distinct peaks with magmatic maxima in the late Cretaceous (implied), late Eocene (41 ma), early Miocene (22 ma), and late Miocene (10 ma). This diagram also suggests a tendency for peaks in tectonic activity to slightly precede magmatic ones.

Figure 3.6b shows Pitcher's (1978) interpretation of this episodic sequence. These workers agree in general terms although the diagrams are not strictly comparable because they refer to different time spans and slightly different locales.

An interesting feature of figure 3.6b is the eastward migration of the pluton locations. This migration is not as

FIGURE A

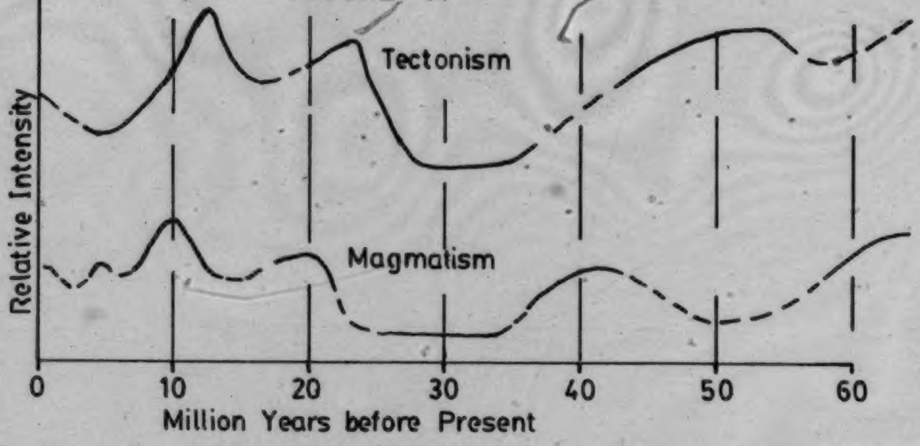

FIGURE B

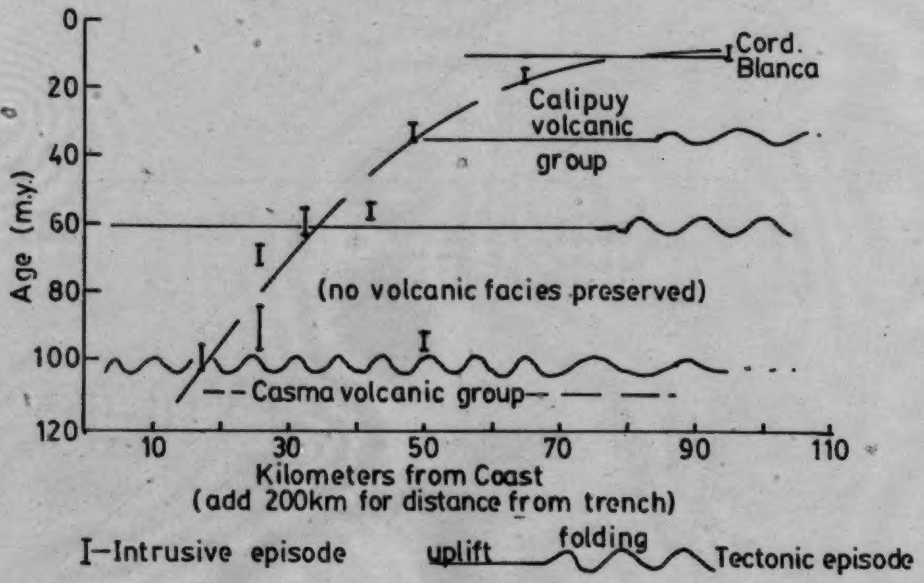

Figure 3.6 shows two views of episodic orogenic activity in Peru. Figure A is adapted from Noble et. al. (1974) and Figure B is modified from Pitcher (1978).

"distinct" as that found in northern Chile (section 3.6.2). Most authors (especially Pitcher, Cobbing and Myers) consider that the Peruvian Coastal Batholith emplacement took place on a single system of feeder fractures. Superficially however, this diagram would indicate an eastward migration of magmatic foci at an average rate of .75mm/yr. This is comparable to the rate in Chile (Clark et al. 1976).

## 3.4 Tectonics of Central Peru

### 3.4.1 Vertical Block Tectonics

An adequate tectonic model for Peru (Ham and Herrera 1961) incorporates dominantly vertical movements. The main cordillera were probably uplifted by motion along two major fault systems: a horst-graben system along the coast, and the Subandean reverse fault system along the eastern margin of the Eastern Cordillera. This general scheme of vertical motion and very little crustal shortening has been confirmed by numerous workers since then. A high-grade basement of Precambrian metamorphics under Peru makes the mobile belt highly resistant to horizontal compressive stresses (Cobbing and Pitcher 1972b, Cobbing et al. 1977) (figure 3.5).

Another model for the evolution of the Peruvian Andes since the Cretaceous (Myers 1975b) postulates dominantly vertical movements between a series of 7 crustal blocks. These blocks are a series of striplike assemblages which strike parallel to the coast. The suggested blocks include the oceanic plate, the continental shelf, and the elements of Cobbing's geosynclinal model of Peru (figure 3.5). The Tapacocha Axis, the injection route for the Peruvian Coastal Batholith, is also a boundary between two of these blocks.

Cobbing's model is similar to that proposed by Myers but involves a greater number of strips in the area of Cobbing's special interest, the eugeosynclinal - miogeosynclinal belt. He also takes issue with Myers on the tectonic importance of the Tapacocha Axis, arguing that it is secondary to the Cordillera Blanca fault. Both workers agree that the Peruvian Andes are everywhere underlain by a structurally rigid basement of Precambrian metamorphics (Cobbing and Pitcher 1972b, Cobbing et al. 1977) which resists significant horizontal deformation. Instead, plate margin forces (arising from the subduction-collision process) fracture the basement. Myers contrasts this model with the broad deformation found in the North American Cordillera which, he asserts, is due to lack of a rigid basement.

Cobbing (1978) compares the Peruvian structure with the Alpine orogenic structure and notes such differences as:

1. A general absence of ophiolite assemblages in Peru.
2. Andesitic volcanism and granitic plutonism (dominantly tonalite) are the major manifestations of magmatism in the Andes (and are perhaps common to all circum-Pacific volcanism). The Alps, in contrast, show few andesites with ophiolites being the dominant magmatic sequence.

3. The tectonic style of the Andes is generally that of tight, upright folds without significant development of nappes (or large horizontal thrust sheets).

Andean orogenies may be typical of subduction of large open oceans. The Alps, in contrast, seem to be better modeled by a process of opening and closing of small intercontinental seas (Cobbing 1978).

The idea that Andean tectonic movements and volcanism are controlled by large vertical basement faults is certainly not the only possible explanation. The longitudinal shape of the Peruvian Coastal Batholith and associated fractures is just what would be expected from a uniformly subducting oceanic plate melting at a critical depth (Shackleton 1977). From this viewpoint, the longitudinal fractures are an effect rather than the control of the Peruvian Coastal Batholith.

### 3.4.2 Present Day Tectonics of Central Peru

The preceding section might lead one to expect large vertical stresses and normal faults in Peru. A case can be made for a number of normal faults especially in the area of the Cordillera Blanca (Megard and Philip 1976). However, a detailed structural analysis of Recent faults and their apparent motions (Megard and Philip 1976) suggests the maximum principal stress in Central Peru is east-west compression. There are two preferred directions for horizontal compression in Pliocene - Recent structures. An older direction, N70°E, is roughly aligned with the relative motion vector for the Nazca and South American plates. The other direction, associated with recent structures, is N40°W, which does not seem to have a simple plate tectonics explanation.

The fault plane solutions (Chinn and Isacks 1980) for earthquakes occurring in the continental crust support these conclusions. They found horizontal east-west compression axes in Central Peru and in Argentina south of 30°S. Significantly, both areas are devoid of Quaternary volcanic activity (figure 3.10).

Thus, while the modern stress state in central Peru appears to be anomalous, it is contemporaneous with a paucity of volcanism. This observation is consistent with the model for magmatic activity (Aguirre et al. 1974, Pitcher 1978) in which volcanism is associated with extensional tectonics and compressive tectonic eras are amagmatic. (Modern tectonics south of the Pisco Deflection are extensional and modern volcanism starts there.)

## 3.5 Plutonism and Volcanism in the Central Andes

The magmatic history of the Central Andes differs markedly from that of the Peruvian Andes. In Peru, the major magmatic episode began in the middle Cretaceous and occupied the same physical location for the next 70 million years. In contrast, the intrusion of the Chilean Coastal Batholith began in the Jurassic (195ma) and, since then, the site of major activity has migrated eastward at a well established rate of about .8mm/yr (Zentilli 1974). (However see figure 3.6b and section 3.3.4) The Miocene volcanic outbreak is strictly limited to the Central Andes and is perhaps the most extreme spatio-temporal discontinuity in Andean history (Clark et al. 1976).

### 3.5.1 Intrusive Chronology

The major reference used for this section is M. Zentilli (1974). If not stated otherwise, facts cited here are from that work. Zentilli's study included a major contribution to the K-Ar chronology of intrusive events between 26°S and 29°S. These are:

1. The Paleozoic basement, 267-222ma
2. The Coastal Cordillera, 191-176ma (Lower Jurassic)
3. The eastern flank of the Coastal Cordillera, 156-137ma (Upper Jurassic)
4. The Western Cretaceous Batholith, 128-117ma (Lower Cretaceous)
5. The Eastern Cretaceous Batholtih, 107-87ma (Upper Cretaceous)
6. The Paleocene Batholith, 67-59ma
7. The Eocene-Oligocene Batholith, 44-34ma

There is a possible eighth pulse in the Miocene (23-22ma) found on the western slopes of the Western Cordillera. The studies of the Peruvian Coastal Batholith argue strongly that volcanism is the surface expression of simultaneous intrusion at depth. If this model is adopted for the Central Andes, the existence of a Miocene to Pliocene intrusive pulse seems almost certain. Indeed, with this model, another "modern" pulse should be occurring today.

Further evidence for the idea of simultaneous intrusion-extrusion is found in the Central Andes. Zentilli indicates that a given plutonic sequence is commonly found intrusive at a high level in a volcanic pile. Specifically, the Cretaceous batholith intruded the Bandurrias Formation, a thick sequence of continental and marine sediments and andesites; and, the Paleocene intrusion is found high in the Hornitos Formation, another volcanic pile. The notion that plutons rise into their own cloud of "ejecta" (Myers 1975a) seems consistent with these relationships.

### 3.5.2 Eastward Migration of Magmatic Foci

Figure 3.7a is adapted from Clark et al. (1976) and shows the eastward migration of magmatic foci with time as documented by their K-Ar age determinations. These authors have documented a rate of eastward progression increasing from .6mm/yr in the Jurassic to 1.1mm/yr in the Eocene - Oligocene. Additionally, there has been a gradual increase in the $Sr^{87}/Sr^{86}$ initial ratios since the middle Cretaceous from about .7022 to .7077 (Clark et al. 1976). This trend is followed by magmatic rocks of all types and is taken by Clark et al. to reflect a gradual change in the source process and materials rather than progressively greater

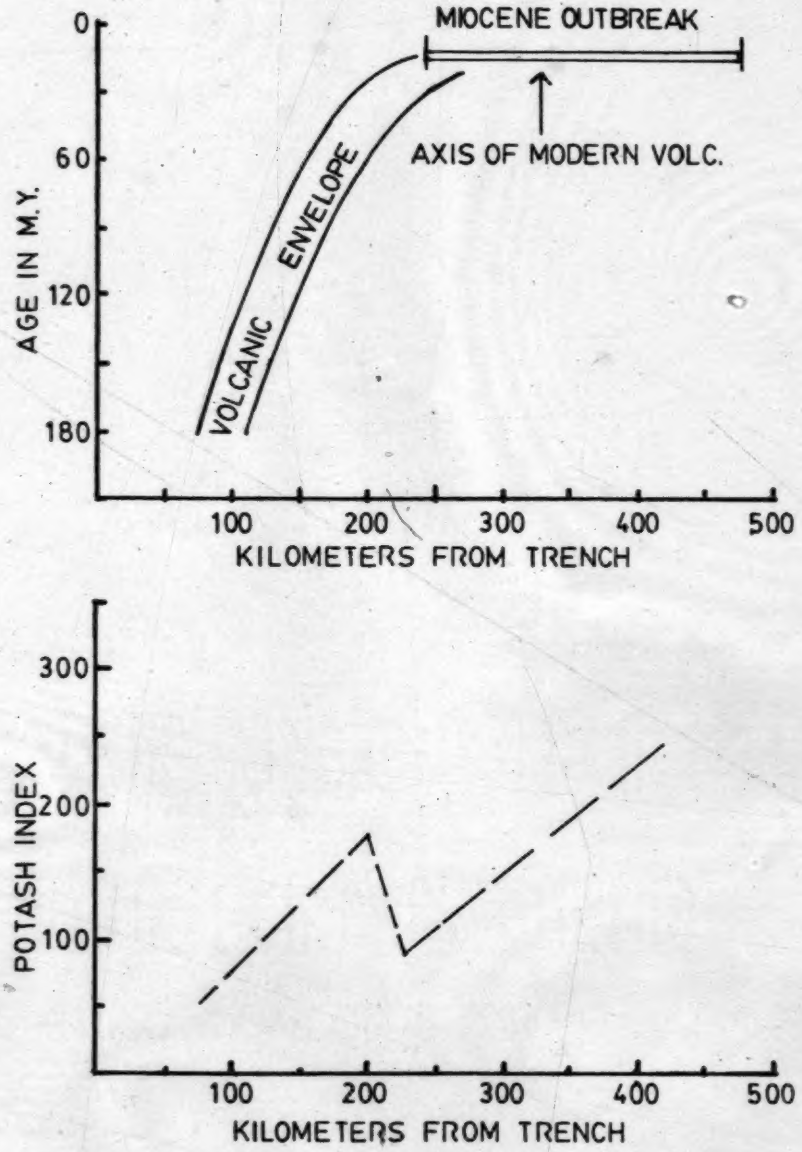

Figure 3.7a is adapted from Clark et. al. (1976) and shows the eastward migration of magmatism in northern Chile. (Compare with figure 3.6b.) Figure 3.7b is modified from Zentilli (1974) and shows the variation of Potash index across a transect of the Andes at about 26°S.

sialic contamination.

There is an orderly eastward increase (Zentilli 1974) in the potash index (Bateman and Dodge 1970) which, according to Dickinson (1970), reflects the depth to the point of magma generation (figure 3.7b). This pattern is broken only by the volcanics of the Miocene outbreak which show an abrupt decrease in potash content consistent with a shallowing of the magma source. For all rocks except the Miocene, these results suggest magma generation at progressively greater depths along the same inclined plane throughout the history of the Central Andes. Thus the suggestion of James (1971b) that the eastward younging of magmatic rocks may be due to a gradual reduction of the dip of the Benioff zone dip can be discounted (Zentilli 1974). James also suggested several other possible mechanisms, including migration of the trench and local depression of mantle isotherms due to the underthrusting of cold lithosphere.

The eastward migration might reflect a gradual increase of the rate of subduction since the Jurassic, or the continuous underthrusting of cold oceanic lithosphere may have resulted in a progressive lowering of mantle geotherms (Clark et al. 1976). These mechanisms are quite possibly related and both assume partial melting of the uppermost crustal layers of the subducting slab in some critical temperature - pressure range.

Another possibility requires the existence of an asthenospheric wedge for magma production (Ringwood 1977). If such is the case, then the gradual thickening of the crust beneath the Central Andes (James 1971b) might imply a consequent lithification of asthenospheric material and a downdip retreat of the requisite "wedge."

### 3.5.3 The Miocene-Pliocene Magmatic Outbreak

Orogeny in the Central Andes has been a "steady state" process over most of its history (Clark et al. 1976). Few events of a sudden or "catastrophic" nature are required to model the data. The only known exception to this generalization is the sudden outbreak of volcanism, on a wide front, in the middle Miocene (Sillitoe 1976). Prior to this, magmatic belts had widths of the order of a few tens of km; but, in the Miocene they widened to a few hundred km. Relaxation to the present volcanic belt occurred late in the Pliocene (3ma) (Clark et al. 1976). Between 19.5°S and 22.5°S the activity seems to have begun with ignimbrite eruptions between 20 and 15ma while the vast majority of the lava flows occurred in the last 10ma (Baker and Francis 1978).

The Miocene to Recent lava flows and associated ignimbrites occur in enormous volumes. Some $1.2\times10^4$km$^3$ of extrusives exist between 19.5°S and 22.5°S with the rate of simultaneous intrusive activity estimated as more than 5 (and perhaps as much as 10) times that of extrusion (Baker and Francis 1978). This means that at least $7\times10^4$km$^3$ of new material has been added to the South American continent in the last 15-20 million years in this region alone. This represents about 200Km$^3$ per Kilometer of length along the trench. If this is a representative figure throughout the Central Andes, then 4x10$^5$Km$^3$ of new material was added to the continent in the Central Andes (between the Pisco Deflection and 30°S).

The cause of this outbreak is unknown. Initial activity seems to coincide with a rather sudden reduction of the depth of magma generation and the reorganization of oceanic spreading centers in the Pacific about 26ma (Handschumacher 1976).

### 3.5.4 Chemistry and Origin of Central Andean Andesites

The idea that the volcanics originated through fusion of the lower continental crust (Pichler and Zeil 1969 and 1972) is not popular (James et al. 1976, Clark et al. 1976). The geochemistry of two Pliocene - Quaternary flows in southern Peru shows "anomalously high" initial $Sr^{87}/Sr^{86}$ ratios of .7061 and .7044 (James et al. 1976). Such magmas can develop from subduction zone melting of the thick South American lithosphere or they may originate as melt from oceanic crust which isotopically equilibrates with the South American lithosphere as it rises (James et al. 1976). A possible problem with this mechanism is that it requires the point of magma generation to be beneath some 200-300Km of continental lithosphere. The Benioff zone is currently about

125km beneath the modern Central Andean volcanic line.

There are high initial strontium ratios across a transect of the Chilean Andes (26°S) (Clark et al. 1976) and there may be a gradual increase in initial ratio with time. This may be due to a mixing of two different source materials with different $Sr^{87}$ content. A low content material, probably oceanic basalt, is one suggested source material ($Sr^{87}/Sr^{86}=.702$) while the other material (unidentified) is relatively enriched ($Sr^{87}/Sr^{86}=.710$).

Presently the crustal contamination hypothesis is favored. Peruvian andesites show higher $O^{18}/O^{16}$ ratios than typical island arcs (Margaritz et al. 1978), and this suggests crustal contamination. In this light, James (1978b) proposed that the lavas are contaminated with subducted greywackes which formed from erosives from the Precambrian shield outcropping in Peru.

Southern Peruvian volcanics exhibit some of the lowest $Pb^{206}/Pb^{204}$ ratios ever found in Recent volcanics and $Nd^{143}/Nd^{144}$ ratios are lower than those found in typical oceanic ridge basalts or pelagic sediments (Tilton 1979). Ratios from a site in Chile, south of the probable Precambrian shield, appear more like typical island arc volcanics than do the results from the Peruvian intercratonic volcanism.

Pb and Nd data for the volcanics from Southern Peru support the notion of crustal contamination and specifically implicate the shield as the source of contaminants (Tilton

1979). The greywacke hypothesis is unlikely because greywacke sediments are rare in Peru and sample greywackes from similar settings in North America show high $Pb^{206}/Pb^{204}$ ratios incompatible with the Pb data for Peruvian andesites.

It seems likely that the andesites of the Central Andes are the ejecta of gabbroic melt originating from near the subducting plate. These are subjected to considerable contamination as they rise through thick crust and competent shield rocks.

### 3.5.5 Crustal and Lithospheric Thicknesses in the Central Andes

Figure 3.8 shows the estimated depth to the Moho in kilometers as determined from surface wave dispersion in the Altiplano (James 1971a), the approximate extent of the underlying Precambrian shield estimated by (Cobbing et al. 1977) and the locations of active volcanoes.

The South American crust beneath the Central Andes is among the thickest found anywhere in the world. The 70km thick zone begins at the Pisco Deflection and follows the course of the Altiplano to approximately 23°S. Clearly the source magmas for Central Andean Volcanoes must penetrate at least 60 Km and in some cases 70 km of continental crust.

Seismic and gravity traverses across the central Andes (Ocola and Meyer 1973, figure 3.9) indicate a maximum crustal thickness approaching 75 km. Figure 3.9 shows how the contours of figure 3.8 might be corrected to agree with

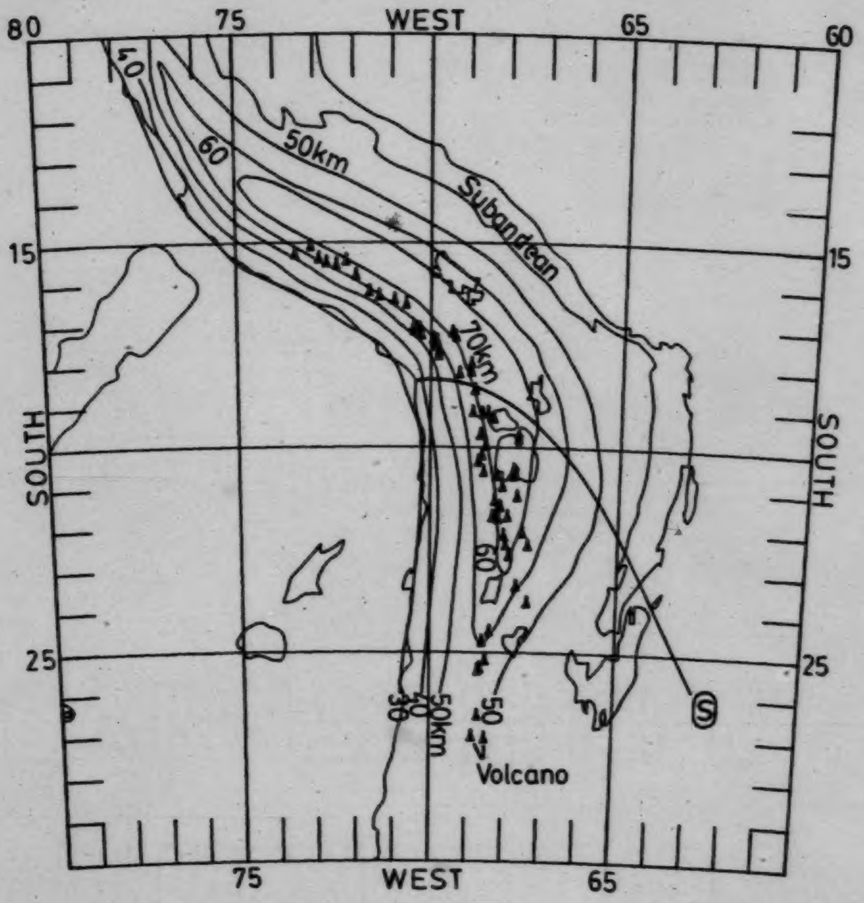
80
75
WEST
65
60
40
60
50km
Subandean
15
15
70km
SOUTH
SOUTH
60
25
25
30
40
50km
50
Volcano
Ⓢ
75
WEST
65

Ⓢ Probable limit of Precambrian shield after Cobbing et. al. (1977)

Figure 3.8 displays contours of the approximate depth to the Moho beneath the Central Andes as estimated by James (1971a). Also shown is the approximate southern limit of the underlying Precambrian shield after Cobbing et. al. (1977).

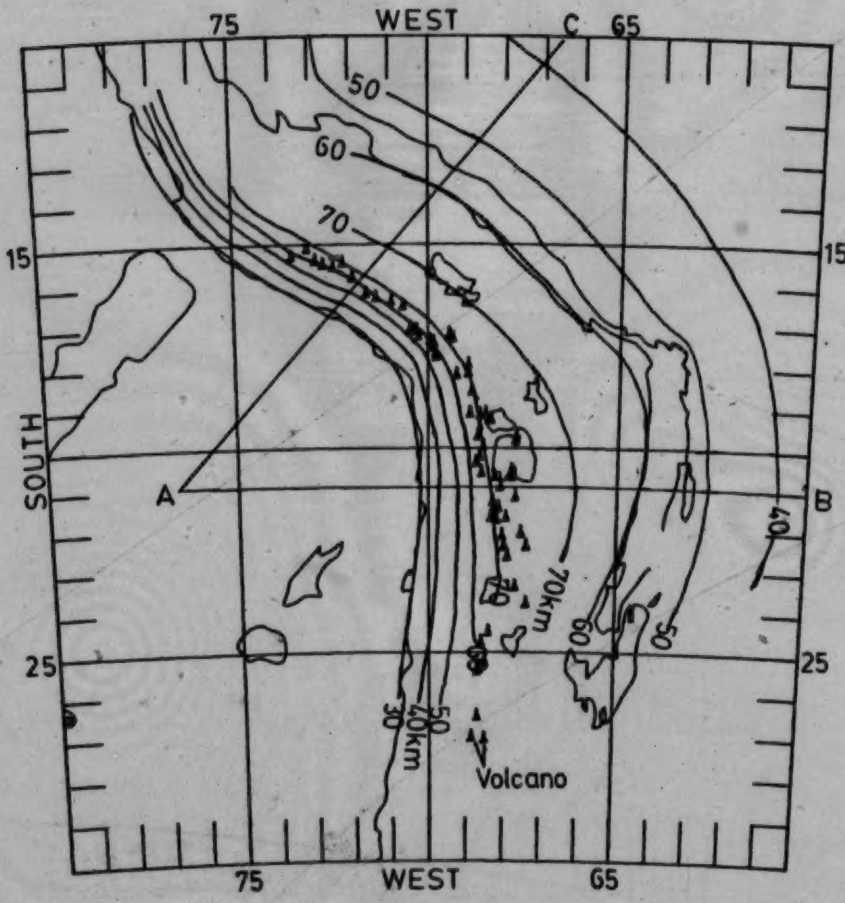

75
WEST
C
65
50
60
70
15
15
SOUTH
A
B
107
70km
60
50
30
50
40km
25
25
Volcano
75
WEST
65

Figure 3.9 indicates how the contours of figure 3.8 might be modified to agree with two seismic and gravity contours done by Ocola and Meyer (1973). The traverses are denoted by "AB" and "AC". Contours agree with Ocola and Meyer along the traverses and are hypothetical elsewhere.

the traverses. These contours coincide with the estimates of Ocola and Meyer along the traverses and are inferred elsewhere. According to James, 60 kilometer thick crust ends at the eastern border of the Altiplano, but the Ocola and Meyer traverses show 60 kilometer crust extending beneath the Eastern Cordillera all the way to the Subandean Ranges. If this is the correct picture, then the amount of new material added to the continental crust since the Mesozoic is considerably greater than estimated by James (1971b).

Q studies beneath South America suggest lithospheric thicknesses approaching 300 km (Sacks 1969, Sacks and Okada 1974, Sacks 1976). Island arcs typically have high Q regions corresponding to a descending slab and an overriding slab 50 - 100 km thick. Between the upper surface of the descending slab and bottom of the overriding slab is a low Q asthenospheric wedge.

Beneath South America in central Peru, the high Q region extends continuously down to some 300 km. There is no evidence of an asthenospheric wedge separating two lithospheric plates. A low Q region appears between 300 - 500 km. Beneath southern Peru and northern Chile (the volcanically active region) there is a definite, thin low Q region along the top of the descending slab. The high Q region still extends to slightly more than 300 km depth.

## 3.6 Tectonic Style of the Central Andes

Here, as in Central Peru, tectonic evolution can be described in terms of vertical motion between striplike crustal blocks. There is little evidence anywhere in the Andes for significant crustal shortening. All of Chile is probably underlain by a high-grade metamorphic basement (Munoz Christi 1956) which controls the tectonic style in much the same way as in Peru.

Vertical tectonics and some folding and faulting, normal and reverse, in association with plutons are found in northern Chile (Zentilli 1974). The gentle, open folds of the coast range increase in intensity eastward until, in the main cordillera, Mesozoic sequences have been intensely folded (Kausel and Lomnitz 1969). The Bolivian Andes (Altiplano and Eastern Cordillera) probably originated in a major folding phase which began in the Miocene (Lohmann 1970). Folding was dominant until the Pliocene when vertical movements became primary.

### 3.6.1 The Altiplano, Pampean Ranges, and Central Valley

The model of coastal tectonics dominated by block faulting with folding increasing inland is somewhat like that in Peru, but there are major differences. Such tectonic elements as the central valley, the Altiplano, and the Pampean Ranges have no counterparts north of the Pisco Deflection.

The Altiplano may be a granitic mass of early or pre-Andean origin which was uplifted in the Tertiary and served as a buttress against which the Andes were folded (Lohmann 1970). It has been a depositional basin for erosives from both Eastern and Western Cordillera and today has more than 10,000 meters of sediments (Lohmann 1970 and 1975).

It seems likely that the Pampean Ranges are the southern extension of the Altiplano structure. These are a series of disconnected blocks which begin to rise out of the Pampas about 33°S and increase in height as they trend northwest into the Altiplano. Maximum elevations in the Pampean Ranges approach 6000m. Block faulting, which formed these horst structures, began in the middle Miocene (Herrero-Ducloux 1963). Each block has a Precambrian granitic core (Tectonic Map of South America, 1978) and is capped by Mesozoic sequences. If the Altiplano is the continuation of these structures, then it can be inferred to have a Precambrian core.

Figure 3.10 shows the regions of significant Quaternary volcanism in South America. There is a clear correlation between the presence of a central valley and Quaternary volcanism (figure 3.10). D'Angelo and Le Bert (1969) suggest that the central valley is downthrown along deep normal faults. This is further evidence for the correlation between extensional tectonics and active volcanism.

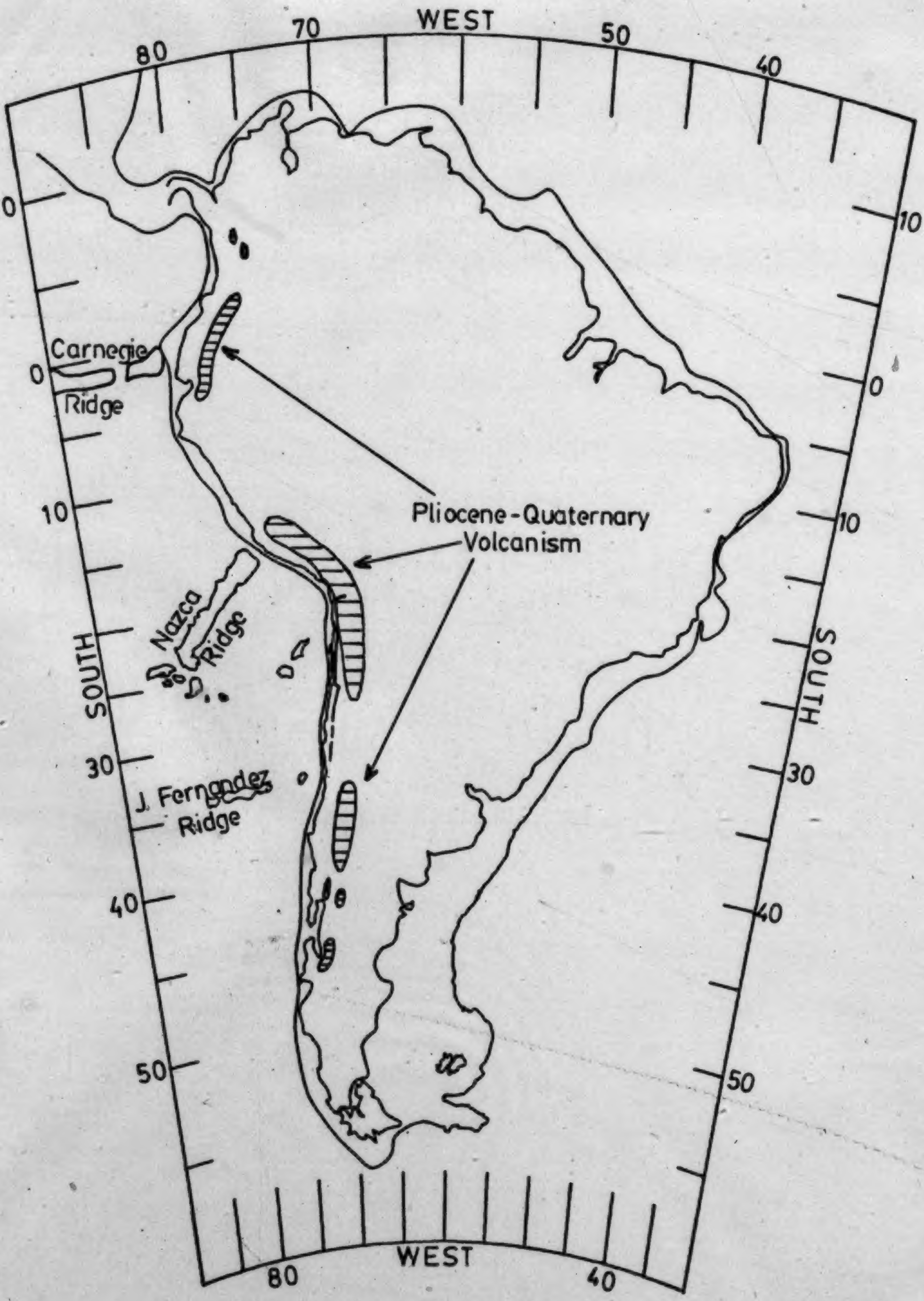
WEST
80
70
50
40
10
0
10
30
40
50
SOUTH
Carnegie Ridge
Nazca Ridge
J. Fernandez Ridge
Pliocene-Quaternary Volcanism
WEST
80
40

Figure 3.10 shows where significant Pliocene through Quaternary volcanism has been found in South America. Adapted from the Tectonic Map of South America (1978).

### 3.6.2 The Atacama Fault

The Atacama Fault is a vertical fault parallel to the coast through much of Chile. It has been suggested that this is a major dextral strike slip system comparable to the San Andreas system (St. Amand and Allen 1960, Allen 1963 and 1965), but more recent work (Arabasz 1971) suggests offsets do not exceed a few tens of kilometers. The period of lateral activity is variously stated as "Mesozoic to early Pliocene" (Arabasz 1971) or "middle Cretaceous to 20ma" (Lomnitz 1974).

Just south of Taltal (about 26°S), the dextral Atacama Fault is offset some 10 km by a sinistral, possibly conjugate, fault active from middle to late Tertiary. It has Recent vertical subsidence of the western block of several kilometers (Arabasz 1971).

It seems clear that the Atacama Fault is not now, and probably never was, a transform fault. In the next chapter, it will be suggested that the fault is a strike slip fault that developed in response to highly oblique subduction. Such faults may be common whenever a plate convergence vector has a significant component parallel to the plate boundary (Fitch 1972) (section 1.2.4). In fact, it may well have played a dual tectonic role by also functioning as a major vertical slip plane.

### 3.6.3 The Ojos del Salado Lineament

The southern boundary of the Puna (or southern

Altiplano) is an abrupt fault scarp with a normal throw of at least 1500 meters called the Ojos del Salado Lineament (OSL) (Zentilli 1974). It lies just south of the Ojos del Salado strato-volcanic complex and strikes east-west at approximately 27.25°S (figure 3.2) from the Western Cordillera at about 69.5°W to at least 67°W. (See Bonatti et al. (1977), figure 17.) While the OSL does not quite mark the southern limit of Quaternary volcanism (at 28°S), there is an order of magnitude decrease in the areal density of Miocene to Recent volcanic craters across the line from north to south (Zentilli 1974). It is found at the same latitude as the southern limit of the central valley.

A large quasi-circular aseismic zone is also found here centered on 68°W and 26.5°S (see figure 3.15). This may be a true aseismic zone (not a region of strain accumulation premonitory to a large earthquake) if the aseismicity is caused by an unspecified modulation of the subduction process by the Sala y Gomez "ridge" (Hanus and Vanek 1978).

The Peru-Chile Trench shallows from 7500 to 6000 meters and is offset at 27.5°S (Fisher and Raitt 1962). There is a continuous linear tectonic feature across the Andes at this latitude (Carter 1974).

## 3.7 On the Genesis of the Modern Andes

### 3.7.1 The Central Andes

It is difficult to define precisely the temporal beginning of the Andes since the mobile belt shows a history of deformation and magmatism since at least the Paleozoic. A Permian orogeny is in evidence in Peru (Jenks, 1956) and Chile (Munoz Christi 1956, Clark et al. 1976). However, events ancestral to the modern Andes in Chile are generally considered to have begun in the late Triassic to early Jurassic (200 ma) (James 1971b, Zentilli 1974, Clark et al. 1976), about the time of the opening of the South Atlantic. (Sillitoe (1976) links the Permian activity to the modern Andes and thus gives the "Permo-Triassic" as the beginning period.)

An ensialic island arc environment probably was probably present off the Chilean Central Andes in the late Triassic to early Jurassic (James 1971b, Zentilli 1974, Clark et al. 1976). There are few ophiolitic suites to be found in South America and none have been found to date in the Central Andes. If there was marginal basin activity here, it was terminated by some process such as subsidence beneath a sediment load rather than obduction.

### 3.7.2 Evidence from Patagonia

A Jurassic volcanic formation, the Tobifera Formation (dominantly rhyolite and rhyodacite) is common throughout Patagonia (Figure 3.11, Dott 1976). A sequence of eugeosynclinal facies which includes parts of the Tobifera may be a remnant arc (Dalziel and Palmer 1979). Associated with the Tobifera in the southernmost Andes are the Rocas Verdes, one of the few ophiolite formations which have been

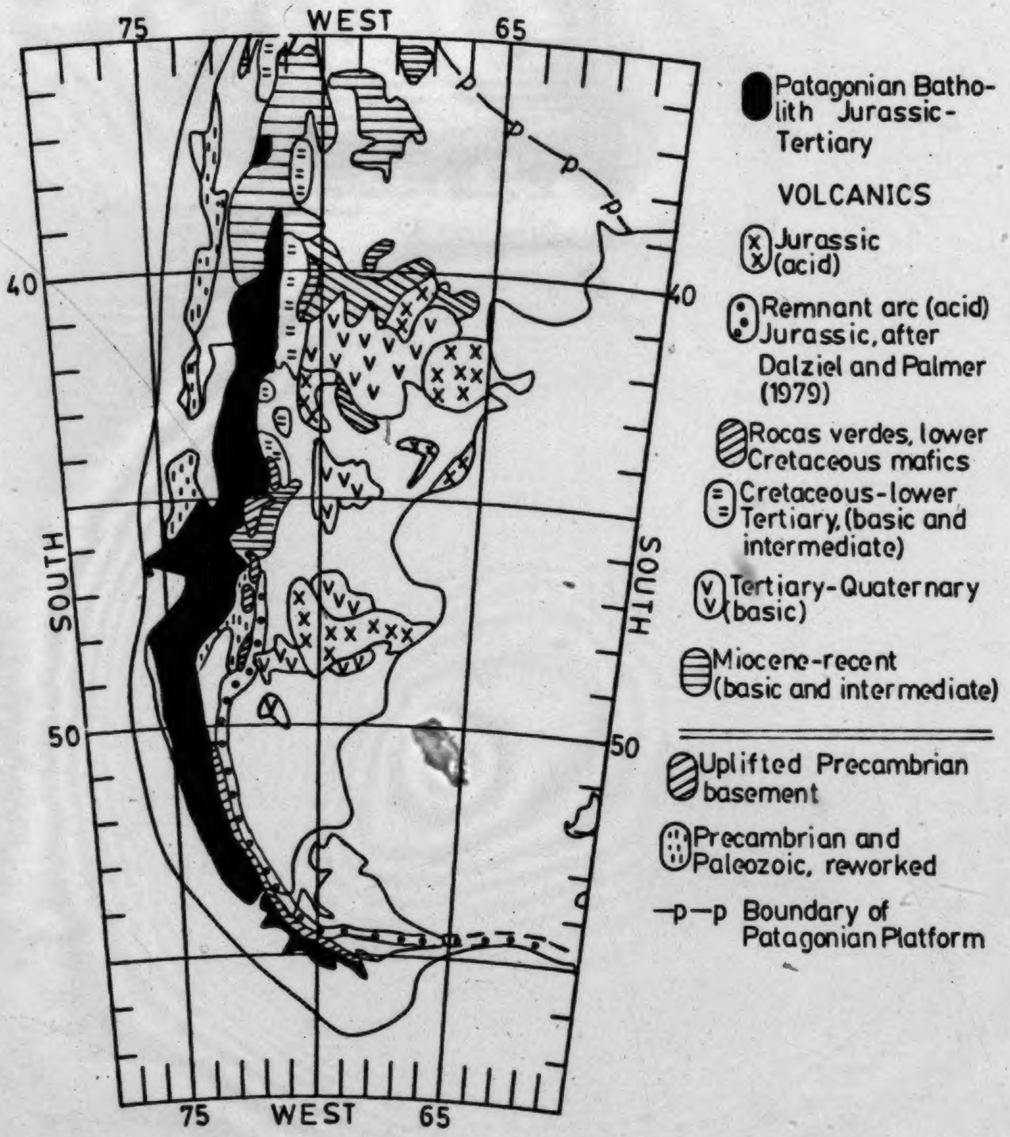
75
WEST
65
40
40
SOUTH
SOUTH
50
50
75
WEST
65
Patagonian Batholith Jurassic-Tertiary
VOLCANICS
Jurassic (acid)
Remnant arc (acid) Jurassic, after Dalziel and Palmer (1979)
Rocas verdes, lower Cretaceous mafics
Cretaceous-lower Tertiary, (basic and intermediate)
Tertiary-Quaternary (basic)
Miocene-recent (basic and intermediate)
Uplifted Precambrian basement
Precambrian and Paleozoic, reworked
—p—p Boundary of Patagonian Platform

Figure 3.11 is a geological sketch map of Patagonia. Primary source map was the Tectonic Map of South America (1978).

found in the Andes (Dalziel et al. 1974). (Ophiolites are also found in the Colombian coastal ranges (Gansser 1973).) The Rocas Verdes have been the subject of numerous studies (Bruhn and Dalziel 1976, Saunders et al. 1979) which have established them as representing the floor of a marginal basin which formed in the late Jurassic - early Cretaceous and was crushed and uplifted in the mid-Cretaceous.

The Patagonian Batholith (figure 3.11) is one of the largest continuous intrusive bodies in the world and one of the least studied. Whole-rock Rb-Sr ages indicate that the batholith was emplaced in three major phases from the Jurassic through the Tertiary (Halpern 1973). These are late Jurassic to early Cretaceous (155-120ma), late Cretaceous (100-75ma), and late Paleocene through early Pliocene (50-10ma). Initial $Sr^{87}/Sr^{86}$ ratios average about .705. There is no evidence for migration of magmatic foci.

### 3.7.3 Peruvian Andes

While there is ample evidence that the Chilean Andes were volcanically active throughout the Jurassic, the modern Peruvian Andes are generally considered to have begun with the emplacement of the Peruvian Coastal Batholith, firmly dated at 105ma. Few traces of significant plutonism prior to the emplacement of the Peruvian Coastal Batholith are found north of 17°S. Some of the more northerly occurrences are the isolated minor plutons of the Bolivian Cordillera Real just east of Lake Titicaca (Lohmann 1970). (Lohmann quotes an age range for these intrusives of 199-180 ma but nevertheless refers to them as Triassic.) Also, Stewart et al. (1974) report one age determination of 204 ma from the southern Peruvian coast near 16°S, which was used by Pitcher (1978) as evidence that the San Nicholas Batholith (figure 3.4a) is Jurassic.

Despite these isolated occurrences of Jurassic plutonism in Peru, there seems to be no evidence to indicate Jurassic magmatic activity which was comparable in intensity to that in Chile. Pitcher (1978) argues that the position of the San Nicholas Batholith on the Paracas Peninsula implies that other Jurassic plutons are now submerged along the Peruvian continental shelf. This idea lacks supporting evidence. If the continental shelf is isostatically compensated, then it is unlikely that it contains large amounts of buoyant plutonic material. Furthermore, Jurassic plutonism and volcanism in Chile were not restricted to the coastal cordillera but are found as far east as the Argentine Precordillera (Lautero Formation, Zentilli 1974.). If Jurassic activity in Peru had been even within a few orders of magnitude of that in Chile, traces of it should be found scattered throughout the cordillera. It is, therefore, difficult to escape the conclusion that the modern Andean mobile belt began forming some 100 my earlier in Chile than Peru with a dividing line somewhere near the Arica Elbow or even the Pisco Deflection. Even if Jurassic plutons do reside within the Peruvian shelf, it would still be necessary to conclude that activity in the south (Patagonia) was much more intense than further north. (See Dalziel and Palmer 1979.) Implications of this will be discussed later in the light of further evidence to be presented in chapter 4.

## 3.8 Seismicity of South America

The seismicity of western South America has been the subject of many detailed studies (e.g. Santo 1969, Stauder 1973 and 1975, Barazangi and Isacks 1976 & 1979 and Hanus and Vanek 1978). Here I review the conclusions of these workers and present new interpretations. The terms shallow, intermediate, and deep refer here to earthquakes occurring in the depth ranges 0-100Km, 100-300Km, and 300-700Km respectively.

Vertical seismicity profiles are a basic tool of this study. The references above are the better compilations of such profiles. There is considerable variation regarding the direction and width of the profiles used to "define" the geometry of the descending Nazca Plate. The value obtained for the dip of the plate is obviously dependent on the direction in which representative profiles are taken. A common practice is to take profiles perpendicular to the trench (Hanus and Vanek 1978). This can lead to a considerable distortion in the case of highly oblique subduction. Also, extremely wide profiles can mask the details of the subduction process.

Profiles should be taken in the direction of relative motion between the two colliding plates. (It may also be argued that profiles should be taken in the direction of spreading on the East Pacific Rise; however, in this case, it makes little difference. See figures 3.1b and 3.1c) The NOAA data tape is sufficiently complete that good results can be obtained in South America with 1° wide profiles using a threshold magnitude of 4.0 (body wave). Accordingly, Appendix 2 contains a complete set of such profiles all taken in the direction of relative motion between the Nazca Plate and South America. The trench system from northern Peru to 26°S is represented.

### 3.8.1 On the Accuracy of Hypocentral Determinations

Figure 3.12 is a seismicity map of South America adapted from the NOAA catalogue showing all recorded events from 1963 to 1977 and having Mb>5.0. The symbol type used has been chosen to indicate the approximate hypocentral depth. Much has been published regarding the accuracy (or lack thereof) of these earthquake locations. They are determined "teleseismically"; that is, a world wide net of seismographs is used. Ideally, such a net would have an even, but random, distribution of stations around the world. If this were so, hypocentral locations should depend only on "average earth" seismic velocity structure which is fairly well known. Local structural anomalies from such things as subducting slabs, or mountain roots should have only second

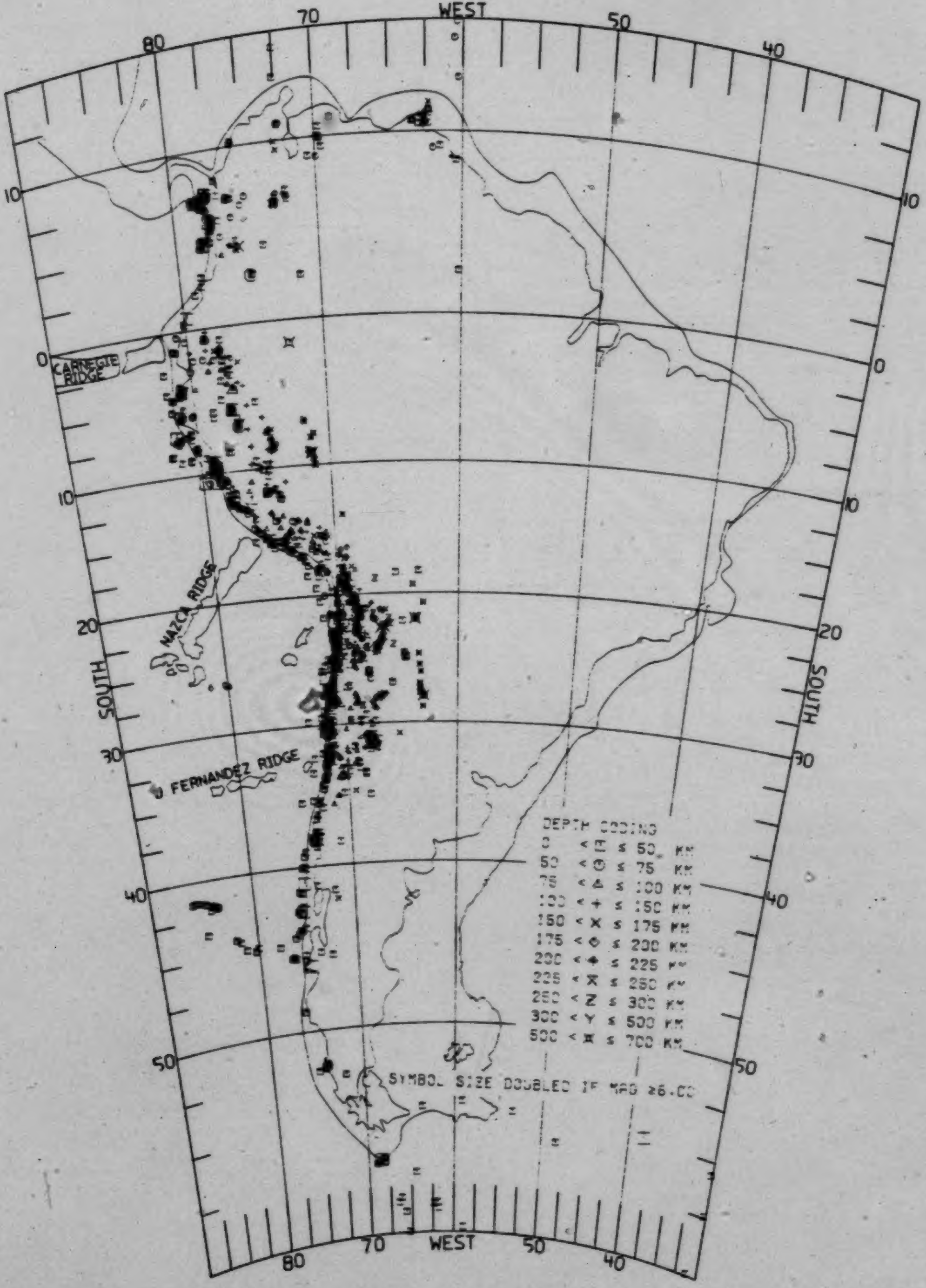
WEST
80
70
50
40
10
0
10
20
30
40
50
SOUTH
CARNEGIE RIDGE
NAZCA RIDGE
J. FERNANDEZ RIDGE
DEPTH CODING
0 < ⊟ ≤ 50 KM
50 < ⊙ ≤ 75 KM
75 < △ ≤ 100 KM
100 < + ≤ 150 KM
150 < × ≤ 175 KM
175 < ◇ ≤ 200 KM
200 < ◆ ≤ 225 KM
225 < ⧖ ≤ 250 KM
250 < Z ≤ 300 KM
300 < Y ≤ 500 KM
500 < ⊠ ≤ 700 KM
SYMBOL SIZE DOUBLED IF MAG ≥6.00

Figure 3.12 displays the seismicity of South America. Data are taken from the NOAA catalogue from 1963 through 1977. Only events having body wave magnitude greater than 5.0 are shown.

order effects. Unfortunately seismic observatories are almost all located on continental crust, and they are much more numerous in developed areas, especially North America, than in other parts of the world.

It is self-evident that hypocentral accuracy must increase with increasing earthquake magnitude. Not so obvious are the effects of the geometry of the observing net and anomalies in seismic velocity structure. The accuracy in the ISC catalogue does increase with magnitude, but not in a simple manner (Barazangi and Isacks 1979). A lower body-wave magnitude (Mb) threshold of 5.4 will eliminate all poorly located events from the data set but will also exclude some valuable information. A lower limit of about 4.0 will include all "good" data but will also pass many poorly constrained results. A sharper distinction requires a detailed evaluation of each event (Barazangi and Isacks 1979).

Workers at the Carnegie Institution distrust such selection techniques because of their inherently subjective nature (e.g. James 1978a). They prefer instead to use the entire data set. Nevertheless, most of the maps and figures shown here have been generated with some threshold magnitude, generally between 4 and 5. The presentation of such maps in small format imposes a practical need for a threshold to avoid producing a black blur. Fortunately, the data set appears to be sufficient for good results even with a fairly high threshold value (5 to 5.5).

It is very difficult to attach a specific value to the accuracy of a given hypocentral location. However, after spending many hours examining the data and observing patterns with high spatial coherence, I believe that events of magnitude 4 - 4.5 and greater probably are accurate to a few tens of kilometers or better in any dimension.

### 3.8.2 General Patterns

The seismically active zone of South America (figure 3.12) consists of a narrow belt parallel to the coast, extending south to the Gulf of Penas in Southern Chile where the Chile Rise intersects the Peru-Chile Trench. A significant east-west offset occurs in both coast and seismicity between the Pisco Deflection and the Arica Elbow (see figure 3.1). A general trend towards deeper hypocentral locations eastward from the trench is also apparent. In profile (see figures 3.16, 3.17, 3.20, and 3.21) this trend is seen to resolve into the inclined seismic "planes" first recognized by Benioff (1954) and hence named Benioff Zones. This is part of the primary evidence for the plate tectonic theory of subduction. The earthquake pattern is generally taken to reflect areas in a high state of stress. Benioff Zones are interpreted as directly giving the position of a subducting slab of oceanic lithosphere which is stressed as it thrusts beneath another plate into the mantle. Under this assumption, the geometry of the Benioff Zones is taken to be identical with the geometry of the descending slab. In practice, earthquakes in the over-riding slab and scatter in the data complicate this picture.

There is a tendency for earthquakes to group into globular clusters or quasi-linear patterns. Clustering occurs in time as well as space due to aftershock and foreshock sequences associated with larger events. If earthquakes are indicative of highly stressed material, then the presence of such clusters implies a very variable stress (and, hence, strain) field.

Discussion of the relationship between seismicity patterns and geological structures and processes requires comparison of phenomena whose time scales differ by some $10^4$ years. Large earthquakes typically show return times on the order of $10^2$ years while a characteristic time for mountain building processes must be at least $10^6$ years. It is possible that earthquake catalogues do not span sufficient time to comprise a statistically valid sample. Hence conclusions such as those in the last paragraph may not be correct on geological time scales.

### 3.8.3 Central Peru

Figure 3.13 is a seismicity (Mb>4.0) map of the Andes from 5°S to 30°S; figure 3.14 is an expanded view from 5°S to 18°S; and figure 3.15 covers 15°S to 30°S. The contours indicate geological features such as volcanic flows, plutons and the Subandean Basin. These have been labeled with a suggestive code which is evident upon comparison with figure

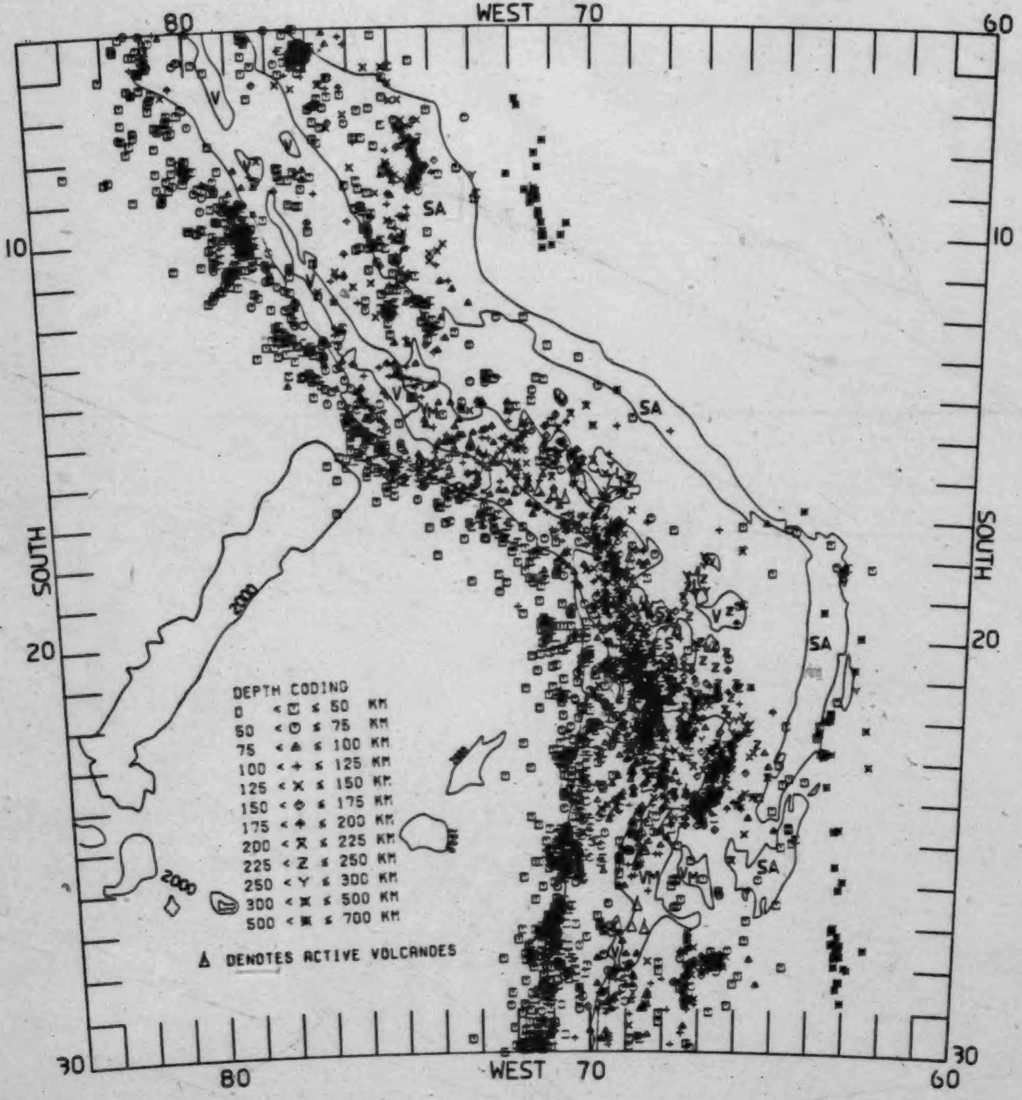
WEST
80
70
60
10
20
30
SOUTH
SA
V
VM
MC
2000
DEPTH CODING
0 < ⊡ ≤ 50 KM
50 < ⊙ ≤ 75 KM
75 < ▲ ≤ 100 KM
100 < + ≤ 125 KM
125 < X ≤ 150 KM
150 < ◈ ≤ 175 KM
175 < ✦ ≤ 200 KM
200 < ⧗ ≤ 225 KM
225 < Z ≤ 250 KM
250 < Y ≤ 300 KM
300 < ⌘ ≤ 500 KM
500 < ■ ≤ 700 KM
△ DENOTES ACTIVE VOLCANOES

Figure 3.13 is an expanded seismicity map for the Andean region between 5°S and 30°S. All events having Mb greater than 4.0 and which occurred between 1963 and 1977 are shown. Also shown are active volcanoes and contours of major geological features. The key to the labeling of the contours can be deduced from figures 3.4a and 3.4b.

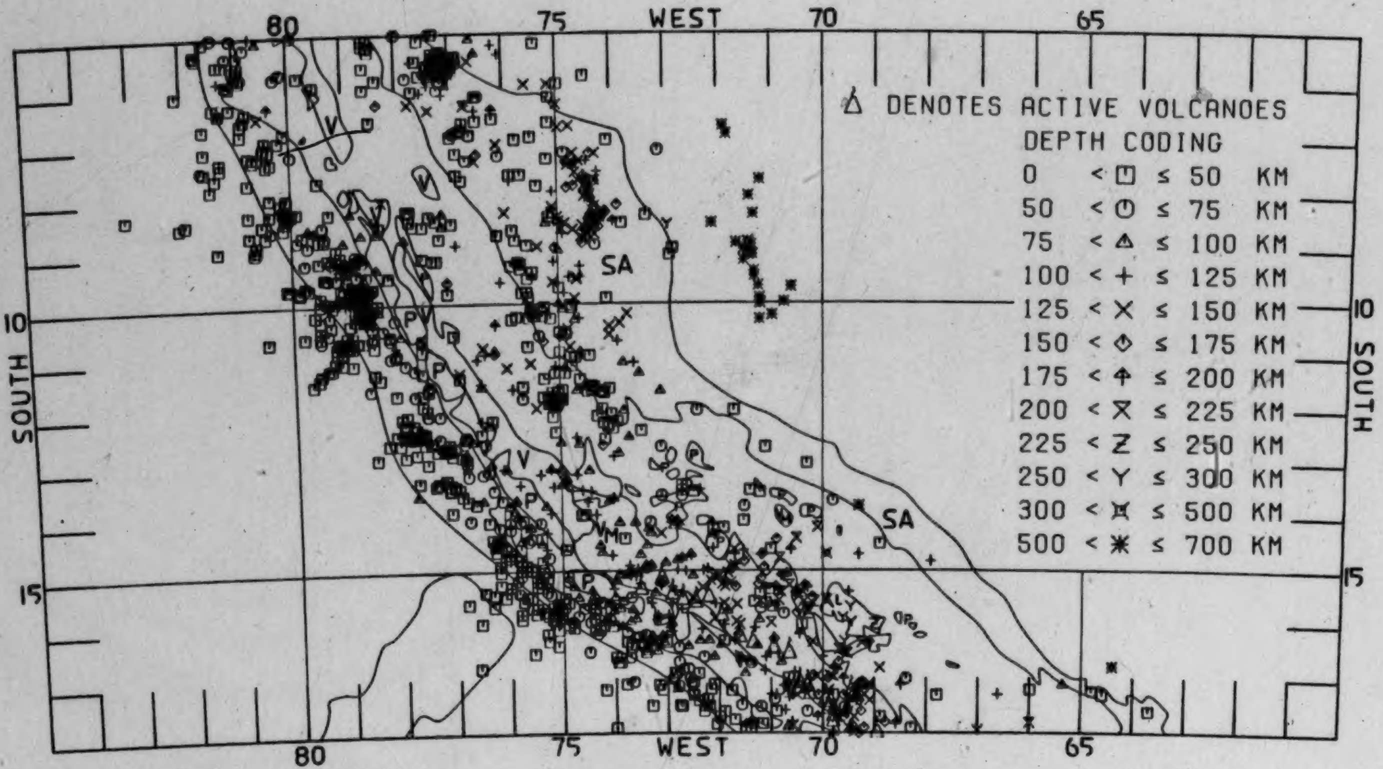
80
75
WEST
70
65
SOUTH
10
15
SA
V
P
Δ DENOTES ACTIVE VOLCANOES
DEPTH CODING
0 < ☐ ≤ 50 KM
50 < ○ ≤ 75 KM
75 < △ ≤ 100 KM
100 < + ≤ 125 KM
125 < X ≤ 150 KM
150 < ◇ ≤ 175 KM
175 < ↑ ≤ 200 KM
200 < X ≤ 225 KM
225 < Z ≤ 250 KM
250 < Y ≤ 300 KM
300 < ⌘ ≤ 500 KM
500 < ✱ ≤ 700 KM

Figure 3.14 is a closeup of the northern half of figure 3.13. Additional detail is included in the geological structure.

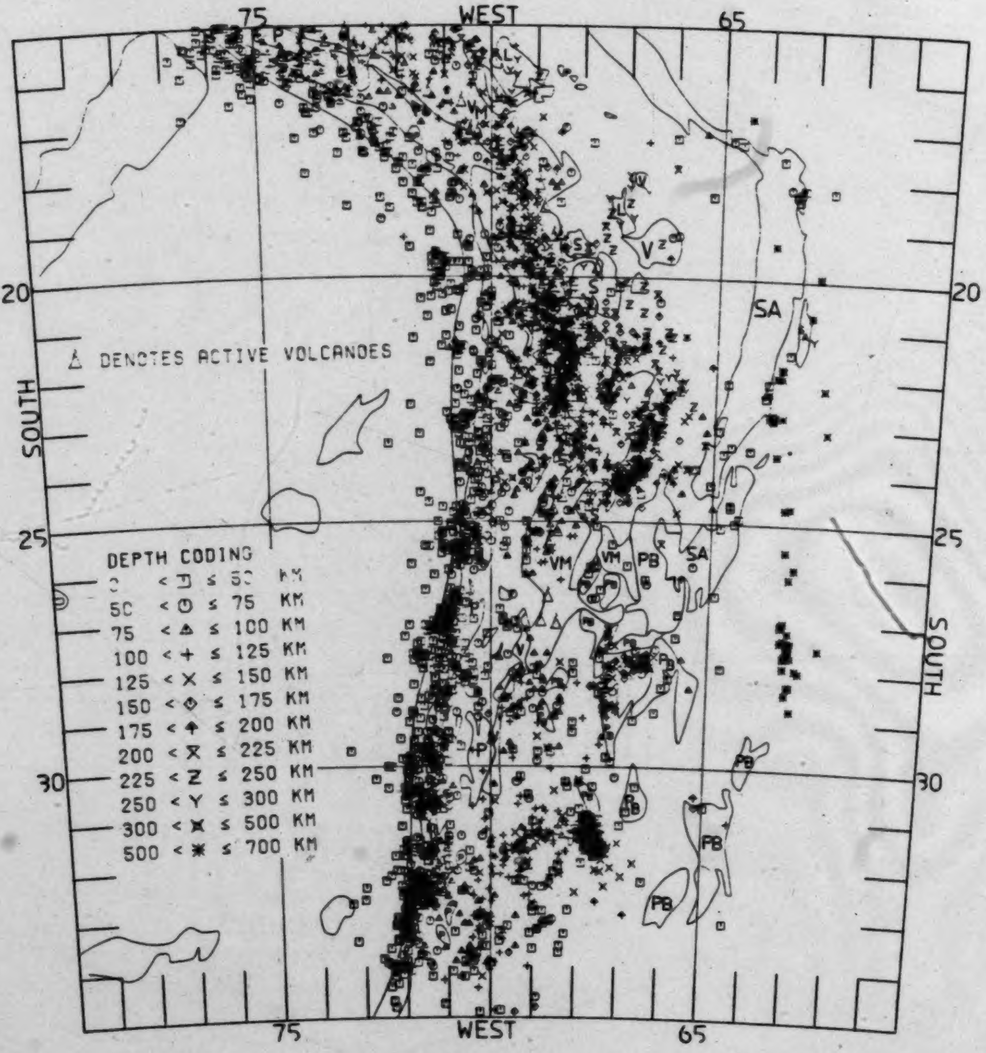
75
WEST
65
20
20
25
25
30
30
SOUTH
SOUTH
△ DENOTES ACTIVE VOLCANOES
DEPTH CODING
0 < □ ≤ 50 KM
50 < ○ ≤ 75 KM
75 < △ ≤ 100 KM
100 < + ≤ 125 KM
125 < × ≤ 150 KM
150 < ◇ ≤ 175 KM
175 < ↑ ≤ 200 KM
200 < X ≤ 225 KM
225 < Z ≤ 250 KM
250 < Y ≤ 300 KM
300 < ✖ ≤ 500 KM
500 < ✱ ≤ 700 KM
SA
SA
VM
VM
PB
PB
PB
PB
PB
P
V
S
75
WEST
65

Figure 3.15 is a closeup of the southern half of figure 3.13.

3.4a and 3.4b.

Figure 3.16a is a vertical seismicity (Mb>4.0) profile taken through central Peru in the direction of relative plate motion. Figure 3.16b shows the same profile but with Mb>5.0. Figure 3.16a illustrates the probable configuration of the Benioff zone while figure 3.16b emphasizes the regions of maximum energy release. The presence of two separate centers of seismic energy release at depths less than 200 km is typical of Peru. One is associated with the trench while the other occurs far inland beneath the Subandean Ranges. The aseismic depth range separating intermediate events from very deep events is a common feature of South American seismicity.

In Central Peru, seismicity can be divided into four zones: a coastal belt, an Andean belt, a Subandean Belt, and an eastern line of deep focus events which actually occur in Brazil. The coastal belt is generally less than 75 km deep and closely follows the trench system. A large cluster of coastal events is found at about 10°S, directly west of the Cordillera Blanca. This cluster represents events associated with two very large earthquakes which occurred here in October of 1966 and May of 1970. Focal mechanisms for these coastal events are generally consistent with underthrusting on an east dipping plane (Stauder 1975). Events in the cluster were more complex.

There is no obvious association between the seismicity patterns in central Peru and the region of Tertiary

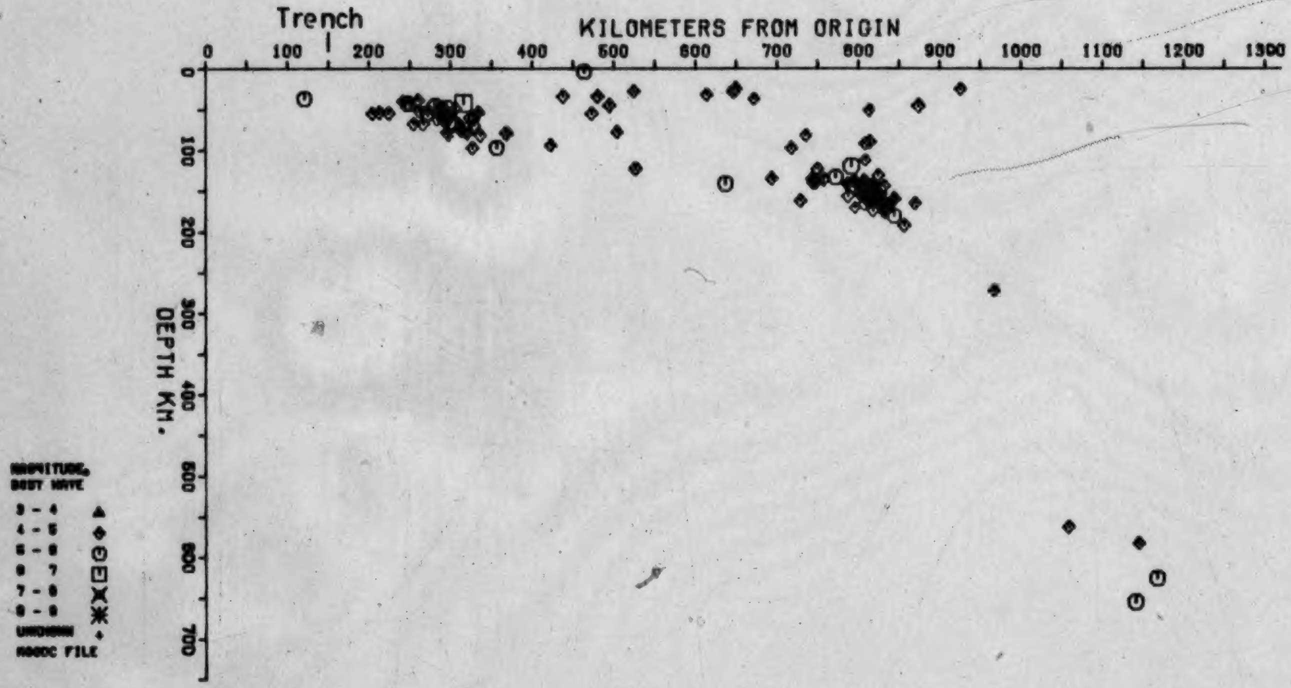

CROSS SECTION 1.0 DEGREES WIDE
BETWEEN 9.5.-81.7 AND -7.8.-69.8

Figure 3.16a shows a vertical profile taken through the Peruvian Andes in the approximate direction of subduction. Only events having Mb greater than 4.0 are shown.

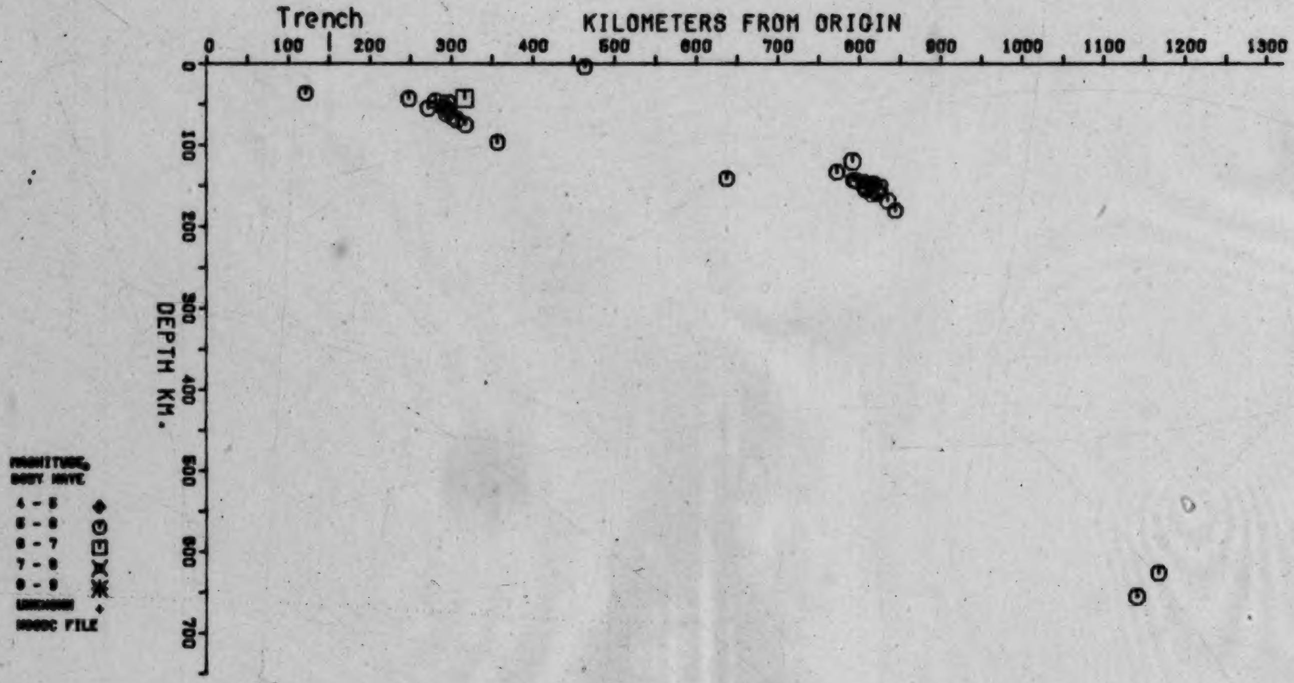

CROSS SECTION 1.0 DEGREES WIDE
BETWEEN -9.5,-81.7 AND -7.8,-69.8

Figure 3.16b is a seismicity profile along the same line as 3.16a but the threshold magnitude has been increase to 5.0. Two major areas of energy release are indicated: near the trench and beneath the Subandean Ranges.

volcanism. Just to the east, beneath the Eastern Cordillera, there is a broad band of somewhat sparse, generally shallow focus (<100 km) events. Our Huancayo survey network is located here. The Pariahuanca earthquakes (July and October 1969) were shallow focus reverse faulting events with a significant left lateral slip component. These earthquakes ruptured the Huaytapallana fault which our microgeodetic network straddles. This fault lies just north of the Pisco Deflection. There are strike slip solutions for one focal mechanism of a crustal event in the Pisco Deflection and several for events in the Huancabamba Deflection (Stauder 1975). Crustal events in between these two deflections were dominantly high angle thrusting. Both sets of data were consistent with approximately east-west compression. A number of large magnitude events with strike slip focal mechanisms have occurred within the Pisco Deflection since 1930 (E. Deza personal communication 1978).

There are shallow focus and intermediate focus (100km< focus <150km) events beneath the Subandean Basin. Barazangi and Isacks (1976 & 1979) used their "selected" earthquake file to resolve these earthquakes into two groups, a set of events clearly within the South American plate and another which probably defines an almost horizontally subducting slab whose upper surface is about 100 km deep.

The continental earthquakes have focal mechanisms consistent with a horizontal east-west compression axis (Chinn and Isacks 1980). The intermediate depth events have focal mechanisms indicating nearly vertical compression axes and N100°W tension axes (Stauder 1975). The quasi-linear cluster between 8° and 9°S lies just east of the Serra do Divisor on the Peru-Brazil border. The Mapa Geologico del Peru (1975) shows three small outcrops of "Tertiary" intrusives here. They may be subduction related (Stewart 1971) "undersaturated alkalic rocks" of 5ma age (James 1978a) from depths on the order of 300Km. This may be evidence for steeper subduction here as late as 5ma.

The deep focus events in western Brazil form a highly linear pattern which strikes about N10°W. These events show an unusually tight clustering of stress axes: compression axes nearly vertical, tension axes horizontal east-west, and null axes aligned along the strike of the seismic lineament (Stauder 1975). This line is the northern part of the Andean Seismicity Lineament (ASL) to be discussed below.

### 3.8.4 The 300-500 Kilometer Aseismic Zone

There are very few earthquakes between 150 and 500 km in Central Peru. In Chile, intermediate depth events are found as deep as 300 km. Throughout the South American seismic belt, events occurring in the depth range 300 to 500 km are extremely rare. Deep earthquakes are found only in western Brazil and northwestern Argentina (figure 3.13). These deep events form a linear pattern which is separated from intermediate events by an aseismic zone. This may indicate a piece of the slab which has been detached from the rest, or that the subduction process is aseismic in this depth range. There appears to be a correlation between the presence of aseismic ridges (buoyant zones) at a trench and detached slabs (Kelleher and McCann 1976) in South America; however the reason for this remains obscure.

### 3.8.5 The Shape of Subducting Plate beneath Central Peru

The shape of the subducted Nazca Plate beneath Central Peru has been a matter of some controversy. Stauder (1975), Barazangi and Isacks (1976), Megard and Philip (1976), Wortel and Vlaar (1978), Barazangi and Isacks (1979), and others are of the opinion that the spatial distribution of hypocenters directly reflects the shape of the subducted slab. Barazangi and Isacks (1979), using only "accurately located" hypocenters as a data base, clearly showed two seismic zones. One begins at the trench and dips at about 10° to a point 700 Km east of the trench. where it reaches a depth of about 150Km. The other zone is confined to depths less than about 50Km and appears beneath the Subandean Ranges 300 to 500 Km from the trench. In "classical" plate tectonics these zones are a shallow, almost horizontally subducting slab and a seismic region within the continent.

This model may be criticised on two counts (James 1978a). First, the data used were filtered through an inherently subjective quality control process. Second, the "definitive" profile which resolves the two seismic zones was unusually wide (9°). The seismicity in Central Peru is somewhat diffuse and shows significant clustering and the use of wide profiles may be misleading in such a circumstance.

Snoke and Sacks (1978) and Snoke et al. (1979) report the observation of seismic phases in Central Peru which they interpret as ScS converted to P at the upper boundary of the descending slab. The conversion interface defines a planar surface dipping some 30° to the east beneath the continent. This surface coincides with the Benioff zone only at depths less than about 100 km. On this basis they advance a model of an aseismic slab descending at about 30° and regard most of the seismicity east of the trench as occurring within the continental lithosphere. This dip is approximately the same as that determined in northern Chile by conventional methods and thus implies a smoothly continuous slab across the Pisco Deflection.

Barazangi and Isacks (1979) found no clear evidence of the ScS to P converted phase in Central Peru but Snoke et al. (1979) counter that Barazangi and Isacks (1979) incorrectly interpreted the evidence for ScSp phases by examining seismograms with a low signal to noise ratio. They contend that the ScSp phase is clearly evident in all records with "a low enough noise level." Hasegawa and Sacks (1979) may have proposed a satisfactory compromise. They advance a model in which the slab dips steeply (30°) until it reaches 100 km depth and then abruptly flattens. Nearly horizontal subduction continues for some 400 km to a point beneath the Serra do Divisor.

Figure 3.17 is my interpretation of the shape of the Nazca Plate beneath Central Peru. The cross section is drawn along the same line as figure 3.16 which is in the direction of relative motion between the South American and Nazca plates (figure 3.1a). This view is similar to that advanced by Hasegawa and Sacks (1979) and, in fact, differs very little from previous models proposed by Stauder (1975) and Barazangi and Isacks (1976). The sharp bend in the plate is as proposed by Hasegawa and Sacks and, while consistent with the seismicity, is not required by it.

### 3.8.6 Low Angle Subduction and Peruvian Tectonics

The apparently anomalous compressional tectonics and lack of volcanism of modern Central Peru (section 3.4.2) seem to be related phenomena. It has been suggested that low angle subduction is responsible for both (Barazangi and Isacks 1976 and 1979, Megard and Philip 1976 and others). Such a process may have been responsible for the North American Laramide orogeny of the late Cretaceous to early Tertiary (Dickinson and Snyder 1978). This tectonic episode saw the volcanic Sevier orogeny give way to the amagmatism and vertical block motions of the Laramide while the zone of deformation advanced further into the continent. Smithson et al. (1979) have recently presented deep reflection seismic data for the Wind River Laramide structures in Wyoming. They were able to continuously map the Wind River thrust to a

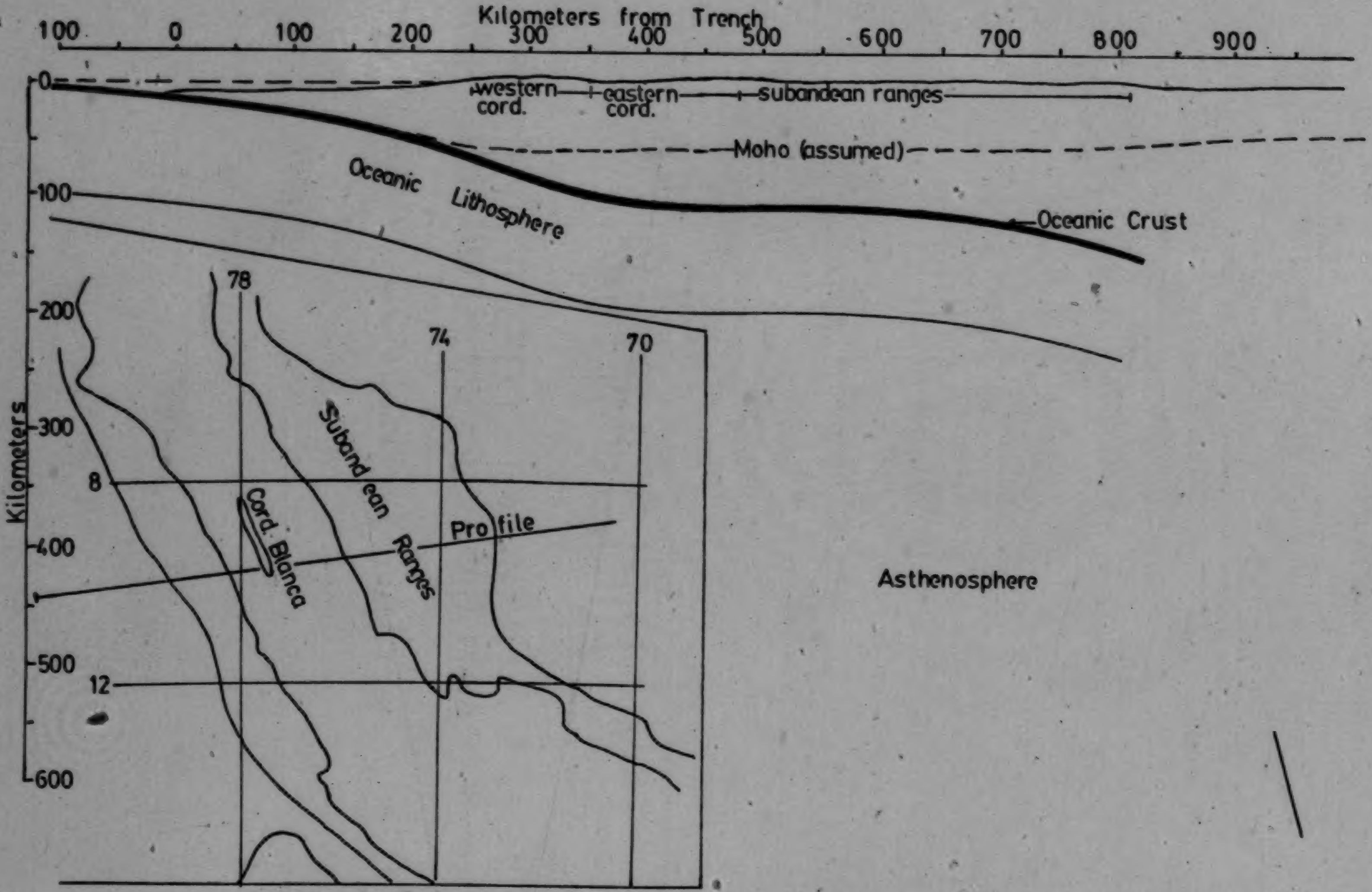
Kilometers from Trench
100
0
100
200
300
400
500
600
700
800
900
Kilometers
0
100
200
300
400
500
600
western cord.
eastern cord.
subandean ranges
Moho (assumed)
Oceanic Lithosphere
Oceanic Crust
Asthenosphere
78
74
70
8
12
Subandean Ranges
Cord. Blanca
Profile

Figure 3.17 is a cartoon showing a probable geometry for the subducted Nazca Plate beneath central Peru.

depth near 24 km. The high angle reverse faulting on the surface can be seen to flatten out with depth on these sections in a manner suggestive of horizontal compressional tectonics.

These facts provide evidence for a model in which a young, buoyant oceanic plate is forced beneath a continental plate before it has cooled sufficiently for more passive subduction. The oceanic plate "scrapes" along the bottom of the continent causing compressional stresses above it. Volcanism would subside either because compression sufficient to close magma routes or because the continent is isolated from the asthenosphere.

### 3.8.7 The Central Andes

Barazangi and Isacks (1976 and 1979) have used seismicity patterns in Southern Peru to infer a tear in the Nazca Plate. Figure 3.18 shows only shallow and intermediate depth events for the Central Andes having Mb>4.0. The hypocentral depth display has been expanded to give better resolution than figure 3.14. The location of the proposed tear is indicated by the line just to the southeast of the Nazca Ridge on figure 3.19. The evidence cited by Barazangi and Isacks (1979) for this tear consists of two vertical profiles, one on either side of the line, taken in a direction perpendicular to the trench. In this manner, they demonstrated a steeply dipping Benioff zone south of the "tear" and shallow, virtually horizontal subduction to the

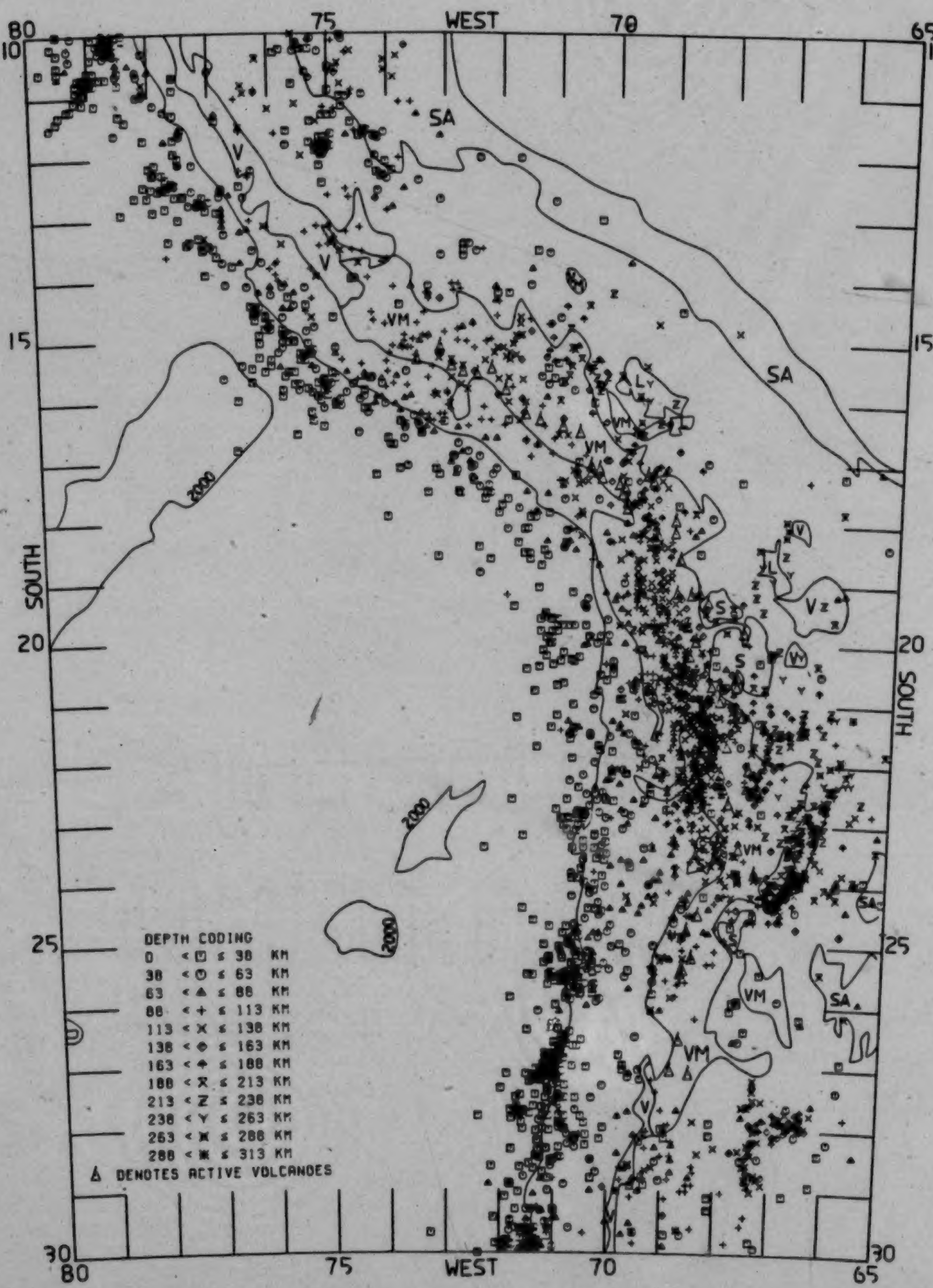
80
75
WEST
70
65
10
15
20
25
30
SOUTH
SA
V
VM
L
Z
S
2000
DEPTH CODING
0 < □ ≤ 38 KM
38 < ○ ≤ 63 KM
63 < ▲ ≤ 88 KM
88 < + ≤ 113 KM
113 < X ≤ 138 KM
138 < ◆ ≤ 163 KM
163 < ♠ ≤ 188 KM
188 < X ≤ 213 KM
213 < Z ≤ 238 KM
238 < Y ≤ 263 KM
263 < ✖ ≤ 288 KM
288 < ✖ ≤ 313 KM
△ DENOTES ACTIVE VOLCANOES

Figure 3.18 is a seismicity map of a portion of the Central Andes similar to 3.13. Only shallow and intermediate depth events are shown and depth coding has been chosen to be compatible with figure 3.19.

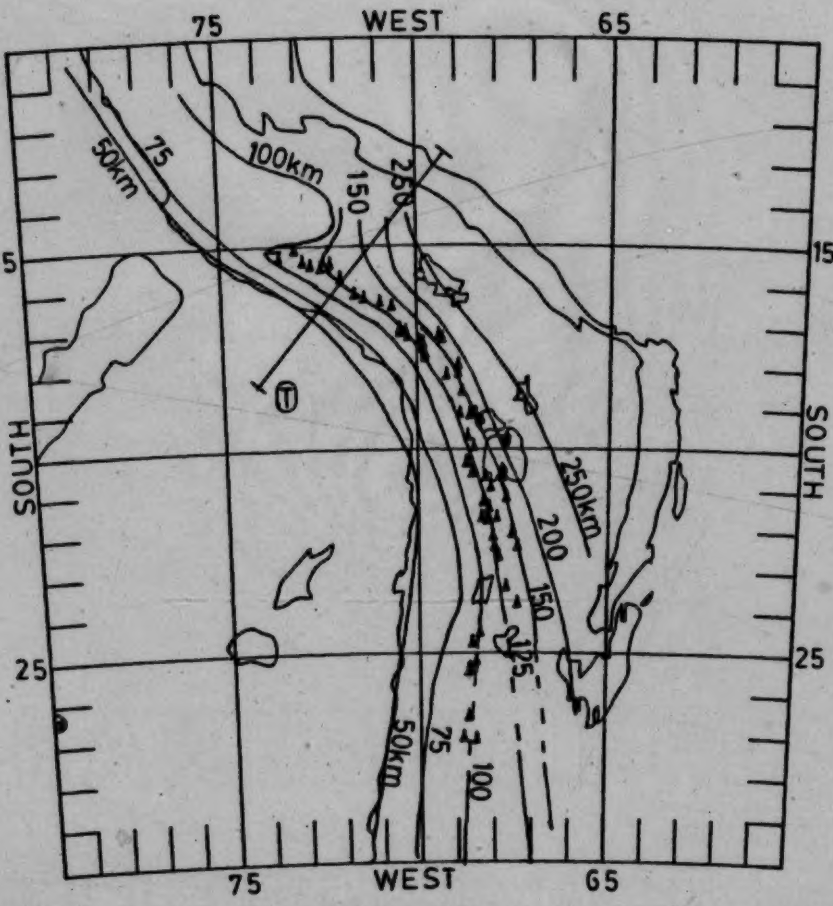
75
WEST
65
15
15
SOUTH
SOUTH
25
25
75
50km
100km
150
250
250km
200
150
125
100
75
50km
Ⓣ
75
WEST
65

▲ DENOTES ACTIVE VOLCANOES

Ⓣ "Tear"of Barazangi and Isacks (1976 & 1979)

Figure 3.19 shows approximate contours of the depth to "maximum" seismic activity beneath the Central Andes. Contours were constructed from a detailed analysis of numerous intersecting vertical profiles (not shown, but see Appendix 1). Most of the features of these contours can be confirmed in figure 3.18. Also shown is the location of the "tear" in the Nazca Plate postulated by Barazangi and Isacks (1976 and 1979.

north. Earthquakes to the north occur no deeper than about 100km while, to the south, the deepest event is nearly 300km over the same horizontal range.

The tear model is based on the comparison of only two profiles taken normal to the trench which, in this region, is definitely not the same as the direction of subduction (figure3.1a). I examined the spatial distribution of hypocenters in detail from 14°S to 23°S and came to a different conclusion than Barazangi and Isacks (1976 and 1979). Figure 3.19 shows approximate contours of the depth to "maximum" seismic activity. These contours were constructed by covering the region with an intersecting mesh of vertical profiles each only 1° wide. The depth to maximum seismic activity was visually selected for a number of points on each profile. Fitting smooth contours to the resulting data matrix resulted in figure 3.19. While it is impractical to display all of the profiles used here, the major features of figure 3.19 can be seen in figure 3.18. (Also, the suite of profiles displayed in Appendix 2 provides additional supporting evidence.) The hypocentral depth display used in figure 3.18 was chosen such that any contour on figure 3.19 corresponds to the locus of a single symbol type on figure 3.18.

Figure 3.19 is a model for the geometry of the Benioff zone from the Pisco Deflection to 25°S. The "tear" (Barazangi and Isacks 1979) occurs in a region where the geometry changes rapidly but continuously from horizontal to

30° subduction. Hypocentral locations obtained from a local network in southern Peru support this conclusion (Hasegawa and Sacks 1979 and 1980).

The most striking feature of figure 3.19 is the large eastward deflection of the 100 kilometer contour. The deflection begins where the Nazca Ridge meets the trench and continues eastward beneath the Pisco Deflection (figure 3.3). This is direct evidence that the Pisco Deflection is causally linked to the subduction process and is perhaps a consequence of the interaction of the Nazca Ridge with the trench system.

In figure 3.19 volcanism begins just south of the deflection in the 100 kilometer contour. There are two distinct linear trends in the volcanoes: one in southern Peru which closely follows the 125 kilometer contour, and another in northern Chile which groups more closely about the 150 kilometer contour. (These contours indicate the depth to "maximum" seismic activity which is probably not the upper surface of the descending slab.)

Figure 3.20a is a vertical seismicity section, 1 degree wide, taken in the direction of subduction through northern Chile and showing all events having Mb>4.0. In figure 3.20b the threshold magnitude has been increased to 5.0. Maximum energy release is probably at the point of magma generation but, unlike Central Peru, there is fairly continuous large magnitude activity down to depths of 250 km. Figure 3.21 shows a possible subduction zone geometry for northern

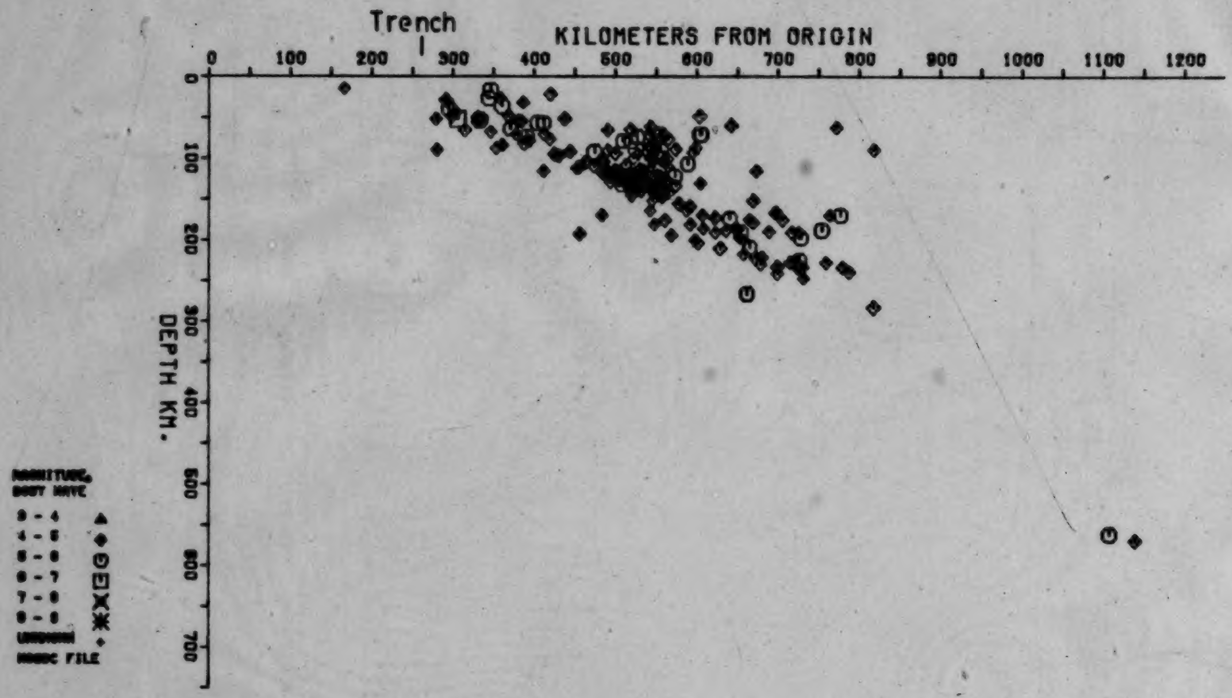

CROSS SECTION 1.0 DEGREES WIDE
BETWEEN -22.5,-73.5 AND -20.0,-61.7

Figure 3.20a is a vertical seismicity profile, 1° wide, taken across northern Chile in the direction of subduction. Only events having Mb greater than 4.0 are shown. The dense cloud of activity between 125 and 150 kilometers is directly beneath the volcanic front.

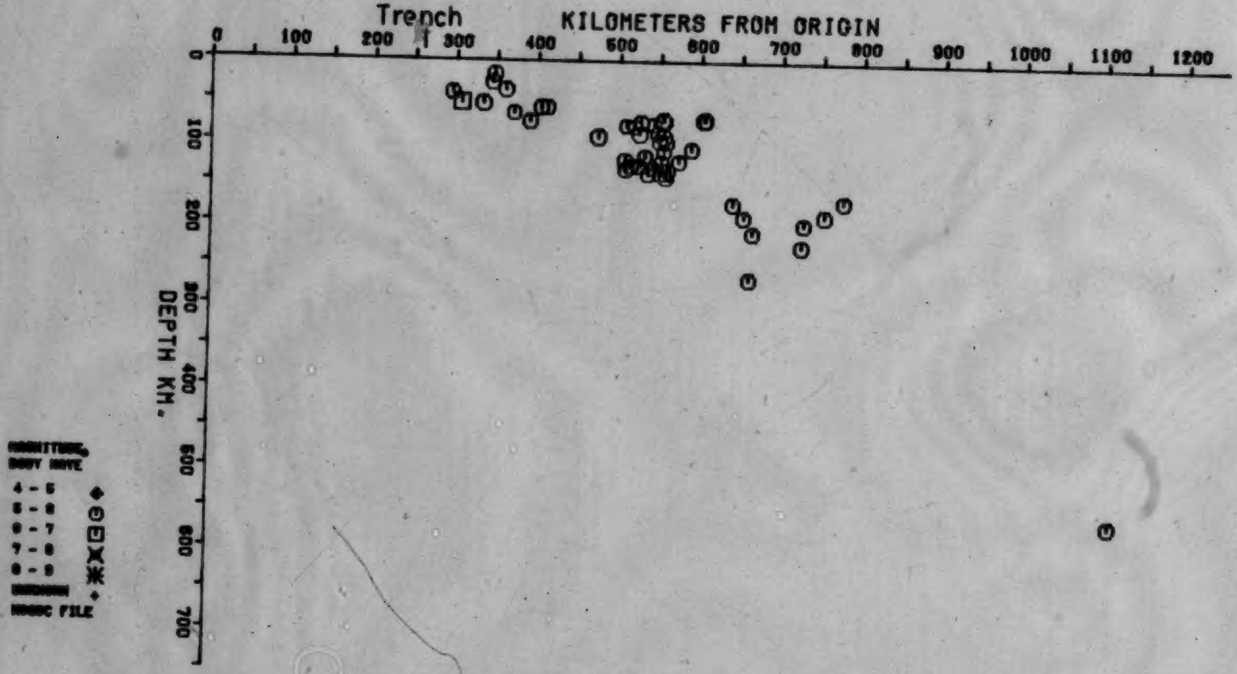

CROSS SECTION 1.0 DEGREES WIDE
BETWEEN -22.5,-73.5 AND -20.0,-61.7

Figure 3.20b shows the same profile as 3.20a but a higher threshold magnitude (5.0) has been used. Energy release is maximal beneath the volcanic front but is distributed continuously along the slab to a depth of 250 kilometers.

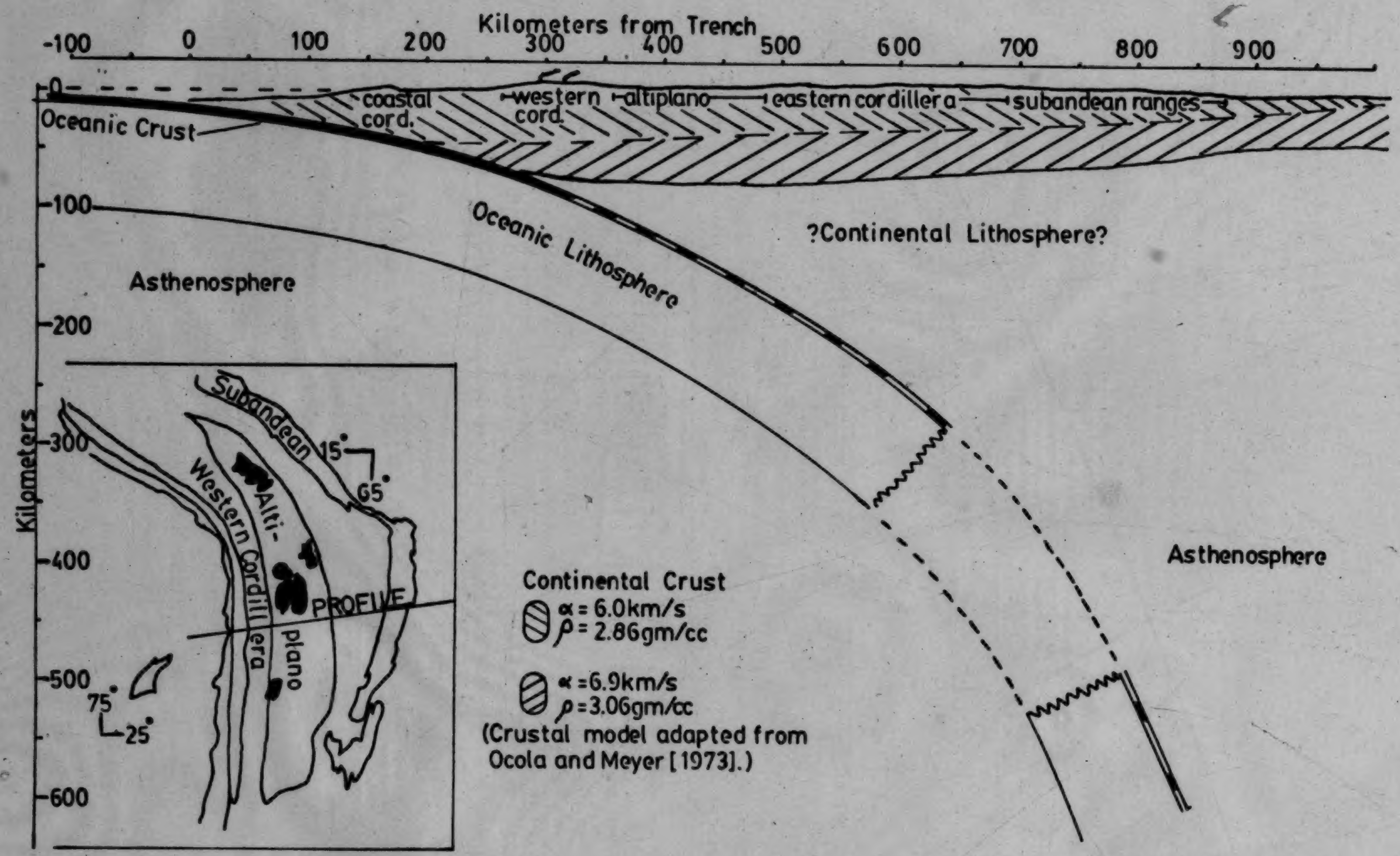
Kilometers from Trench
-100
0
100
200
300
400
500
600
700
800
900
Kilometers
0
-100
-200
-300
-400
-500
-600
coastal cord.
western cord.
altiplano
eastern cordillera
subandean ranges
Oceanic Crust
Oceanic Lithosphere
?Continental Lithosphere?
Asthenosphere
Asthenosphere
Continental Crust
α = 6.0km/s
ρ = 2.86gm/cc
α = 6.9km/s
ρ = 3.06gm/cc
(Crustal model adapted from Ocola and Meyer [1973].)
Subandean
Alti-
plano
Western Cordillera
PROFILE
15°
65°
75°
25°

Figure 3.21 is a cartoon depicting a possible mode of subduction beneath the Central Andes.

Chile.

### 3.8.8 The Andean Seismicity Lineament

Another important seismic feature in the Central Andes, noticed is the linear feature formed by intermediate depth events in northern Chile (figure 3.13) (Barazangi and Isacks 1976 and 1979). This will be referred to as the Andean Seismicity Lineament (ASL). The northern extension of the ASL passes directly through the locus of deep events in western Brazil. Events forming the southern part of the ASL (in northern Chile) occur at an average depth of 100-150km while those to the north are at depths greater than 550km. The ASL has a strike of approximately N12°W and a length in excess of 1500Km.

Seven focal mechanism solutions for events in northern Chile defining the ASL are similar (Stauder 1973). The average solution has one nodal plane dipping 30°N-NE and striking N25°W while the other dips shallowly to the W-SW. The fault motion is thus either normal faulting along the steeply dipping plane or thrusting along the shallow plane. Stauder favors the normal faulting mechanism noting that the steeply dipping nodal plane agrees with the dip of the Benioff zone in northern Chile. The nodal planes are not quite aligned with the ASL; however, shallow focus events occurring on or near the trench have an average direction of underthrusting of N85°E (or nodal plane strike of N15°W) which is essentially perpendicular to the ASL (Stauder

1973).

Focal mechanisms of some events defining the northern part of the ASL are quite consistent and show an average nodal plane strike of N10°W. and a near vertical axis of compression (Stauder 1975).

Figure 3.22 shows the same seismicity map as figure 3.13 with a spherical polar grid drawn about the relative motion pole for the South American and Nazca plates (Minster and Jordan 1978). One of the great circles (striking N12°E) fits the ASL almost perfectly. A similar grid drawn about the pole of relative motion for the Pacific and Nazca plates (figure 3.23) yields a good but slightly more discordant fit. The best fit circle in this case strikes N10°W.

These results imply that the geometric principles of plate tectonics can be extended to continental geology. If the fit in figure 3.22 is real, the ASL is a "front" of some sort normal to the direction of relative motion. The ASL also appears in the surface geology as shown in figure 3.24. Here the best fitting line of figure 3.22 is compared to the modern volcanic belt and the Pampean basement blocks. The volcanic belt groups very tightly about this line for nearly 800 km , from 17°S to 24°S. At 24°S a dextral shift of the volcanic trend causes it to deviate from this front. From 25°S to 33°S the Pampean horst structures outcrop along the same line.

From 24°S to 26°S, the ASL loses its definition as the regional seismicity becomes very sparse. In this same

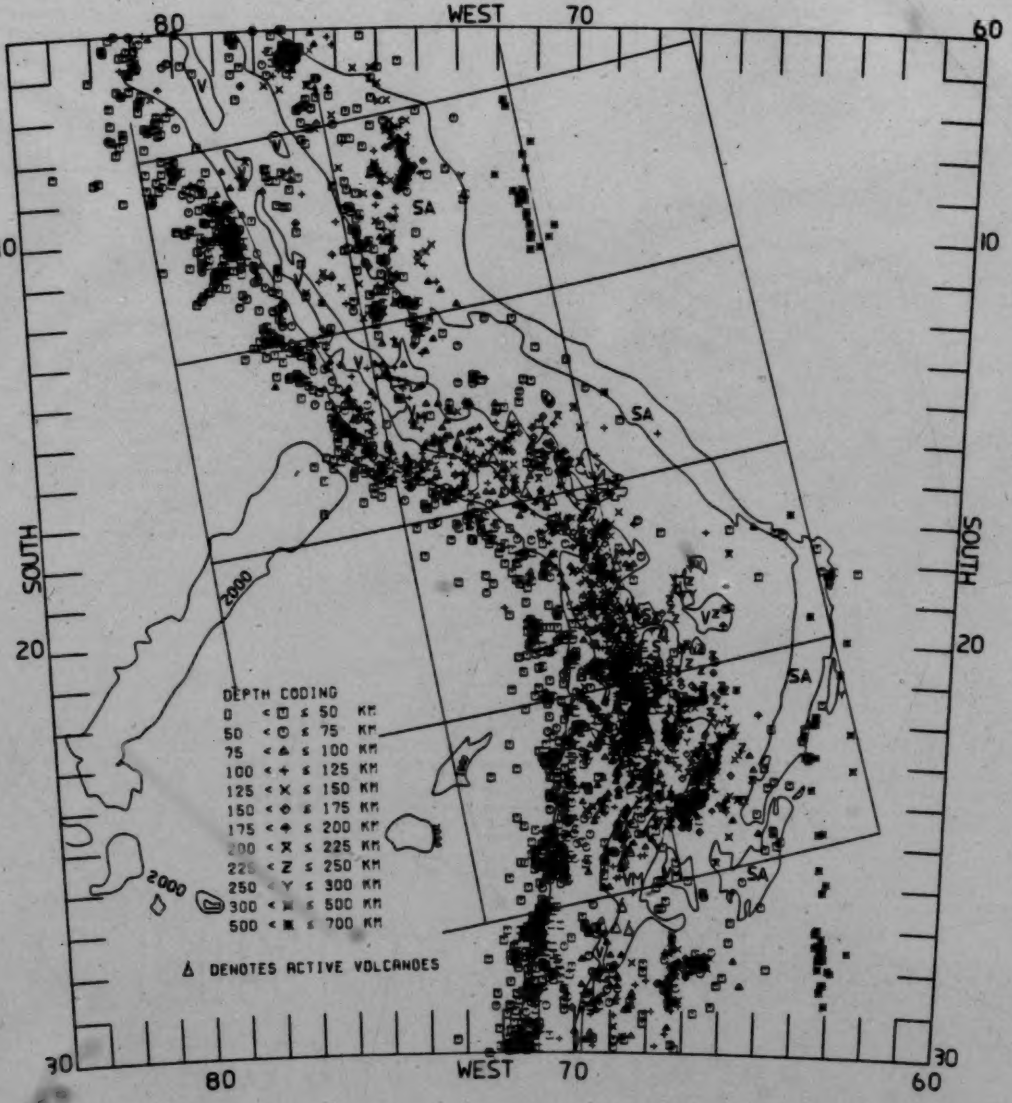
80
WEST
70
60
10
10
SOUTH
SOUTH
20
20
30
30
80
WEST
70
60
V
SA
SA
SA
SA
VZ
VM
2000
2000
DEPTH CODING
0 < □ ≤ 50 KM
50 < ○ ≤ 75 KM
75 < △ ≤ 100 KM
100 < + ≤ 125 KM
125 < × ≤ 150 KM
150 < ◇ ≤ 175 KM
175 < ♠ ≤ 200 KM
200 < X ≤ 225 KM
225 < Z ≤ 250 KM
250 < Y ≤ 300 KM
300 < ▪ ≤ 500 KM
500 < ■ ≤ 700 KM
Δ DENOTES ACTIVE VOLCANOES

Figure 3.22 shows the same seismicity map as figure 3.13 with a spherical coordinate grid drawn about the relative motion pole for the Nazca and South American plates. Pole position is 94.75°W and 59.08°N and is from earth model RM2 of Minster and Jordan (1978).

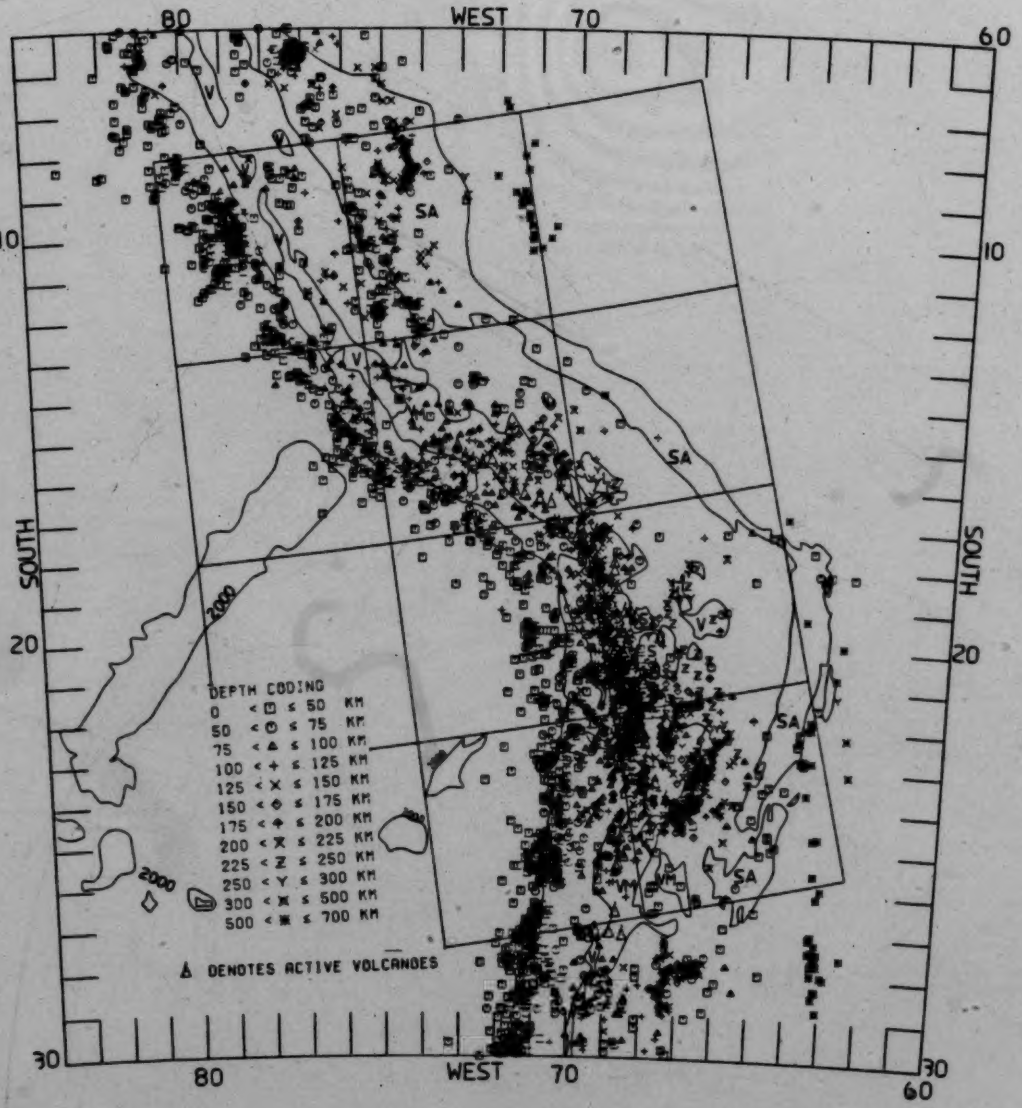
80
WEST
70
60
10
SOUTH
20
30
V
SA
2000
DEPTH CODING
0 < ⊡ ≤ 50 KM
50 < ⊙ ≤ 75 KM
75 < ▲ ≤ 100 KM
100 < + ≤ 125 KM
125 < × ≤ 150 KM
150 < ◈ ≤ 175 KM
175 < ♠ ≤ 200 KM
200 < X ≤ 225 KM
225 < Z ≤ 250 KM
250 < Y ≤ 300 KM
300 < ⊠ ≤ 500 KM
500 < ■ ≤ 700 KM
Δ DENOTES ACTIVE VOLCANOES

Figure 3.23 is similar to figure 3.22 except the superimposed grid is drawn about the Nazca - Pacific pole of relative motion. Pole position is 87.88°N and 56.64°W after Minster and Jordan (1978).

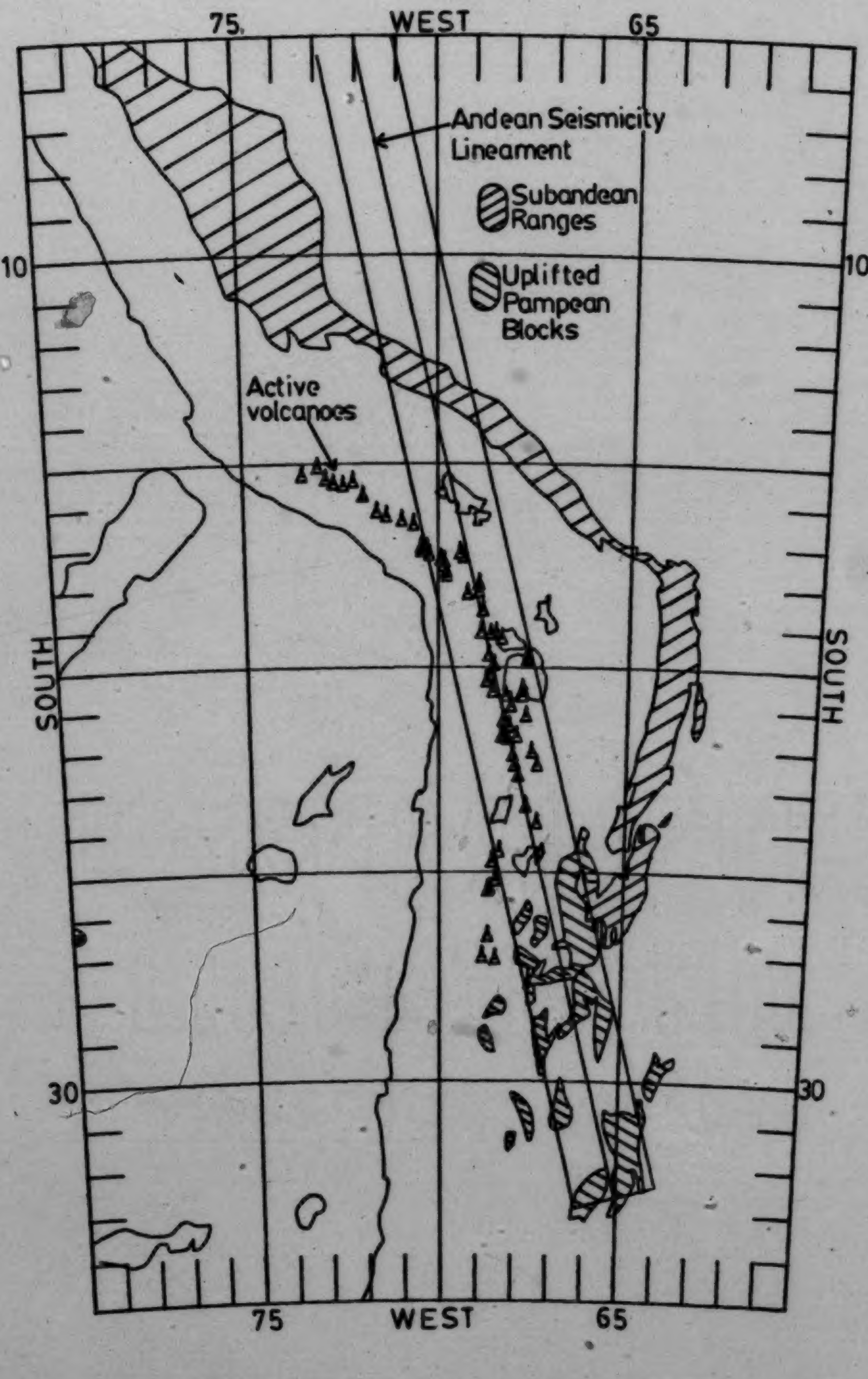
75
WEST
65
Andean Seismicity Lineament
Subandean Ranges
Uplifted Pampean Blocks
Active volcanoes
10
SOUTH
30

Figure 3.24 compares the Andean Seismic Lineament as defined by the best fitting line of figure 3.22, with the locations of modern volcanism and the Pampean basement horsts.

interval on the Nazca Plate, several bathymetric highs are found in the vicinity of the trench. Centered on the ASL at about 26°S is an aseismic region which may be an extension of the Easter Fracture Zone (Sala y Gomez Ridge) (Bonatti et al. 1977, Hanus and Vanek 1978).

I do not suggest that plate tectonics principles make transparent the reasons for all of these geometric relationships. Nevertheless, an underlying geometric coherence has key tectonic structures along "fronts" normal to the direction of relative motion. Such a result is a consequence of the relative motion of two spherical caps but does not reveal the dynamics of the Pampean uplift or Andean volcanism. The ASL may imply a great fault in the Nazca Plate and perhaps indicates a zone of weakness along which a piece of the plate may break off and form a detached slab (Barazangi and Isacks 1979).

The association of volcanic centers with the line suggests another explanation. Evidence that the Peruvian Coastal Batholith was emplaced by magma intrusions along a linear fracture extending through the crust (Tapacocha Axis) was presented earlier. The ASL may indicate such a giant vertical fracture (or system of fractures) which extends from Lago Titicaca to at least 35°S. Volcanic centers would be found along such a line whenever the subduction process brings the melting zone beneath the fracture. The Pampean blocks and Altiplano could then represent vertical tectonic activity along the fault. Along the volcanic segment of the

ASL, it is both a route for magma migration and a tectonic fault showing many km of relative vertical motion.

If this is correct, linear batholith chains like the Peruvian Coastal Batholith may provide valuable constraints on the positions of paleo-poles of relative motion. Handschumacher's (1976) study suggests that subduction in the Eocene was normal to the Peruvian Coastal Batholith as would be expected.

This model does not explain why the zone of deep focus events in western Brazil aligns with the ASL. There is little doubt that the Nazca Plate is discontinuous along this line; therefore, any explanation requiring the transmission of mechanical stresses to "align" the plate is ruled out. The model advanced previously for Peruvian subduction implies that these deep focus events represent a detached piece of the slab which has been passively sinking into the mantle. If that is so, then the alignment is either a remarkable coincidence or it may imply something about plate driving forces and mantle convection currents. Alternately, the ASL may be controlled by the deep structure of the South American continent. Perhaps it indicates the western boundary of a substructure associated with the South American craton.

If the ASL in Chile represents a megafracture penetrating the South American plate, then it is interesting to ask when and how it formed. This is a major topic of the next chapter where I will argue that the fracture is an extremely old feature which formed during the disruption of the western Gondwana continent in Mesozoic times. Such fractures would exert a controlling influence on subsequent tectonics.

### 3.8.9 Observations and Speculations on Geometric Symmetries

It is often remarked that the two lines of deep earthquakes in South America show discordant trends (Stauder 1973, Hanus and Vanek 1978). Since it seems likely that the western Brazil deep quakes form a seismic front normal to the relative motion of either the Nazca - South America plates or the Nazca - Pacific plates, it might be hoped that a similar thing might be true for the western Argentina deep events. A study of the relative motion poles for all nearby plates has been fruitless.

These two trends would not be considered in discord if it could be shown that they lie along different great circles about the same pole. From figure 3.12, the point of intersection of these trends may be seen to be near 62°W and 43°S on the southern Argentina shelf. No present plate tectonics scheme has ever been proposed with a relative motion pole here. If such a pole did exist, it might correspond to a new plate organization or an unknown system of mantle currents. Alternately, since both deep focus zones probably represent detached slabs, it is also possible that such a pole could reflect a plate arrangement which was operable some 15my ago but no longer exists.

There are several other geometric relationships in evidence in South American seismicity patterns, some of which are listed below:

1. The strike of the Nazca Ridge points directly towards the western Brazil deep earthquakes.
2. The Nazca Ridge, ASL, western Brazil deep quakes, and the aseismic zone at 26.5°S and 68°W form a triangular structure whose southern side can be closed by a small circle about either the Nazca - South America or the Nazca - Pacific poles (figures 3.22 and 3.23).
3. Two dense clusters of shallow - intermediate events lie along the strike of the J. Fernandez ridge when projected into the continent (figure 3.15).
4. A dense, elongate cluster at 23°-24°S and 67°W seems to run parallel to the eastern edge of the Miocene to recent volcanism (compare figures 3.4b and 3.15).
5. Generally speaking, the positions of the three major aseismic ridges, the Carnegie, the Nazca, and the J. Fernandez, coincide with changes in both seismicity patterns and geology. On figure 3.12, it can be seen that all deep earthquakes and most intermediate depth events lie between the Carnegie and the J. Fernandez ridges. The Nazca Ridge denotes a major style change in between. The Sala y Gomez ridge points out the disruption of the ASL and other features associated with the Ojos del Salado Lineament.

## 3.9 The South American Interior

Here I will present brief sketches of several structures in the continental interior which I feel to be of key importance in the tectonic evolution of the continent. The relationship between them and the Andes will become apparent in the next chapter.

### 3.9.1 The Argentine Basins

The tectonic style of the eastern margin of Argentina has largely been one of rifting and subsidence since late Jurassic time (Zambrano and Urien 1970). Figure 3.25 is adapted from Zambrano and Urien (1970) and Urien and Zambrano (1973) and shows the locations of major basins and shear zones. The area consists of a series of wedge shaped basins with their long axes oriented more or less perpendicularly to the coast. Seismic reflection studies reveal rift-like fault structures beneath the basins (Zambrano and Urien 1970 and Urien and Zambrano 1973).

The history of the modern basins began in Jurassic times (Zambrano and Urien 1970) with the emplacement of the Tobifera formation, a rhyolitic complex common throughout southern South America (Dott 1976) (figure 3.11). This event was roughly contemporaneous with the beginning of the extrusion of the Parana flood basalts. By the late Jurassic the pattern of regional subsidence was established with the formation of the Salado and Colorado basins.

Subsidence continued through the early Cretaceous when

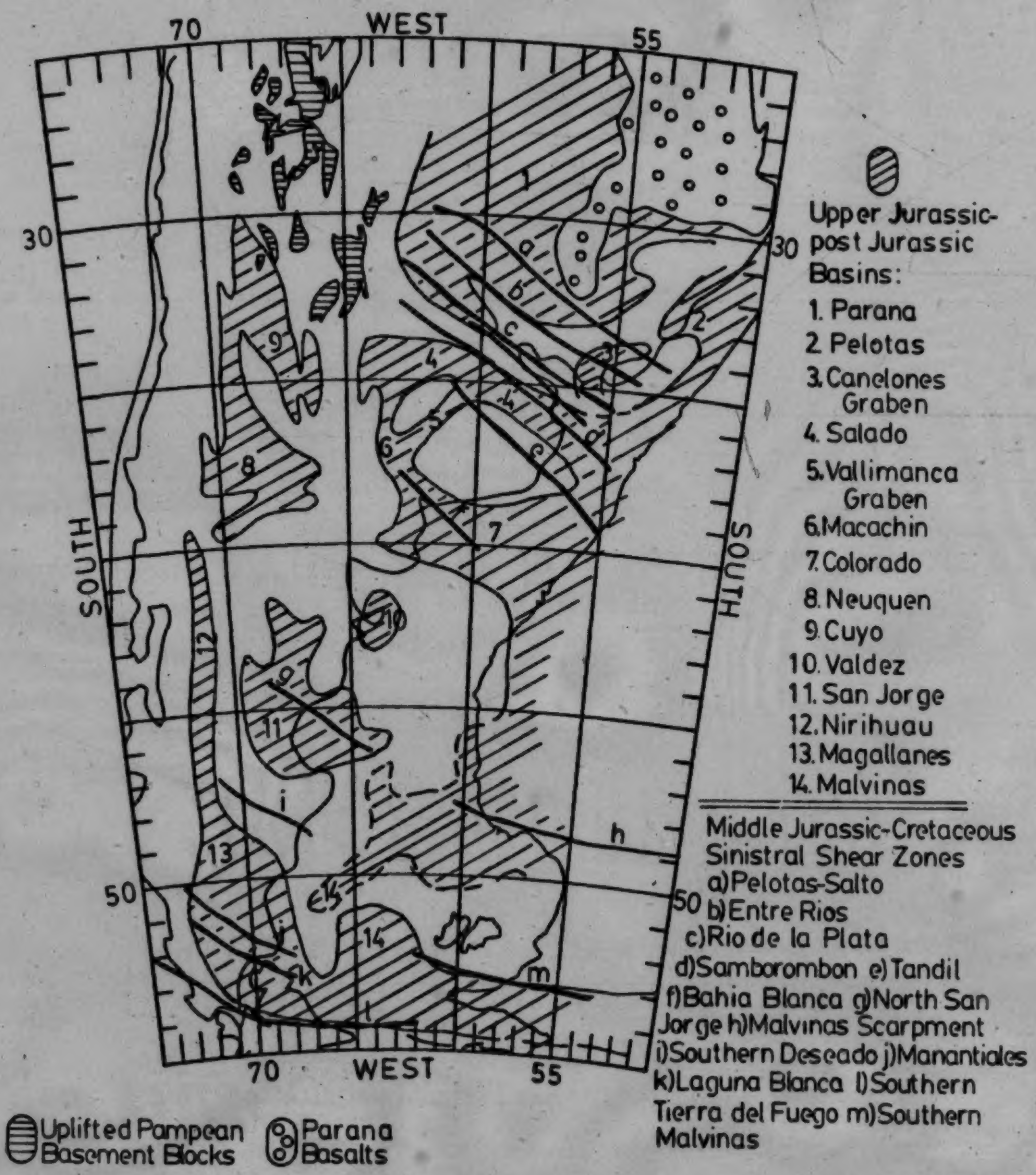
70
WEST
55
30
30
50
50
SOUTH
SOUTH
70
WEST
55
Upper Jurassic-post Jurassic Basins:
1. Parana
2. Pelotas
3. Canelones Graben
4. Salado
5. Vallimanca Graben
6. Macachin
7. Colorado
8. Neuquen
9. Cuyo
10. Valdez
11. San Jorge
12. Nirihuau
13. Magallanes
14. Malvinas
Middle Jurassic-Cretaceous Sinistral Shear Zones
a) Pelotas-Salto
b) Entre Rios
c) Rio de la Plata
d) Samborombon
e) Tandil
f) Bahia Blanca
g) North San Jorge
h) Malvinas Scarpment
i) Southern Deseado
j) Manantiales
k) Laguna Blanca
l) Southern Tierra del Fuego
m) Southern Malvinas
Uplifted Pampean Basement Blocks
Parana Basalts

Figure 3.25 is adapted from Zambrano and Urien (1970) and Urien and Zambrano (1973) and shows major sedimentary basins and shear zones in Argentina which have formed since the Jurassic.

sediments filled all basins including the Neuquen and Paraná and massive basaltic flows appeared in Uruguay, the Chaco-Parana plains, Central Argentina and in the seaward extension of the Salado basin. Deposition in the San Jorge and Magallenes basins may have been interrupted in the mid-Cretaceous by an orogeny (Lesta 1968).

During the late Cretaceous through the Paleocene subsidence continued unabated in all basins. Detrius derived from Andean volcanism filled the basins, and the regional slope changed from inclined towards the Pacific to towards the Atlantic, resulting in the first of many transgressions by the Atlantic into southern Argentina.

The Eocene seems to have been a period of relative quiesence. Sedimentary breaks occurred in the Salado-Colorado basins. Some sedimentation took place in the San Jorge and Magallenes basins. Oligocene deposition is also scarce in southern Argentina.

The Miocene was a period of renewed activity. Extensive subsidence which was probably related to the Andean Miocene orogeny (Zambrano and Urien 1970) occurred in all basins. There was significant acid and basic volcanism in central and western Argentina. Most of the Chaco-Pampas was submerged beneath a shallow sea.

The Pliocene was a period of emergence and extensive basic igneous activity which continued during the Quaternary. Large basalt flows occurred on the northern Patagonia and Desado massifs. Similar activity is seen in the Magallenes and Neuquen basins.

Figure 3.25 also shows major lineations and areas of strike-slip faulting. Activity along these faults began in the middle Jurassic and continued through most of the Cretaceous. Offsets are dominantly left lateral. Many of these faults are found along lines which coincide with the strike of the basins.

### 3.9.2 The Parana Flood Basalts

Approximately 130 million years ago southwestern Brazil, eastern Paraguay, all of Uruguay, and parts of northeastern Argentina were the site of one of the largest outpouring of basic magmas yet discovered on the earth. Covering an area of at least $1.2\times10^6$ km$^2$ (Maack 1952) (see figure 3.1) and reaching depths of more than 1500 meters (Cordani and Vandoros 1967, Bowen 1966), the Parana basalts (also known as the Serra Geral basalts) represent a truly enormous volume of extrusive material. Using an average depth of 500 meters and an areal extent of $1\times10^6$ km$^2$, the total volume is estimated as being some $6.5\times10^5$ km$^3$. These numerical estimates are all based on the present visible surface of the basalts and are almost certainly conservative (Cordani and Vandoros 1967).

$Sr^{87}/Sr^{86}$ and K/Rb ratios obtained are consistent with direct derivation from the mantle (Verhoogen et al. 1970, Cordani and Vandoros 1967). There is little evidence of significant contamination from crustal material (Cordani and

Vandoros 1967). K/Ar age determinations have been summarized by Hertz (1966) and Cordani and Vandoros (1967). Figure 3.26 is adapted from Hertz (1966) and shows histograms of the age determinations. As can be seen activity may have begun as long ago as 165ma and the event was certainly in progress by 145ma. Maximal activity was between 130 and 120ma with the peak at 120. There are some age determinations below 120ma but these are probably due to argon loss (Hertz 1966). Hence, the outpouring seems to have had a fairly sharp cutoff immediately after the period of maximal activity.

There is no evidence of explosive activity (Eckel 1959, Hertz 1966, Cordani and Vandoros 1967), instead the lavas seem to have flowed quietly from tension cracks (Cordani and Vandoros 1967). This system of tension cracks is in evidence today as a large system of diabase dikes and sills. These dikes range in width from a few centimeters to as much as 100 meters and often have lengths approaching 100 km. (Cordani and Vandoros 1967). The dikes strike more or less perpendicular to the axis of the basin and, collectively, indicate a regional extension of 5% or more parallel to the continental margin (Verhoogen et al. 1970).

There are some associated alkaline igneous rocks found in neighboring areas (mostly in southern Sao Paulo state) as reported by Hertz (1966). These are much smaller in areal extent and show two peaks of activity. The first peak occurs between 136 and 122ma while the second is between 82 and 51ma. These may represent a fractionation of the Parana

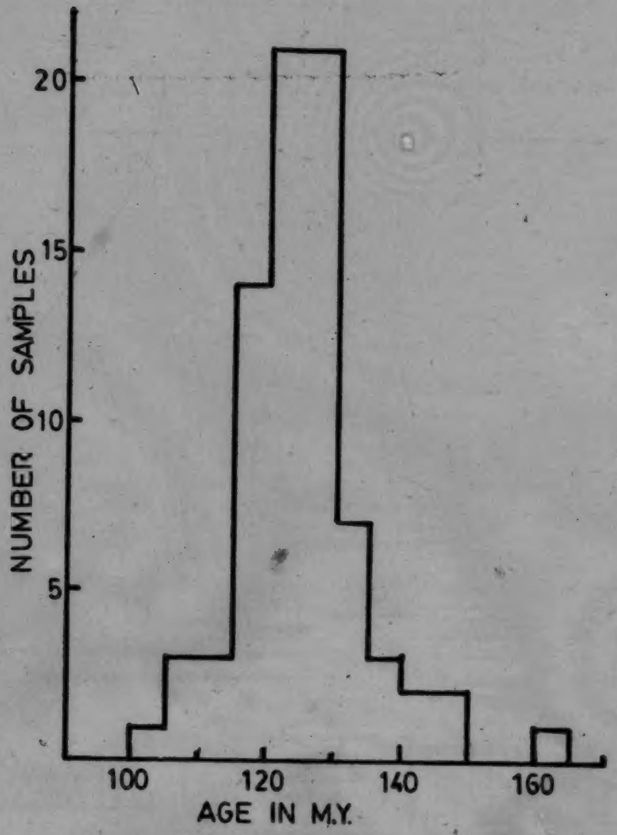

Figure 3.26 is adapted from Hertz (1966) and shows the age distribution of K-Ar dating for the Parana Basalts. Determinations were made by various authors and summarized by Hertz.

basalts though the latter shows no second period of activity in the Tertiary.

The Parana basalts are definitely not contemporaneous with the Karoo basalts in southern Africa. McDougal (1963) found K/Ar ages for the Karoo dolerites cover the range 190 to 154ma. Ages of the Kakao basalts of southwestern Africa show a similar distribution to the Parana basalts and are probably related (Siedner and Miller 1968). However, the areal extent of the Brazilian Serra Geral formation is vastly greater than its South African cousin.

### 3.9.3 The Chaco-Pampas Plains

Eckel (1959) interpreted the Gran Chaco of Paraguay as a vast depositional basin with sedimentary thicknesses of at least 3000m and structurally controlled by a series of major faults, downthrown to the west, that parallel the course of the Parana river. Harrington (1956) states that the high seismic velocity basement of the Argentine pampas is at least 5000m below sea level. These plains show a thin covering of Quaternary continental sediments covering a thick lens of continental Pliocene, marine upper Miocene, continental upper Tertiary (and volcanics), and on down to a presumed Precambrian basement (Harrington 1956). Faults parallel to the Parana river are dominated by a major fault with a vertical throw of some 700 meters (Harrington 1956).

Thus, the Chaco-Pampas plains are a downfaulted basin which has served as the major depository for detrius from the Andean uplift.

## 3.10 Summary

1. The Huancabamba Deflection and the Pisco Deflection are regions of major structural change in the Andes and coincide with the positions of the Carnegie Ridge and the Nazcá Ridge respectively.
2. Peruvian igneous history is dominated by the emplacement of the Peruvian Coastal Batholith from 105ma until possibly 30ma. Associated volcanism can be viewed as simply the "ejecta" of the plutons.
3. The emplacement of the Peruvian Coastal Batholith took place on the same system of linear fractures throughout its history. These fractures, the Tapacocha Axis, probably penetrate the South American crust and allowed magma formed at the Benioff zone to migrate to the surface.
4. The Cordillera Blanca Batholith was emplaced along a similar linear fault system beginning about 12ma.
5. Pliocene - Quaternary volcanism is insignificant in Peru between the Huancabamba Deflection and the Pisco Deflection.
6. Peruvian tectonic history can be understood in terms of the vertical oscillations of a series of crustal strips paralleling the coast. There is little evidence for crustal shortening.
7. Pliocene - Quaternary tectonics of Peru north of the

Pisco Deflection are anomalous in a historical perspective evidencing strong horizontal compression in the direction of subduction.

8. Volcanism is associated with extensional tectonics.
9. Igneous activity began in Chile in late Triassic - early Jurassic times. At least 8 major intrusive events have been documented.
10. Magmatic foci in Chile (and possibly Peru) have migrated regularly eastward at a rate near .8mm/yr.
11. A great outbreak of volcanism occurred in the Central Andes about 15ma and ceased about 4ma. This is probably the major discontinuity in Andean history.
12. Trace element geochemistry of Central Andean andesites indicates they derive from Benioff zone melt but undergo considerable crustal contamination while rising to the surface.
13. Maximum crustal thickness in the Central Andes occurs beneath the Western Cordillera and Altiplano and exceeds 70 km. Lithospheric thickness beneath South America is probably everywhere greater than 300 km.
14. The Central Andes also show dominantly vertical tectonics.
15. The Altiplano and Pampean ranges are probably similar uplifted blocks of Precambrian - early Paleozoic basement.
16. The Chilean central valley is associated with areas of modern volcanism and probably is a graben.

17. The Ojos del Salado Lineament marks another structural boundary and coincides with the offshore position of the Sala y Gomez Ridge - Easter Fracture Zone.
18. The beginning of the Andean orogeny is coincident with the breakup of western Gondwana. Activity south of about 18° may have begun as much as 100my before activity to the north.
19. Seismicity patterns in central Peru are consistent with a shallow underthrusting of the Nazca Plate. The plate probably subducts horizontally for some 800 km beyond the trench.
20. A diffuse zone of crustal earthquakes is present in the South American continent in central Peru above the subducting slab. These earthquakes indicate horizontal compressive stresses in the lower crust.
21. A zone of deep focus events probably represents a piece of lithosphere physically detached from the rest.
22. Subduction beneath the volcanic Central Andes is much steeper. The transition from one zone to the other is sudden but continuous.
23. The Pisco Deflection is reflected in the seismicity structure as a large eastward deflection of 100 km activity. The Nazca Ridge is implicated as the cause of the Pisco Deflection through an unknown mechanism.
24. Beneath the volcanic front, maximum seismic activity occurs between 125 and 150 km.
25. The Andean Seismicity Lineament is a linear feature

formed by the seismicity beneath the volcanic front and the deep focus events in western Brazil. It is geometrically fitted by a great circle drawn through the Nazca - South America pole of relative motion.

26. The ASL indicates that the geometrical principles of plate tectonics do have application on land. The modern volcanic belt conforms to the ASL for some 800 km. The Pampean basement horsts also outcrop along the strike of the ASL for nearly 1000 km.
27. The ASL in Chile may represent a megafracture penetrating the entire South American crust. The fracture is the site of large vertical relative motions and, when the zone of melting on the subducting slab comes beneath it, it serves as a migration route for magma. It represents a modern equivalent of the Tapacocha Axis along which the Peruvian Coastal Batholith was emplaced.
28. Geometric alignments abound in the seismicity patterns of South America and are mostly unexplained.
29. The Argentine basins have a history of subsidence which begins in the Jurassic and has continued to Recent times. Large sinistral shears were active from the middle Jurassic through the Cretaceous. Episodes of subsidence correlate in time with Andean movements.
30. The Parana basalts were effused between 165ma and 120ma with peak activity between 130ma and 120ma. They were probably derived directly from the mantle and indicate

crustal extension of at least 5% parallel to the coast. Areal and volumetric considerations indicate this was one of the largest outpourings of volcanic material in earth history.

31. The vast sedimentary basins of Argentina, Paraguay, Bolivia and western Brazil are downfaulted depositories for erosives from the Andes.

# 4. On the Tectonic Evolution of South America

## 4.1 Introduction

The rigid plate model has proved very successful in the kinematic analysis of large scale motions of crustal plates. Such studies indicate that orogenic processes are characteristic of convergent plate margins, but are of little direct aid in understanding their detailed tectonic evolution. There is a basic contradiction inherent in the application of "rigid" plate theories to the problem of orogenesis. At a convergent margin, plate interaction is obviously not rigid.

Plates have frequently suffered irreversible deformation which need not be localized to convergent margins. (Molnar and Tapponier 1977), The Asian Plate is subject to plastic deformation quite far from its boundary with the Indian Plate (Molnar and Tapponier 1977). At divergent margins such as continental riftlands, permanent deformation features include aulacogens or failed rift-arms (Burke and Dewey, 1973), large scale flood basalts, and even thermal uplift such as is found along the African rift valley. While the presence of such deformations is usually undeniable, speculations about their causes have been controversial.

## 4.2 The Fit of South America to Africa along their Continental Shelves

It is widely believed that the present continental masses were joined in one large megastructure through most of the Mesozoic and that disruption of this "Pangea" continent marks the beginning of a modern plate tectonics era. Accordingly, an appropriate starting point for this chapter is an examination of the fit of the South American and African continents.

It will be shown that the South American shelf can be fitted very precisely to the African shelf, but the northern portion (from Uruguay to the Amazon) requires a different composite rotation from the southern portion (Rio de la Plata and south). This implies a history of relative motion between these two blocks.

### 4.2.1 The Bullard Fit

Carey (1958b) used a model globe with a crust broken into movable spherical caps to demonstrate that the fit of South America to Africa is remarkably good when made at the edge of the continental shelf rather than the coastline as previous workers had done (Du Toit 1937). The fit of all the continents around the Atlantic using a least squares technique (Bullard et al. 1965) confirmed this result in a quantitative way. Various other authors have re-examined the problem (Smith and Hallam 1970, Le Pichon and Hayes 1971, Barron et al. 1978, Rabinowitz and LaBreque 1979) but did not improve the Bullard et al. fit of South America to Africa significantly.

Figure 4.1 shows a computer reconstruction of the Bullard et al. fit. They adopted the angular difference in "longitude" about a possible rotation pole as a convenient measure of misfit. Once a mathematically tractable expression for measuring the misfit is adopted, the rigid rotation giving minimum misfit can be calculated for any given pole. An optimum pole position as well as an optimum rotation angle may be estimated by first guessing the approximate pole position and then conducting a systematic search to find the pole-angle pair giving minimum misfit.

Using 100 points on each side of the Atlantic for each of the 100, 500, 1000, and 2000 fathom isobaths, Bullard et al. examined the fit of South America and Africa at these levels. The results showed a weak dependence on the contour used with the best fit being obtained at the 500 fathom level. Figure 4.1 recreates their best fit. Africa is shown rotated clockwise 57.0° about a pole located at 30.6°W and 44.0°N. (This is fit #9 from their table 1 and is equivalent to their figure 4.) The 100 points used for comparison were taken between the points marked "P" on each continent. Bullard et al. (1965) estimated an r.m.s. (root mean square) misfit of 0.93° or about 88 km. Significant overlap occurs mainly near the delta of the Niger River which is a post separation feature. The large gaps on both the northern and southern ends were not included in the estimation of the

Figure 4.1 shows the fit of Africa and South America according to Bullard et. al. (1965). The continents were matched at the 500 fathom isobath using a least squares technique. Africa is shown rotated clockwise 57.0° about a pole located at 30.6°W and 44.0°N. The average misfit according to Bullard et. al. is 88 kilometers. The points "P" indicate the limits of the continental shelves that were digitized.

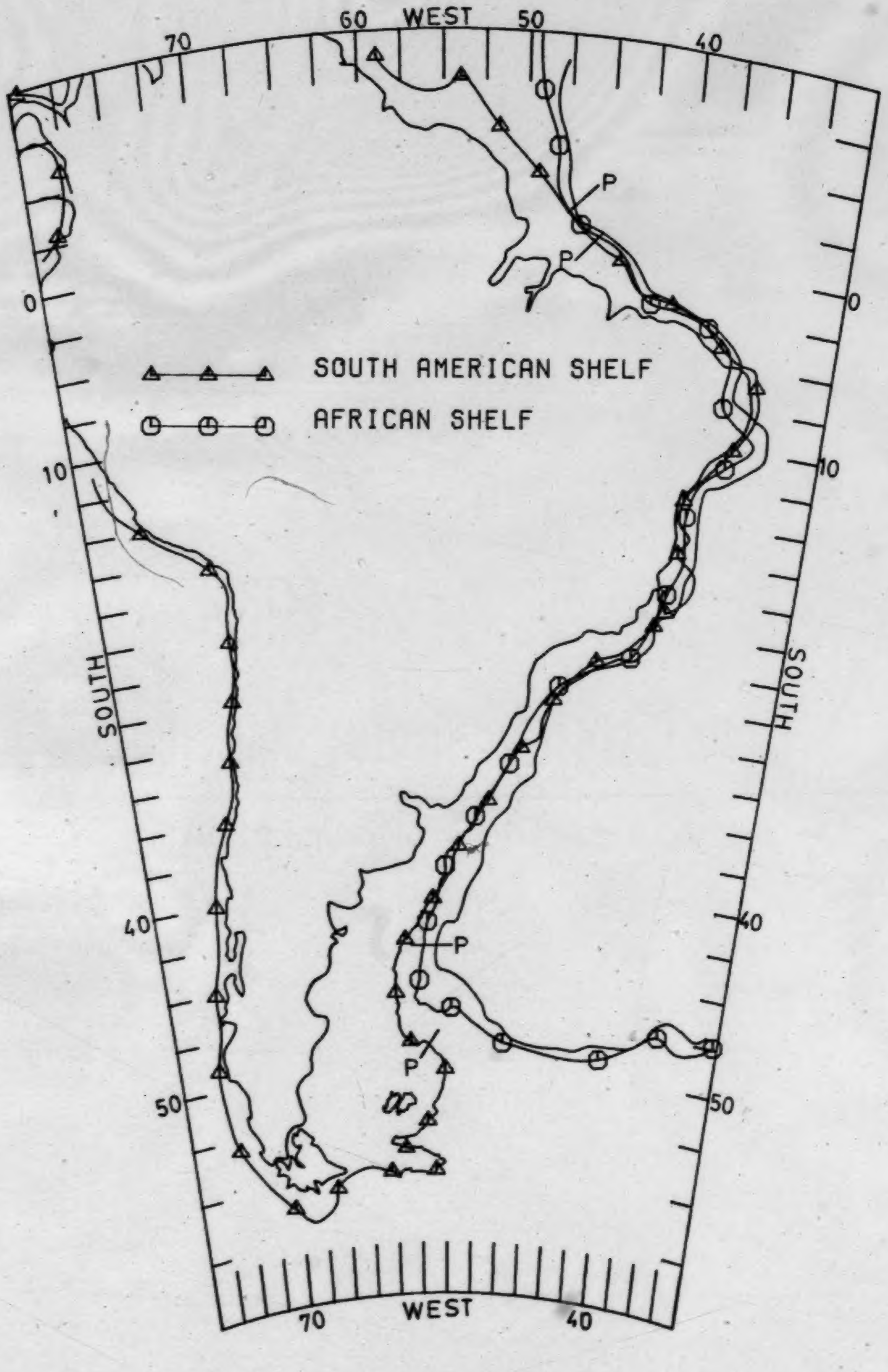
WEST
70
60
50
40
0
10
40
50
SOUTH
△—△—△ SOUTH AMERICAN SHELF
○—○—○ AFRICAN SHELF
P
P
P
P
WEST
70
40

0.93° misfit. The significance of the northern gap will not be considered here, but the southern one will be used as a primary evidence for the model to be presented.

### 4.2.2 A Revised Least Squares Method

The southern gap in figure 4.1 implies that there has been relative motion between southern and northern South America since the beginning of disruption of the megacontinent. (The idea that the Palmer Peninsula of Antarctica should be placed in this gap in a western Gondwana reconstruction is structurally impossible because of the intervening Falkland Plateau. See Barron et al. (1978) for a detailed discussion.) The southern portion of South America will be referred to as the Patagonian block and the northern portion as the craton or cratonic block. The postulated boundary between these blocks will be defined more precisely later (see figure 4.9).

With pencil and tracing paper, it is easy to verify that this southern gap can be closed by a counter clockwise rotation of the Patagonian block by some 10°-15° degrees about a pole near 65°W and 40°S. To quantify this idea, a computer technique for the least squares rotation and comparison of continental masses was developed. The method used is a modification of that devised by Bullard et al. (1965) and is described in detail in appendix 3. Briefly, minimization of the angular misfit between continents (as was done by Bullard et al.) was not found satisfactory. This is because, when the angular extent in latitude of the continents is small, there is a tendency to minimize the angular misfit with a pole 90° from the continents. This was not a problem in the Bullard reconstruction since the South American and African continents subtend large angles.

The modified method measures the continental misfit using the actual distance between opposing points on each continent. This choice is non-unique until the definitions of "opposing points" and "distance between them" are established. The method used is illustrated in figure 4.2. Following Bullard et al. (1965), opposing points were taken to be those points being on the same small circle drawn about the rotation pole. (Finding two such points from digital data sets generally involves linear interpolation on one continental boundary or the other.) The distance between points was assumed to be the arclength of the small circle connecting them.

Thus, a unique mathematical expression of the continental misfit (in km) can be formed and readily minimized. For a given pole position, a unique rotation angle yielding minimum misfit is defined. Rather than use a numerical search procedure to find the optimum pole position, I generated contour maps of the "polar region" showing the continental misfit in km as a function of pole position. This technique requires only a rough guess of the region in which the pole is thought to lie. The map can then be refined by narrowing the bounds of the region once its

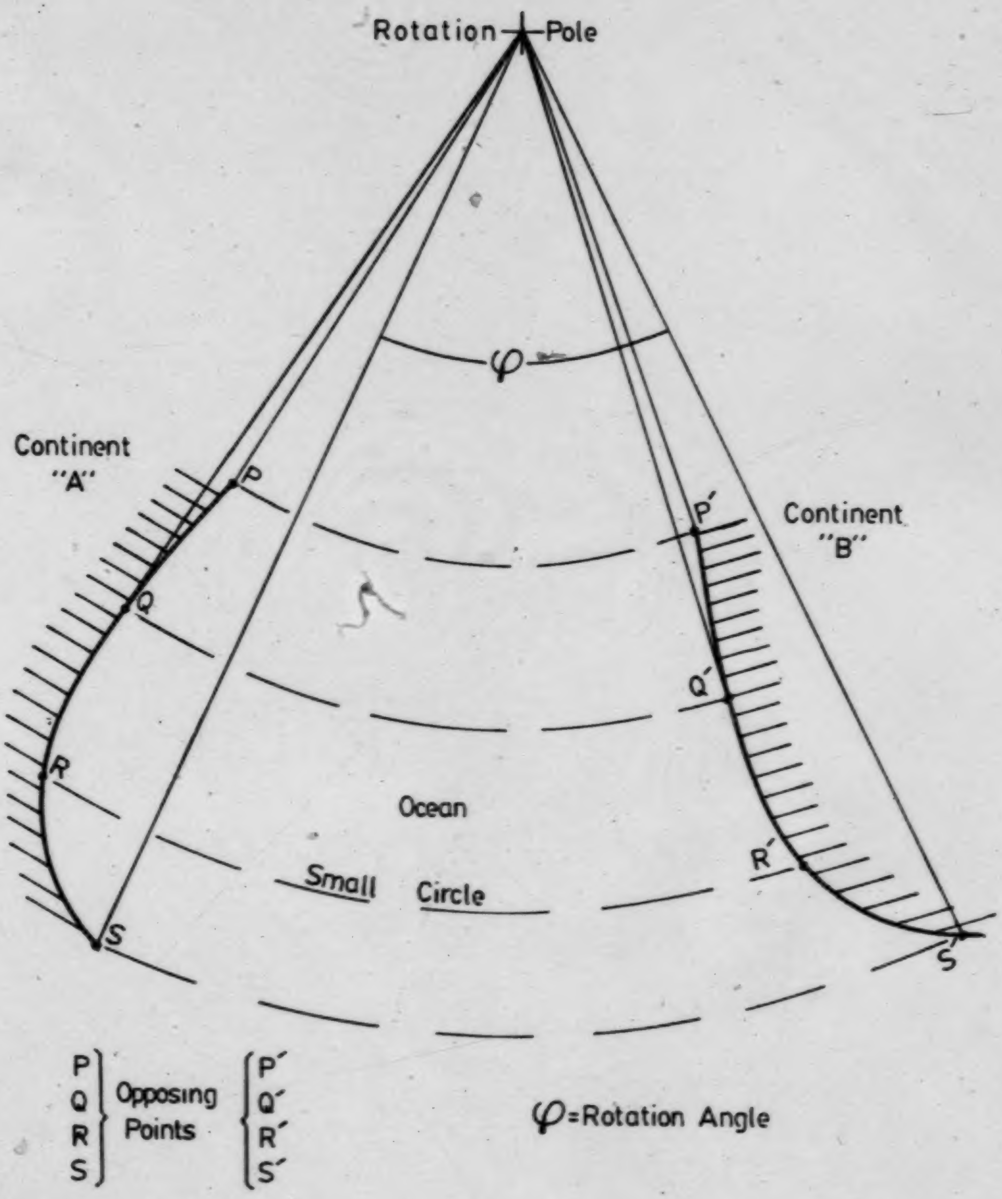
Rotation Pole
φ
Continent "A"
Continent "B"
P
Q
R
S
P′
Q′
R′
S′
Ocean
Small Circle
P Q R S Opposing Points P′ Q′ R′ S′
φ=Rotation Angle

Figure 4.2 illustrates the technique of fitting continents together as discussed in the text. Opposing points are defined as pairs of points, one on each continent, lying on the same small circle about the rotation pole. The best rotation angle is chosen mathematically to minimize the squared misfit measured in kilometers along the small circles.

gross structure is determined.

### 4.2.3 The Bullard Fit Revisited

As a test of this method, a digitized version of the 500 fathom isobaths of the continental shelves (on file at the University of Alberta) was used to repeat the work of Bullard et al. (1965) in fitting South America to Africa. This data file was not intended for this use (and probably does not compare in accuracy to the data used by Bullard et al.), but it proved sufficient to verify the accuracy of the method.

Using a procedure virtually identical to that of Bullard et al. (minimization of angular misfit and systematic searching), gives a best pole position of 31.27°W and 45.07°N, a rotation angle of 56.34°, and an r.m.s. angular misfit of 1.2°. Bullard et al. obtained a pole at 30.6°W and 44.0°N, a rotation angle of 57.0°, and an r.m.s. misfit of 0.93°.

The method described in the last section was used to generate figure 4.3. This shows contours of the continental misfit in km for the area immediately surrounding the pole of Bullard et al. While broadly consistent with the Bullard pole, the contour map conveys much more information and gives an idea of the accuracy of the pole position. Since it is difficult to assess the accuracy of the data used, a particular contour cannot be taken as defining the 95% confidence ellipse. Nevertheless, it is possible to state

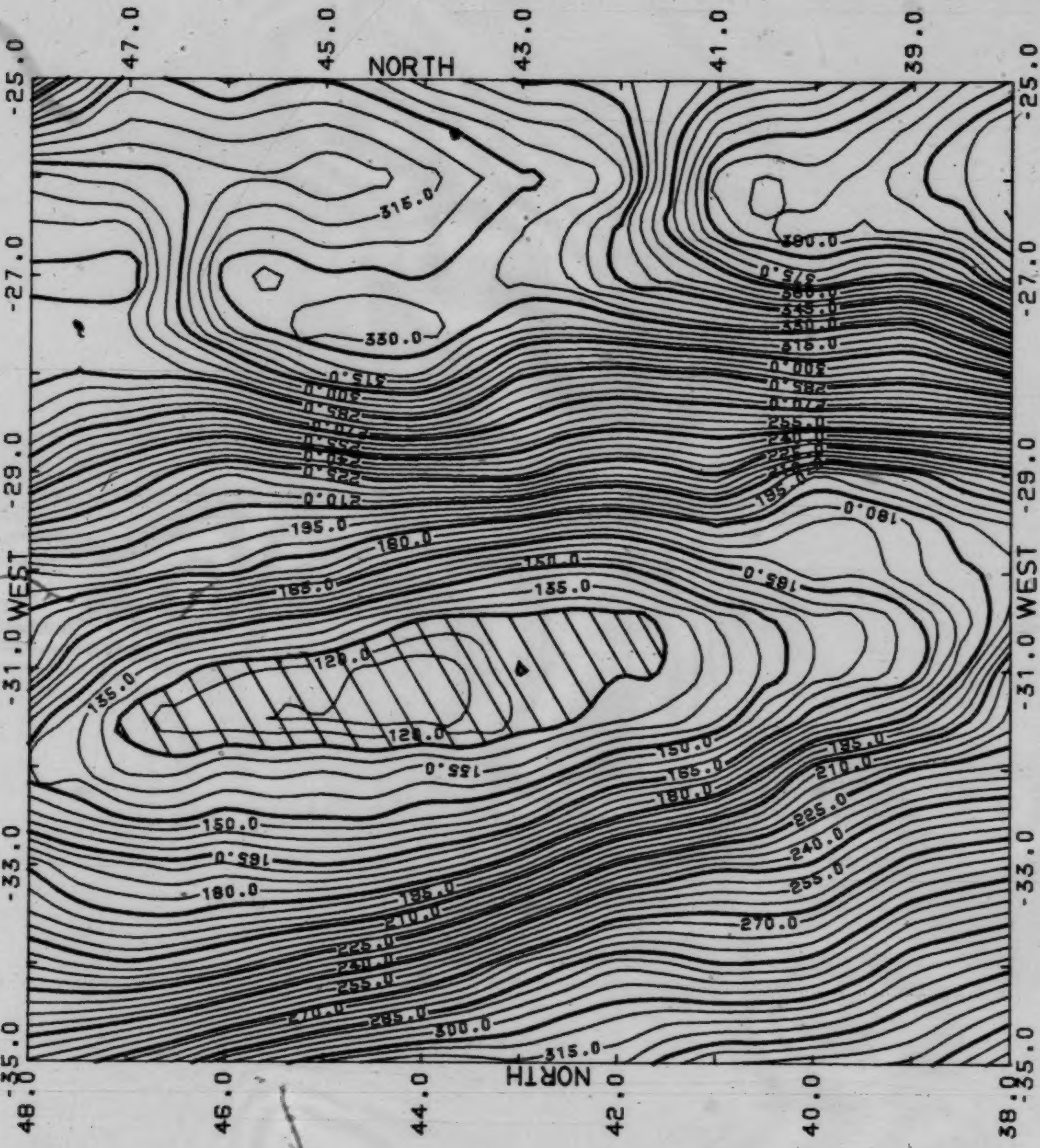

Figure 4.3 displays contours (at 5km intervals) of the misfit in kilometers between South America and Africa for the area in the immediate vicinity of the Bullard pole (figure 4.1). The Bullard pole is much better constrained in longitude than latitude. The shaded region indicates the possible range of optimal pole positions as discussed in the text.

that the pole position is defined much more precisely in longitude than latitude. Systematic study and examination of figures like 4.1 shows that visually "pleasing" fits may be obtained with any pole position lying within the 125-130km contours. Thus, while the pole position is probably constrained to within a degree or so in longitude, its latitude is uncertain by some 5 degrees.

### 4.2.4 A Composite Pole for the Southernmost Regions

In order to apply this same technique to the postulated rotation of the Patagonian block, the relevant portions of the continental shelves of Africa and South America were digitized from maps available at the University of Alberta. The 1000 meter isobaths (550 fathoms) were used for both continents. For the Argentine margin, data were taken from the excellent chart by Rabinowitz et al. (1978). Data for the African continental margin came from a chart compiled by the Brazilian navy and listed in the bibliography under "Oceano Atlantico da America do Sul a Africa, (1978)." These charts differ somewhat in scale and probable accuracy with the chart by Rabinowitz et al. being the most reliable. Both are of sufficient quality for this work, however.

The southernmost portions were not included in the estimation of the fit shown in figure 4.1. It is interesting to see what sort of continental fit results if only the Argentine and South African shelves are matched and the rest of the continents are simply carried along with rigid body motion.

The African shelf south of 20°S was fitted to the South American shelf south of 30°S at the 1000 meter isobath, starting from the modern continental positions. Over this region, 63 points were used to represent the African shelf and 101 were used to represent the South American shelf.

Figure 4.4 shows contours of the misfit in kilometers as a function of pole position. The best pole position is well constrained in one dimension only, but it definitely differs from the Bullard et al. pole. The best misfit using the Bullard et al. pole (at 30.6°W and 44.0°N) is about 220km. Yet a pole position of 31°W and 36°N and a rotation of 58.7° gives a misfit of only 89km. The reconstruction using these parameters, shown in figure 4.5, opens a large gap between the continental shelves to the north.

Thus, it has been demonstrated that a highly accurate fit (90km misfit) may be obtained along the continental shelves from the Amazon to the Falkland Escarpment but that different composite poles are required for the northern and southern portions. The excellent match between the shelves over such long distances cannot be due to random processes. The fit of figure 4.1 has historical precedence over that of figure 4.5 but they have similar intrinsic value. A valid physical theory must explain both.

### 4.2.5 On the Validity of Continental Shelf Reconstructions

The question of what features to match when doing

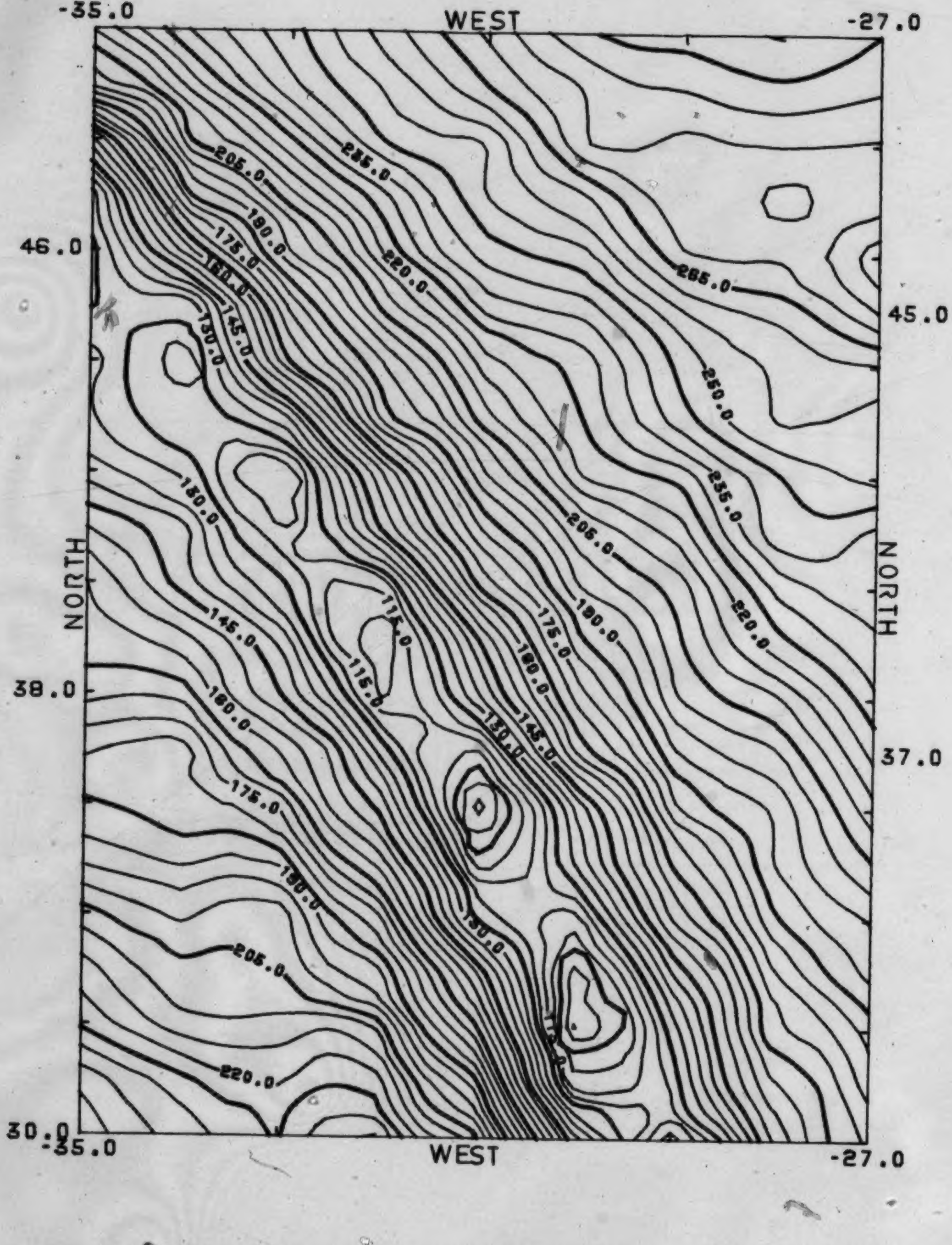

Figure 4.4 shows contours of the continental misfit when only the southern portions of Africa and South America are matched. Contour interval is 5 kilometers. Minimum misfit is about 89 kilometers at 31°W and 36°N.

Figure 4.5 shows the best fit obtained when the southern portions of the continents are matched. Africa has been rotated clockwise 58.7° about a pole at 31°W and 36°N. This achieves a misfit of only 89 kilometers between the limits marked "P".

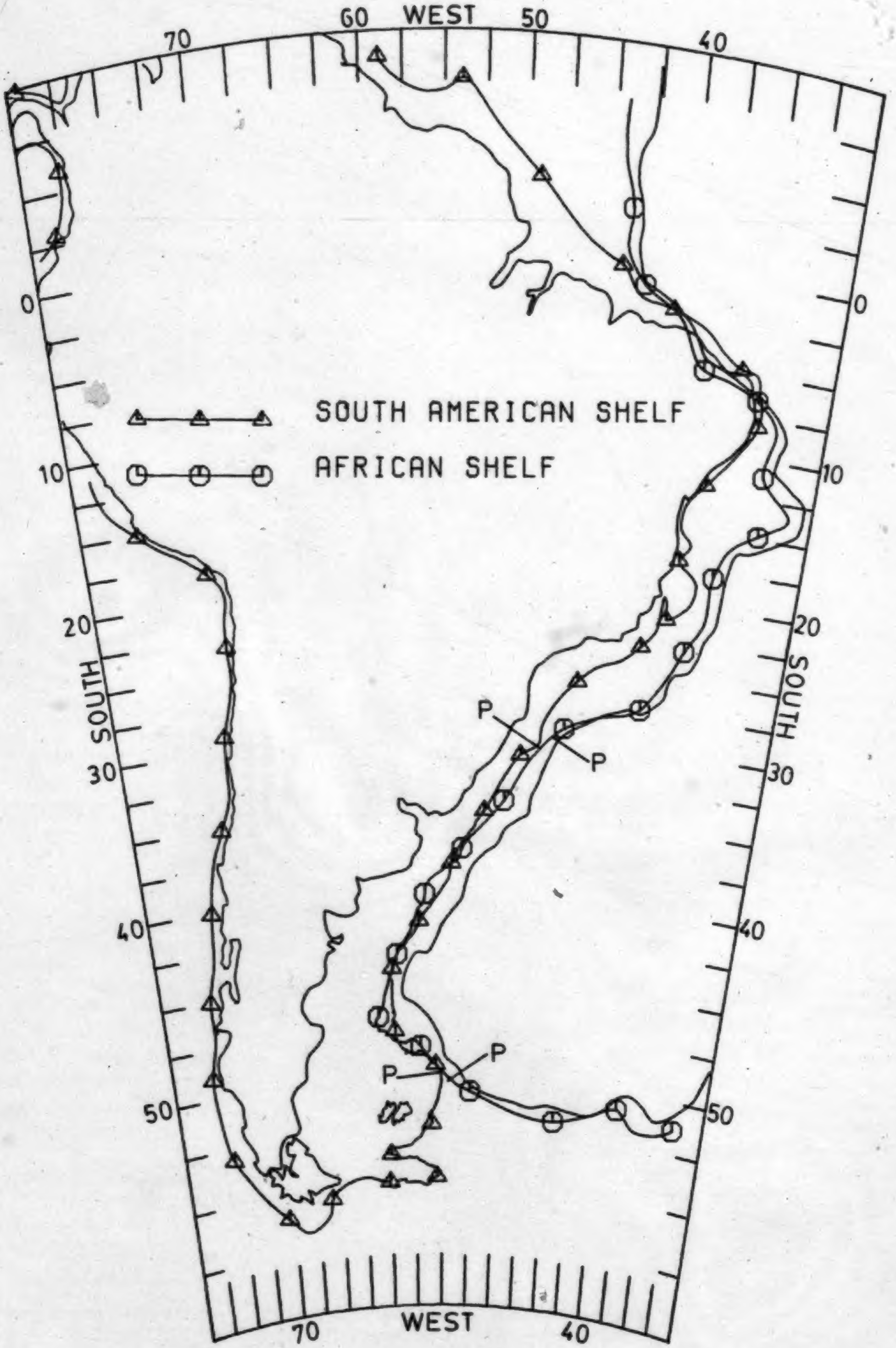
60 WEST 50
70
40
0
10
20
30
40
50
SOUTH
△—△—△ SOUTH AMERICAN SHELF
○—○—○ AFRICAN SHELF
P
P
P
P
WEST
70
40

continental reconstructions is non-trivial. If the rifting process postulated in section 1.4 approximates reality, then there may be no single correct position at which to do the fitting. On the other hand, if the rifting process is uniform along the length of the boundary, matching the resulting shelves may be satisfactory. Previous reconstructions have accepted, on faith, some isobath along the continental shelves as the correct location. If such an assumption is made here, we have a strong case for relative motion between the northern and southern portions of either South America or Africa or both.

If this "constant isobath" assumption is rejected, then the evidence just presented must be explained on other grounds. Rabinowitz and Labreque (1979) have proposed that the fit should be made along the course of a prominent magnetic anomaly, "anomaly G," found along the margins of both continents and thought to represent the boundary between oceanic and continental crust. They have mapped and matched those portions of the anomaly in the southern regions and obtained a "good" fit (the quality of their fit was not assessed quantitatively). They did not examine the fit of the continental shelves in this area. Their model will be presented in section 4.4 as an alternative to that proposed in the next few sections.

It is possible that differences in the style of rifting could be invoked to explain these results. For example, if rifting proceeded much more slowly along the southern margins than in the north, then we might expect to find greater crustal stretching in the south. Ludwig et al. (1979) found the seismic velocity structure of the basement beneath the Colorado Basin (figure 3.25) to be suggestive of stretching. Such an explanation would require about 100km more stretching along the Argentine margin than along Brazil and similarly for Africa. Ludwig et al. (1979) found that continental crust extends 80-110km from the shelf edge or about 50-80km from the 1000 meter isobath.

## 4.3 A Continental Distortion Model

I suggest that, in the course of the rifting of western Gondwana, South America deformed in a manner that is well modeled by differential motion between a southern part, the Patagonian block, and a northern part, the craton. Before the model is presented in detail, further evidence from the fit of the continental shelves will be presented. Figure 4.6 is an enlargement of the southern gap of the Bullard et al. fit (figure 4.1). This gap can be closed by a rigid rotation of Patagonia with respect to the craton. In all of the reconstructions done in the next few sections, the African continent was first rotated into the position shown in figure 4.1. From there the possibility of closing the southern gap via rotations of the Patagonian block has been investigated.

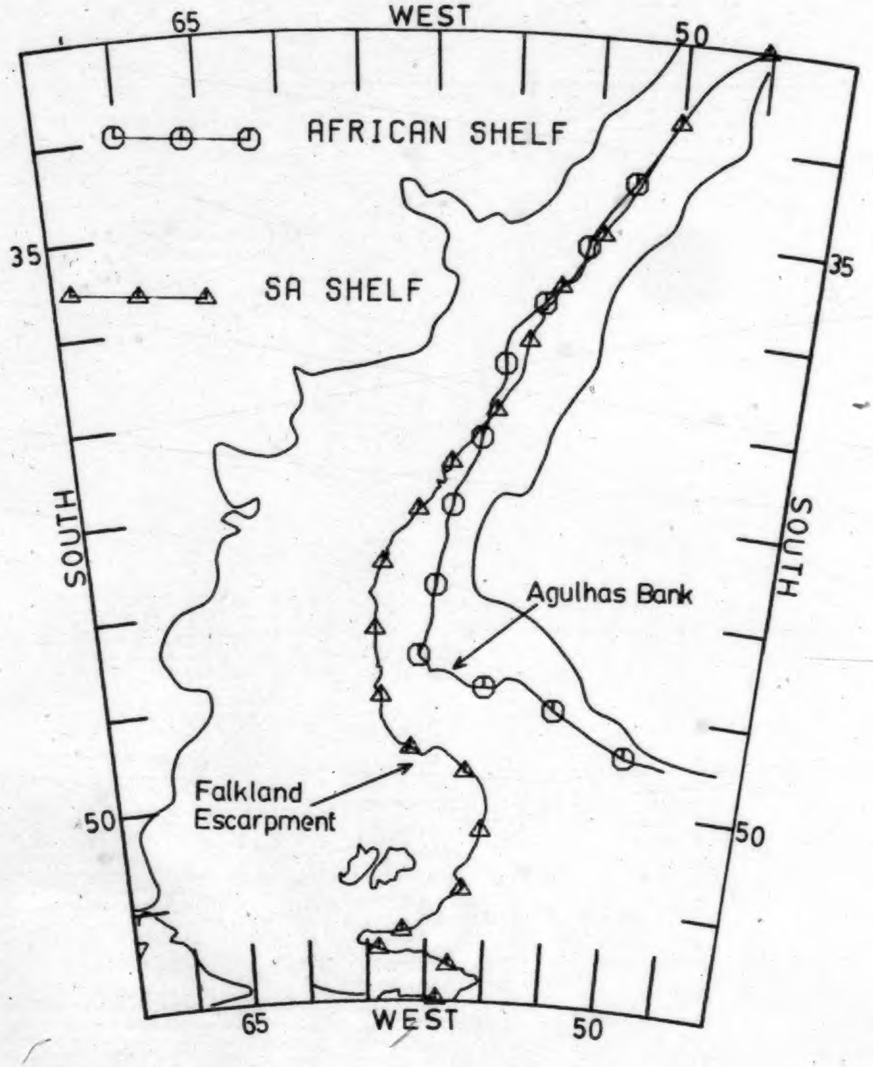
WEST
65
50
AFRICAN SHELF
SA SHELF
35
35
SOUTH
SOUTH
Agulhas Bank
Falkland
Escarpment
50
50
65
WEST
50

Figure 4.6 is a closeup of the southern gap between the continents as defined by the Bullard fit of figure 4.1. Note the matching offsets on the east flank of Agulhas Bank and the Falkland Escarpment.

### 4.3.1 Fit of the Falkland Escarpment to Agulhas Bank

A good evidence for relative motion between the Patagonian block and the craton is shown in figure 4.7. The African shelf from Agulhas Bank (about 21°E) to Port Elizabeth (26°E) has been fitted to the corresponding part of the Falkland Escarpment. A rotation of this section of the Falkland Escarpment (northeast of the Falkland Islands) counter clockwise by 16.2° about a pole located at 65°W and 42.5°S gives the reconstruction of figure 4.7. This reconstruction yields a very small r.m.s. misfit of 17km. The matching offsets on the east flank of Agulhas Bank and the Falkland Escarpment form good small circles about the pole.

Figure 4.8 shows misfit contours for the immediate vicinity of the pole. This figure indicates that the pole position, while reasonably well determined, is tightly constrained in one dimension only. The reconstruction of figure 4.7 is not quite that of minimum misfit; however, it is one of the most "visually pleasing." A pole position of 64.8°W and 43.2°S gives a misfit of about 16km but separates the matching offsets slightly in order to achieve a better overall fit.

The extreme precision of the fit shown in figure 4.7 is strong evidence in favor of a continental reconstruction in which the southern gap is closed. However, if this rotation is extended further north, it worsens the gap there. This is an indication that at least two instantaneous poles are

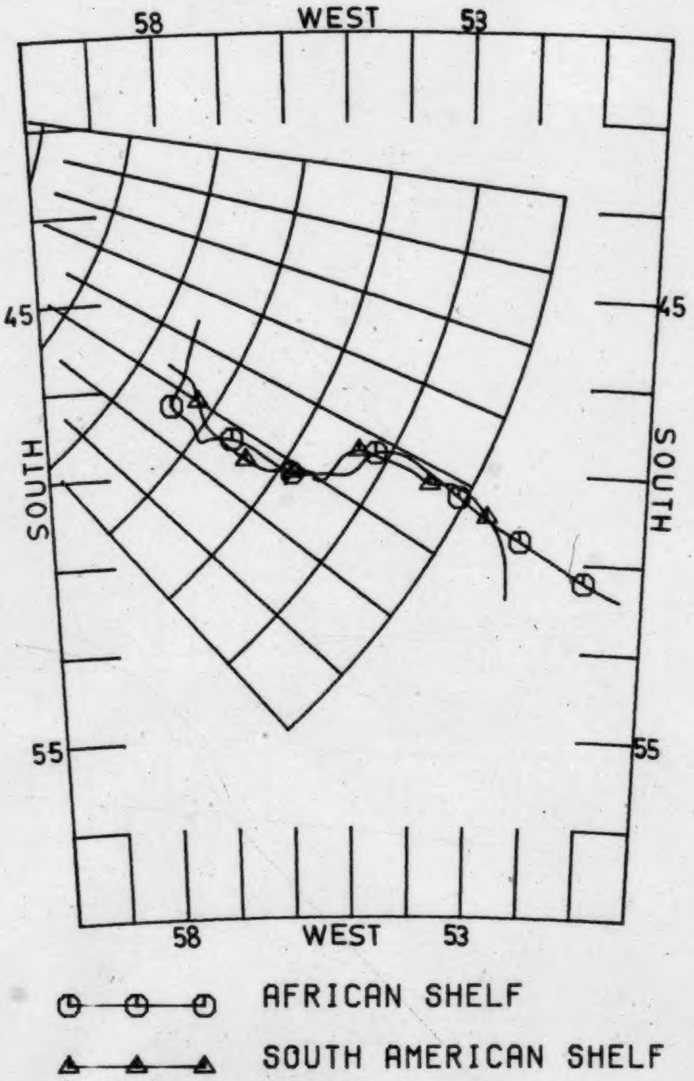
58
WEST
53
45
45
SOUTH
SOUTH
55
55
58
WEST
53
AFRICAN SHELF
SOUTH AMERICAN SHELF

Figure 4.7 shows the fit of the Agulhas Bank region of South Africa to the corresponding section of the Falkland Plateau. The continents were first rotated into the position of figure 4.1, then the Falkland Plateau was rotated counter clockwise 16.2° about a pole at 65°W and 42.5°S. The average misfit is about 17 kilometers. The superimposed grid is drawn about the rotation pole.

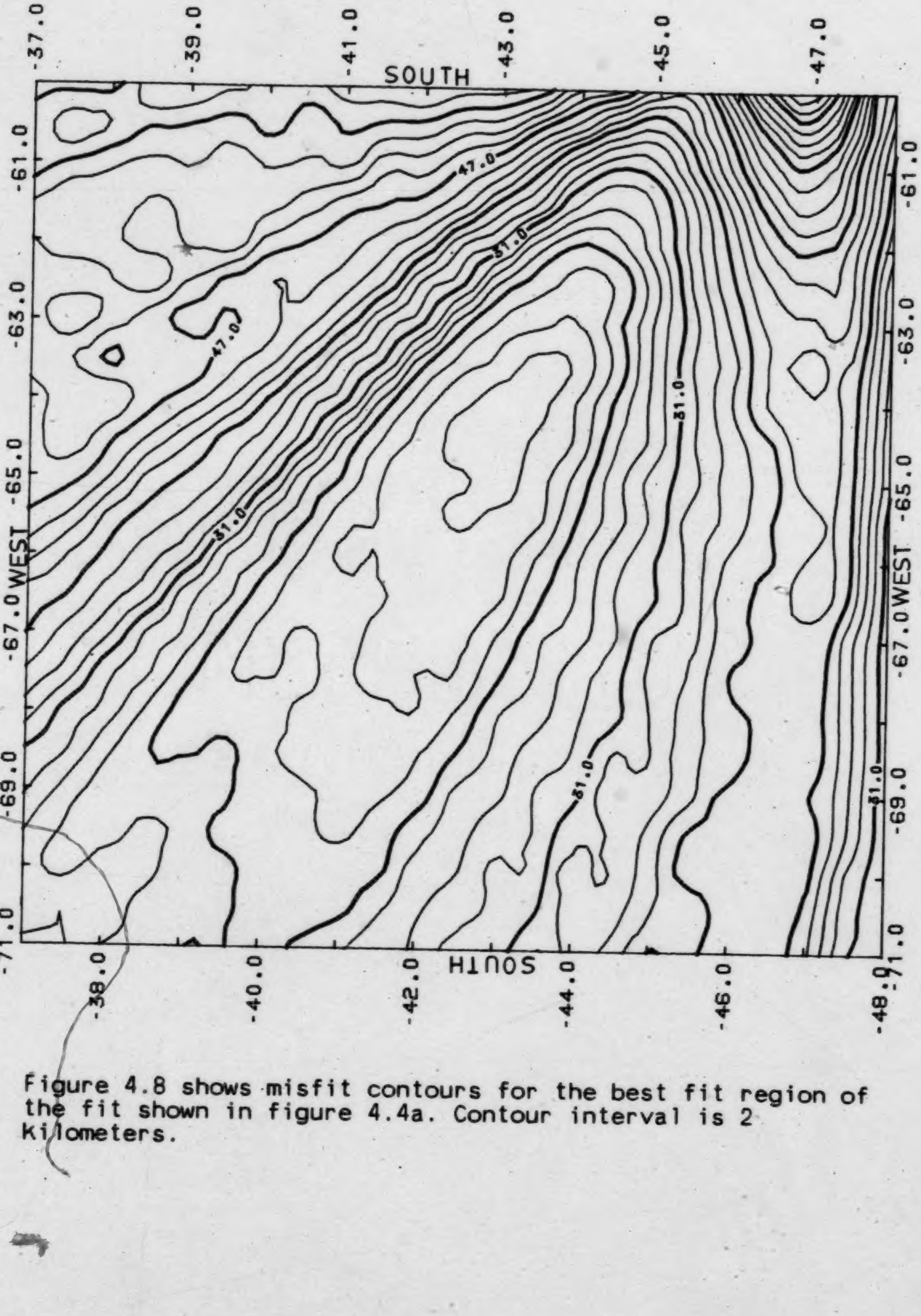

Figure 4.8 shows misfit contours for the best fit region of the fit shown in figure 4.4a. Contour interval is 2 kilometers.

necessary to close the gap.

### 4.3.2 Boundaries of the Patagonian block

The northern limit of the Atlantic coast of the Patagonian block is important to this argument. It is likely that a precise boundary does not exist; rather, the rotated Patagonian Block may connect to the rest of South America by a plastic shear zone. However, for this exercise, it is necessary to define one. From figure 4.1 it is evident that it must extend at least to latitude 40°S (off the coast of Bahia Blanca). There is additional geological evidence to support a northern boundary in the Rio Salado Basin - Rio de la Plata area. This was a zone of major left lateral shear beginning in the middle Jurassic (Urien and Zambrano, 1973) which was probably related to the Parana basalt effusions (see section 3.10.1). These facts together with a a 75km left lateral offset of magnetic anomaly G in the Rio Salado Basin (Rabinowitz and LaBreque 1979) makes this a good choice for the boundary. Moving it by as much as 200km north or south does not seriously change the results.

The proposed Pacific boundary of the Patagonian block is the Arica Elbow at latitude 18°S on the Peru-Chile border. The reasons for this choice are mainly structural and can be suggested by another pencil and tracing paper exercise using figure 4.1. If the southern gap is closed with a rotation about a pole near 65°W and 40°S, the same rotation will erase the offset in the western coast at

Arica. While there is no obvious reason to expect that the Pacific coast of South America should have been a linear feature, nevertheless, this is an intriguing consequence and identifies small circle geometry with the Arica Elbow.

The location of the boundary was probably factors such as the sites of early rifting, the consequent force balance on the continent, and the southern extent of competent shield rocks. Figure 4.9 (adapted from Cobbing et al. 1977) shows the approximate southern limit of the South American craton. Since this line coincides with the postulated coastal limits of the Patagonian block, it is a reasonable extrapolation to make it the boundary between the Patagonian block and the craton. These arguments suggest that the size of the Patagonian block was controlled by the location of the South American shield. Since the rifting between Africa and South America started in the south and migrated northwards, it is plausible that this northward progression controlled the active westward motion of South America. Until rifting and sea-floor spreading forces had advanced northward to a point sufficient to affect the craton, this model predicts separate westward motion of the less rigid Patagonian block.

### 4.3.3 Composite Pole of Opening for the Southern Gap

If this model is correct, the early history of the opening of the South Atlantic was a time of considerable irreversible deformation in southern South America.

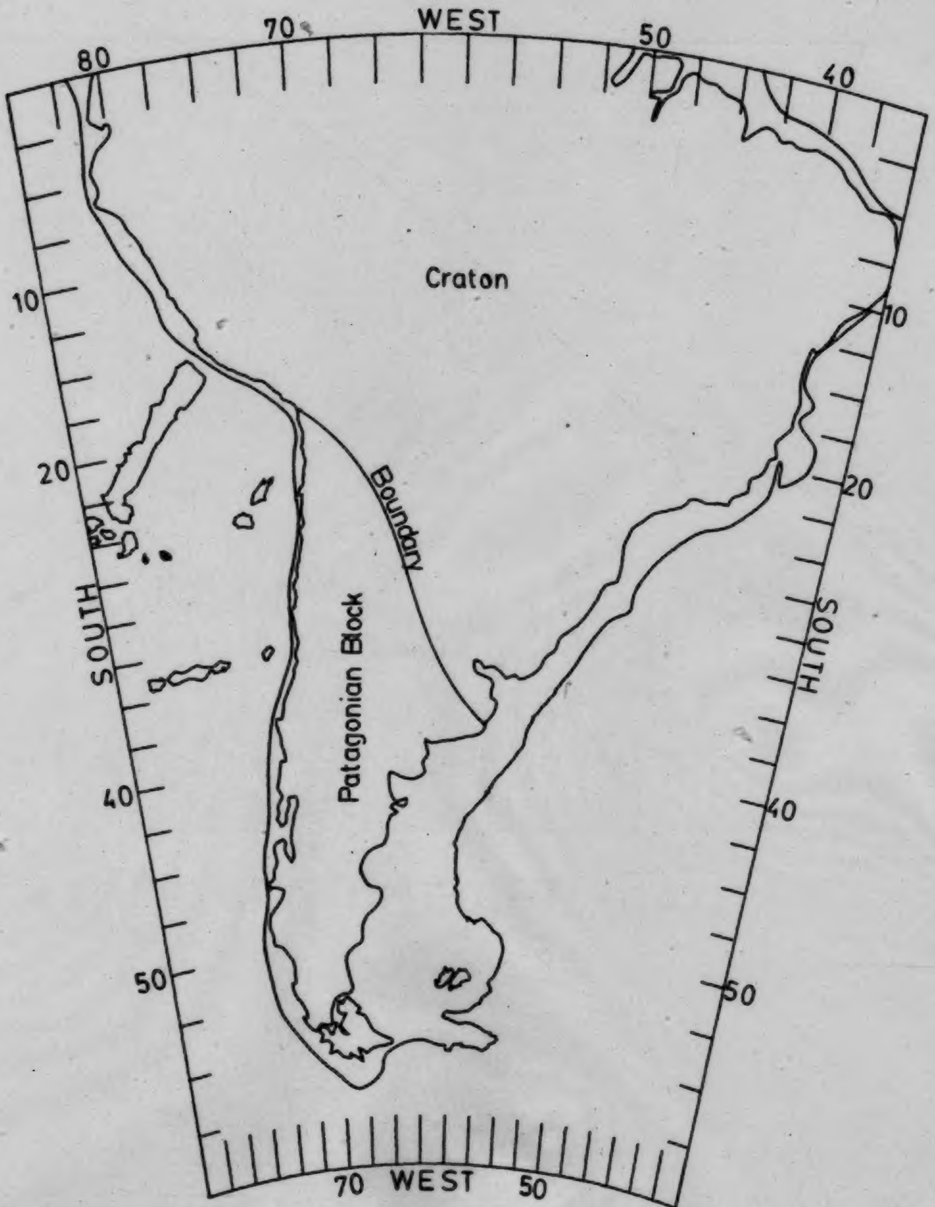
WEST
80
70
50
40
Craton
10
10
20
20
Boundary
Patagonian Block
SOUTH
SOUTH
40
40
50
50
70 WEST 50

Figure 4.9 shows the postulated boundary between the Patagonian Block and the Craton. The boundary is taken to be coincident with the southern extent of the shield as estimated by Cobbing et al. (1977).

Therefore, the discussion of poles of relative motion between rigid bodies may seem unwarranted. However, this is a useful first approximation to a kinematic description. In fact, the location of a composite pole lends a geometric unity to structures which have not previously been viewed as related. A useful conceptualization of the postulated process is that of two rigid basement blocks in relative motion, connected and overlain by a deformable rubber sheet.

A composite pole for opening the southern gap was determined by matching the continental shelf of South America from 55.9°W,40.2°S to 55.4°W,51.0°S with the African shelf from 6°E,32°S to 28°E,33.5°S. 68 points were used to define the South American shelf and 39 points were used for Africa. The different number of points reflects the relative accuracy of the maps used as source materials.

Figure 4.10 shows contours of the misfit at intervals of 2km for the neighborhood of the best possible pole positions. This pole position is well determined in one direction only, the locus of possible pole positions being restricted to a line. The smallest misfits are about 61km.

Since least squares fitting does not suffice to localize the pole position to a meaningfully small area, I assumed further that:

1. The rotation must eliminate the Arica Elbow.
2. The Arica Elbow and the Santa Cruz (Bolivia) Shoulder of the Subandean Ranges must lie along the same small circle.

Figure 4.10 is a contour map of the misfit obtained by closing the southern gap between the continents in figure 4.1 with a rigid rotation of the Patagonian Block. The best pole position is well defined in one dimension only. Contour interval is 2 kilometers.

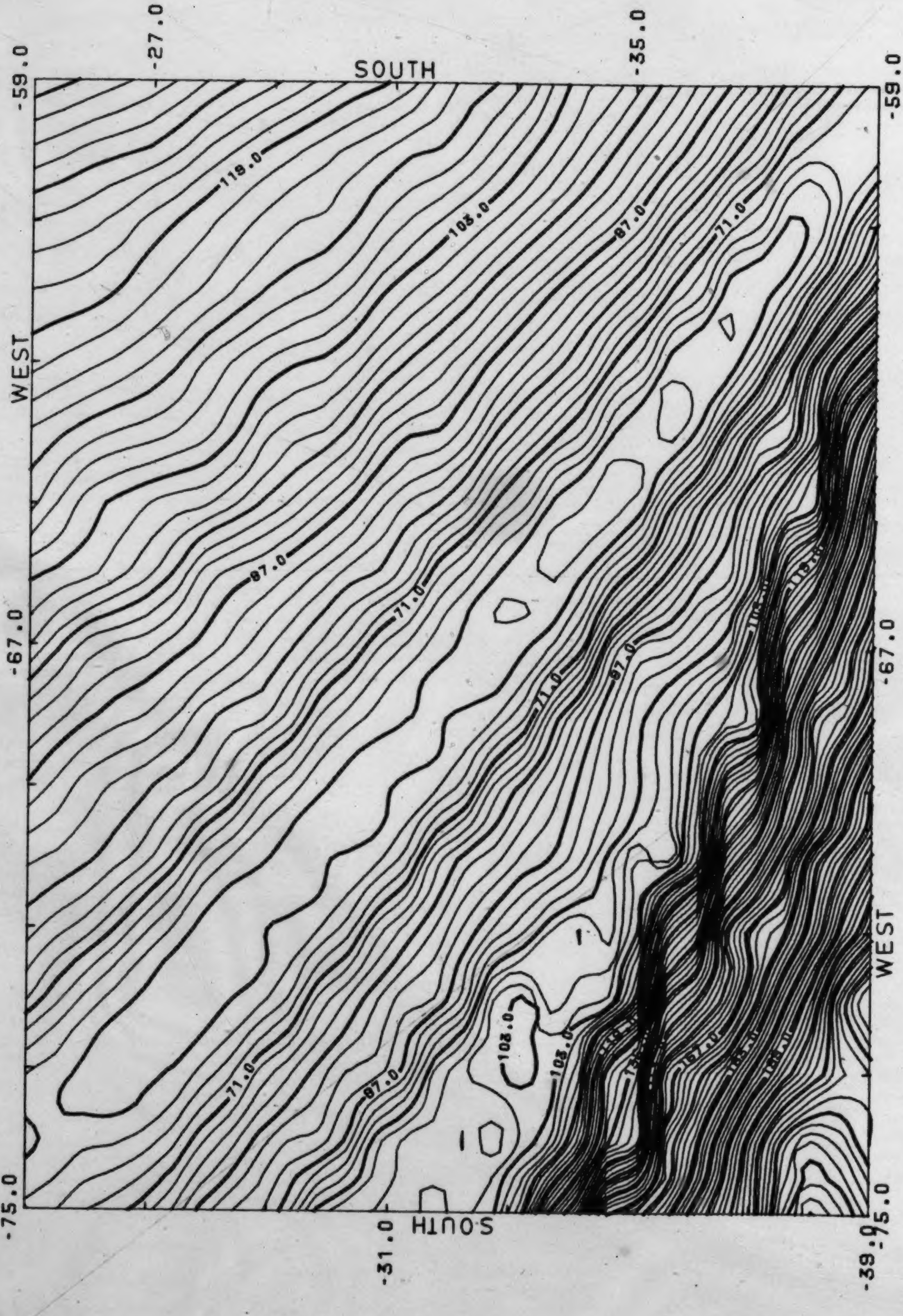
SOUTH
WEST
SOUTH
WEST
-59.0
-27.0
-35.0
-59.0
-67.0
-67.0
-75.0
-31.0
-39.0
-75.0
119.0
103.0
87.0
71.0
87.0
71.0
71.0
87.0
71.0
87.0
103.0
103.0
167.0
119.0
103.0

The first constraint is the weaker and limits the pole position to the southeastern end of the line of possibilities. The second, stronger constraint confines the possible pole positions to a small region centered on 63°W and 36.5°S. The uncertainty in pole position is no more than ±1° in either latitude or longitude.

Figure 4.11 shows this reconstruction with Patagonian block rotated counter clockwise by 12.5° about the pole at 63°W and 36.5°S, which shall be referred to as the Patagonian pole. Portions of South America connecting the Patagonian block and the cratonic block have been omitted.

The overall fit is excellent; major overlap occurs only in the Agulhas Bank area and the average misfit is somewhat less than that achieved by Bullard et al. (1965) for the rest of South America - Africa. Note that this reconstruction does not give the best possible fit of Agulhas Bank to the Falkland Escarpment. (Compare figures 4.11 and 4.7.) This is perhaps another indication of internal deformation not readily modeled by rigid plate theories. Figure 4.12 shows a close-up view of the southern portion of figure 4.11 and allows visual assessment of the quality of the fit. (Compare with figure 4.6.)

### 4.3.4 Statement of the Model

The precision with which the Atlantic continental shelves of Africa and South America can be matched from the Amazon to the Falkland Escarpment is strong evidence that

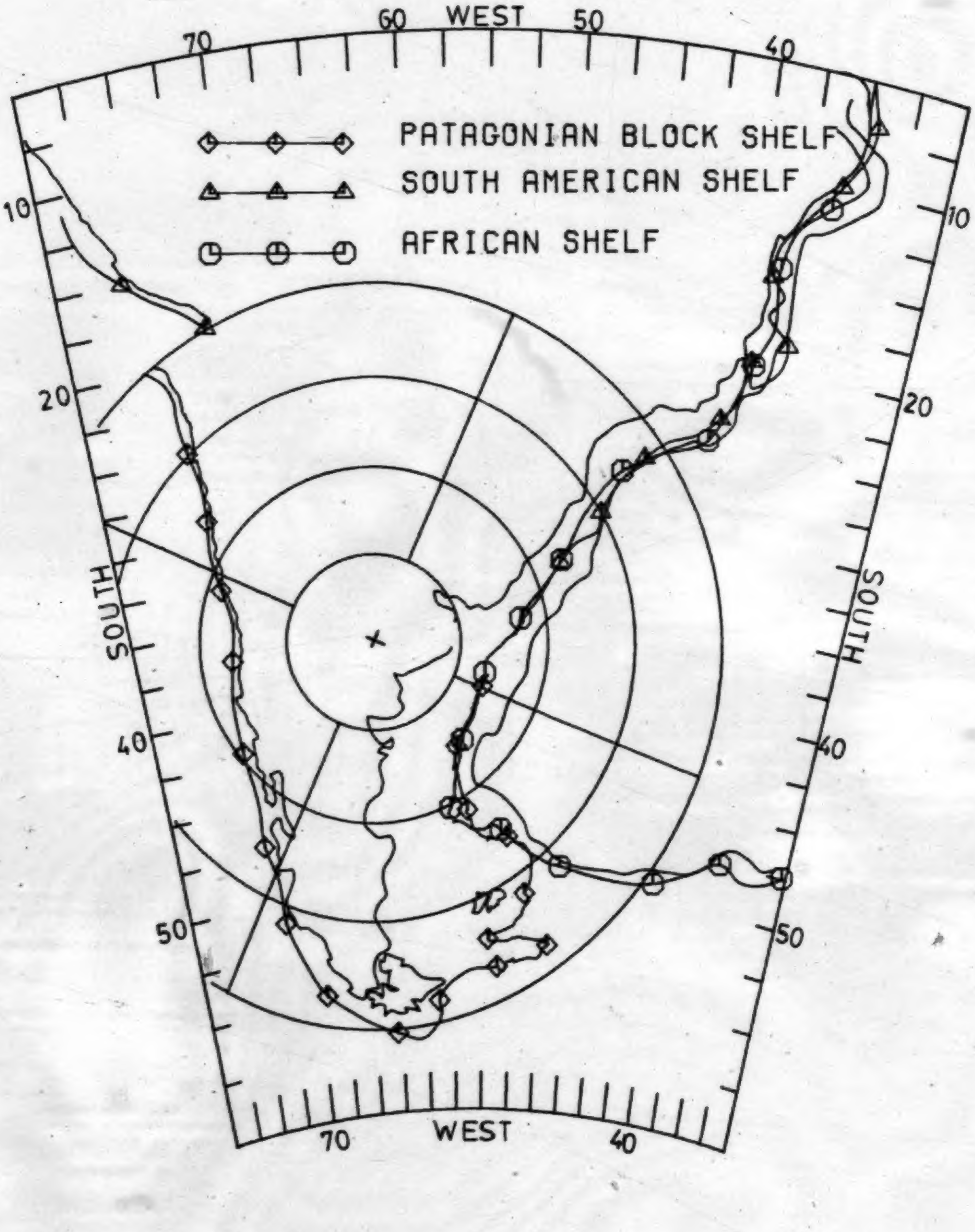
60 WEST 50
70
40
PATAGONIAN BLOCK SHELF
SOUTH AMERICAN SHELF
AFRICAN SHELF
10
20
SOUTH
40
50
10
20
SOUTH
40
50
70
WEST
40

Figure 4.11 shows the "best" rotation which closes the southern gap of figure 4.1. The pole position was chosen from figure 4.10 using the additional constraints described in the text. The average misfit is about 61 kilometers. The Patagonian block has been rotated counter clockwise 12.5° about a pole at 63°W and 36.5°S.

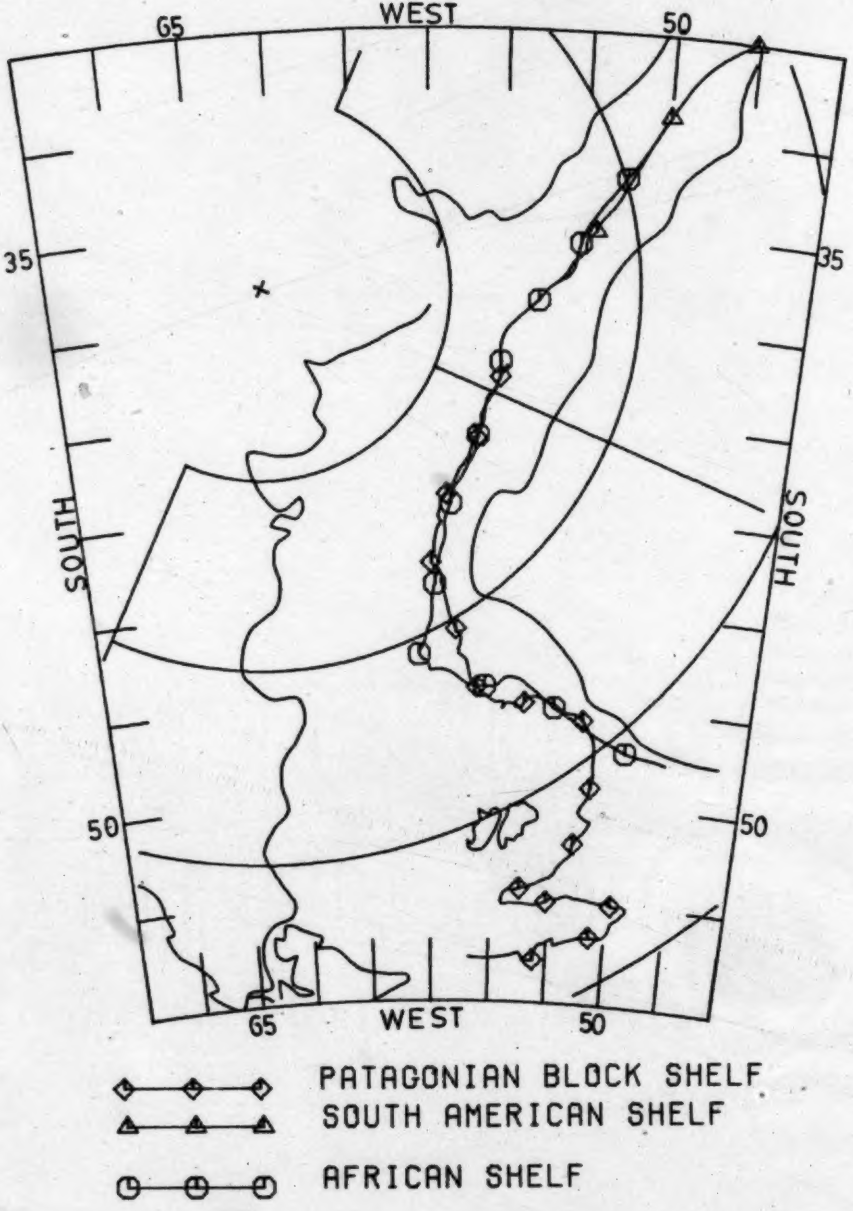
WEST
65
50
35
35
SOUTH
SOUTH
50
50
WEST
65
50
PATAGONIAN BLOCK SHELF
SOUTH AMERICAN SHELF
AFRICAN SHELF

Figure 4.12 is an enlargement of the southern portion of figure 4.11 showing the closure of the southern gap. Compare with figure 4.6.

they were once united over this length. This reconstruction implies considerable deformation in the continental interior of South America. I suggest that most of this deformation occurred between the late Triassic and the middle Cretaceous and was caused by relative motion between the Patagonian block and the western Gondwana craton (Africa and the South American shield).

Figure 4.13 illustrates the proposed sequence of events through the late Cretaceous. Initial rifting began in the South Atlantic in late Triassic - early Jurassic times coincident with the beginning of continental disruption in the Northern Hemisphere and with events leading to the separation of Antarctica and India from Africa (Dietz and Holden 1970, Cox 1970). The primary evidence for this is:

1. The initiation of subsidence and shearing in the Argentine Basins.
2. The Jurassic platform volcanism in Patagonia.
3. The Triassic - Jurassic plutonic events associated with the beginning of the subduction process in Chile.

Figure 4.13a shows the predisruption configuration of the continents with the west coast of South America appearing as a linear feature. The southern limit of cratonic material as shown is adapted from information found in Cobbing et al. (1977) and Windley (1977). Subduction is shown occurring all along the western boundary of the Patagonian block and increases in intensity to the south in accord with information presented in the last chapter. The initial

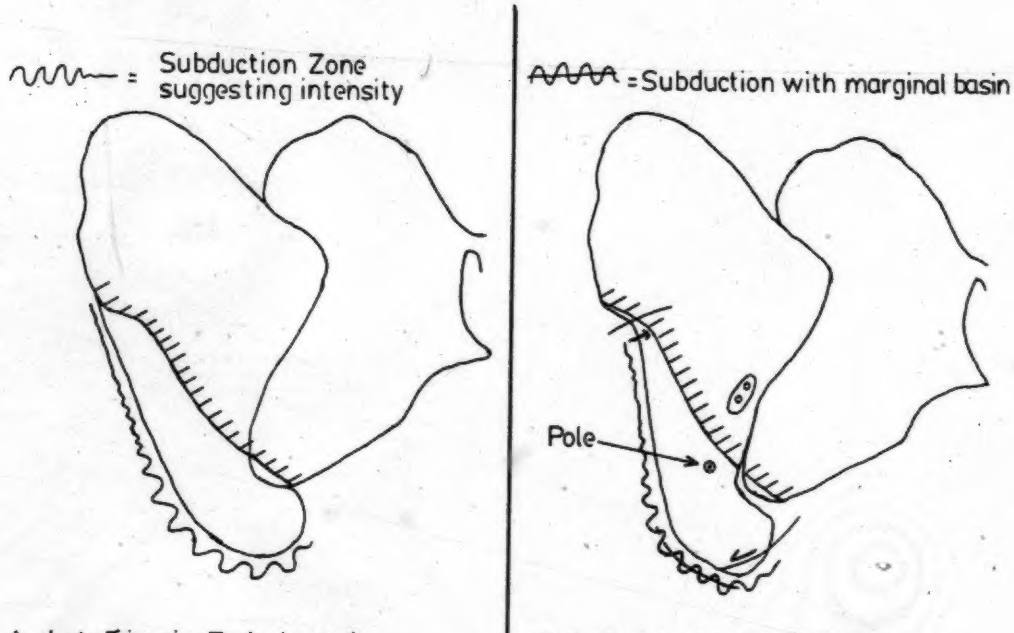
Subduction Zone suggesting intensity
=Subduction with marginal basin
Pole

A. Late Triassic-Early Jurassic (195ma)

B. Late Jurassic-Early Cretaceous (135ma)

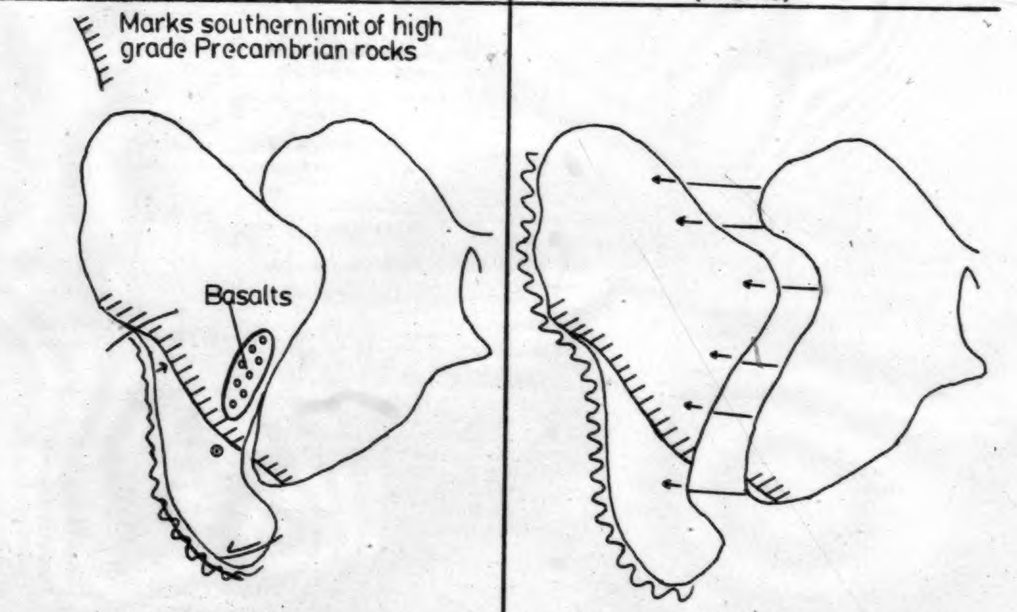
Marks southern limit of high grade Precambrian rocks
Basalts

C. Middle Cretaceous (120ma)

D. Late Cretaceous (90ma)

Figure 4.13 is a cartoon sequence illustrating the continental distortion model proposed in the text.

direction of subduction was probably normal to the linear portion of the coast (see sections 4.3.10 and 4.3.11).

It is not clear whether a causal connection existed between the western subduction and the rifting process. They seem to have at least a temporal relation. It is possible that one process drives the other much like marginal basin spreading is thought to be driven by "trench suck." Indeed, the South Atlantic might be simply the marginal basin for the entire eastern Pacific subduction system.

By the late Jurassic a large gap had opened between the Falkland Escarpment and Agulhas bank. Motion of the Patagonian block in figure 4.13b and 4.13c is shown as rotation about the composite Patagonian pole. (This is done for simplicity; actual motion was probably more complicated.) Subsidence of the Argentine basins, caused by horizontal tensile stresses, was widespread and crustal disruption had initiated the basement fracturing in the Parana basin allowing extensive basaltic effusion. (Mesozoic basalts underlying the Amazon and Parnaiba basins (Bigarella 1973) may also be related to this process.) Marginal basin formation had begun in the southernmost Andes, probably enhanced by the very slow westward motion of the Patagonian block. The Arica Elbow had started to form as the northern boundary of the Patagonian block and as a small circle about the Patagonian pole.

The southern rifting process was much slower than that in the north taking some 80my to proceed to the latitude of the Parana Basalts but requiring only another 30my (at most) to rift the entire western Gondwana craton. Such slow rifting would allow time for crustal stretching along the Argentine margin, though probably not sufficiently to allow the entire southern gap of figure 4.13b to be underlain by stretched continental crust. Thus this model predicts Jurassic oceanic crust in this region perhaps along the entire northern margin of the Falkland Escarpment.

By the middle Cretaceous the crustal distortion process had reached its maximum intensity and the Patagonian block had probably completed most of its relative motion with respect to the Craton (figure 4.13c). Basaltic igneous activity in the Parana basin had peaked, and rifting had migrated to a point sufficiently far north to begin the active western motion of the South American craton. The Patagonian marginal basin was at maximum extension.

The westward motion of the shield was fully underway by Aptian times (107ma). This was geometrically manifest in a change in the pole of spreading for the South Atlantic from a point in northeastern Brazil to one in the northern hemisphere (Rabinowitz and LaBreque 1979). Thus, the period of active continental distortion lasted roughly 100my. The final rifting process and the beginning of westward motion was coincident with the initial emplacement of the Peruvian Coastal Batholith and the closure and uplift of the Patagonian marginal basin. The continents were completely separated before 90ma. A period of fast spreading on the Mid

Atlantic Rise followed immediately (LePichon and Hayes, 1971).

This completes an overview of the proposed model, now individual geologic points will be examined to illustrate to what extent they support the model.

### 4.3.5 The Patagonian Pole

In section 4.2.4 it was shown that the total apparent relative motion between the Patagonian block and the South American craton can be described by a rotation of 12.5° about a pole at 63°W and 36.5°S. Available data are not sufficient to determine if this composite rotation was composed of several smaller rotations about other poles. The fit of figure 4.7 and the early - middle Cretaceous pole position estimated by Rabinowitz and Labreque (1979) (section 4.4) imply that it was. The reconstruction of figure 4.12 suggests that the South American shelf has undergone stretching near where it matches the Agulhas Bank. It is possible that such stretching was associated with a change of pole position.

Despite its possible composite nature, many diverse structural elements in South America form well defined geometrical relationships with the Patagonian pole. However, these seem to fall into two distinct temporal classes: those whose genesis was contemporaneous with the continental rifting, and those which were formed primarily in the Miocene - Recent phase of the Andean orogeny. Before examining the possible meaning of this temporal duality, the structural relationships will be presented.

### 4.3.6 The Parana Basalts and Crustal Disruption

The Parana Basalt flows are a dominant symptom of the proposed relative motion between Patagonia and the craton. Figure 4.14 shows the areal extent of these basalts, the location of the Sao Paulo dike swarm, and the proposed Patagonian pole. The probable origin of these basalts was direct derivation from the mantle implying large basement fractures penetrating the craton. The most likely foci of extrusion include the axes of the Uruguay and Parana rivers (Cordani and Vandoros, 1967). The Parana River follows the long axis of the basalt flows which is more or less radially situated with respect to the Patagonian pole. The majority of tributary streams of the Parana River form good small circles about the Patagonian pole.

The average strike of dikes in the Sao Paulo (Brazil) region also compares well with small circles. (Positions of dikes in figure 4.14 were taken from the Mapa Geologico do Estado do Parana, 1953) These dikes lie longitudinally along a major structural arch known as the Ponta Grosa Arch and are probably the result of axial tension associated with its formation (Neill 1973). The Ponta Grosa Arch is thus the primal tectonic feature.

The Parana Basalts and the Ponta Grosa Arch lie north of the postulated boundary (figure 4.9) well within the

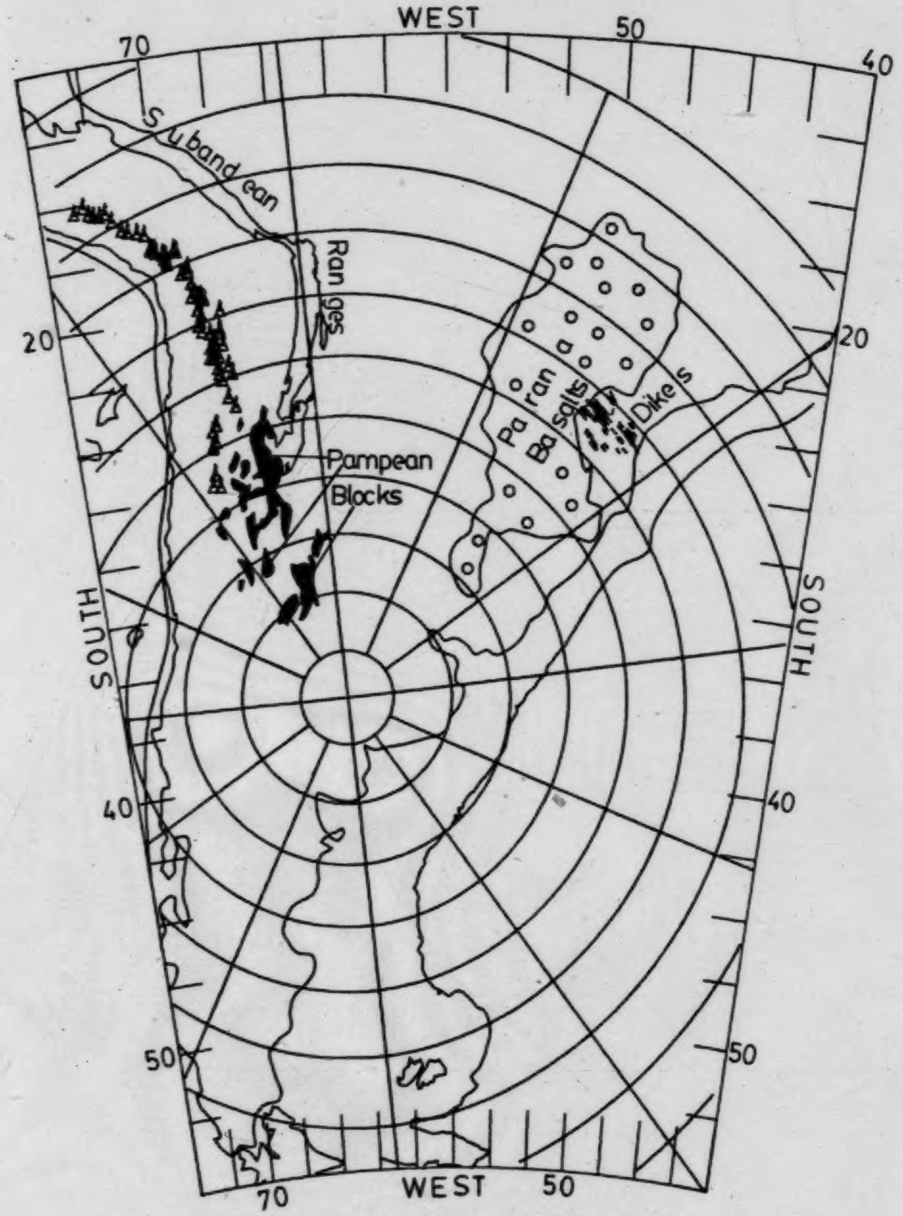
WEST
70
50
40
Subandean
Ranges
20
20
Pampean
Blocks
Parana Basalts
Dikes
SOUTH
SOUTH
40
40
50
50
70
WEST
50

▲ DENOTES ACTIVE VOLCANOES

Figure 4.14 illustrates the geometric harmony found between the Patagonian pole and various geological features. See text for discussion.

craton. Therefore, in this model, they must be attributed to a complex set of boundary tractions induced along the edges of the craton. If a single large fracture was responsible for these magmas, then the most likely position would be along the long axis of the modern outcrop. Such a fracture might have been, in some sense, a conjugate to the ASL (see section 4.3.10). Note that the northern limit of the basalts is approximately on the same small circle as the northernmost Central Andes. In figure 4.14, the Parana basalts appear as an image of the uplifted Altiplano region.

Qualitatively, the Parana Basalts are just the sort of major continental disruption that would be expected. That they are spatially and temporally identifiable with the Kaoko Basalts of southwest Africa (Siedner and Miller 1968) poses no difficulties since this model implies that South America and Africa were still physically connected at this latitude while rifting and deformation proceeded further south.

If this explanation for the tectonic forces responsible for the Parana Basalts can be accepted, then a clear timetable for these events is established from the extensive K-Ar age determinations which are available (see section 3.10.2 and figure 3.26). The oldest dates obtained are around 165ma or middle Jurassic, indicating that deformation had reached a stage just sufficient to rupture the crust. Activity was well under way by 145ma and culminated in a sharply defined maximum between 130 - 120ma. Few reliable age determinations younger than 120ma have been reported. Such a sharp cutoff in activity could be explained by this model as the time at which the South American craton began to actively move westward. It is tempting to move this date forward slightly and identify it with the Aptian change of spreading pole for the South Atlantic.

### 4.3.7 The Southern Argentine Basins

This model predicts that the basins of southern Argentina (figure 3.25) were formed by a horizontal tensile stress field. The actual mechanics of subsidence may have been either graben formation from downfaulted blocks or crustal stretching as was discussed in section 1.4 or both. The history of subsidence is certainly compatible with the model (section 3.10.1), with major vertical motions beginning in the Jurassic. If stretching was responsible, then deep seismic sections across the basins should show a basement of thinned continental crust and lateral boundaries formed by systems of listric normal faults.

### 4.3.8 The Cretaceous Marginal Basin in Patagonia

It is interesting to compare this timetable with that given by Dalziel et al. (1974) for the formation and closure of a marginal basin in the southernmost Patagonian Andes. The existence of this basin is deduced from the "rocas verdes," an ophiolite complex found east of the present outcrop of the Patagonian Batholith (figure 3.11). Batholith intrusion probably had begun by the late Jurassic (150ma) (Halpern, 1973) and continued until the late Cretaceous. Dalziel et al. (1974) argue that the rocas verdes were extruded beginning in the early Cretaceous and extension continued until the Aptian.

Basin closure began later than the Aptian and was complete by 88ma. Dalziel et al. note that this coincides with the period of fast spreading and suggest that there may be a causal relationship. They refer to the model of Wilson and Burke (1972) which attributes the opening and closing of marginal basins to the relative motions of crustal plates with respect to the mantle. That is, marginal basins form in front of an overriding plate which is stationary with respect to the mantle and close when that plate advances trenchward.

As mentioned in section 3.8.2, Jurassic volcanism is present here as a remnant arc (figure 3.11). The slow westward progression of the Patagonian block allowed a marginal basin to form by early Cretaceous times. The extension ceased and closure began when the entire continent was mobilized in the Aptian.

Orogenic history in Chile shows greater Mesozoic intensity in Patagonia than further north (section 3.8). Note that the latitude of the Patagonian pole corresponds with the northern limit of the Patagonian Batholith (figure 3.11). This means the the batholith is found in the region of strongest westward motion. Extensional tectonics would be expected along western margin of the continent south of the Patagonian pole and compressional tectonics to the north. These facts agree with the conclusion reached in the last chapter that magmatism is simultaneous with extensional tectonics.

### 4.3.9 The Structure of the Central Andes

Some of the most intriguing consequences to emerge from this model are found in the Central Andes. Figure 4.15 compares some of the structural elements of the Central Andes with spherical geometry about the Patagonian pole. The two curves labeled "Sonnenberg's lines" are the approximate traces of two tectonic lines identified by Sonnenberg (1963). These lines, while not well defined, are said by Sonnenberg to represent boundaries of major tectonic zones. Sonnenberg feels that they may represent Precambrian lines of weakness which have been reactivated in later orogenies. Their general trend is not unlike the small circles shown, though one definitely has a smaller radius of curvature.

The Arica - Santa Cruz Elbow, defined in figure 4.15 by the bend in the coastline at Arica and the left lateral offset of the Subandean Ranges near Santa Cruz, corresponds with a small circle about the Patagonian pole. Though folding in the Subandean Ranges is generally Pliocene and younger (Lohmann 1970), it may reflect an older basement structure. There is no superficial strike slip fault along this line though there is evidence of some left lateral

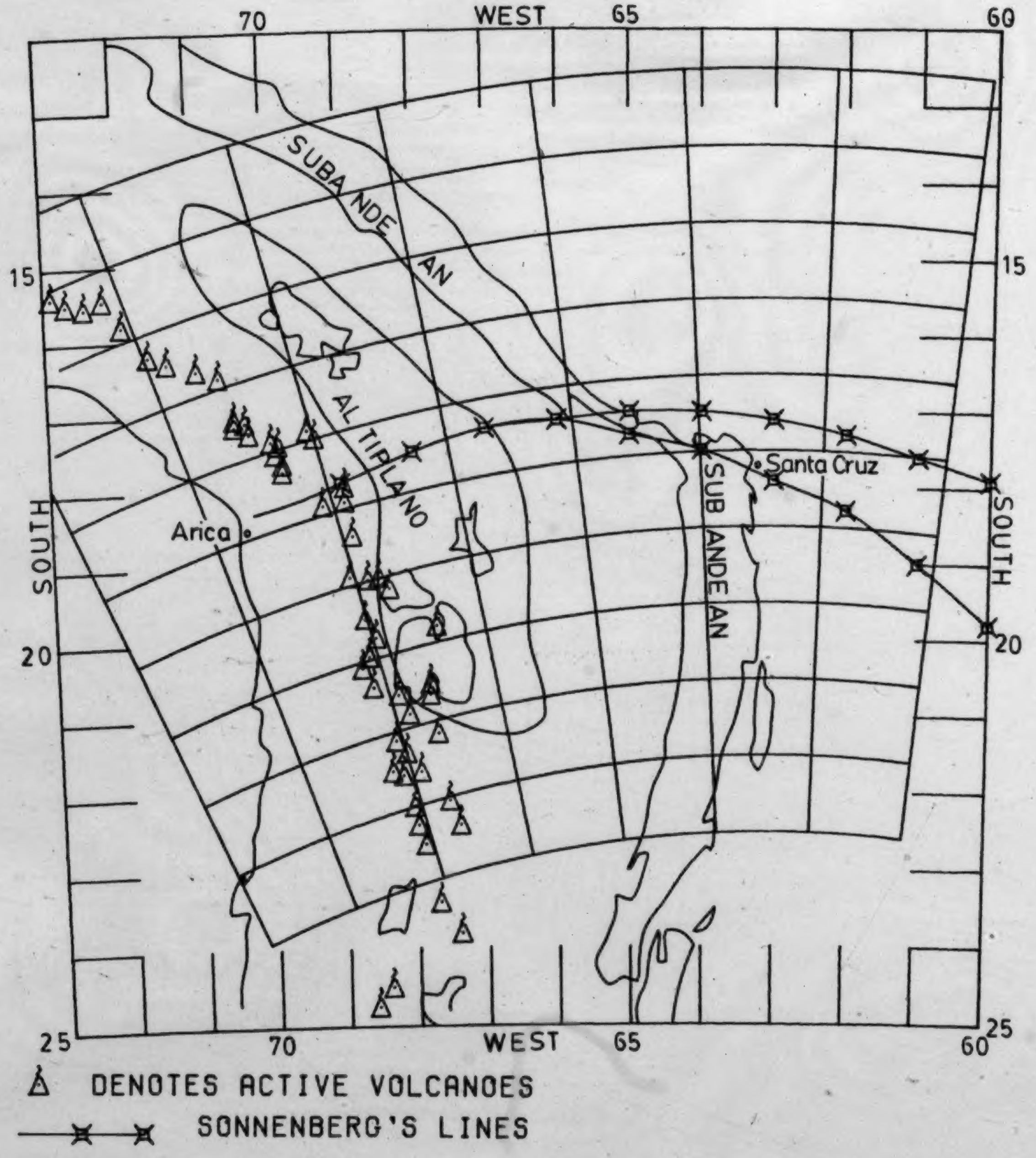
70
WEST
65
60
15
SOUTH
20
25
SUBANDEAN
ALTIPLANO
Arica
Santa Cruz
SUB ANDEAN
DENOTES ACTIVE VOLCANOES
SONNENBERG'S LINES

Figure 4.15 compares the structure of the modern Central Andes with the spherical geometry of the Patagonian pole. Sonnenberg's lines are major tectonic boundaries postulated by Sonnenberg (1963). Notice the remarkable alignment between the modern volcanic belt and a great circle. Compare with figures 3.24 and 4.14.

movement (Sonnenberg 1963). In view of the extensive volcanic activity which has occurred here since the Miocene, it seems quite likely that evidence of earlier lateral movement would be obscured.

### 4.3.10 The Andean Seismicity Lineament Revisited

The alignment between the modern volcanic line and a line of "longitude" about the Patagonian pole (figure 4.14, and figure 4.15) is excellent. As was discussed in the previous chapter, this volcanic line, there called the Andean Seismicity Lineament (ASL), is only one manifestation of a seemingly fundamental tectonic lineament. The line is also defined by:

1. The strike of the Western Cordillera between 18°S and 25°S.
2. A line of intermediate depth earthquake activity directly beneath the volcanic front and another line of deep activity further north.
3. The outcrop of the uplifted Pampean massifs in Chile and Argentina.
4. A line of "longitude" drawn through the modern Nazca - South America pole as determined by Minster and Jordan (1978). (See figure 3.22.)

The Patagonian pole seems also to lie along the ASL. This fact is evidence for the formation of major basement fractures at the time of the disruption of the continents which have controlled the evolution of South America since then.

The postulated model predicts the rising of basement blocks, like the Pampean structures, as the Patagonian block north of the Patagonian pole is compressed against the shield. The uplift of such blocks beginning immediately north of the pole is a method of crustal shortening. However, the uplift of these structures probably occurred in the Miocene, not the Cretaceous. If such an uplift did occur in the Cretaceous, there has been sufficient time to erode it. The modern Pampean Blocks would thus be interpreted as a Miocene resurgence of this motion along a Mesozoic basement fracture.

The ASL itself seems curiously associated with the geometry of relative motion poles. It should be re-emphasized that the position used for the Patagonian pole was not entirely a consequence of the geometry of the continental shelves. Other assumptions were found necessary, the most important being that the Arica Elbow should be a small circle about the pole. Thus, the alignment found here is really an indication that the ASL and the Arica Elbow form a good large and small circle pair.

### 4.3.11 The Atacama Fault as a Consequence of Oblique Subduction

The association of the ASL with great circles about motion poles has been demonstrated and discussed. In the last chapter it was suggested that the volcanic activity along the ASL in northern Chile indicates that plutonic injection is taking place beneath it today. It was argued that this is a modern equivalent of the Tapacocha Axis, the injection fracture for the Peruvian Coastal Batholith. This line of reasoning leads to the conclusion that linear plutonic chains may be valuable constraints on paleo-pole positions. Then, the history and structure of the Peruvian Coastal Batholith show that the direction of subduction beneath central Peru, from 105ma to 30ma, was approximately normal to the coast. This model has South America behaving as a unit through this time; therefore, we can conclude that subduction in Chile was highly dextral oblique. (This conclusion is not unique to this model.)

In section 1.2.5 it was suggested that oblique subduction can induce sympathetic strike-slip faulting within the continental plate. The Atacama Fault, as discussed in section 3.6.2, is thus readily modeled as a Fitch fault (Fitch 1972). The probable period of active dextral motion (middle Cretaceous to middle Miocene) fits very well with this idea. Motion started when the rotation of the Patagonian block had caused oblique subduction of a magnitude sufficient to induce shear failure in the continent. The cessation of motion coincides with the Miocene reorganization of spreading in the eastern Pacific (Handschumacher 1976) which brought about more nearly normal subduction.

### 4.3.12 Critical Evaluation of the Continental Distortion Model

As presented, the model is basically conjectural. The fundamental proven facts are the accuracy of the fit of the continental shelves (90 Km) from the Amazon to the Falkland Escarpment and the impossibility of matching the entire length of the shelves with rigid plate motions. The model is a conjecture advanced to explain this observation. Strong points of the theory include:

1. It is formulated in terms of spherical geometry and plate tectonics.
2. It is sufficiently quantitative to lend itself to further physical modeling and experimental testing.
3. It offers a plausible explanation for the observed synchronism of tectonic events on opposite sides of the continent, such as the subsidence events in the Argentine basins coinciding with major Andean movements.
4. It leads to the recognition of a geometric harmony of structure in the continent which has previously escaped notice.
5. It offers physically realistic explanations for a wide range of known tectonic events which have not previously been considered related.

The model is not without significant drawbacks. It rests on a structure of three interdependent speculations:

1. Continental reconstructions done at a particular isobath (1000 meters) are valid. That is, they give a true

picture of the former continent.

2. The reconstruction of South America and Africa implies relative motion between the Patagonian block and the South American craton.
3. The majority of this motion occurred during the rifting of western Gondwana.

Care has been taken in the presentation to make these appear as reasonable as possible, but they remain unproven points. Other possibly objectionable points include:

1. It constitutes a major departure from orthodox plate tectonic theory because the continents are not regarded as rigid. However, it should be stressed that distortion of the Archean nucleus is not postulated. The proposed distortion followed the boundary between high strength Precambrian rocks and less competent Phanerozoic sequences.
2. It is only quantitative in a kinematic (or geometric) sense. Dynamic explanations suggested for various events are entirely qualitative.
3. It is not, at present, bolstered by any paleomagnetic data.

The spatial and temporal scope of the theory are large; hence, it is certain to find discord with various localized observations. As a generalized plate tectonic evolutionary scheme for the South American continent, it is probably unique. Therefore, it cannot be compared with competing theories. The model of Rabinowitz and Labreque (1979) (section 4.4) for the early opening of the south Atlantic will be presented as an alternative theory, but it is really much more limited in scope. So, also, such theories as James' (1971b) discussion of the evolution of the Central Andes or Dalziel and Palmer's (1979) evolution of Patagonia are not strictly comparable. Key elements from these works have been incorporated into this theory and they are generally compatible with the continental distortion model.

### 4.4 The Model of Rabinowitz and Labreque

The most recent and comprehensive study to emerge on the opening of the South Atlantic is that of Rabinowitz and Labreque (1979). A major result of that work is the estimation of a new pole (at 2.5°S and 45°w) describing the relative motion of the African and South American plates from the early Cretaceous (130 ma) until the the Aptian (107 ma). This pole position was determined by visually fitting small circles to the earliest portions of the Falkland-Agulhas fracture zone. It thus represents an "instantaneous" pole rather than a composite one. A critical examination of this work is appropriate here because a major conclusion reached by the authors was that South America and Africa have suffered little or no deformation since the initiation of rifting in the proto South Atlantic. This is directly in conflict with my model.

### 4.4.1 The Rabinowitz and Labreque Fit

Figure 4.16 is a reconstruction of the western Gondwana continent as proposed by Rabinowitz and Labreque showing the location of their postulated early pole. This figure was generated using their composite pole of opening for the South Atlantic at 45.5°N and 32.2°W and a rotation angle of 57.5° (South America fixed).

With the data set used to generate figure 4.3, the method described in this chapter can be used to express the accuracy of this fit at the 500 fathom level. The rotation angle giving minimum misfit for the composite pole used by Rabinowitz and Labreque is 55.8°. This minimum misfit is about 143Km while the reconstruction of figure 4.16 gives an r.m.s. misfit of 223Km. Thus the overall misfit of the continental shelves obtained in this reconstruction is significantly greater than that obtained by Bullard et al. (1965). The fit is particularly poor along the northeastern Brazilian coast where major overlap of the continental shelf occurs.

### 4.4.2 The Ocean-Continent Boundary

The reconstruction of Rabinowitz and Labreque differs from all previous attempts in that an unambiguous definition of the continent - ocean boundary was used. Their claim is that the boundary is determined by a certain magnetic anomaly, anomaly G, interpreted as a "magnetic edge effect" at the oceanic plate boundary (Talwani and Eldholm 1973)

Figure 4.16 shows the fit of the continents as postulated by Rabinowitz and Labreque (1979). The location of their early to middle Cretaceous pole for spreading on the South Atlantic is also shown (45°W and 2.5°S). Africa has been rotated clockwise 57.5° about a pole at 32.2°W and 45.5°N. The average misfit at the 500 fathom isobath is estimated in the text as 223 kilometers. The worst misfit is along the northeastern coast of Brazil. Compare with figure 4.1.

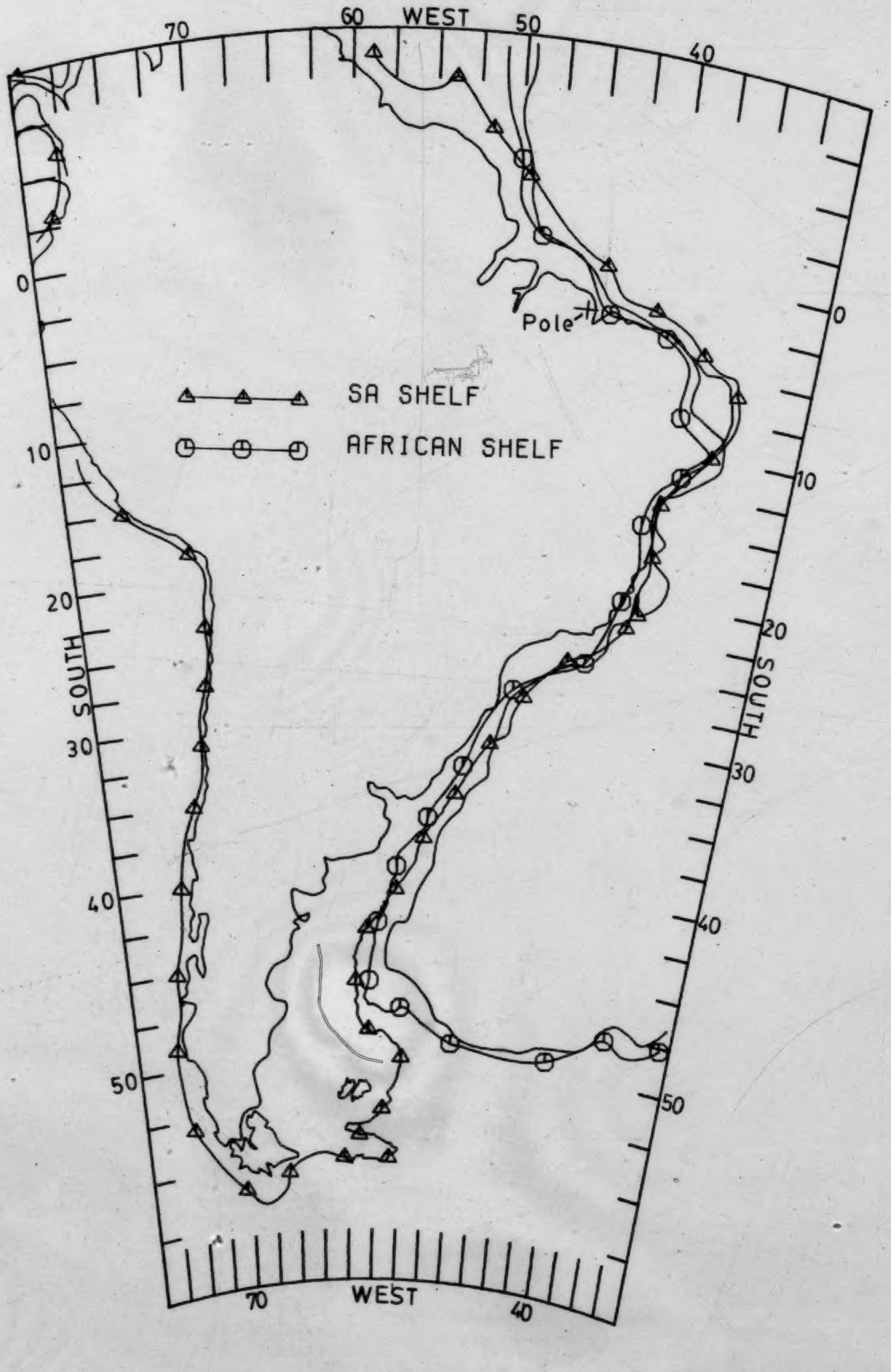
70
60
WEST
50
40
0
10
20
SOUTH
30
40
50
Pole
SA SHELF
AFRICAN SHELF
0
10
20
SOUTH
30
40
50
70
WEST
40

which should be coincident with an isostatic gravity gradient. Anomaly G does not conform to any particular isobath. This is a major reason for relatively large r.m.s. misfit at the 500 fathom level. The following points should be considered when interpreting these results (all were noted by Rabinowitz and Labreque):

1. The continent - ocean boundary was determined only for those portions of Africa and South America south of the Walvis Ridge and Rio Grande Rise respectively. The fit of the more northerly boundaries was not examined and is simply a consequence of fitting the southern portions using rigid plate tectonics.
2. North of about 30°S, anomaly G for Africa is found about 150km landward from the continental shelf edge. To the south (south of 34°S) it is on the continental slope as much as 2 km below the shelf.
3. The South American anomaly G is very near the shelf edge north of 36°S (the mouth of the Rio de la Plata). South of here, the boundary changes abruptly to the continental slope where it is found as much as 2-3 km below the shelf edge.
4. Along the southernmost margins of both continents the magnetic anomaly is not well defined. Seaward isostatic gravity gradients are present, however.
5. The fit was obtained by an undefined "trial and error" method.

### 4.4.3 Comparison with the Fit at the Continental Shelves

The fit of the continental shelves shown in figure 4.5 was made over the region in which Rabinowitz and Labreque matched anomaly G. 63 points on the African shelf south of 20°S were fitted to 101 points South American shelf south of 30°S at the 1000 meter isobath. Figure 4.4 shows contours of the misfit in km as a function of pole position. The best fit pole position is near 31°W and 36°N giving a misfit of 89km with a rotation angle of 58.7°. For the composite pole suggested by Rabinowitz and Labreque (32.2°W and 45.5°N) the optimal rotation angle is 58.2° giving a misfit of 209km. The pole-angle combination suggested by them increases the misfit to 222km.

The reconstruction of Rabinowitz and Labreque is far from an optimal one for the fit of the continental shelves. In fact, it does not significantly improve the misfit for the southern region over that obtained with the Bullard et al. pole. (See figure 4.9.) The method of Rabinowitz and Labreque does provide an unambiguous definition of the continental boundary, but it is disturbing that the results are in such discord with those obtained from comparison of the shelves.

### 4.4.4 Evaluation of the Rabinowitz and Labreque Model

The reconstruction of Rabinowitz and Labreque poses more problems than it was intended to solve. It seems likely that the location of the boundary as defined by them will show strong dependence on the thermo-mechanical style and temporal history of the rifting process. (See section 1.4.) The reconstruction of Rabinowitz and Labreque was done at a position which probably corresponds to the first occurrence of oceanic crust in figure 1.5. The horizontal distance between there and the continental shelf will depend on the speed with which the rifting process occurred. Slow rifting will allow much more ductile flow and hence more crustal stretching than a rapid process. This model could well explain why the magnetic edge anomaly is found on the shelf north of the Patagonian block and in the abyssal plain south of there. If this is the case, then fitting the continents together along this magnetic boundary will be erroneous.

It is undeniable that a good match may be obtained between those anomalies of the Argentine and South African coasts; however, the conclusion that this indicates no deformation in the continental blocks seems hasty for several reasons. First, no data from the northern coastlines was used to constrain the model. Second, since the defining magnetic anomaly is most likely an edge effect of a magnetized slab of oceanic crust, the fit indicates only that the Atlantic sea floor has spread according to the geometric principles of plate tectonics. Certain types of relative motion can occur along this boundary without destroying the anomaly, such as spreading and stretching of the continent parallel to the boundary.

The early pole position calculated by Rabinowitz and

Labreque is probably a good approximation since it was determined geometrically from the Falkland-Agulhas fracture zone. The early time limit given for probable activity around this pole (130 ma) was based on the identification of Mesozoic oceanic crust just west of Capetown, South Africa (Larson and Ladd 1973). As can be seen from figure 4.1b, rigid body relative motion of South America and Africa about this pole predicts tension along the continental suture south of the pole and, to the north, compression.

Rabinowitz and Labreque postulate 11.1° of relative motion about this pole until the change of pole positions in the Aptian. Thus, starting either from the Bullard et al. (1965) reconstruction or that of Rabinowitz and Labreque, rigid plate motion predicts a period of considerable compressive stresses along the northeastern coast of Brazil. Possible consequences of such compression include large scale crustal shortening and resulting thrusting and orogenic activities typical of continental collision. There is little supporting evidence for such an event (e.g. Almeida 1968). Rabinowitz and Labreque cite scattered references on this subject which, by their own admission, lack cohesiveness.

In the area under consideration, both continents are predominantly composed of highly competent shield rocks which might be expected to withstand considerable stress. Thus, it is reasonable to expect yielding elsewhere in response to stresses applied on the northeastern Brazilian coast. Such deformation could have involved left-lateral slip along a major shear zone through the Amazon Basin or tension and stretching in a direction parallel to the continental coast in the Chaco-Pampas plains, or both.

A major shear zone along the Amazon has been postulated before (Carey 1958a). Neev (1977) has suggested the extension of this shear zone through the African Basin on an arcuate path through the Benue Basin, Lake Chad, the Ghazal Basin, the Nile Delta,and into Israel. This possibility has not been investigated in detail, focusing instead on possible deformation further south. Since the early opening was primarily a southern event, it is likely that local compensation via stretching in the Pampas was an important mechanism. If a trans-Amazon shear zone did develop, after the separation of the continents it would remain as a zone of weakness and serve to decouple northern South America from the rest of the continent.

Thus, the data presented by Rabinowitz and Labreque can also be interpreted as supporting the continental distortion model of section 4.3. Their model faces serious structural difficulties along the northeastern coast of Brazil. If these can be overcome, then the model would be considerably more viable. Certainly, the concept of rigid body motion about their Cretaceous pole must be abandoned. If this were done, the two models might even be compatible. Figure 4.12 is quite similar to their figure 14 showing the match of anomaly G. Both show a close fit everywhere except around the Agulhas Bank where the Falkland Escarpment appears to have stretched.

### 4.5 On Events Subsequent to the Western Gondwana Breakup

The continental distortion theory has so far been concerned with events from Triassic to middle Cretaceous times. From the Aptian (107ma) to the late Oligocene(30ma). was a period of major orogeny throughout the Andes. During this time more than any other, the Andes come closer to being the elusive type example of cordilleran orogeny. Key tectonic and magmatic events have already been discussed in chapter 3. The history is complicated but appears to be well described by "classic" steady state subduction beneath an ensialic volcanic arc (Clark et al. 1976). Continued episodic subsidence and platform tectonics to the east appear to correlate with Andean events (e.g. Urien and Zambrano 1973). Such a correlation could be exist if the sedimentary basins received erosives from each uplift phase and continued to subside along faults established during the continental breakup. This era will not be given further treatment here. Refer to Zentilli (1974) or Clark et al. (1976) for detailed, consistent models of Central Andean evolution.

#### 4.5.1 The Miocene Events

Many of the structures forming definite geometric relationships with the ASL and the Patagonian pole are of

Miocene age. This may be due to a resurgence of motion along the same geometric lines as were established in the Mesozoic, and may, therefore, indicate a renewal of the relative motion of the Patagonian block. It might seem tempting to suggest that all of the relative motion of the Patagonian block occurred in the Miocene. However, this is inconsistent with the history of the associated events elsewhere, such as the Parana Basalts, the subsidence of the Argentine basins, and Mesozoic Patagonian tectonics.

A renewal of the relative motion of the Patagonian block is not a necessary prerequisite to the observed Miocene motions. Once large continental fractures like the ASL have been formed, they will accomodate other types of motion and play a fundamental role in guiding the later tectonics.

### 4.5.2 On Aseismic Ridges

The question of what caused the Miocene event arises. I was originally led to the idea of the motion of the Patagonian block by studying possible modes of interaction between aseismic ridges and subduction zones. Such buoyant objects might well serve as obstacles to subduction and the westward motion of South America. If westward motion of South America in the vicinity of Bolivia were to stop while Patagonia proceeded unrestrained, the result would be relative motion of the Patagonian block similar to that postulated previously.

Variations in tectonic style along the western margin of South America often coincide with the position of aseismic ridges on the Nazca Plate. (Deza 1970, Herron 1972, Gansser 1973, Vogt et al. 1976, Pilger 1977, Kelleher and McCann 1977.) The crustal structure of the Nazca Ridge (section 3.2.2) is similar to many other aseismic ridges worldwide (Detrich and Watts 1979) and supports the notion that they represent zones of relatively high buoyancy in the oceanic plate. Since subduction is probably a consequence of cold, dense lithosphere sinking into a less dense mantle, it seems likely that the presence of buoyant zones will modulate the subduction process.

An enlightening model for ridge subduction has been presented by Vogt et al. (1976). The model supposes that the presence of a buoyant zone at a trench will slow down the subduction process and, consequently, affect all related activities such as back-arc spreading. This was used to explain the frequent association of cusps in island arcs with buoyant zones.

In addition to their cusp-forming effect, Vogt et al. postulate that reduced volcanism and seismicity are also to be expected where a buoyant zone encounters a trench. These rules seem to apply in some situations (especially with island arcs) but fail in a number of specific cases mostly along the eastern Pacific. For example, the intersection of the Nazca Ridge with the Peru-Chile Trench is manifest on the continent by the Pisco Deflection (see sections 3.2.2

and 3.8.7). Contrary to predictions of the Vogt et al. theory, low level volcanism does not occur just in the immediate vicinity of the contact point but extends virtually the entire length of Peru. In contrast, the volcanic Central Andes begin abruptly at the Pisco Deflection and extend south some 1500 km. This volcanism is strictly bounded between about 14°S and 28°S, a longitudinal regime which closely corresponds to the projection of the Nazca Ridge onto the continent in the direction of subduction (see figures 3.1b and 3.10).

### 4.5.3 Aseismic Ridges and the Miocene Event

The immense scale of the Miocene - Pliocene magmatic outbreak (section 3.5.3) tempts speculation regarding the cause. The Nazca Ridge and associated bathymetric highs form a close geometric relationship with these magmas suggesting a causal connection. As mentioned in section 3.2.2, the Nazca Ridge is the only one of the major aseismic ridges on the Nazca Plate which is not aligned approximately in the direction of subduction.

It was suggested in section 3.8.7 that the Nazca Ridge is causally related to the Pisco Deflection, the northern limit of the magmas. Figure 4.17 gives additional evidence in this matter. Here, the structure of the Pisco Deflection region is compared with spherical coordinate nets drawn about the Nazca - South America pole (upper figure) and the Nazca - Pacific pole (lower figure). The location of the

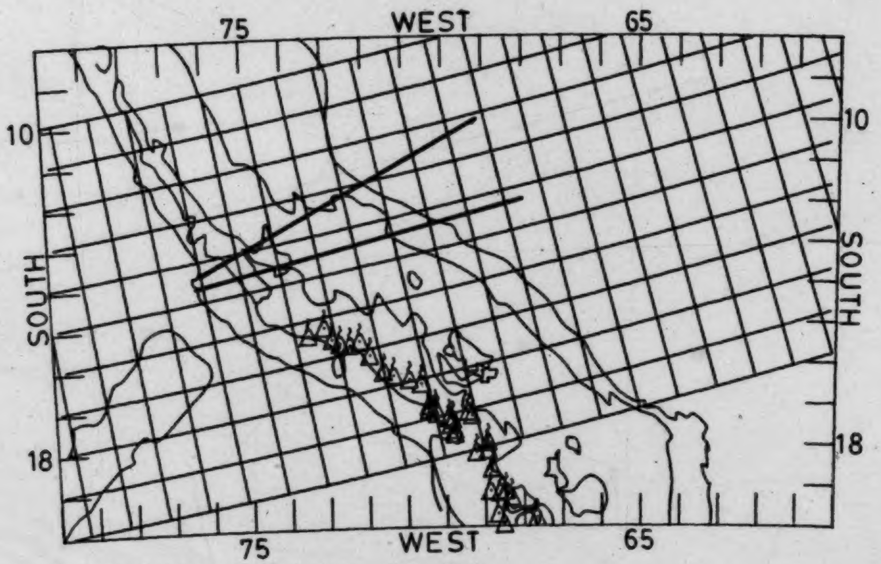
75
WEST
65
10
10
SOUTH
SOUTH
18
18
75
WEST
65

A: Nazca-South America Pole

Bold lines indicate Pisco Deflection Zone

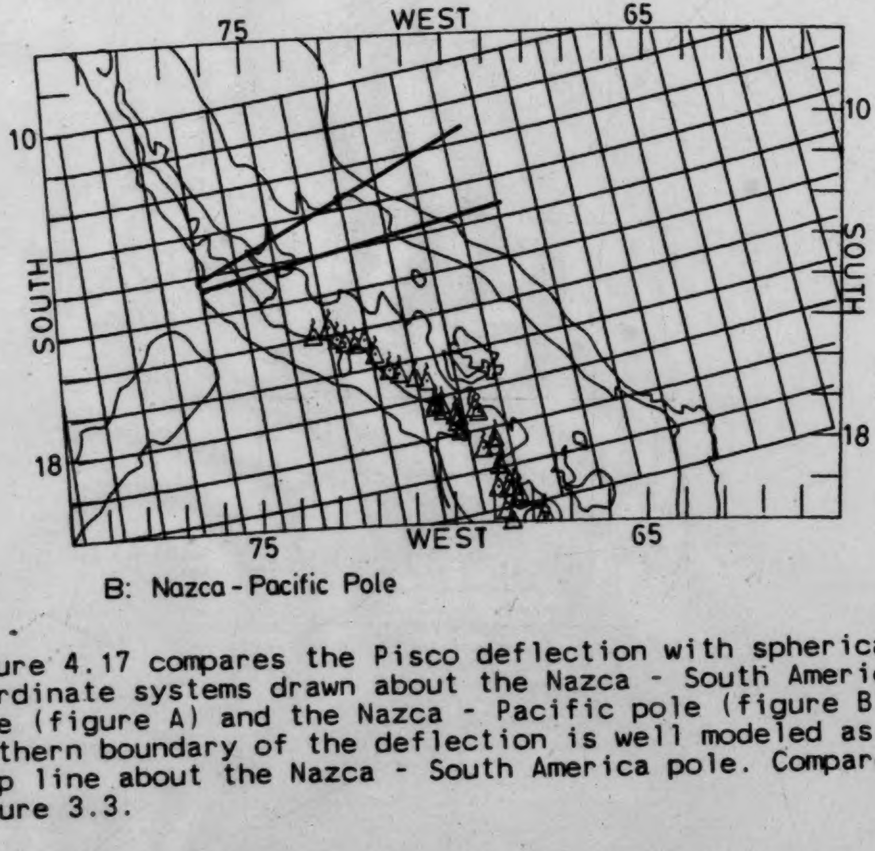
75
WEST
65
10
10
SOUTH
SOUTH
18
18
75
WEST
65

B: Nazca-Pacific Pole

Figure 4.17 compares the Pisco deflection with spherical coordinate systems drawn about the Nazca - South America pole (figure A) and the Nazca - Pacific pole (figure B). The southern boundary of the deflection is well modeled as a slip line about the Nazca - South America pole. Compare with figure 3.3.

Pisco Deflection is taken from Megard and Philip (1976) and the various geologic features may be identified from figure 3.4a. The lower boundary of the Pisco Deflection is a close match with a small circle about the Nazca - South America pole.

Thus, the Pisco Deflection may be interpreted as a plastic shear zone oriented in the direction of relative motion between the Nazca and South American plates. This supports the idea that the Nazca Ridge is an obstacle both to subduction and to the westward motion of South America.

In section 4.3.11, it was argued that the direction of subduction from 105ma to 30ma was normal to the coast of central Peru. The northern boundary of the Pisco Deflection forms a good plastic slip line for this subduction direction. Thus, there is evidence to suggest that the Nazca Ridge has been in the same position relative to South America since Mesozoic times. (Ganseer (1973) arrived at a similar conclusion by an independent line of reasoning.) If such a large buoyant object were here at the time of the initial breakup of western Gondwana, it may have exerted some control over the northern boundary of the Patagonian block and the consequent location of the "Arica Elbow."

Such reasoning also explains why the Nazca Ridge is not aligned in the approximate direction of spreading on the East Pacific Rise (or in the direction of subduction). It is most likely a relic left over from the plate motion patterns existing prior to the Miocene breakup of the old Farallon plate.

It is possible that the present pattern of shallow subduction beneath central Peru is a consequence of aseismic ridge interaction. Such a model has been presented by Pilger (1977). (However, this model conflicts with the last few paragraphs in that it has the Nazca Ridge striking the northern Peruvian coast about 20ma. The present position of the Nazca Ridge would then be due to more northerly portions being subducted. This model must attribute the association of the Nazca Ridge with the Pisco Deflection as coincidence.) Perhaps the combined effects of the Nazca Ridge and the Carnegie Ridge are sufficient to buoy up the Nazca Plate in between. Figure 4.18 illustrates a possible sequence of events which could lead to a subduction zone much like that found today in central Peru.

Figure 4.18 is a cartoon depicting the possible evolution of a subduction system as a zone of buoyant oceanic crust encounters the trench. The figure reads from top to bottom. This construction was drawn assuming that both the buoyant slab (A) and the normal slab (B) move with the same horizontal velocity but that B feels a greater (constant) gravitational force. Thus the slabs follow parabolic trajectories with different curvatures.

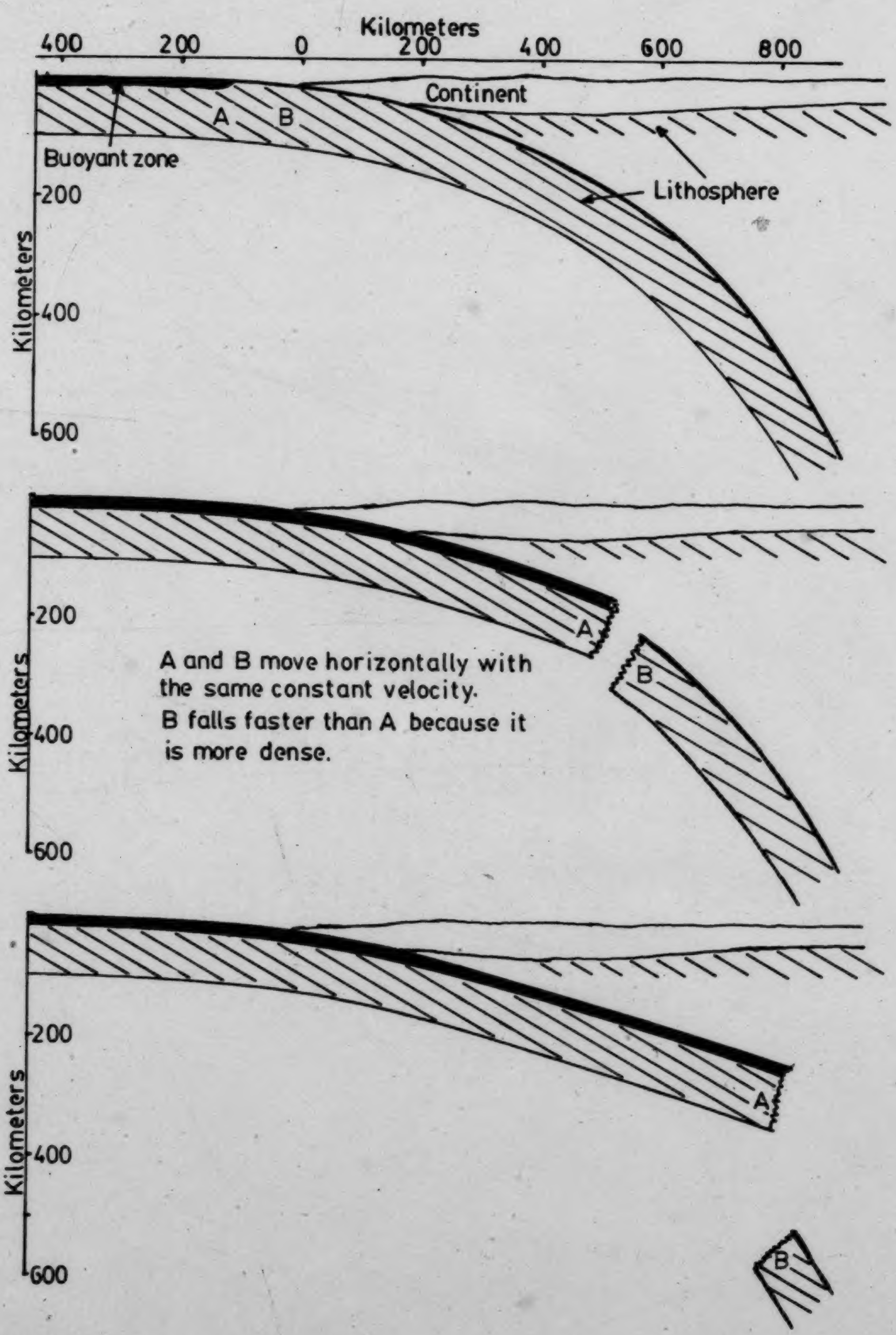
Kilometers
400
200
0
200
400
600
800
Continent
A
B
Buoyant zone
Lithosphere
200
Kilometers
400
600
200
A
B
Kilometers
400
600
200
A
Kilometers
400
600
B

A and B move horizontally with the same constant velocity.
B falls faster than A because it is more dense.

# 5. Future Directions in Tectonophysics

The initial Peruvian microgeodesy project has greatly expanded since its conception. Two networks are now in operation with others in planning stages. At the University of Alberta, the focus of activity with microgeodesy has shifted in the last two years from Peru to Mexico. Several networks have been installed there. Two are on active plate boundaries, and another is across a canyon being filled with a water reservoir. I have not been directly involved with these projects and cannot comment on their possible future. In South America, however, the results from the Huancayo network merit further discussion.

## 5.1 The Value of the Huancayo Microgeodetic Experiment

It was originally hoped that the tectonic studies summarized in the last few chapters would lead to a better insight into the meaning of the data gathered on the Huancayo network and possibly to a dynamic model of the Huaytapallana thrust fault. While the fog of ignorance has thinned, it remains a peculiar fog allowing sight at a distance but not nearby. With respect to the general tectonic evolution of South America, a plausible model has been advanced and examined. There remains a gulf between our understanding of the continental tectonics and our small survey measurements which is not easily bridged. The relation (if any) between large scale plate convergence rates and straining on one small thrust fault, high in the Andes, is obscure. Little is known of the details of the intervening structure; even with such knowledge, direct modeling would require a theoretical complexity beyond current abilities.

The Huancayo experiment is best regarded as a developmental study of a methodology for strain measurement. As such, it has been highly successful demonstrating that tectonic strains can be measured cheaply and rapidly. The technique can be employed by any organization possessing ordinary commercial surveying equipment. The total capital outlay required to begin operations is less than $10,000. It provides a practical means of monitoring tectonic strains, within the grasp of third world and developing countries.

The magnitude of the Huaytapallana strain event is surprisingly large compared to expected tectonic strains (section 2.1). The event appears far too temporally consistent to be illusory but its significance remains unclear. Perhaps future modeling to determine the magnitude and distribution of possible body forces will be illuminating. Certainly the development of the requisite mathematical technique would be a valuable contribution to geophysics.

## 5.2 Directions in Design and Analysis

The mathematical analysis requires access to modern computational facilities. This should pose no problem since the opportunity for cooperative studies is usually available should no facilities be present locally. The strain deduction method presented in chapter 2 is quite successful in achieving strain estimates approaching 1 microstrain. It seems quite possible that this could be extended to perhaps .5 microstrains with simple changes in the surveying technique such as:

1. Measuring only distances and repeating as many times as possible during a two week interval.
2. The use of slightly more sophisticated EDM's.
3. Using sophisticated targets whose position can be changed systematically along the line of sight by a precisely known amount. This idea (suggested by R.I. Walcott, personal communication 1980) has yet to be investigated, but may allow the accuracy of a given distance measuring device to be extended.

The possibility of extended accuracy through advanced network design remains an unknown. The mathematical technique of chapter 2 is suitable for forward modeling studies of the response of various geometries. However, it gives little direct insight into any fundamental design principles. It may be possible to do the singular value decomposition analytically for the simplest case of constant strain analysis by assuming a certain number of points, but leaving their coordinates arbitrary. This would be a major step in network design studies and would allow the analytical study of the fundamental modes of deformation of the network. The use of an algebraic computer language such as "Reduce" to do the decomposition seems feasible.

### 5.3 A Backus-Gilbert Formulation of the Strain Problem

It is possible to formulate the strain deduction problem as a linear inverse problem which could be solved by any of the many techniques developed in the geophysical literature for these problems (Parker 1977, Backus and Gilbert 1970 for example). The methods were devised to deal with inaccurate, incomplete and probably inconsistent data, which are far more common in geophysics than in geodesy. A linear inverse problem must be formulated such that the data, $A_i$ , (in this case observations of linelength and angle changes) are related to the model, M(x) (in this case a postulated form for the variation of strain over the survey area) by a linear relation having the general form

$$A_i = \int G_i M(x) dx \qquad 33$$

The quantities, {Gi}, are called the Frechet kernels of the data and are related to the way the response of the model changes with changing model parameters. Other terms, which are at least partially correct, are Green's functions, response functions, or Frechet derivatives. Suppose there exists a set of constants, {Bi}, such that we can write:

$$\delta(x-x_o) = \sum_i B_i G_i \qquad 34$$

where, $\delta(x-x_o)$ , is the Dirac delta function. Then, multiply 33 by {Bi}, sum over i, and reverse the order of integration and summation. This gives:

$$\sum_i B_i A_i = \int \delta(x-x_o) M(x) dx = M(x_o) \qquad 35$$

Thus, the properties of the delta function can be used to determine the value of the model at any point provided the set {Bi} can be found. A set {Bi}, satisfying 34 exactly, does not exist. This is because the {Gi} do not usually form a complete set of expansion functions. It is possible however to construct a pseudo-delta function, $\tilde{\delta}(x-x_o)$ , that is as sharply peaked as possible. (This pseudo-delta function is called the resolution function.)

Once the Frechet kernels have been identified for a given problem, then it is said to have been formulated as a Backus-Gilbert inversion problem. The actual construction of the resolution function is a difficult task which will depend on the properties of the particular set of Frechet kernels.

The problem of estimating strains from repeated survey data is equivalent to the mathematical problem of achieving the best possible approximation to a function of 2 variables given a finite number of values of its averages along a set of straight line segments (see chapter 2). Therefore, consider the following problem: Let {Li} be a set of N finite line segments defined in Euclidean two-space. Let x and y be Cartesian coordinates in that space and let R denote a rectangular region formed of coordinate lines which contains the set {Li}. If F=F(x,y) is any unknown, piecewise continuous function, then the values:

$$A_i = \frac{1}{d_i} \int_{o}^{d_i} F(x(s_i),y(s_i))ds_i \qquad 36$$

are known and are the average values of F along each of the {Li}. Construct the best possible estimate for the value of F(x0,y0) where x0,y0 is a point in R.

The method of analysis proceeds as follows:
If x(si),y(si) is any point on line segment Li, then we can write:

$$F(x(s_i),y(s_i)) = \int_R \delta(x-x(s_i),y-y(s_i))F(s,y)dxdy \qquad 37$$

where $\delta(x,y)$ is the two dimensional Dirac delta function. Substituting 37 into 36 and reversing the order of integration gives:

$$A_i = \int_R G_i F(x,y)dxdy \qquad 38$$

where:

$$G_i = \frac{1}{d_i} \int_0^{d_i} \delta(x-x(s_i), y-y(s_i))ds_i \qquad 39$$

The functions {Gi} are the Frechet kernels of the data {Ai}. These Frechet kernels are a particularly unwieldy set of functions. They are pseudo-functions in the same sense that the Dirac delta function is a pseudo-function. The {Gi} are the integrals of two dimensional delta functions along the straight line segments {Li}. Thus the {Gi} have the values:

$$G_i(x,y) = \begin{cases} \infty, \text{ if } (x,y) \text{ lies on } L_i \\ 0, \text{ if otherwise} \end{cases} \qquad 40$$

Furthermore these functions satisfy the following relations:

$$\int_R G_i(x,y)dxdy = 1 \qquad 41$$

and, if E(x,y) is an arbitrary function defined in R,

$$\int_R G(x,y)E(x,y)dxdy = \text{average value of } E(x,y) \text{ on } L_i \qquad 42$$

The {Gi} also satisfy an interesting sort of "orthogonality" relation:

$$\int_R G_iG_jdxdy = \begin{cases} 0, & L_i \cap L_j = \Phi \\ 1, & L_i \cap L_j \neq \Phi \text{ and } L_i \neq L_j \\ \infty, & L_i = L_j \end{cases} \qquad 43$$

$\Phi$ = The null set

This relation can be demonstrated non-rigorously using 40 and 41 and the properties of the delta function.

The preceeding exercise is by no means complete. Proper solution of the problem requires application of "quelling" (Parker 1977 and references therein) and a much more rigorous statement of the class of admissible strain solutions. It also requires extension of the essentially one dimensional notions of inverse theory to two dimensions. The particular advantage of this approach lies in its ability to quantify the effect of data inaccuracy and in its treatment of the underdetermined problem, the situation in which very few observations were made on a complex strain.

A tentative statement of the Backus-Gilbert inverse problem for strain is:

> Given the set of functions, {Gi}, defined as infinite on a set of line segments {Li} and zero elsewhere, construct a sharply peaked function at the point x0,y0 (in R) from a linear combination of the {Gi}.

Consider a radial network in which all of the {Li} intersect at a central point. Several results follow immediately:

1. The resolution function cannot be constructed at any point which does not lie on one of the line segments.
2. If x0,y0 lies at the center of the network, then we can construct a function which is infinite there but it will also be infinite along all line segments used in constructing the function. Those familiar with Backus - Gilbert theory will recognize that this means the resolution will be of the order of the size of the network. This is a rather abstract verification that,

given no additional knowledge concerning F(x,y), we have no recourse but to assume it constant over the network.

3. If the network includes any lines which do not pass through the central point, they will serve to broaden the resolution even further.

This formulation provides a valuable intuitive approach to the problem. The fundamental difficulty lies with the nature of the {Gi}. Since they are infinite along line segments, any linear combination is also infinite. It is impossible to build a sharply peaked function whose width is less than the network aperture with such a process. Suppose that some assumption about the nature of F(x,y) could be made with the result that the {Gi} became sharply peaked, but finite functions along the set {Li}. Then, for the radial net again, the superposition of 10 {Gi} would result in a function whose value at the center point would be ten times as great as neighboring points.

Such a formalism shows great promise but it needs to be more fully developed. Its intuitive nature may make it a valuable approach to network design analysis. Perhaps the application of physical constraints such as minimum strain energy will serve to broaden the {Gi}. It is hoped that this brief discussion will serve as a starting point for those wishing to investigate the problem further.

## 5.4 Suggestions for Future Microgeodetic Experiments in South America

The interpretation of the Huancayo network results is clouded by the complex tectonic setting of the network. This need not be the case for future experiments since there are areas of vital interest in South America which are probably much more adaptable to tectonic modeling. These include areas expected to show dominantly strike slip (horizontal) deformation such as:

1. The Huancabamba Deflection (section 3.2.4). Here a network along the coast would be valuable in establishing the nature of this zone. A measurement of strong east - west shearing could solidify the idea of this being a transition zone between northern and southern regions. The width and complexity of the Huancabamba Deflection would be a complicating factor, but a detailed study of the tectonic history should suggest specific locales for measurements.
2. The Pisco Deflection (section 3.2.5). In the last chapter, it was argued that this is a zone of plastic shear aligned in the direction of subduction and caused by the interaction of the Nazca Ridge with the Peru-Chile Trench. This model could be bolstered by the detection of strong horizontal shearing in the direction of relative motion between the Nazca and South American plates. Ernesto Deza (personal communication, 1977) has suggested a network in the western end of the Pisco

Deflection near Ica, Peru. This would be an excellent choice since it is close to the trench and the Pisco Deflection has minimum width here. Such conditions should result in strong, measurable strains.

3. The Arica Elbow. In the last chapter, this feature was modeled as a Mesozoic shear zone which may have been periodically reactivated during the Cretaceous. There is known active sinistral fault north and slightly west of Santa Cruz in the Subandean Ranges. A more accessible region of interest might be on the coast near the Arica corner itself.
4. The Atacama Fault (sections 3.6.2 and 4.3.11). The Atacama Fault was modeled as a Fitch fault (section 1.2.4) which ceased dextral activity with the Miocene reorganization of spreading centers in the eastern Pacific. Thus a null result for shearing parallel to the fault would be expected here and would be important as a verification of the model. Straining perpendicular to the fault and vertical motions would be anticipated.

There are other areas where small survey networks would give extremely valuable constraints especially if vertical control of the net could be achieved. Such areas include:

1. The Andean Seismicity Lineament (sections 3.8.8, 3.8.9, 4.3.10). A network situated along the volcanic portion of the ASL would be a fascinating experiment. It could provide direct verification of the association of extensional tectonics with volcanism. The intense

seismicity of the area should cause measurable deformations.

Another interesting local would be along the aseismic portion of the ASL in the Pampean Ranges. Vertical control would be a necessity here.

2. The Ojos del Salado Lineament (section 3.6.3). The OSL has been suggested to be the on-land extension of the Easter Fracture Zone (or Sala Y Gomez Ridge). As discussed in chapter 3, it is defined by a trans-Andean lineament and a normal fault with a throw exceeding 1.5 km. It denotes a major tectonic change from volcanic to non-volcanic. Again vertical control would be helpful here.

## Bibliography

Aguirre, L., R. Charrier, J. Davidson, A. Mpodozis, S. Rivano, R. Thiele, E. Tidy, M. Vergara, and J.-C. Vicente, Andean magmatism: It's paleographic and structural setting in the central part (30°-35°S) of the Southern Andes, *Pacific Geology*, 8, pp1-38, 1974

Allen, C. R., Earthquakes and mountains around the Pacific, *Engineering and Science Magazine*, January, 1963

Allen, C. R., Transcurrent faulting in continental areas, *Philosophical Transactions Royal Society of London*, 258, series A, pp82-89, 1965

de Almeida, F. F. M., Structure and dynamics of the Brazilian coastal area, in: M. Maldonado-Koerdall(ed), *Pan American Symposium on the Upper Mantle, Petrologia, vol 2*, v 2, Mexico Inst. Geofis., pp29-38, 1968

Arabasz, W. J., *Geological and geophysical fault studies of the Atacama fault zone in Northern Chile*, PhD. Thesis, California Institute of Technology, 1971

Atherton, M. P. and P. J. Brenchley, A preliminary study of the structure, stratigraphy, and metamorphism of some contact rocks of the Western Andes near the Quebrada Venado Muerto, Peru. *Geological Journal*, 8, pp161-178, 1972

Atwater, T., Implications of plate tectonics for the Cenozoic tectonic evolution of western North America, *Geological Society of America Bulletin*, 81, pp3513-3536, 1970

Auboin, J., *Geosynclines*, Elsevier, New York, 335pages, 1965

Backus, G. and F. Gilbert, Uniqueness in the inversion of inaccurate gross earth data, *Philosophical Transactions Royal Society of London*, 266, series A, pp123-192, 1970

Baker, M. C. W. and P. W. Francis, Upper Cenozoic volcanism in the central Andes, ages and volumes, *Earth and Planetary Science Letters*, pp175-187, 1978

Bally, A. W. and S. Snelson, *Realms of Subsidence*, Canadian Society of Petroleum Geologists, Memoir 6, pp1-94, 1979

Barazangi, M. and J. Dorman, World seismicity maps compiled from ESSA and Coast and Geodetic Survey epicenter data 1961-1967, *Bulletin of the Seismological Society of America*, 59, pp369-380, 1969

Barazangi, M. and B. Isacks, Spatial distribution of earthquakes and subduction of the Nazca Plate beneath South America, *Geology*, 4, pp686-692, 1976

Barazangi, M and B. Isacks, Subduction of the Nazca Plate beneath Peru:, evidence from spatial distribution of earthquakes, *Geophysical Journal of the Royal Astronomical Society*, 57, pp537-555, 1979

Barron, E. J., C. G. A. Harrison, and W. W. Hay, A revised reconstruction of the southern continents, *EOS*, 59, pp436-449, 1978

Bateman, R. C., and F. C. W. Dodge, Variations in major chemical constituents across the Sierra Nevada Batholith, *Geological Society of America Bulletin*, 81, pp409-420, 1970

Beaumont, C., The evolution of sedimentary basins on a viscoelastic lithosphere: theory and examples, *Geophysical Journal of the Royal Astronomical Society*, 55, pp471-497, 1978

Benioff, H., Orogenesis and deep crustal structure: additional evidence from seismology, *Geological Society of America Bulletin*, 65, pp385-400, 1954

Bonarino, F. Gonzalez, Argentina, in: Fairbridge, R. W. (ed), *Encyclopedia of World Regional Geology Part 1: Western Hemisphere (including Antarctica and Australia)*, pp 15-20, Dowden Hutchinson and Ross, 704pp, 1975

Bonatti, E., C. G. A. Harrison, D. E. Fisher, J. Honnarez, J.-G. Schilling, J. J. Stipp, and M. Zentilli, The Easter volcanic chain, a mantle hot line, *Journal of Geophysical Research*, 82, pp2457-2478, 1977

Bowen, R. L., The Parana basin flood lavas and their structural relations with the Ponta Grossa Arch, in: Guidebook--International Field Institute--Brazil 1966, sponsered by: American Geological Institute, Wash, D. C., 1966

Bruhn, R. L. and I. W. D. Dalziel, Destruction of the early Cretaceous marginal basin in the Andes of Tierra del Fuego, in: Talwani and Pittman (eds), Island Arcs, Deep Sea Trenches, and Back-arc Basins, pp395-406, 1977

Brunner, F. K., On the analysis of geodetic networks for the determination of the incremental strain tensor, Survey Review , 25, pp56-57, 1979

Bullard, E., J. E. Everett, and A. G. Smith, The fit of the continents around the Atlantic, Philosophical Transactions Royal Society of London, 258, series a, pp41-51, 1965

Carey, S. W., The Expanding Earth, Elsevier, 1958a

Carey, S. W., Continental Drift, a Symposium, pp177-355, Hobart, 1958b

Carter, W. D., Evaluation of ERTS-1 data: Applications to geologic mapping of South America, with emphasis on the Andes mountain region, open file report, U.S. Geological Survey, 1974

Chinn, D. S., and B. L. Isacks, Focal mechanisms and accurate depths of crustal earthquakes in the Andean cordilleras (abstract), Transactions American Geophysical Union (EOS) , 61, p370, 1980

Chinnery, M. A., The deformation of the ground around surface faults, Bulletin of the Seismological Society of America, 51, no. 3, pp355-372, 1961

Chrzanowski, A., E. Nyland, M. Dennler, and A. Szcostak, Microgeodetic networks in monitoring tectonic movements, in Proceedings of FIG 2nd International Symposium on Deformatory Movements,1978

Clark, A. H., E. Farrar, J. C. Caelles, S. J. Haynes, R. B. Lortie, S. L. McBride, S. G. Quirt, R. C. R. Robertson, and M. Zentilli, Longitudinal variations in the metallogenetic evolution of the Central Andes, In: D. F. Strong (ed), Metallogeny and Plate Tectonics, Geological Association of Canada, Special Paper 14, pp25-58, 1976

Cobbing, E. J., The tectonic framework of Peru as a setting for batholithic emplacement, Pacific Geology, 8, pp63-65, 1974

Cobbing, E. J., The Andean geosyncline in Peru and its distinction from Alpine geosynclines, Journal of the Geological Society of London, 135, pp207-218, 1978

Cobbing, E. J. and W. S. Pitcher, The coastal batholith of Peru, Journal of the Geological Society of London, 128, pp421-460, 1972a

Cobbing, E. J. and W. S. Pitcher, Plate Tectonics and the Peruvian Andes, Nature Physical Science, 240, pp51-53, 1972b

Cobbing, E. J., J. M. Ozard, and N. J. Snelling, Reconnaissance geochronology of the crystalline basement rocks of the Coastal Cordillera of Peru, Geological Society of America Bulletin 88, pp241-246, 1977

Coney, P. J., Structural evolution of the Cordillera Huayhuash, Andes of Peru, Geological Society of America Bulletin, 82, pp1863-1884, 1971

Cordani, U. G. and P. Vandoros, Basaltic rocks of the Parana basin, in: J. J. Bigarella, R. D. Becker, and I. D. Pinto (eds), Problems in Brazillian Gondwana Geology, International Symposium of the Gondwana Stratigraphy and Paleontology, pp207-231, 1967

Cossio, A., Geologia de los Quadrangulos de Santiago de Chuco y Santa Rosa, Boln. Comn. Carta. Geol. Nac. Peru, 8, pp1-69, 1964

Cox, Keith Gordan, Tectonics and volcanism of the Karoo period and their bearing on the postulated fragmentation of Gondwanaland, in: T. N. Clifford and I. G. Gass (eds), African Magmatism and Tectonics , Oliver and Boyd, Edinburgh, pp211-236, 1970

Cox, Keith Gordan, The Karoo Volcanic Cycle, Journal of the Geological Society of London, 128, pp311-336, 1972

Cutler, S. T., Geophysical investigation of the Nazca Ridge (abstract), Transactions American Geophysical Union, Dec., p1230, 1977a

Cutler, S. T., Geophysical investigation of the Nazca Ridge, MSc Thesis, U. of Hawaii, Honolulu, 1977b

Dalziel, I. W. D., M. J. DeWitt, and K. F. Palmer, A fossil marginal basin in the Andes, Nature, 250, pp291-294, 1974

Dalziel, I. W. D. and K. F. Palmer, Progressive deformation and orogenic uplift at the southern extremity of the Andes, Geological Society of America Bulletin, 90, pp259-280, 1979

D'Angelo, E. P., and L. A. Le Bert, Relacion entre Estructura y Volcanismo Cuaternaio Andino en Chile, in Petrologia, Pan-American Symposium on the Upper Mantle, vol2, Mexico Inst. Geofis., pp39-46, 1969

Dennler, S. M., and A. Chrzanowski,Evaluation of micro-geodetic networks for monitoring tectonic movements in Peru, MSc. Thesis, Dept. of Surveying Engineering, Univ. of New Brunswick, Fredrickton, New Brunswick, 1979

Detrich, R. S. and A. B. Watts, An analysis of isostacy in the world's oceans, 3, aseismic ridges, Journal of Geophysical Research, 84, pp3637-3653, 1979

Dewey, J. F. and J. M. Bird, Mountain belts and the new global tectonics, Journal of Geophysical Research, 75, pp2625-2647, 1970

Deza E, Zonas de transicion sismotectonica en Sudamerica: estudio preliminar de la zona de transicion en el Peru, in: Proceedings of the Upper Mantle Symposium, Buenos

Aires, pp143-155, 1970

Deza, E, The Pariahuanca earthquakes, Huancayo, Peru: July-October 1969, in Recent Crustal Movements, Royal Society of New Zealand, bulletin 9, pp77-83, 1971

Dickinson, W. R., Relations of andesites, granites, and derivative sandstones to arc-trench tectonics, Reviews of Geophysics, 8, pp813-860, 1970

Dickinson, W. R. and W. S. Snyder, Plate tectonics of the Laramide Orogeny, Geological Society of America Bulletin, 151, pp355-366, 1978

Dietz, R. S. and J. C. Holden, Reconstruction of Pangea: break-up and dispersion of the continents, Permian to Recent, Journal of Geophysical Research, 75, pp4939-4956, 1970

Dott, R. H. Jr., Contrasts in tectonic history along the eastern Pacific rim, in: G. H. Sutton, M. H. Manghnani, and R. Moberly (eds), The Geophysics of the Pacific Ocean Basin and its Margin, pp299-308, American Geophysical Union Monograph 19, 1976

Drake, C. L., M. Ewing, and J. Sutton, Continental margins and geosynclines; the east coast of North America, north of Cape Hatteras, in: Aherns, Rankama and Runcorn (eds), Physics and Chemistry of the Earth, pp110-198, Pergamon, London, 1959

Du Toit, A. L., Our Wandering Continents: an Hypothesis of Continental Drifting, Oliver and Boyd, London, 366pages, 1937

Eckel, Edwin B., Geology and Mineral Resources of Paraguay - a Reconnaissance, USGS professional paper, 327, 110 pages, 1959

Eisbacher, G. H., Evolution of successor basins in the Canadian cordillera, in: R. H. Dott and R. H. Shaver (eds), Modern and Ancient Geosynclinal Sedimentation, Society of Economic Paleontology and Minerology, special publication 19, pp274-291, 1974

Fisher, R. L., Preliminary report on Expedition Downwind, Univ. Cal., Scripps Inst. Oceanography, IGY cruise to southeast Pacific, IGY general report, ser. 2, 1958

Fisher, R. L. and R. W. Raitt, Topography and structure of the Peru-Chile Trench, Deep Sea Research, 9, pp423-429, 1962

Fitch, T. J., Plate convergence, transcurrent faults and internal deformation adjacent to Southwest Asia and the Western Pacific, Journal of Geophysical Research, 77, pp4432-4460, 1972

Frank, F. C., Deduction of earth strains from survey data, Bulletin of the Seismological Society of America, 56, no. 1, pp35-42, 1966

Gansser, A., Facts and theories on the Andes, Journal of the Geological Society of London, 129, pp93-131, 1973

Goldstein, H., Classical Mechanics, Addison - Wesley, Reading Mass., 399pages, 1965

Halpern, M, Regional geochronology of Chile south of 50° latitude, Geological Society of America Bulletin, 84, pp2407-2422, 1973

Ham, C. K. and L. J. Herrara Jr., Role of the subandean fault system in the tectonics of eastern Peru and Equador, in: O. E. Childs and B. W. Beebe (eds), Backbone of the Americas, pp47-61, American Association of Petroleum Geologists Memoir 2, 1963

Handschumacher, D. W., Post Eocene plate tectonics of the eastern Pacific, in: G. H. Sutton, M. H. Maghnani, and R. Moberly (eds), The Geophysics of the Pacific Ocean Basin and its Margin, pp177-203, American Geophysical Union monograph 19, 1976

Hanus, V and J. Vanek, Morphology of the Andean Wadati-Benioff zone, andesitic volcanism, and tectonic features of the Nazca Plate, Tectonophysics, 44, pp65-77, 1978

Harrington, H. J., Argentina, in: W. F. Jenks (ed), Handbook of South American Geology, pp129-166, Geological Society of America, Memoir 65, 1956

Hasegawa, A. and I. S. Sacks, Subduction of the Nazca Plate beneath Peru as determined from seismic observations, Carnegie Institute of Washington Year Book, 78, pp276-284, 1979

Hasegawa, A. and I. S. Sacks, The subduction of the Nazca Plate (abstract), Transactions American Geophysical Union (EOS), 61, p371, 1980

Herrero-Ducloux, A., The Andes of western Argentina, in: O. E. Childs and B. W. Beebe (eds), Backbone of the Americas, pp16-28, American Association of Petroleum Geologists Memoir 2, 1963

Herron, E. M., Sea floor spreading and the Cenozoic history of the east central Pacific, Geological Society of America Bulletin, 83, pp1671-1692, 1972

Hertz, Norman, Tholeiitic and alkalic volcanism in southern Brazil, in: Guidebook--International Field Institute--Brazil 1966, sponsored by: American Geological Institute, Wash. D. C., 1966

Hill, R., The Mathematical Theory of Plasticity, Oxford University Press, New York, 1950

Hobbs, B. E., W. D. Means, P. F. Williams, An Outline of Structural Geology, 571 pages, John Wiley and Sons Inc., New York, 1976

Huggett, G. R. and L. E. Slater, Precision of electromagnetic distance-measuring instrument for determining secular strain and fault movement, Tectonophysics, 29, pp19-27, 1975

IMSL, International Mathematical and Statistical Libraries Inc., 6th floor-GNB Bldg, 7500 Bellaire Boulevard, Houston, Texas 77036, 1979

Jackson, D. D., Interpretation of inaccurate, insufficient, and inconsistent data, Geophysical Journal of the Royal Astronomical Society, 28, pp97-109, 1972

James, D. E., Andean crustal and upper mantle structure, Journal of Geophysical Research, 76, pp3246-3271, 1971a

James, D. E., Plate tectonic model for the evolution of the central Andes, Geological Society of America Bulletin, 82, pp3325-3346, 1971b

James, D. E., Subduction of the Nazca PLate beneath central Peru, Geology, 6, pp174-178, 1978a

James, D. E., On the origin of the calc-alkaline volcanics of the Central Andes: a revised interpretation, Carnegie Institute of Washington Year Book, 77, pp562-590, 1978b

James, D. E., C. Brooks, and A. Cuyobamba, Andean Cenozoic volcanism: magma genesis in the light of strontium isotopic composition and trace element geochemistry, Geological Society of America Bulletin, 87, pp592-600, 1976

Jenks, W. F., Peru, in: W. F. Jenks (ed), Handbook of South American Geology, Geological Society of America, memoir 65, pp217-247, 1956

Karig, D. E, Ridges and basins of Tonga - Kermadec island arc system, Journal of Geophysical Research, 75, pp239-255, 1970

Karig, D. E., Evolution of arc systems in the western Pacific, Annual Reviews of Earth and Planetary Sciences, 2, pp51-75, 1974

Kausel, E. and C. Lomnitz, Tectonics of Chile, in: Petrologia, Pan-American Symposium on the Upper Mantle, vol 2, Mexico Inst. Geofis., pp47-68, 1969

Kay, G. M., North American Geosynclines, Geological Society of America, Memoir 48, 143pages, 1951

Kelleher, J. A. and W. McCann, Bouyant zones, great earthquakes and unstable boundaries of subduction. Journal of Geophysical Research, 81, pp4885-4896, 1976

Kulm, L. D., W. J. Schweller, and A. Masias, A preliminary analysis of the subduction processes along the Andean continental margin, 6° to 45°S, in:Talwani and Pittman (eds), Island Arcs, Deep Sea Trenches, and Back-arc Basins, pp285-301, 1977

Lanczos, C., Linear Differential Operators, D. Van Nostrand Co., London, 1961

Larson, R. L. and J. W. Ladd, Evidence for the opening of the south Atlantic in the early Cretaceous, Nature, 246(5430), pp209-212, 1973

Lawson, Charles L., and Richard J. Hanson, Solving Least Squares Problems, Prentice-Hall Inc, Englewood Cliffs, N.J., 1974

LePichon, X., and D. E. Hayes, Marginal offsets, fracture zones and the early opening of the south Atlantic, Journal of Geophysical Research, 76, pp6283-6293, 1971

Lesta, P. J., Estratigrafia de la cuencadel Golfo de San Jorge, Actas de las 3 das. J. Geol. Argentinas, 1, pp251-290, 1968

Lohmann, H. H., Outline of the tectonic history of the Bolivian Andes, American Association of Petroleum Geologists Bulletin, 54, pp735-757, 1970

Lohmann, H. H., Bolivia, in: R. W. Fairbridge (ed), Encyclopedia of World Regional Geology Part 1: Western Hemisphere (including Antarctica and Australia), pp123-126, Dowden Hutchinson and Ross, 704pages, 1975

Lomnitz, C., Global Tectonics and Earthquake Risk, Elsevier, Amsterdam, 320pages, 1974

Ludwig, W. J., J. I. Ewing, C. C. Windisch, A. G. Lonardi, and F. F. Rios, Structure of the Colorado basin and continent - ocean crust boundary off Bahia Blanca, Argentina, in: J. S. Watkins, L. Montadert, and P. W.

Dickerson (eds), Geological and Geophysical Investigations of Continental Margins, American Association of Petroleum Geologists, memoir 29, pp113-124, 1979

Maack, R., Die Entwicklung der Gondwana Schichten Sued Brasiliens und ihre beziehungen zur Karru-formation Sued Africas, Int. Geol. Congress, 19, Alger, Symp. sur les Series Gondwana, pp339-372, 1952

Magaritz, M., D. J. Whitford, and D. E. James, Oxygen isotopes and the origin of high $Sr^{87}/Sr^{86}$ andesites, Earth and Planetary Science Letters, 40, pp220-230, 1978

Mapa Geologico de America del Sur, Commission for the Geological Map of the World, F. Blondel (President), 1964

Mapa Geologico do Estado do Parana, by Reinhard Maack, Servico de Geologia do Instituto de Biologia e Pesquisas Technologicas, Brazil, 1953

Mapa Geologico del Peru, Ministerio de Energia y Minas, Instituto de Geologia y Minas, Republica del Peru, Lima, Peru, 1975

McDougall, I, Potassium-argon age measurements on dolerites from Antarctica and South Africa, Journal of Geophysical Research, 68(5), pp1535-1545, 1963

McKenzie, D. P, The initiation of trenches: a finite amplitude instability, in: Talwani and Pittman (eds), Island Arcs, Deep Sea Trenches, and Back-arc Basins, pp57-62, 1977

Mckenzie, D. P., Some remarks on the development of sedimentary basins, Earth and Planetary Science Letters, 40, pp25-32, 1978

McKenzie, D. P. and W. J. Morgan, Evolution of triple junctions, Nature, 224, pp125-133, 1969

Megard, F. and H. Phillip, Plio-Quaternary tectonomagmatic zonation and plate tectonics in the central Andes, Earth and Planetary Science Letters, 33, pp231-238, 1976

Menard, H. W. and T. Atwater, Changes in the direction of sea floor spreading, Nature, 219, pp463-467, 1968

Minster, J. B. and T. H. Jordan, Present day plate motions, Journal of Geophysical Research, 83, pp5331-5354, 1978

Molnar, P. and P. Tapponier, Cenozoic tectonics of Asia, effects of a continental collision, Science, 189, pp419-426, 1975

Molnar, P. and P. Tapponier, The collision between India and Eurasia, Scientific American, 236, pp30-41, 1977a

Molnar, P. and P. Tapponier, Relation of the tectonics of eastern China to the India-Eurasia collision: applications of slip-line field theory to large scale control tectonics, Geology, 5, pp212-216, 1977b

Monger, J. W. H., J. G. Souther, H. Gabrielse, Evolution of the Canadian cordillera: a plate tectonic model, American Journal of Science, 272, pp577-602, 1972

Montadert, L., D. G. Roberts, O. de Charpal, and P. Guennoc, Rifting and subsidence of the northern margin of the Bay of Biscay, Initial Reports of the Deep Sea Drilling Project, XLVIII, pp1025-1060, 1979

Munoz Christi, J., Geology of Chile, in: W. F. Jenks (ed), Handbook of South American Geology, Geological Society of America Memoir, 65, pp191-214, 1956

Myers, J. S., Cauldron subsidence and fluidization: mechanisms of intrusion of the Coastal Batholith of Peru into its own volcanic ejecta, Geological Society of America Bulletin, 86, pp1209-1220, 1975a

Myers, J. S., Vertical crustal movements in Peru, Nature , 254, pp672-674, 1975b

Neev, D., The Pelusium line - a major transcontinental shear, Tectonophysics, 38, ppT1-T8, 1977

Neill, W. M., Possible continental rifting in Brazil and Angola related to the opening of the South Atlantic, Nature Physical Science, 245, pp104-107, 1973

Noble, D. C., E. H. McKee, E. Farrar, and U. Petersen, Episodic Cenozoic volcanism and tectonism in the central Andes of Peru, Earth and Planetary Science Letters, 21, pp213-220, 1974

Noble, D. C., E. H. McKee, and F. Megard, Early Tertiary "Incaic" tectonism, uplift, and volcanic activity, Andes of Central Peru, Geological Society of America Bulletin, 90, pp903-907, 1979

Nyland, E., Repeated geodetic surveys as experiments in geophysics, Canadian Surveyor (Scientific journal of the Canadian Institute of Surveying), 31, no. 4, pp347-360, 1977

Nyland, E., A. Chrzanowski, M. Dennler, A. Szcostak, G. Margrave, and E. Deza, Measurement and analysis of ground motion using microgeodetic networks, in press Geofisica Internacional , 1979

Oceano Atlantico da America do Sul a Africa, Internacional Serie de Cartas, published by: Directoria de Hidrografia e Navegacao da Marinha do Brasil, 1978

Ocola, L. C. and R. P. Meyer, Crustal structure from the Pacific basin to the Brazilian shield between 12° and 30° south latitude, Geological Society of America Bulletin, 84, pp3387-3404, 1973 Parker, R. L., Understanding inverse theory, Annual Reviews of Earth and Planetary Science, 5, pp35-64, 1977

Penrose, R., A generalized inverse for matrices, Proceedings of the Cambrige Philosophical Society, 51, pp406-413, 1955

Philip H. and F. Megard, Structural analysis of the superficial deformation of the 1969 Pariahuanca earthquakes (central Peru), Tectonophysics, 38, pp259-278, 1977

Pichler, H. and W. Zeil, Andesites of the Central Andes, in:

A. R. McBirney(ed), Proceedings of the Andesite Conference, pp165-174, bull. 65, Dept. of Geology and Mineral Industries, State of Oregon, 1969

Pichler, H. and W. Zeil, The Cenozoic rhyolite-andesite association of the Chilean Andes, Bulletin Volcanology??, 34, pp424-452, 1972

Pilger, R. H. Jr., Plate reconstructions, aseismic ridges, and low angle subduction beneath the Andes (abstract), Transactions American Geophysical Union, Dec., 58, p1232, 1977

Pitcher, W. S., The Mesozoic and Cenozoic batholiths of Peru, Pacific Geology, 8, pp51-62, 1974

Pitcher, W. S., The anatomy of a batholith, Journal of the Geological Society of London, 135, pp157-182, 1978

Pitcher, W. S. and M. A. Bussell, Structural control of batholith emplacement in Peru - a review, Journal of the Geological Society of London, 133, pp249-256, 1977

Prescott, W. H., An extension of Frank's method for obtaining crustal shear strains from survey data, Bulletin of the Seismological Society of America, 66, pp1847-1854, 1976

Prescott, W. H., J. C. Savage, and W. T. Kinoshita, Strain accumulation rates in the western United States between 1970 and 1978, Journal of Geophysical Research, 84, no. B10, pp5423-5436, 1979

Rabinowitz, P. D., M. Delach, M. Truchan, and A Lonardi, Bathymetry of the Argentine Continental Margin and Adjacent Areas (Map), published by: The American Association of Petroleum Geologists, box 979, Tulsa, Oklahoma, 1978

Rabinowitz, Philip D. and John Labreque, The Mesozoic south Atlantic ocean and evolution of its continental margins, Journal of Geophysical Research, 84, pp5973-6002, 1979

Ringwood, A. E., Petrogenesis in island arc systems, in:

Tanwani and Pittman (eds), Island Arcs, Deep Sea Trenches, and Back-arc Basins, pp311-324, 1977

Roeder, D., Continental Collisions, in: D. E. James (ed), U.S. National Report: Papers in Tectonophysics, published in: Reviews of Geophysics and Space Physics, 17, pp1098-1108, 1979

Sacks, I. S., Distribution of absorptive shear waves and its tectonic significance, Carnegie Institute of Washington Year Book, 67, pp339-344, 1969

Sacks, I. S., Interrelationships between volcanism, seismicity, and anelasticity in western South America, Tectonophysics, 37, pp131-139, 1976

Sacks, I. S. and H. Okada, A comparison of the anelasticity structure beneath western South America and Japan, Physics of the Earth and Planetary Interiors, 9, pp211-219, 1974

Santo, T., Characteristics of seismicity in South America, Bulletin of Earthquake Research Institute, Tokyo University, 47, pp635-672, 1969

Saunders, A. D., J. Tarney, C. R. Stern, and I. W. D. Dalziel, Geochemistry of Mesozoic marginal basin floor igneous rocks from southern Chile, Geological Society of America Bulletin, 90, pp237-258, 1979

Savage, J. C., Comment on 'An analysis of strain accumulation on a strike slip fault' by D. L. Turcotte and D. A. Spence, Journal of Geophysical Research, 80, pp4111-4114, 1975

Savage, J. C., Geodetic Measurements of Crustal Motions, in: U. A. Uotila (ed), The Changing World of Geodetic Science, volume 1, report 250, Ohio State University, Department of Geodetic Science, pp99-118, 1977

Savage, J. C., Strain Patterns and strain accumulation along plate margins, in: I. I. Mueller (ed), Applications of Geodesy to Geodynamics, report 280, Ohio State University, Department of Geodetic Science, pp93-98, 1979

Savage, J. C., and W. H. Prescott, Precision of Geodolite distance measurements for determining fault movements, Journal of Geophysical Research, 78, no. 26, pp6001-6008, 1973

Schmucker, U., D. Hartmann, A. A. Giesecke, M. Casaverde, and S. E. Forbush, Electrical conductivity anomalies in the earth's crust in Peru, Carnegie Institution Yearbook, 63, pp354-362, 1964

Schmucker, U., S. E. Forbush, D. Hartmann, A. A. Giesecke, M. Casaverde, J. Castillo, R. Salgueiro, and S. del Poza, Electrical conductivity anomaly under the Andes, Carnegie Institution Yearbook, 65, pp11-28, 1966

Scholz, C. H., M. Barazangi, and M. L. Sbar, Late Cenozoic evolution of the great basin, western United States, as an ensialic interarc basin, Geological Society of America Bulletin, 82, pp2979-2990, 1971

Shackleton, 1977, appears as discussion following Pitcher and Bussell, 1977

Siedner, G. and J. A. Miller, K-Ar age determinations on basaltic rocks from SW Africa and their bearing on continental drift, Earth and Planetary Science Letters, 4, pp451-458, 1968

Sillitoe, R. H., Tectonic segmentation of the Andes: implications for magmatism and metallogeny, Nature, 250, pp542-545, 1974

Sillitoe, R. H., Andean mineralization, a model for the metallogeny of convergent plate margins, in: D. F. Strand (ed), Metallogeny and Plate Tectonics, Geological Association of Canada, special paper 14, pp59-100, 1976

Smith, A. G. and A. Hallam, The fit of the southern continents, Nature, 225, pp139-144, 1970

Smithson, S. B., J. A. Brewer, S. Kaufman, J. E. Oliver, and C. A, Hurich, Structure of the Laramide Wind River uplift, Wyoming, from Cocorp deep reflection data and from gravity data, Journal of Geophysical Research, 84, pp5955-5972, 1979

Snay, R. A., and J. G. Gergen, Monitoring regional crustal deformation with horizontal geodetic data, in: I. I. Mueller (ed), Application of Geodesy to Geodynamics, pp87-92, Ohio State University, Department of Geodetic Science, Report 280, Columbus, Ohio, 1979

Snoke, J. A. and I. S. Sacks, Observations of ScSp arrivals at NNA: Seismological evidence for steeper (30°) subduction beneath central Peru, (abstract) Transactions American Geophysical Union, 59, p383, 1978

Snoke, J. A., I. S. Sacks, and D. E. James, Subduction beneath western South America: evidence from converted phases, Geophysical Journal of the Royal Astronomical Society, 59, pp219-225, 1979

Sonnenberg, Frank P., Bolivia and the Andes, in: O. E. Childs and B. W. Beebe (eds), Backbone of the Americas, American Association of Petroleum Geologists Memoir 2, pp36-46, 1963

St. Amand, P. and C. R. Allen, Strike slip faulting in northern Chile (Abstract), Geological Society of America Bulletin, 71, p1965, 1960

Stauder, W., Mechanism and spatial distribution of Chilean earthquakes with relation to subduction of the oceanic plate, Journal of Geophysical Research, 78, pp5033-5061, 1973

Stauder W., Subduction of the Nazca Plate under Peru as evidenced by focal mechanisms and by seismicity, Journal of Geophysical Research, 80, pp1053-1064, 1975

Stearns, D. W., Faulting and folding in the Rocky Mountains foreland, in: V. Matthews II (ed), Laramide Folding associated with Basement Block Faulting in the Western United States, Geological Society of America, Memoir 151, pp1-38, 1978

Steinmann, G., Geologie von Peru: Heidelberg, Carl Winters Universitats Buchhandlung, 448pages, 1929

Steketee, J. A., On Volterra's dislocations in a semi-infinite medium, Canadian Journal of Physics, pp192-205, 1958

Stewart, J. W., J. F. Evernden, and N. J. Snelling, Age determinations from Andean Peru, a reconnaissance survey, Geological Society of America Bulletin, 85, pp1107-1116, 1974

Sykes, L. R., A possible nacent island arc in the Indian Ocean (Abstract), Transactions American Geophysical Union, 51, 1970

Talwani, M. and O. Eldholm, The boundary between continental and oceanic basement at the margin of rifted continents, Nature , 241(5388), pp325-330, 1973

Tapponier, P. and P. Molnar, Slipline field theory and large scale continental tectonics, Nature, 264, pp319-324, 1976

Tectonic Map of South America, Commission for the Geological Map of the World, Jean Marcais (President), 1978

Thatcher, Wayne, Systematic inversion of geodetic data in central California, Journal of Geophysical Research, 84, no. B5, pp2283-2296,1979

Tilton, G. R., Isotope studies of Cenozoic Andean calc-alkaline rocks, Carnegie Institute of Washington Year Book, 78, pp298-304, 1979

Turcotte, D. L. and D. A. Spence, An analysis of strain accumulation on a strike slip fault, Journal of Geophysical Research, 79, pp4407-4412, 1974

Urien, C. M. and J. J. Zambrano, The geology of the basins of the Argentine continental margin and the Malvinas plateau, in: A. E. M. Nairn and F. G. Stehli (eds), The Ocean Basins and Margins -- Volume 1 the South Atlantic, pp135-169, Plenum Press, N. Y., 1973

Uyeda, S. and A. Miyashiro, Plate tectonics and the Japanese islands: a synthesis, Geological Society of America Bulletin, 85, pp1159-1170, 1974

Uyeda, S. and H. Kanamori, Back-arc opening and the mode of subduction, Journal of Geophysical Research, 84, pp1049-1062, 1979

Vandoros, P., N. R. Ruegg, and U. G. Cordani, On potassium-argon age measurements of basaltic rocks from southern Brazil, Earth and Planetary Science Letters, 1(6), pp449-452, 1966

Verhoogen, J., F. J. Turner, L. E. Weiss, and C. Wahrhaftig, The Earth - An Introduction to Physical Geology , Holt, Rinehart, and Winston, 748pages, 1970

Vogt, P. R., A. Lowrie, D. Bracey and R. Hey, Subduction of aseismic ocean ridges: effects on shape seismicity, and other characteristics of consuming plate boundaries, Geol. Soc. Amer. Spec. Paper 172, 59pages, 1976

Walcott, R. I., Lithospheric flexure, analysis of gravity anomalies, and the propagation of seamount chains, in: G. H. Sutton, M. H. Maghnani, and R. Moberly (eds), The Geophysics of the Pacific Ocean Basin and its Margin, pp431-438, American Geophysical Union monograph 19, 1976

Walcott, R. I., Present tectonics and late Cenozoic evolution of New Zealand, Geophysical Journal of the Royal Astronomical Society, 52, pp137-164, 1978

Welsch, W., A review of the adjustments of free networks, Survey Review, 25, pp167-180, 1979

Wiggins, Ralph A., The general linear inverse problem: implication of surface waves and free oscillations for earth structure, Reviews of Geophysics and Space Physics, 10, no. 1, pp251-285, 1972

Wilson, J. T., A new class of faults and their bearing on continental drift, Nature, 207, pp343-347, 1965

Wilson, J. T. and K. Burke, Two types of mountain building, Nature, 239, pp448-449, 1972

Windley, B. F., The Evolving Continents, John Wiley and Sons Inc., New York, 385pages, 1977

Wortel, M. J. R. and N. J. Vlaar, Age dependent subduction of oceanic lithosphere beneath western South America, _Physics of the Earth and Planetary Interiors_, 17, pp201-208, 1978

Zambrano, J. J., and C. M. Urien, Geological outline of the basins in southern Argentina and their continuation off the Atlantic shore, _Journal of Geophysical Research_, 75, pp1363-1396, 1970

Zentilli, M., _Geological evolution and metallogenetic relationships in the Andes of northern Chile between 26° and 29°S._, PhD. thesis, Queens University, Kingston, Ontario, 446pages, 1974

# Appendix 1: Survey Data

These tables present the Huancayo survey data used for the analysis in chapter 2. Distances are given in meters from station "L" to station "M". Angles are given in Deg.mmss format. That is, the numbers before the decimal give the number of degrees, the next two numbers denote the number of minutes, and the last two give the number of seconds. A horizontal angle is specified as angle I,J,K where J refers to the station at which the angle was based, I denotes the station on the left (for an observer at station J) and K is the number of the station on the right. The columns labeled "Error" give the estimated standard deviations. In all cases, the distances have been corrected for atmospheric effects and elevation differences between target and instrument. (Corrections were done at UNB and are not discussed here.) As discussed in chapter 2, horizontal angle information is only given for 1975 and 1976.

Reduced horizontal distances (meters) for 1975.

| L | M | Distance | Error |
|---|---|---|---|
| 1 | 3 | 375.705 | 0.004 |
| 1 | 4 | 1232.191 | 0.004 |
| 1 | 5 | 1325.423 | 0.004 |
| 1 | 10 | 305.247 | 0.004 |
| 1 | 11 | 333.695 | 0.004 |
| 2 | 3 | 712.650 | 0.004 |
| 2 | 4 | 1387.819 | 0.004 |
| 2 | 5 | 936.133 | 0.004 |
| 2 | 6 | 403.446 | 0.004 |
| 2 | 7 | 923.925 | 0.004 |
| 2 | 9 | 198.264 | 0.004 |
| 2 | 10 | 558.406 | 0.004 |
| 3 | 4 | 1584.342 | 0.004 |
| 3 | 5 | 1519.545 | 0.004 |
| 3 | 6 | 1020.670 | 0.004 |
| 3 | 10 | 176.824 | 0.004 |
| 3 | 11 | 540.234 | 0.004 |
| 4 | 5 | 928.174 | 0.004 |
| 4 | 6 | 1098.285 | 0.004 |
| 4 | 7 | 652.178 | 0.004 |
| 4 | 8 | 939.471 | 0.004 |
| 4 | 11 | 1091.061 | 0.004 |
| 5 | 6 | 534.145 | 0.004 |
| 5 | 8 | 558.195 | 0.004 |
| 6 | 7 | 543.206 | 0.004 |
| 6 | 8 | 188.486 | 0.004 |
| 6 | 9 | 528.978 | 0.004 |
| 7 | 8 | 463.116 | 0.004 |
| 7 | 11 | 851.653 | 0.004 |
| 8 | 9 | 529.770 | 0.004 |
| 8 | 10 | 785.731 | 0.004 |
| 8 | 11 | 454.535 | 0.004 |
| 9 | 10 | 360.647 | 0.004 |
| 9 | 11 | 338.177 | 0.004 |
| 10 | 11 | 373.205 | 0.004 |

University of Alberta

```
Horizontal angles for 1975 (Deg.mmss format)
  I    J    K                Angle                  Error
  4    1   10           0.1290207E+03            0.26E-03
  4    1    3           0.1564435E+03            0.26E-03
  3    1    4           0.2031527E+03            0.26E-03
  5    1   11           0.1521120E+02            0.26E-03
 10    1    3           0.2742320E+02            0.26E-03
  4    1   11           0.5742520E+02            0.26E-03
  4    1    5           0.4221360E+02            0.26E-03
 11    1    3           0.9901400E+02            0.26E-03
 11    1   10           0.7119070E+02            0.26E-03
  3    2    7           0.1153354E+03            0.26E-03
  3    2    6           0.1301138E+03            0.26E-03
  5    2    3           0.2260714E+03            0.26E-03
 10    2    5           0.1260120E+03            0.26E-03
  3    2    4           0.9212290E+02            0.26E-03
  9    2    5           0.1224532E+03            0.26E-03
  1    3    4           0.1753020E+02            0.26E-03
  4    3   11           0.1942280E+02            0.26E-03
 11    3    5           0.1500440E+02            0.26E-03
  1    3    5           0.5236140E+02            0.26E-03
  2    3    1           0.2810201E+03            0.26E-03
  5    3    2           0.2621420E+02            0.26E-03
  5    3   10           0.4652000E+00            0.26E-03
 10    3    6           0.8002600E+01            0.26E-03
 10    3    2           0.2534450E+02            0.26E-03
  6    3    2           0.1734250E+02            0.26E-03
  5    4   11           0.5912300E+02            0.26E-03
  5    4    1           0.7411390E+02            0.26E-03
  6    4    1           0.4508580E+02            0.26E-03
  5    4    2           0.4206380E+02            0.26E-03
  5    4    3           0.6849120E+02            0.26E-03
  7    4    1           0.6615070E+02            0.26E-03
  2    5    1           0.3246220E+02            0.26E-03
  8    5    4           0.7343150E+02            0.26E-03
  4    5    2           0.2634658E+03            0.26E-03
  3    5    4           0.7627370E+02            0.26E-03
  6    5    4           0.9326020E+02            0.26E-03
  5    6    9           0.1923909E+03            0.26E-03
  5    6    2           0.1733148E+03            0.26E-03
  5    6   10           0.2072552E+03            0.26E-03
  2    6    8           0.9906210E+02            0.26E-03
  2    6    7           0.1543332E+03            0.26E-03
  4    6    2           0.2310308E+03            0.26E-03
  6    7    4           0.1331713E+03            0.26E-03
  2    7    4           0.1222830E+03            0.26E-03
  8    7    4           0.1134201E+03            0.26E-03
 11    7    4           0.9203060E+02            0.26E-03
  4    7    6           0.2264247E+03            0.26E-03
  6    8   11           0.1184546E+03            0.26E-03
```

University of Alberta

```
 5   8  10        0.1750818E+03        0.26E-03
 7   8   9        0.1842800E+03        0.26E-03
 9   8  11        0.3915360E+02        0.26E-03
11   8   5        0.1681844E+03        0.26E-03
 5   8   9        0.1522544E+03        0.26E-03
11   9   2        0.1203530E+03        0.26E-03
 2   9  10        0.1745635E+03        0.26E-03
10   9  11        0.6427560E+02        0.26E-03
 8   9   2        0.6218520E+02        0.26E-03
10   9   6        0.1431504E+03        0.26E-03
 2  10   3        0.1463337E+03        0.26E-03
 8  10   9        0.3432550E+02        0.26E-03
 9  10   2        0.1473600E+01        0.26E-03
11  10   8        0.2017560E+02        0.26E-03
11  10   2        0.5638250E+02        0.26E-03
 1  10  11        0.5753250E+02        0.26E-03
 2  10  11        0.3032133E+03        0.26E-03
 3  10   1        0.9854300E+02        0.26E-03
 3  11   1        0.4322440E+02        0.26E-03
 9  11   1        0.1112828E+03        0.26E-03
10  11   7        0.1944619E+03        0.26E-03
 7  11   9        0.1043230E+03        0.26E-03
 9  11   4        0.2184634E+03        0.26E-03
 1  11   8        0.1660340E+03        0.26E-03
 8  11   3        0.1503331E+03        0.26E-03
```

1976 reduced horizontal distances (meters).

| L | M | Distance | Error |
|---|---|---|---|
| 1 | 3 | 375.710 | 0.002 |
| 1 | 4 | 1232.198 | 0.002 |
| 1 | 5 | 1325.428 | 0.002 |
| 1 | 10 | 305.250 | 0.002 |
| 1 | 11 | 333.692 | 0.002 |
| 2 | 3 | 712.651 | 0.002 |
| 2 | 4 | 1387.812 | 0.002 |
| 2 | 5 | 936.123 | 0.002 |
| 2 | 6 | 403.445 | 0.002 |
| 2 | 7 | 923.921 | 0.002 |
| 2 | 9 | 198.260 | 0.002 |
| 2 | 10 | 558.405 | 0.002 |
| 3 | 4 | 1584.338 | 0.002 |
| 3 | 5 | 1519.558 | 0.002 |
| 3 | 6 | 1020.667 | 0.002 |
| 3 | 10 | 176.823 | 0.002 |
| 3 | 11 | 540.235 | 0.002 |
| 4 | 5 | 928.175 | 0.002 |
| 4 | 6 | 1098.282 | 0.002 |
| 4 | 7 | 652.179 | 0.002 |
| 4 | 8 | 939.471 | 0.002 |
| 4 | 11 | 1091.059 | 0.002 |
| 5 | 6 | 534.146 | 0.002 |
| 5 | 8 | 558.193 | 0.002 |
| 6 | 7 | 543.207 | 0.002 |
| 6 | 8 | 188.496 | 0.002 |
| 6 | 9 | 528.979 | 0.002 |
| 6 | 10 | 845.922 | 0.002 |
| 7 | 8 | 463.114 | 0.002 |
| 7 | 11 | 851.659 | 0.002 |
| 8 | 9 | 529.771 | 0.002 |
| 8 | 10 | 785.734 | 0.002 |
| 8 | 11 | 454.543 | 0.002 |
| 9 | 10 | 360.641 | 0.002 |
| 9 | 11 | 338.173 | 0.002 |
| 10 | 11 | 373.203 | 0.002 |

```
1976 horizontal angles (Deg.mmss format)
  I    J    K              Angle                  Error
  4    1    5          0.4221410E+02            0.22E-03
  5    1   11          0.1521120E+02            0.22E-03
  4    1   11          0.5742520E+02            0.22E-03
  4    1   10          0.1290204E+03            0.22E-03
 11    1   10          0.7119100E+02            0.22E-03
 11    1    3          0.9901410E+02            0.22E-03
 10    1    3          0.2742280E+02            0.22E-03
  3    1    4          0.2031523E+03            0.22E-03
  4    1    3          0.1564434E+03            0.22E-03
  3    2    4          0.9212250E+02            0.22E-03
  5    2    3          0.2260705E+03            0.22E-03
  3    2    6          0.1301142E+03            0.22E-03
  3    2    7          0.1153355E+03            0.22E-03
 10    2    5          0.1260123E+03            0.22E-03
  9    2    5          0.1224536E+03            0.22E-03
  1    3    4          0.1753040E+02            0.22E-03
  4    3   11          0.1942280E+02            0.22E-03
 11    3    5          0.1500360E+02            0.22E-03
  1    3    5          0.5236090E+02            0.22E-03
  2    3    1          0.2810204E+03            0.22E-03
  5    3   10          0.4651000E+00            0.22E-03
  5    3    2          0.2621420E+02            0.22E-03
 10    3    2          0.2534490E+02            0.22E-03
 10    3    6          0.8002200E+01            0.22E-03
  6    3    2          0.1734260E+02            0.22E-03
  6    4    1          0.4509000E+02            0.22E-03
  5    4    1          0.7411350E+02            0.22E-03
  1    4    5          0.2854823E+03            0.22E-03
  5    4    2          0.4206350E+02            0.22E-03
  5    4   11          0.5912320E+02            0.22E-03
  5    4    3          0.6849180E+02            0.22E-03
  7    4    1          0.6615070E+02            0.22E-03
  6    4    3          0.3946380E+02            0.22E-03
  8    4   11          0.2426050E+02            0.22E-03
  3    5    4          0.7627360E+02            0.22E-03
  4    5    2          0.2634657E+03            0.22E-03
  8    5    4          0.7343110E+02            0.22E-03
  6    5    4          0.9326020E+02            0.22E-03
  1    5    4          0.6326420E+02            0.22E-03
  2    5    1          0.3246190E+02            0.22E-03
  5    6    9          0.1923910E+03            0.22E-03
  4    6    2          0.2310310E+03            0.22E-03
  2    6    7          0.1543331E+03            0.22E-03
  5    6    2          0.1733149E+03            0.22E-03
  5    6   10          0.2072552E+03            0.22E-03
  2    6    8          0.9906180E+02            0.22E-03
  3    6    4          0.9642530E+02            0.22E-03
 11    7    4          0.9203040E+02            0.22E-03
```

University of Alberta

```
 6   7   4        0.1331712E+03          0.22E-03
 4   7   6        0.2264246E+03          0.22E-03
 8   7   4        0.1134158E+03          0.22E-03
 2   7   4        0.1222829E+03          0.22E-03
 7   8   9        0.1842803E+03          0.22E-03
 5   8   9        0.1522547E+03          0.22E-03
11   8   4        0.9648190E+02          0.22E-03
 5   8  10        0.1750823E+03          0.22E-03
 5   8  11        0.1914118E+03          0.22E-03
 6   8  11        0.1184558E+03          0.22E-03
 9   8  11        0.3915360E+02          0.22E-03
10   9  11        0.6427560E+02          0.22E-03
10   9   8        0.1224427E+03          0.22E-03
11   9   2        0.1203528E+03          0.22E-03
 8   9   2        0.6218530E+02          0.22E-03
 2   9  10        0.1745643E+03          0.22E-03
10   9   6        0.1431500E+03          0.22E-03
 8  10   6        0.1234410E+02          0.22E-03
 2  10  11        0.3032130E+03          0.22E-03
 3  10   1        0.9854220E+02          0.22E-03
11  10   8        0.2017590E+02          0.22E-03
11  10   2        0.5638280E+02          0.22E-03
 1  10  11        0.5753230E+02          0.22E-03
 8  10   9        0.3432580E+02          0.22E-03
 9  10   2        0.1473400E+01          0.22E-03
 2  10   3        0.1463338E+03          0.22E-03
 1  11   8        0.1660336E+03          0.22E-03
10  11   7        0.1944612E+03          0.22E-03
 3  11   1        0.4322460E+02          0.22E-03
 9  11   1        0.1112831E+03          0.22E-03
 8  11   3        0.1503342E+03          0.22E-03
 7  11   9        0.1043236E+03          0.22E-03
 4  11   9        0.1411328E+03          0.22E-03
```

1977 reduced horizontal distances (meters)

| L | M | Distance | Error |
|---|---|---|---|
| 1 | 3 | 375.707 | 0.003 |
| 1 | 4 | 1232.199 | 0.003 |
| 1 | 5 | 1325.430 | 0.003 |
| 1 | 10 | 305.245 | 0.003 |
| 1 | 11 | 333.693 | 0.003 |
| 2 | 3 | 712.650 | 0.003 |
| 2 | 4 | 1387.817 | 0.003 |
| 2 | 5 | 936.128 | 0.003 |
| 2 | 6 | 403.445 | 0.003 |
| 2 | 7 | 923.925 | 0.003 |
| 2 | 8 | 471.560 | 0.003 |
| 2 | 9 | 198.260 | 0.003 |
| 2 | 10 | 558.404 | 0.003 |
| 3 | 4 | 1584.336 | 0.003 |
| 3 | 5 | 1519.555 | 0.003 |
| 3 | 6 | 1020.661 | 0.003 |
| 3 | 9 | 519.522 | 0.003 |
| 3 | 10 | 176.824 | 0.003 |
| 3 | 11 | 540.239 | 0.003 |
| 4 | 5 | 928.177 | 0.003 |
| 4 | 6 | 1098.276 | 0.003 |
| 4 | 7 | 652.178 | 0.003 |
| 4 | 8 | 939.471 | 0.003 |
| 4 | 11 | 1091.064 | 0.003 |
| 5 | 6 | 534.142 | 0.003 |
| 5 | 8 | 558.192 | 0.003 |
| 5 | 12 | 21.612 | 0.003 |
| 6 | 7 | 543.204 | 0.003 |
| 6 | 8 | 188.494 | 0.003 |
| 6 | 9 | 528.973 | 0.003 |
| 6 | 10 | 845.923 | 0.003 |
| 7 | 8 | 463.114 | 0.003 |
| 7 | 11 | 851.657 | 0.003 |
| 7 | 12 | 274.688 | 0.003 |
| 8 | 9 | 529.771 | 0.003 |
| 8 | 10 | 785.732 | 0.003 |
| 8 | 11 | 454.539 | 0.003 |
| 9 | 10 | 360.644 | 0.003 |
| 9 | 11 | 338.175 | 0.003 |
| 10 | 11 | 373.203 | 0.003 |

1978 reduced horizontal distances (meters)

| L | M | Distance | Error |
|---|---|---|---|
| 1 | 3 | 375.706 | 0.003 |
| 1 | 4 | 1232.204 | 0.003 |
| 1 | 5 | 1325.424 | 0.003 |
| 1 | 10 | 305.248 | 0.003 |
| 1 | 11 | 333.692 | 0.003 |
| 2 | 3 | 712.650 | 0.003 |
| 2 | 4 | 1387.817 | 0.003 |
| 2 | 5 | 936.128 | 0.003 |
| 2 | 6 | 403.443 | 0.003 |
| 2 | 7 | 923.920 | 0.003 |
| 2 | 8 | 471.555 | 0.003 |
| 2 | 9 | 198.259 | 0.003 |
| 2 | 10 | 558.401 | 0.003 |
| 3 | 4 | 1584.340 | 0.003 |
| 3 | 5 | 1519.553 | 0.003 |
| 3 | 6 | 1020.664 | 0.003 |
| 3 | 9 | 519.526 | 0.003 |
| 3 | 10 | 176.820 | 0.003 |
| 3 | 11 | 540.241 | 0.003 |
| 4 | 5 | 928.177 | 0.003 |
| 4 | 6 | 1098.280 | 0.003 |
| 4 | 7 | 652.183 | 0.003 |
| 4 | 8 | 939.477 | 0.003 |
| 4 | 11 | 1091.068 | 0.003 |
| 5 | 6 | 534.143 | 0.003 |
| 5 | 8 | 558.188 | 0.003 |
| 6 | 7 | 543.203 | 0.003 |
| 6 | 8 | 188.492 | 0.003 |
| 6 | 9 | 528.977 | 0.003 |
| 6 | 10 | 845.925 | 0.003 |
| 7 | 8 | 463.112 | 0.003 |
| 7 | 11 | 851.655 | 0.003 |
| 8 | 9 | 529.772 | 0.003 |
| 8 | 10 | 785.730 | 0.003 |
| 8 | 11 | 454.536 | 0.003 |
| 9 | 10 | 360.645 | 0.003 |
| 9 | 11 | 338.176 | 0.003 |
| 10 | 11 | 373.205 | 0.003 |

# Appendix 2: Vertical Seismicity Profiles

These profiles were taken from data on the NOAA catalogue and show all recorded events having body wave magnitude greater than 4.0 and which occurred between 1963 and 1977 inclusive. Profiles are all 1 degree wide and were taken in the approximate direction of relative motion between the Nazca and South American plates as determined by Minster and Jordan (1978). The coverage is complete from northern Peru to 26°S in Chile.

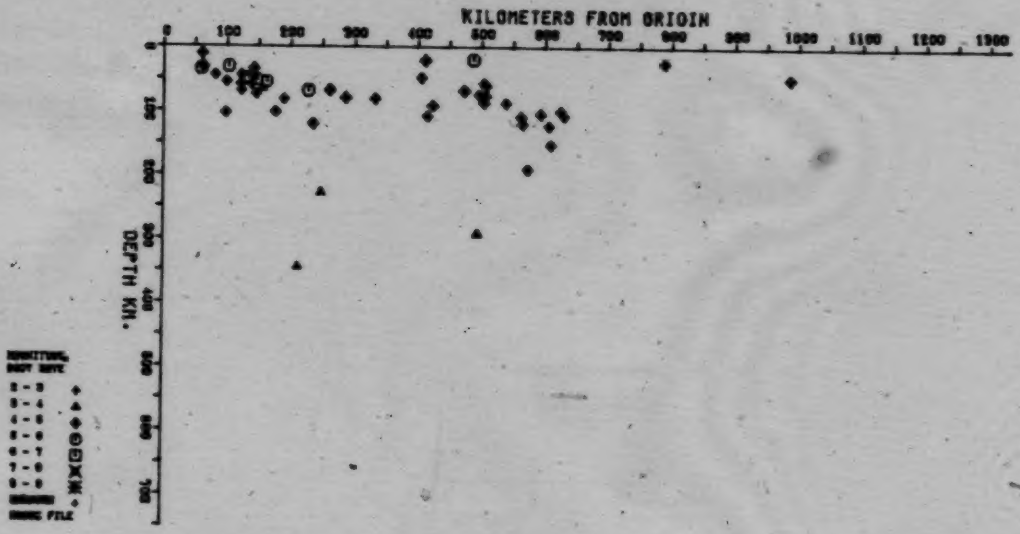

CROSS SECTION 1.0 DEGREES WIDE
BETWEEN -5.6,-82.2 AND -3.6,-70.3

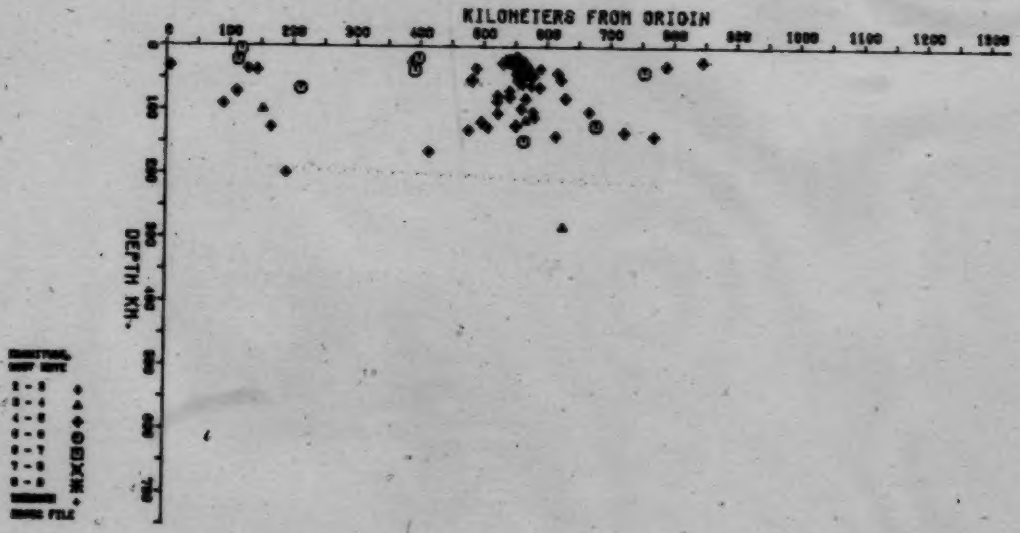

CROSS SECTION 1.0 DEGREES WIDE
BETWEEN -6.6,-82.1 AND -4.8,-70.2

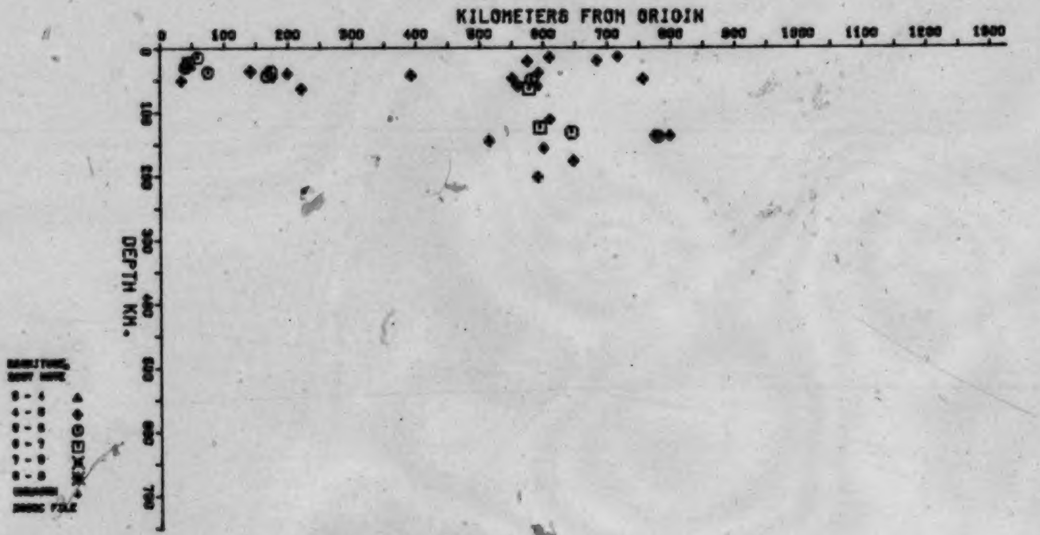

CROSS SECTION 1.0 DEGREES WIDE
BETWEEN -7.5,-82.0 AND -5.9,-70.1

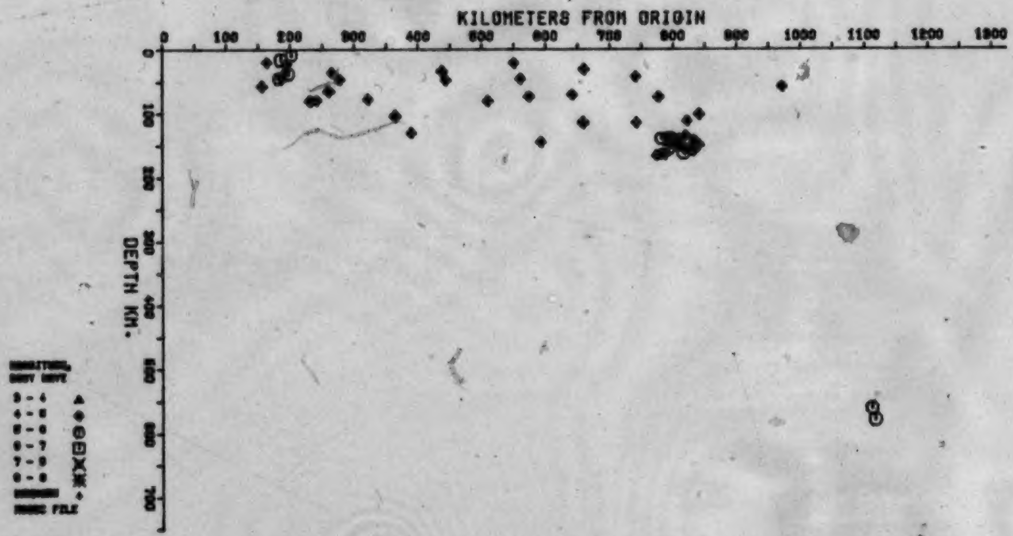

CROSS SECTION 1.0 DEGREES WIDE
BETWEEN -8.5,-81.9 AND -6.9,-69.9

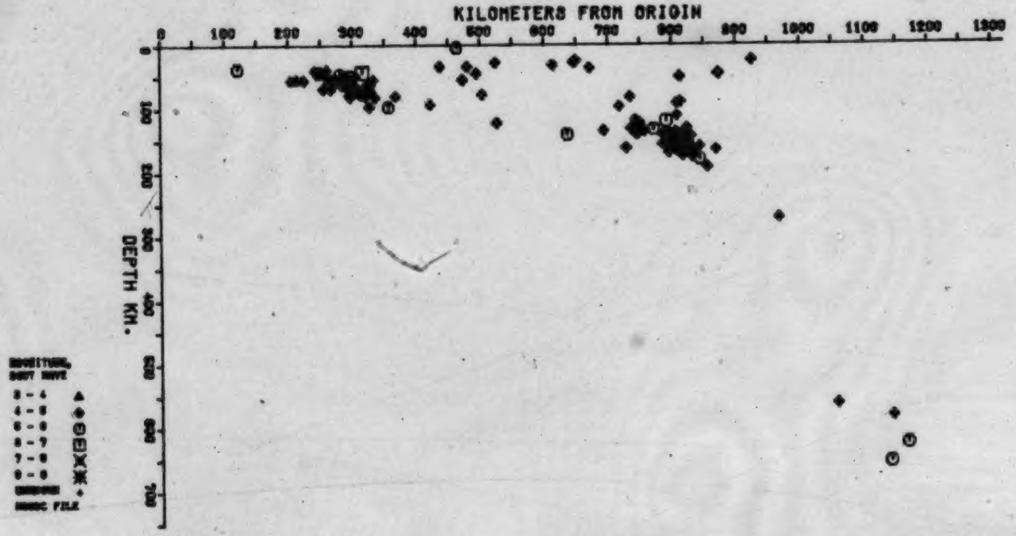

CROSS SECTION 1.0 DEGREES WIDE
BETWEEN -8.5,-81.7 AND -7.8,-69.8

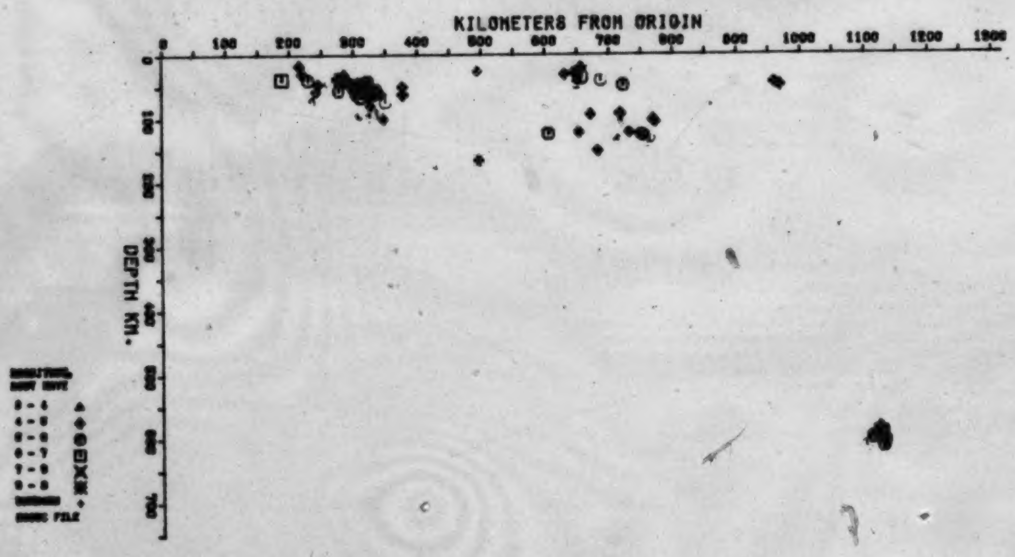

CROSS SECTION 1.0 DEGREES WIDE
BETWEEN -10.4,-81.8 AND -8.8,-68.7

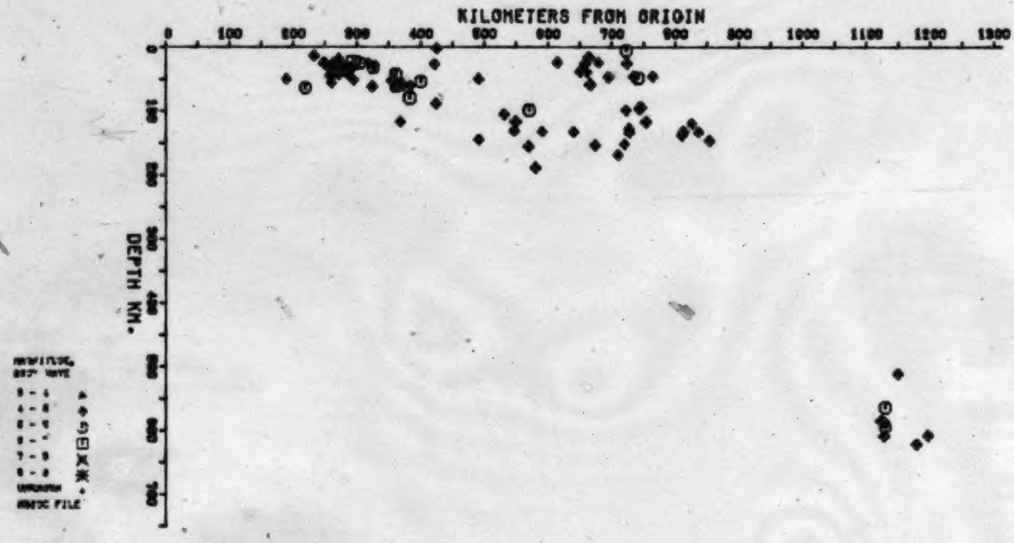

CROSS SECTION 1.0 DEGREES WIDE
BETWEEN -11.4,-81.4 AND -9.6,-69.5

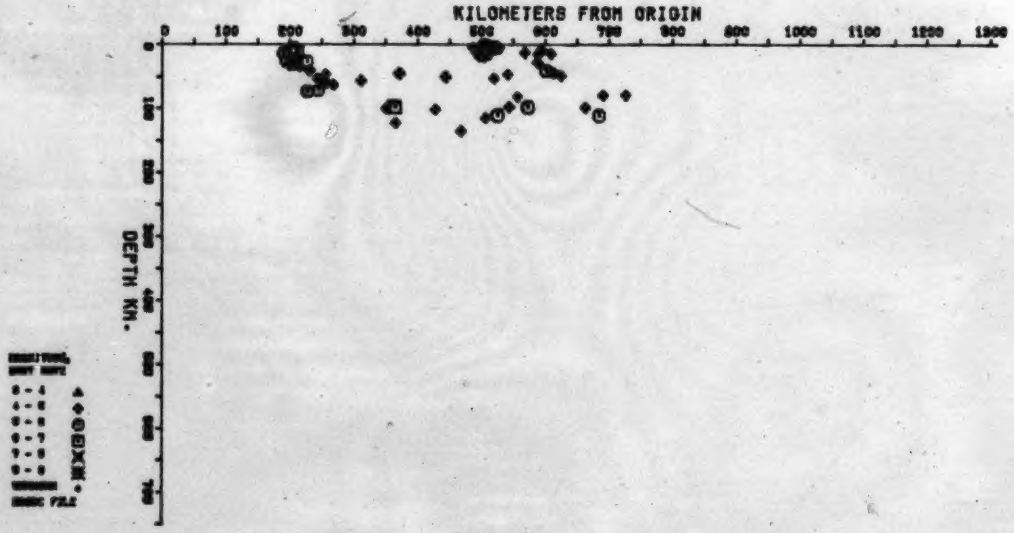

CROSS SECTION 1.0 DEGREES WIDE
BETWEEN -12.6,-78.7 AND -10.2,-67.9

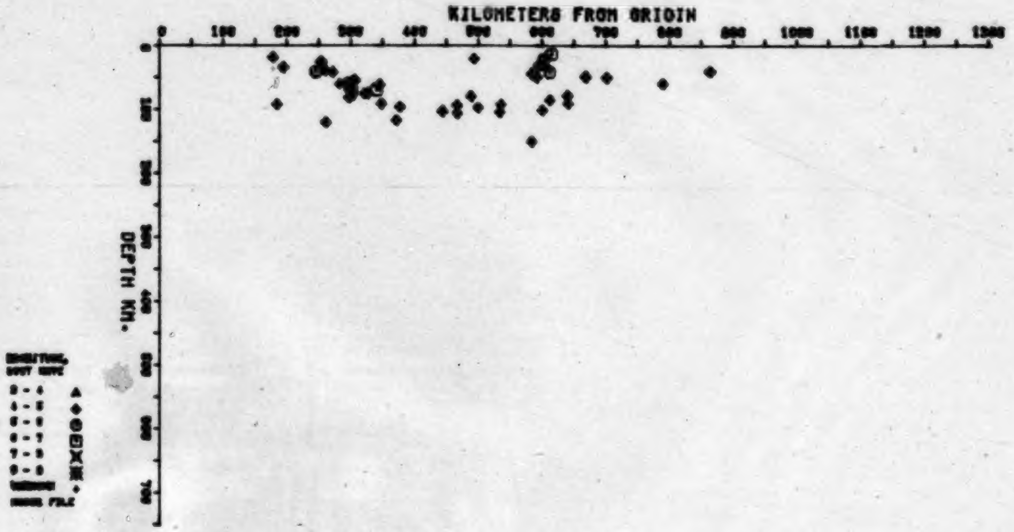

CROSS SECTION 1.0 DEGREES WIDE
BETWEEN -13.6,-70.5 AND -11.2,-67.7

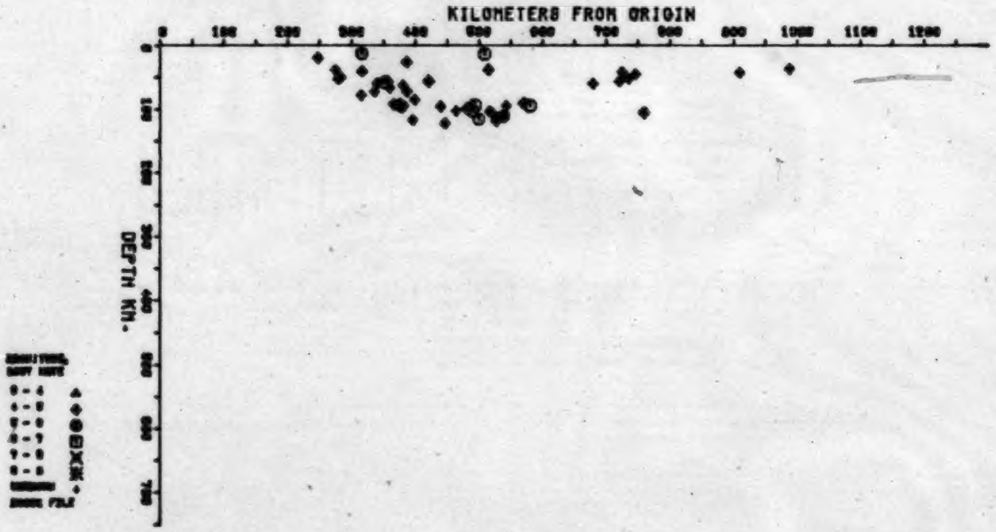

CROSS SECTION 1.0 DEGREES WIDE
BETWEEN -14.5,-70.3 AND -12.1,-67.5

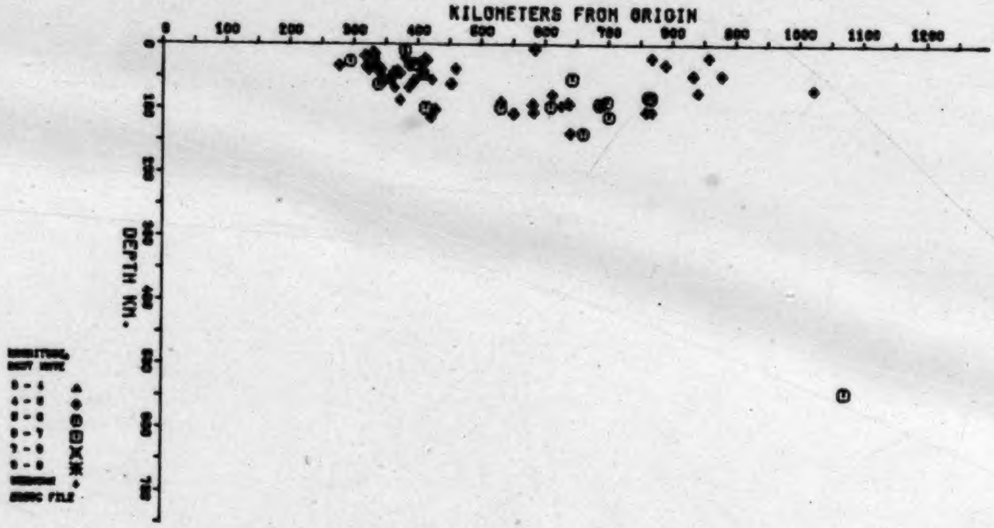

CROSS SECTION 1.0 DEGREES WIDE
BETWEEN -15.5,-78.1 AND -13.1,-67.3

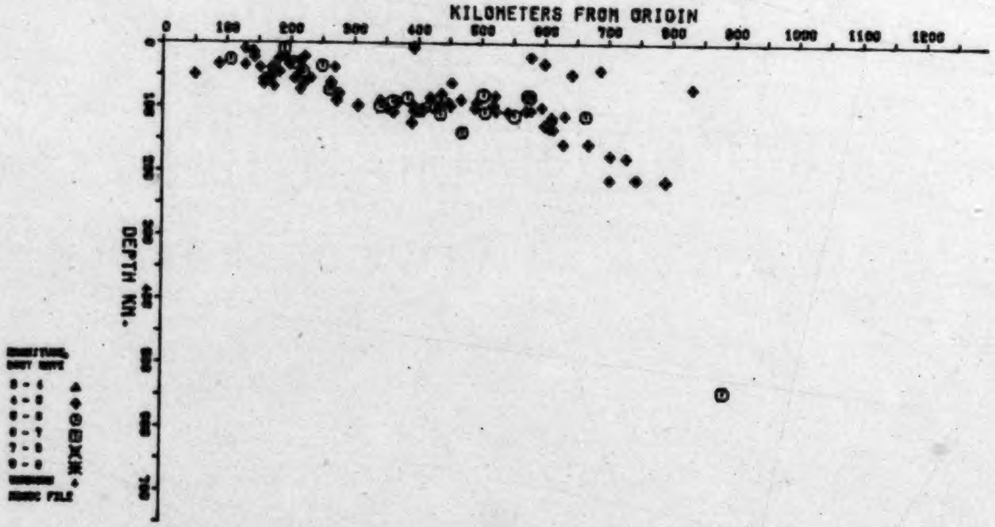

CROSS SECTION 1.0 DEGREES WIDE
BETWEEN -16.5,-77.3 AND -19.4,-66.6

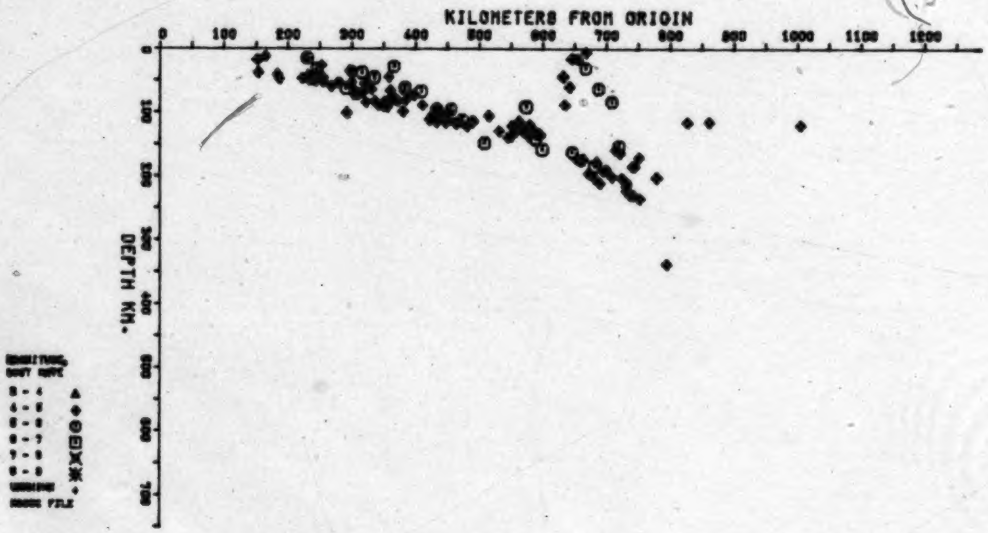

CROSS SECTION 1.0 DEGREES WIDE
BETWEEN -10.6,-77.1 AND -14.4,-66.3

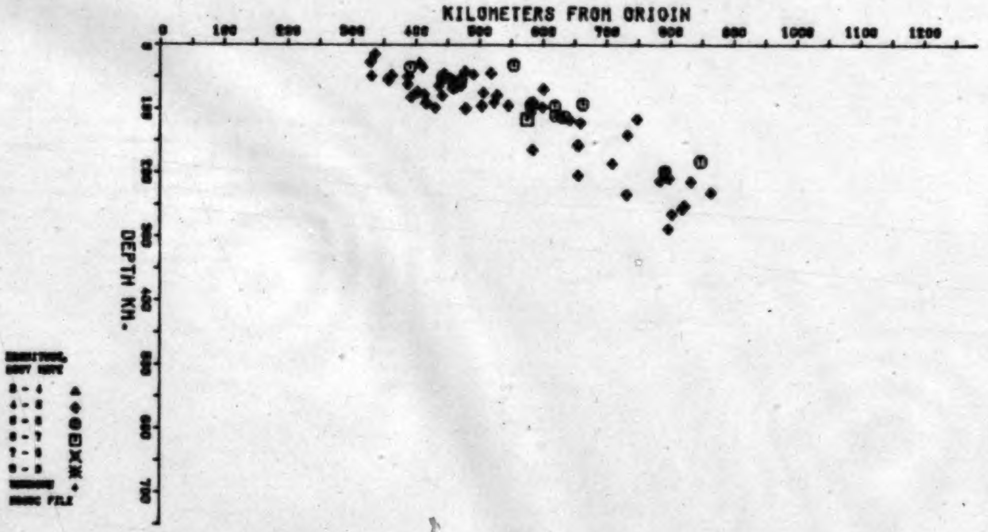

CROSS SECTION 1.0 DEGREES WIDE
BETWEEN -17.6,-77.0 AND -15.4,-66.1

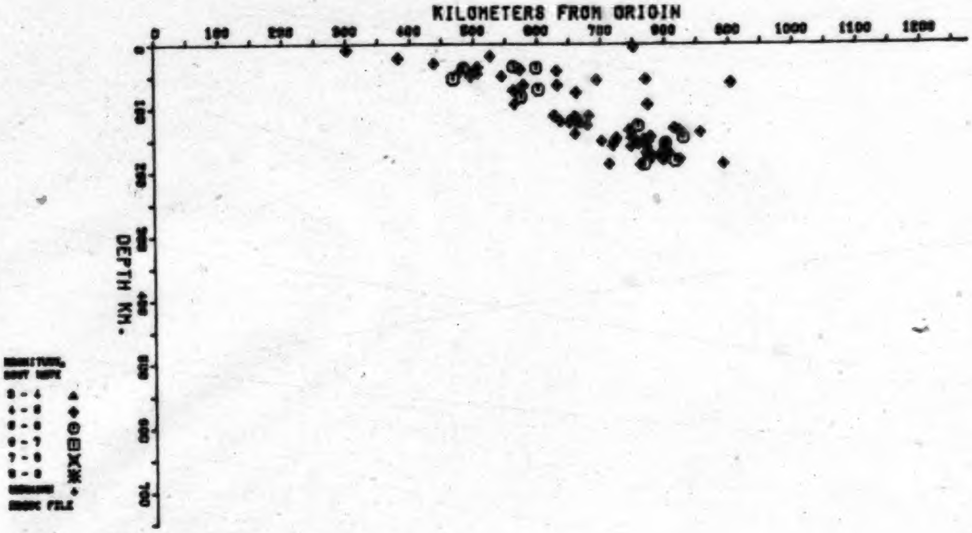

CROSS SECTION 1.0 DEGREES WIDE
BETWEEN -18.4,-70.8 AND -16.3,-66.0

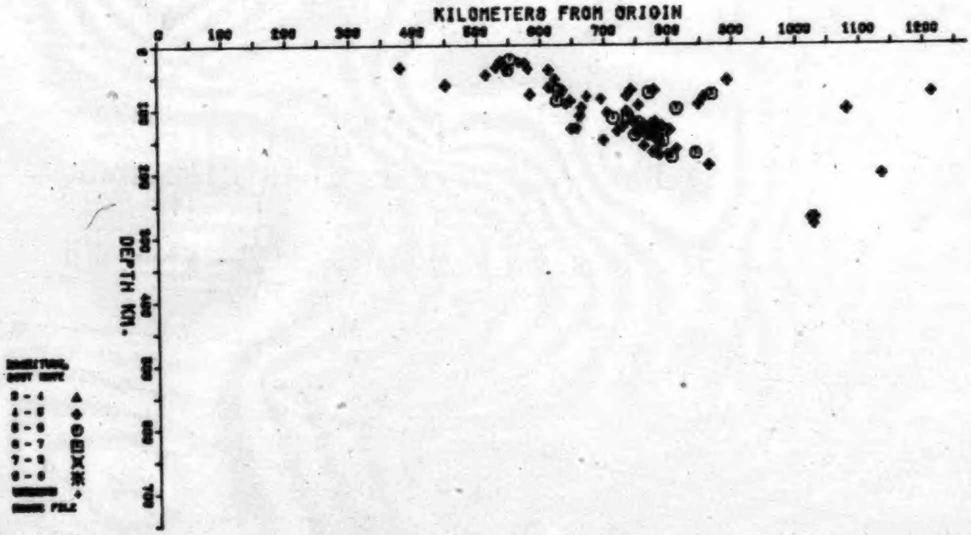

CROSS SECTION 1.0 DEGREES WIDE
BETWEEN -19.4,-70.8 AND -17.3,-64.8

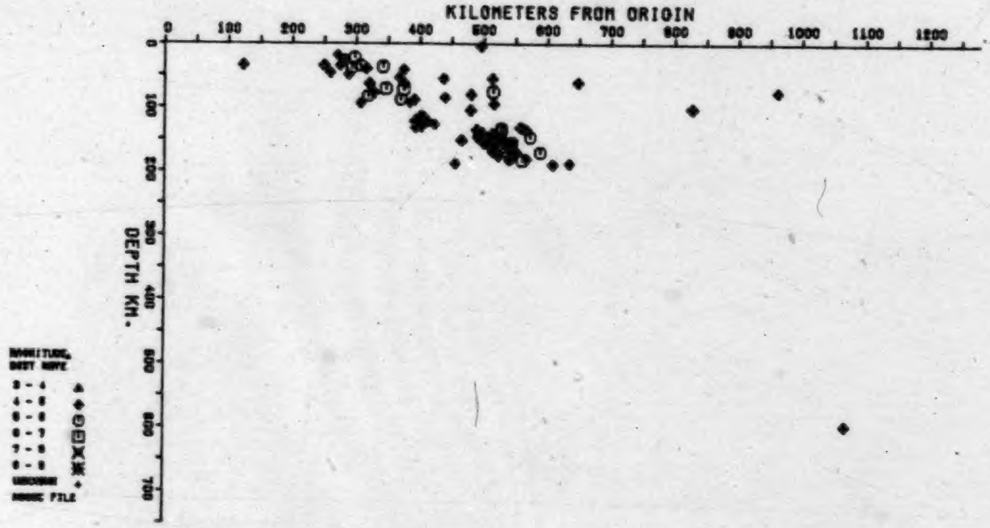

CROSS SECTION 1.0 DEGREES WIDE
BETWEEN -18.6,-74.3 AND -16.1,-62.8

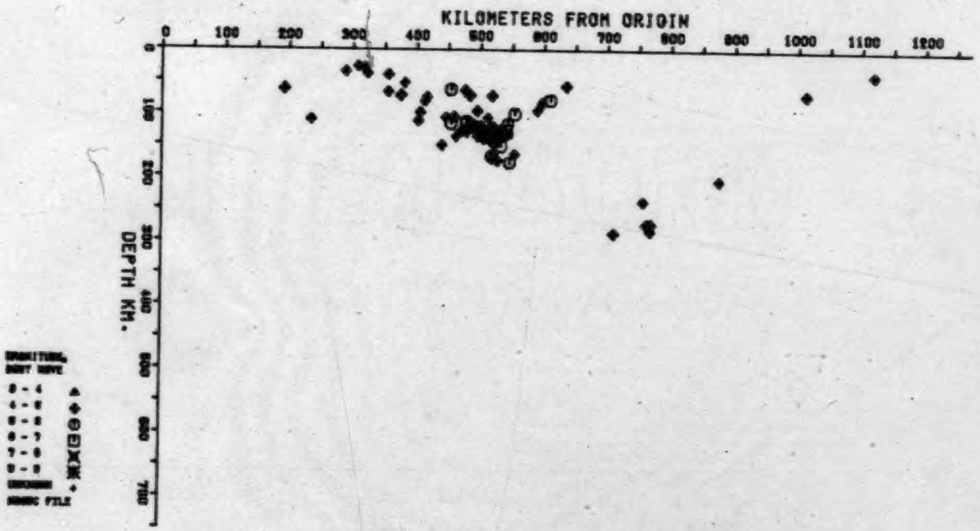

CROSS SECTION 1.0 DEGREES WIDE
BETWEEN -19.6,-74.1 AND -17.1,-62.4

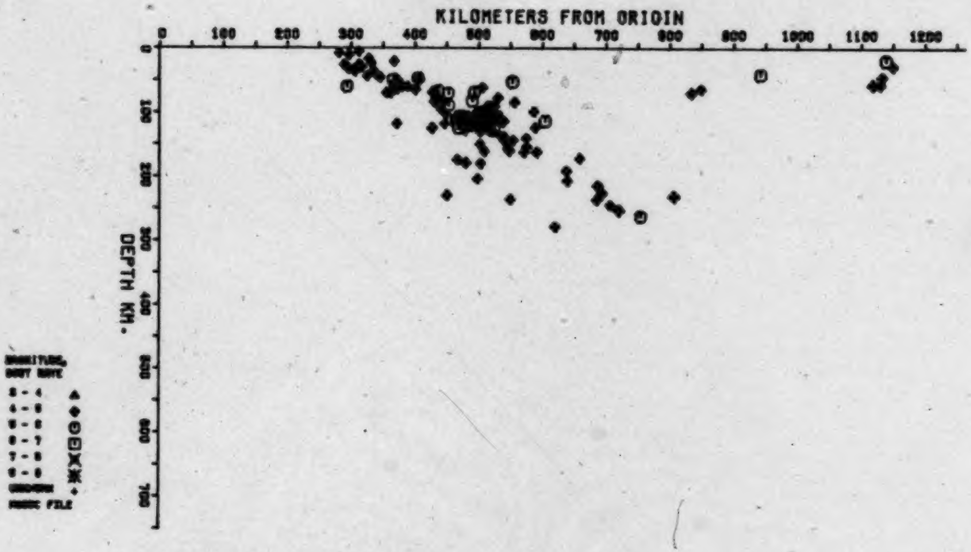

CROSS SECTION 1.0 DEGREES WIDE
BETWEEN -20.5,-73.9 AND -19.0,-62.1

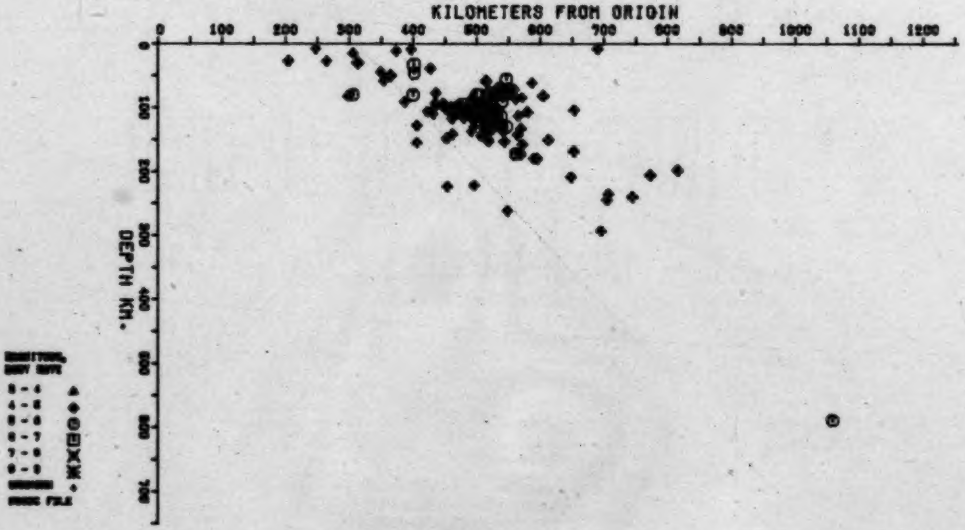

CROSS SECTION 1.0 DEGREES WIDE
BETWEEN -21.5,-73.7 AND -19.0,-61.8

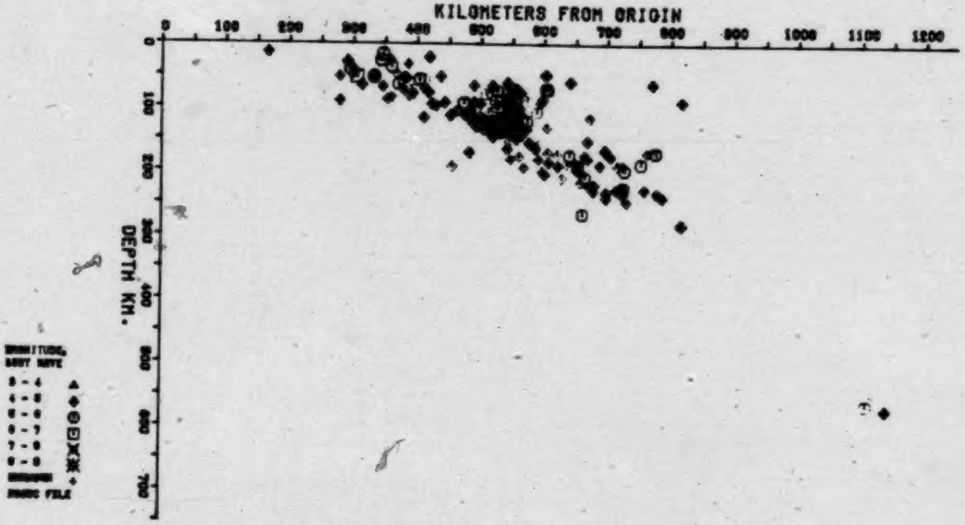

CROSS SECTION 1.0 DEGREES WIDE
BETWEEN -22.6,-73.6 AND -20.9,-61.7

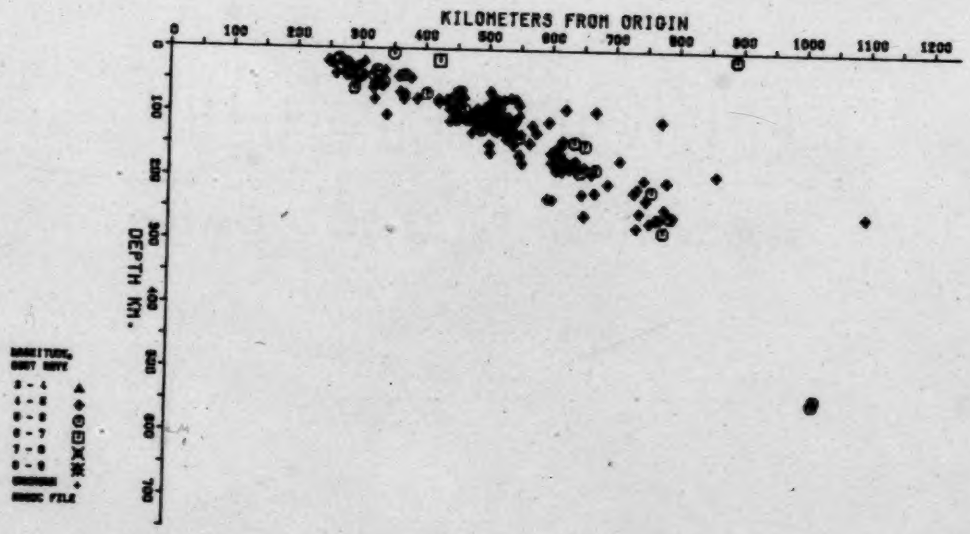

CROSS SECTION 1.0 DEGREES WIDE
BETWEEN -23.5,-73.3 AND -21.0,-61.6

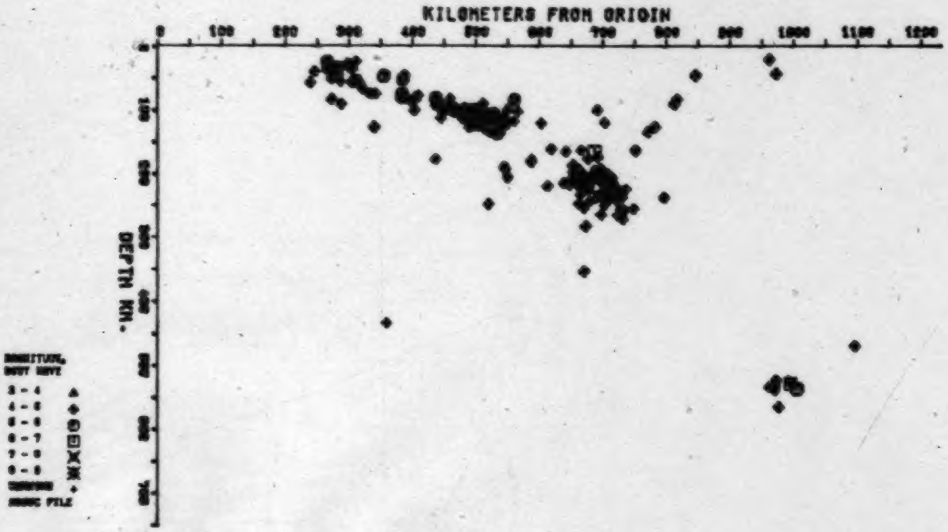

CROSS SECTION 1.0 DEGREES WIDE
BETWEEN -24.5,-73.0 AND -22.0,-61.3

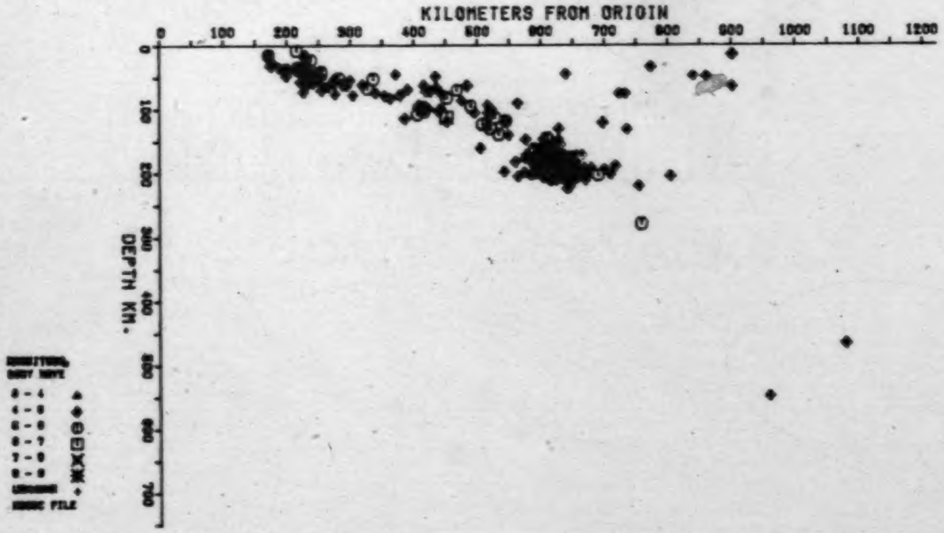

CROSS SECTION 1.0 DEGREES WIDE
BETWEEN -25.4,-72.8 AND -22.8,-61.1

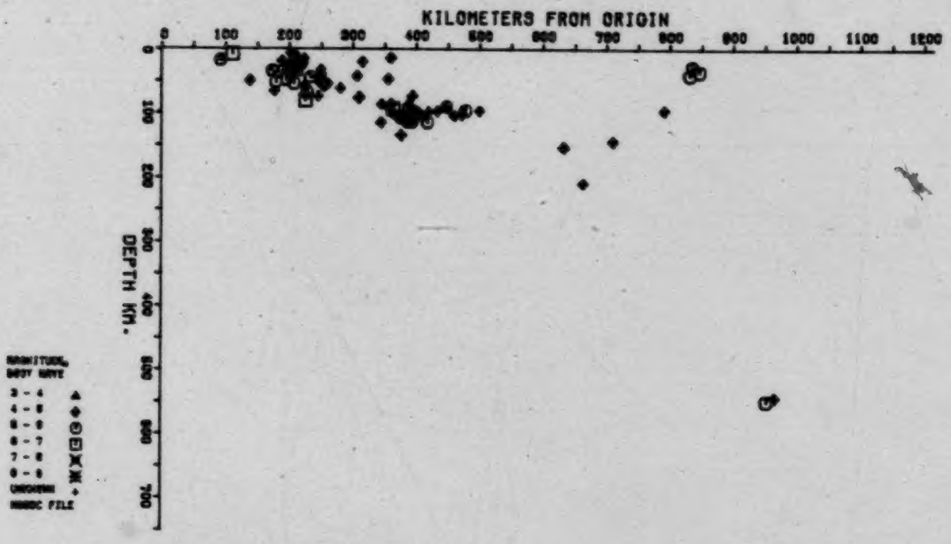

CROSS SECTION 1.0 DEGREES WIDE
BETWEEN -28.4,-72.6 AND -23.5,-60.9

## Appendix 3: Method for the Least Squares Matching of Plate Boundaries

Idealize the problem as that of rotating one contour into another (figure 4.2). Bullard et al. (1965) solved this by finding the rotation angle, $\Phi_o$, which minimizes the difference in "longitude" between the contours. As discussed in section 4.2.2, this method is not satisfactory for continents whose angular extent in "latitude" is small. The method presented here minimizes the difference in arclength (in km) measured along lines of "latitude."

Consider a point, n, in the digitized data set representing curve 1 (say the left curve in figure 4.2). It is desired to compute the distance in km between this point and a point on curve 2 which has the same "latitude." This will usually require linear interpolation between two points in the curve 2 data set. The distance in km between these points is given by:

$$d_n \cong \alpha_n \Phi_n$$

where $\alpha_n \cong 111 \sin \Psi_n$, $\Phi_n$ is the difference in "longitude" and $\Psi_n$ is the "latitude." The total number of such comparisons, say N12, which can be made will usually be less than the number of points representing curve 1.

In a completely analogous manner, any point in the digitized data set representing curve 2 can be compared to curve 1 giving a distance difference, $d'_n$. Let N21 be the total number of these comparisons. Then following Bullard et al., the average squared misfit, Q², is:

$$Q^2 = \frac{1}{2N_{12}} \sum_{1}^{N_{12}} (\Phi_n - \Phi_o)^2 \alpha_n^2 + \frac{1}{2N_{21}} \sum_{1}^{N_{21}} (\Phi'_n - \Phi_o)^2 \alpha'^2_n$$

It is not difficult to show that the rotation angle, , which minimizes this quantity is given by:

$$\Phi_o = \left( N_{21} \sum_{1}^{N_{12}} \Phi_n \alpha_n^2 + N_{12} \sum_{1}^{N_{21}} \Phi'_n \alpha'^2_n \right) \Bigg/ \left( N_{21} \sum_{1}^{N_{12}} \alpha_n^2 + N_{12} \sum_{1}^{N_{21}} \alpha'^2_n \right)$$

The average misfit is then found by using this result in the previous equation and computing the square root.